Applications of Model-Based Lung Mechanics in the Intensive Care Unit

Ashwath Sundaresan

A thesis presented for the degree of

Doctor of Philosophy

in

Mechanical Engineering

at the

University of Canterbury,

Christchurch, New Zealand.

13 May 2010

Acknowledgements

To Professor Geoff Chase. Thank you for being a solid supervisor and constantly pushing me to improve my work.

To Dr Geoff Shaw. Cheers for always making time for me. Could not have done this project without your inputs.

To the ICU staff. Thanks for putting up with me and assisting me in my trials. Somehow I always got in your way, and yet you guys were always patient!

To Dr Chris Hann. Thank you for your technical and mathematical advice during my research.

To the Bioeng suite. Cheers for the good times and laughs. Loved the goss, loved the jokes and appreciate the accumulation of random knowledge I now have thanks to you guys!

To Messer's Fleury and Jackson. PG for life! Enjoyed living with you guys and also appreciated the support from you guys during the first two years of our postgrad.

To my Dad (Sundar). Thank you for all your wisdom and guidance. You have been an awesome role model to me and appreciate all the advice you have imparted on me.

To my Mum (Narayani), Mythrayee & Frances. Thank you heaps for your love and support. Also, thank you for putting up with me when I was difficult. Love you lots.

Table of Contents

List of Figures

List of Tables

Nomenclature

Intensive Care Unit (ICU)
Mechanical Ventilation (MV)
Endotracheal (ET)
Ventilator Induced Lung Injury (VILI)
Acute Respiratory Distress Syndrome (ARDS)
Acute Lung Injury (ALI)
Positive End Expiratory Pressure (PEEP)
Centimetre of Water – Pressure Measurement (cmH2O)
Tidal Volume (V_t)
Peak Inspiratory Pressure (PIP)
Functional Residual Capacity (FRC)
Dynamic Functional Residual Capacity (dFRC)
Volume Controlled Ventilation (VCV)
Pressure Controlled Ventilation (PCV)
Carbon Dioxide (CO_2)
Pressure Volume (PV)
Lower Inflection Point (LIP)
Upper Inflection Point (UIP)
Zero End Expiratory Pressure (ZEEP)
Computed Tomography (CT)
Threshold Opening Pressure (TOP)
Threshold Closing Pressure (TCP)
Hounsfield unit (HU)
Static Pressure Volume (SPV)
Finite Element (FE)
Chronic Obstructive Pulmonary Disease (COPD)
Standard Deviation (SD)
Transpulmonary Pressure (P_L)
Specific Lung Elastance (E_{Lspec})
Plateau Airway Pressure (P_{aw})
Lung Elastance (E_L)
Chest Wall Elastance (E_{CW})
Ratio of lung elastance to total respiratory elastance (α)
Normal Mean (μ')

Normal SD (σ')
Lognormal Mean (μ)
Lognormal SD (σ)
Total Lung Capacity (TLC)
PEEP Stress (β)
Millisieverts (mSv)
International Commission on Radiological Protection (ICRP)
Linear No Threshold Model (LNT)
Medical Radiation Technologists (MRT)
Partial Pressure of Arterial Oxygen (P_aO_2)
Fraction of Inspired Oxygen (F_iO_2)
Fraction of Expired Oxygen (F_EO_2)
Synchronised Intermittent Mandatory Ventilation (SIMV)
Rocuronium Bromide (ROC)
Interquartile Range (IQR)
Cardiac Output (CO)
Oxygen Saturation (S_aO_2)
Oxygen Consumption (VO_2)
Diffusion Resistance (R)
Pulmonary Shunt (f_s)
Oxygen Dissociation Curve (ODC)
Proof of Concept (POC)

Abstract

Mechanical ventilation (MV) therapy has been utilised in the intensive care unit (ICU) for 50 years to treat patients with respiratory illness by supporting the work of breathing, providing oxygen and removing carbon dioxide. MV therapy is utilised by 30-50% of ICU patients, and is a major driver of increased length of stay, increased cost and increased mortality. For patients suffering from acute respiratory distress syndrome (ARDS), the optimal MV settings are highly debated. ARDS patients suffer from a lack of recruited alveoli, and the application of positive end expiratory pressure (PEEP) is often used to maintain recruitment to maximise gas exchange and minimise lung damage. However, determining what level of PEEP is best for the patient is difficult. In particular, it involves a complex trade off between patient safety and ventilation efficacy.

Currently, no clinical protocols exist to determine a patient-specific "best" PEEP. Model-based approaches provide an alternative patient-specific method to help clinical diagnosis and therapy selection. In particular, model-based methods can utilise a mix of both engineering and medical principles to create patient-specific models. The models are used for optimising ventilation settings and providing greater physiological insight into lung status than is currently available.

Two model-based approaches are presented here. First, a quasi-static, minimal model of lung mechanics is presented based solely on fundamental lung physiology and mechanics. Secondly, a model of dynamic functional residual capacity (dFRC) is developed and presented based on model-based status of lung stress and strain. These models are validated with retrospective clinical data to evaluate the potential of such model-based approaches. Finally, the models are further validated with real time clinical data over a broader spectrum of pressure-volume ranges than prior studies to evaluate the clinical viability of model-based approaches to optimise MV therapy.

When validated with real-time clinical trials data, the outputs of the recruitment model provide a range of optimal patient-specific values of PEEP based on different clinically and physiologically derived criteria. The recruitment model is also shown to have the ability to track the disease state of ARDS over time. The dFRC model introduces the PEEP stress parameter, β, which represents a unique population constant. The dFRC model

suggests that clinically reasonable estimates of dFRC can be achieved by using this novel value of β, rather than the current, potentially hazardous, methods of deflating the lung to atmospheric pressure.

Finally, a third model, combining the principles of recruitment and gas exchange is introduced. The combined model has the ability to estimate cardiac output (CO) changes with respect to PEEP changes during MV therapy. In addition, the model relates the coupled areas of circulation and pulmonary management, as well as linking these MV decision support models to oxygenation based clinical endpoints. A proof of concept is shown for this model by combining two different retrospective datasets and highlighting its ability to capture clinically expected drops in CO as PEEP increases. The model allows valuable cardiovascular circulation data to be predicted and also provides an alternative method and clinical end point by which PEEP could be optimised. The model requires further clinical validation before clinical use, but shows significant promise.

The models developed and tested in this research enable rapid parameter identification from minimal, readily available clinical data, and thus provide a novel way of guiding therapy. The models can potentially provide clinicians with information to select an optimal patient-specific level of PEEP using only standard ventilation data, such as pressure-volume curves. In addition, the development of a dFRC stress model provides a unique population constant, β. Overall, the modelling approaches developed and validated in this research provide several novel methods of guiding therapy setting mechanical ventilation parameters and tracking and assess a patient's lung condition. This research thus creates and provides novel validated methods for improving MV therapy with minimal cost or added invasiveness.

Chapter 1 - Introduction

The rapid development of technology has made many aspects of human life easier. Innovations introduced in the past century have transformed the world and improved human life. Medical technologies represent a small portion of the technology umbrella and are used to diagnose, monitor or treat a wide range of conditions. Medical technologies are used to improve the quality of care by providing earlier diagnosis, less invasive treatment options and reduction in hospital times.

Although medical technologies can incorporate pharmaceuticals, procedures, and organisational systems, an important category is medical devices. The purpose of medical devices can range from diagnosis to treatment of disease conditions. The range of medical devices available can be seen in a typical Intensive Care Unit (ICU), with patients being monitored and managed through invasive catheters, ventilators and infusion pumps. The technologies used in the ICU are used to deliver drug therapies, support circulation and breathing, and provide several other specific treatments.

1.1 MECHANICAL VENTILATION

The most common treatment in the ICU is Mechanical Ventilation (MV) therapy, and is used to aid patients who have respiratory failure. MV aids patient breathing by delivering bulk movement of air into and out of the lung, and thus supplements or replaces spontaneous breathing. Through the application of additional pressure to the patient's airway, air is delivered invasively through an endotracheal (ET) tube or non-invasively through a face mask. To prevent air from leaking, the ET tube is sealed with a pressure cuff, to ensure the patient is accurately ventilated.

Patients who suffer from respiratory failure are treated with MV to improve gas exchange and oxygenation. However, additional complications may arise if incorrect ventilation settings are used. Ventilator Induced Lung Injury (VILI) can occur if patients are ventilated with excessive pressures (barotrauma) or tidal volumes (volutrauma) [Dasta et al., 2005, McLean et al., 2006]. This injury exacerbates the existing condition and increases a

patient's length of time under MV, resulting in increased length and cost of stay [Dasta et al., 2005].

Ventilators offer a range of parameters to change. However, in practice, only a few variables are considered of significant clinical relevance to patients. Positive End Expiratory Pressure (PEEP) and Tidal Volume (V_t) are two key parameters that define a state of MV. PEEP represents the pressure at the end of expiration to which the lung is allowed to deflate and is greater than atmospheric pressure. MV status is also well described by V_t, which represents the volume of air that enters the lung per breath. If PEEP describes the minimum pressure which the lung experiences, the Peak Inspiratory Pressure (PIP) describes the maximum pressure the lung experiences. Therefore, during ventilation, the patient inspires a certain Vt of air from a pressure of PEEP up to a resulting PIP, as shown on Figure 1.1, thus defining a typical breath in terms of pressure and volume.

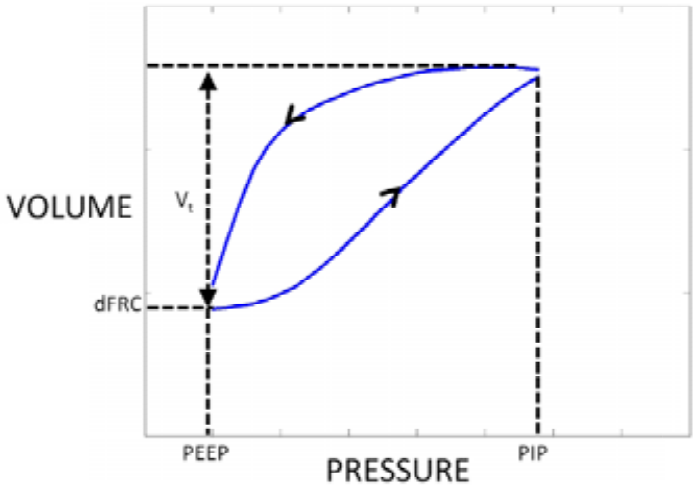

Figure 1.1 – Pressure Volume curve showing dFRC, V_t, PEEP and PIP

Under normal breathing conditions, the pressure of the lung drops to atmospheric pressure with the associated relaxed volume known as Functional Residual Capacity (FRC). When MV is applied, the application of PEEP will produce extra recruitment or retain additional lung volume at the end of expiration. Hence, there is an extra volume of gas to be exchanged. This additional volume due to PEEP is known as Dynamic Functional Residual Capacity (dFRC) and is caused due to alveolar distension or additional recruitment maintained at the end of expiration above atmospheric pressure.

Most commonly, two basic modes of ventilation exist: 1) Volume Controlled Ventilation (VCV) and 2) Pressure Controlled Ventilation (PCV). Under PCV, the clinician directly sets PEEP and PIP, with the patients compliance (volume change per pressure change) determining the level of V_t. In contrast, if the clinician chooses VCV, then the PEEP and V_t are set, with the PIP being the result. Thus, depending on the mode of ventilation, the resulting PIP or V_t may be highly variable.

Ideally, MV should be applied for the least amount of time to prevent ventilator dependence and other complications. Hence, the ability to choose optimal ventilator settings and provide the best treatment is very important. Thus, the ideal MV therapy aims to combine maximum recruitment and oxygenation, while minimising the risk of VILI. In addition, it seeks to be as minimally invasive as possible (lower PEEP) without compromising these goals. However, with the absence of any standardised protocol in MV therapy or a readily available gold standard [Howman, 1999, Stather and Stewart, 2005], it is often difficult to achieve this optimal balance in real time, especially as the patient condition varies.

Numerous attempts to create standardised MV therapies have been trialled [Girard and Bernard, 2007, Ware and Matthay, 2000]. In all the studies, the primary focus was to control tidal volume [Brochard et al., 1998, Eichacker et al., 2002, Kallet et al., 2005, The ARDS Network, 2000] and PEEP [Amato et al., 1998, Brower et al., 2004, Rouby et al., 2002, Takeuchi et al., 2002]. In all the studies, no significant improvement in survival rates was observed with the respective protocols, and there is still no standard method in which to set ventilators.

The process of standardisation is difficult as the needs of the individual ICU patient can vary significantly by patient condition and over time. Because the condition of the lung is highly patient-specific and can also change with time, it means that a “one size fits all” protocol may not work. As a consequence, the absence of patient-specific protocols adoptive to these inter and intra-patient variability’s, mean that clinically chosen ventilation settings are still highly dependent on the clinician’s experience and intuition [Ferguson et al., 2005, Thompson et al., 2001].

1.2 LUNG PHYSIOLOGY

The human body requires a constant supply of oxygen to provide energy and sustenance. When oxygen is delivered to the body, the by-product of respiration is carbon dioxide (CO_2). Thus, the function of the lungs is to provide oxygen to the body, while simultaneously removing CO_2 and other waste gas products. The oxygen is delivered to the blood stream through lung alveoli via diffusion, while CO_2 is similarly removed in exchange.

The two primary objectives of the respiratory system are to provide bulk transport and treatment of air and to provide maximum surface area to allow sufficient gas exchange. However, before the lung can perform these functions, air must be drawn from the atmosphere into the body. By itself, the lung does not draw in air during inspiration. Rather, the process of inflation is determined by the movement of the diaphragm and the intercostal muscles of the ribs. During inspiration, the diaphragm moves down and the intercostal muscles move the ribs outwards and upwards, as shown in Figure 1.2. This movement causes a sudden increase in volume and results in a negative pressure gradient between the lung and the atmosphere. As a result, the air is drawn from the atmosphere into the lungs and allows for the pressure gradient to equilibrate, thus forming the process of inspiration.

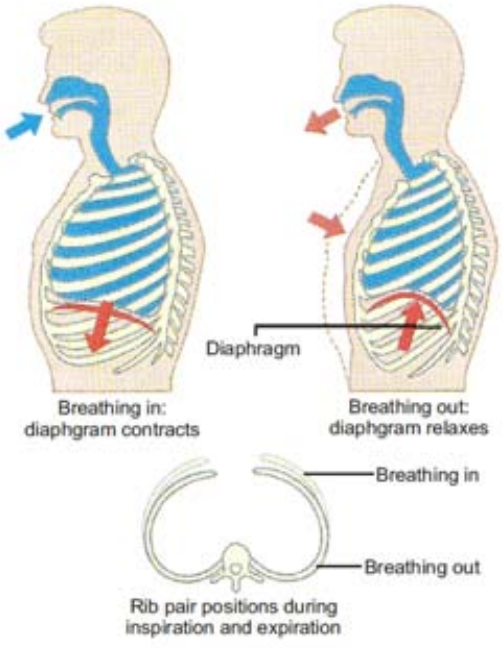

Figure 1.2 - Diaphragmatic movement during inspiration and expiration [Sebel et al., 1985]

In contrast, under normal breathing, the deflation process occurs due to the elastic recoil of tissues. At the end of inspiration, but prior to expiration, the intercostal muscles and diaphragm are under elastic deformation. When the pressure in the lung is at equilibrium with the atmosphere, the elastic recoil causes the muscles to relax. This forces all the air out of the lung and the lung resumes its original value. The outgoing air now contains the waste products of respiration, such as CO_2.

When inspired air enters the body, it enters through the nasal cavity or mouth, moves through the larynx and then into the trachea. The role of the upper respiratory system is to treat the incoming air by filtering, heating and humidifying the air. This filtering and treatment process ensures that the more delicate surfaces of the airways are not damaged and remain protected. Just above the heart, the trachea begins to bifurcate, with the airway diameter eventually decreasing and forming the bronchi. The bronchi then branch off to feed air to the respective sides of the lung. As the bronchi spread further into the lung, the airway diameter continues to decrease at each bifurcation, becoming steadily smaller, as shown in Figure 1.3. Eventually, the diameter ceases to decrease, while bifurcation continues, thus increasing the total surface area of the lung. Up till now, the primary function of these airways is to transport air and maintain humidity and temperature [Sebel et al., 1985, Martini, 2006].

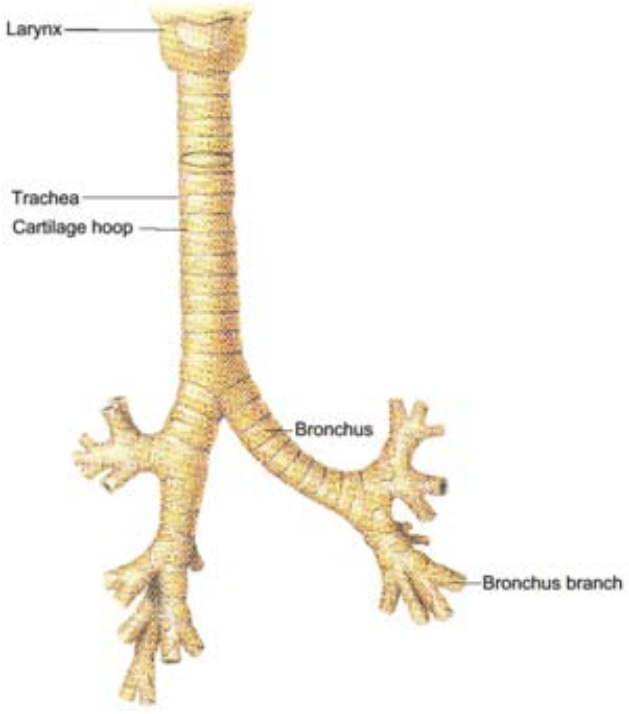

Figure 1.3 - Trachea and airway bifurcation into bronchial branch [Sebel et al., 1985]

Eventually, the cartilage lining supporting the bronchial branch begins to be replaced by alveoli, known as respiratory bronchioles. With each generation of airways, the number of bronchioles continues to increase. This change in lung structure marks the transition of the role of the lung from gas transport to gas exchange. The airway walls gradually become dominated with alveoli, thus increasing the total surface area available for gas exchange. As air continues to flow through the bronchial branch, it finally reaches the alveolar sac. The alveolar sac differs from the alveolar duct, as it represents an end to the bronchial branch and contains roughly half the total alveoli in the lung [Sebel et al., 1985].

The alveoli perform the second primary function of the lung, which is gas exchange. The number of total alveoli significantly varies depending on the individual's sex and the size of the lung [Ochs et al., 2004]. However, the average human has about 600 million alveoli with each approximately 200 μm in diameter [Seeley et al., 2003]. Each alveolus is surrounded by capillaries, which carry red blood cells, shown in Figure 1.4. The capillaries and the alveolus are separated by an epithelium of about 0.2 μm thick, which allows fast gas transfer between them [Vander et al., 2001]. The gas exchange between the alveoli and the capillaries occurs through diffusion, with oxygen moving from the alveoli to the capillaries and CO_2 moving in the opposite direction, as a result of a partial pressure gradient.

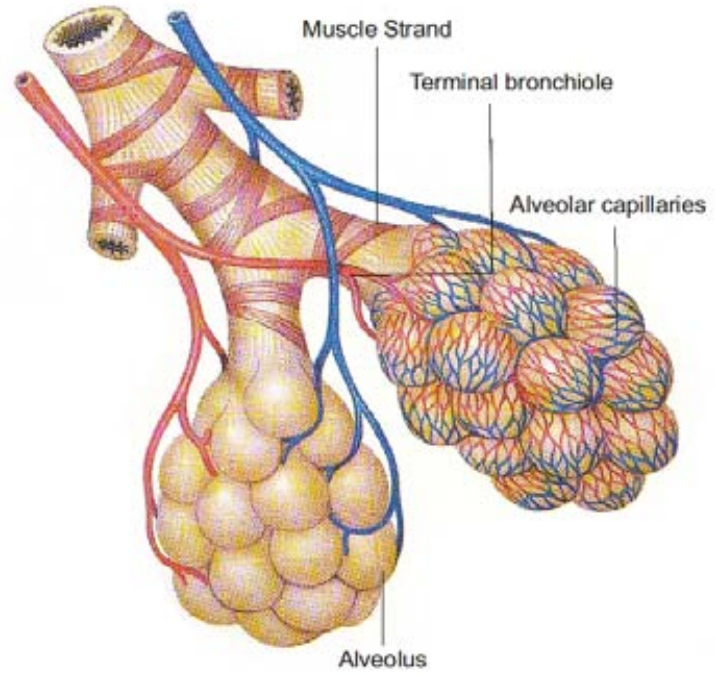

Figure 1.4 - Alveolar sac surrounded by capillaries. Difference in partial pressure of the gas causes gas exchange to occur [Sebel et al., 1985]

1.3 ARDS

Acute Respiratory Distress Syndrome (ARDS), is a severe form of Acute Lung Injury (ALI), and is a condition where the lung is inflamed and filled with fluid. As a result, the lung loses its ability to exchange gas effectively, resulting in oxygen deficient blood. In addition, the inflammation in the alveoli results in less surfactant being produced, which causes alveoli to collapse. This situation results in bronchioles and alveoli filling up with fluid or collapsing, preventing them from filling with air. Thus, alveoli are lost to the diseased state and the lung volume is decreased, resulting in the "baby lung" [Gattinoni and Pesenti, 2005].

A formal definition of ARDS was first defined in 1967 [Ashbaugh et al., 1967]. The study recognised that ARDS was a consequence of a wide variety of illness, which resulted in common symptoms among patients. Hence, it is a syndrome, rather than a specific infection or virus. Although the study highlighted the importance of positive pressure ventilation, there are still no specific criteria in treating ARDS patients. This deficiency is due to the fact that ARDS does not present any unique disease specific symptoms [Artigas et al., 1998, Rouby et al., 2000].

The additional fluid in the alveoli has the overall effect of making the lung stiffer. A stiffer lung requires a larger pressure gradient to inflate, which leads to an increase in the work of breathing required by the patient. Thus, the ARDS lung is characterised by being stiffer and smaller. It is thus, less effective at optimal gas exchange, requiring in these cases, mechanical support.

When gas exchange has been limited or impaired, the vital organs do not obtain the necessary oxygen, a condition known as hypoxemia. The onset of severe hypoxemia can be fatal for these vital organs, which cannot function without oxygen. In addition, when alveoli collapse, tidal ventilation from the collapsed region is transferred to other areas and causes an increase in local pressure. This increase in local pressure can restrict blood flow in the capillaries, a phenomenon known as shunt, and can make CO_2 elimination more difficult, further complicating the ventilation problem.

ARDS can be caused either directly or indirectly. Direct lung injury, such as smoke inhalation, near drowning or direct physical injury, can lead to the onset of ARDS. In

addition, ARDS can also be caused indirectly though sepsis, severe trauma to other body parts, or an inflammatory response to surgery.

Prior to the implementation of ICU's, patients with ARDS typically did not survive long enough for detailed investigations [Girard and Bernard, 2007]. ARDS incidence rates have been reported to range from 3 to 74 cases per 100,000 of total population per year from various parts of the world [Bersten et al., 2002, Luhr et al., 2000, Phua et al., 2009, Reynolds et al., 1998]. Mortality for those hospitalised in the ICU with moderate to severe ARDS, ranges from 22 to 66% [Ferguson et al., 2005, Esteban et al., 2002, Suchyta et al., 1997 , Zilberberg and Epstein, 1998]. With the advance of technology and increasingly better equipped ICU's, as well as the increased availability of positive pressure ventilators and trained staff, patients now survive much longer and in greater numbers [Baudouin, 1998, Hudson and Steinberg, 1999]. However, improvements in mortality rates have plateaued since 1994 with no further improvements in therapy [Phua et al., 2009].

1.4 VENTILATION & ARDS TREATMENT

Because no patient-specific or adaptive treatments exist for ARDS, the only option is for clinicians to provide an environment that ensures the patient can recover by themselves with time. Although clinical therapies such as anti-inflammatory and surfactant therapy exist, these approaches have been shown so far to be ineffective [Ware and Matthay, 2000]. Because ARDS increases the work of breathing, patients can find it difficult to spontaneously breathe, and most require additional support to assist them. MV therapy is therefore used to assist the patient and help minimise the work of breathing.

In essence, the ventilator is a precision pump that delivers a fixed amount of air to the lung through an ET tube or a face mask. The ventilator can either assist or replace the work of breathing depending on the clinically assessed requirements of the patient. In addition, it can be used to prevent alveolar collapse and/or prevent further alveolar damage, allowing the lung a better chance of recovery.

PEEP is therefore one of the most important settings in MV therapy. When PEEP is applied, the ventilator stops the airflow at a certain expiratory pressure. This restriction prevents the lung from deflating to the low FRC's that ARDS patients can exhibit. In particular, this additional pressure is important for ARDS patients, because without it,

ARDS affected alveoli are highly susceptible to collapsing due to fluid build up and inflammation. When alveoli collapse, the pressure required to open them up is higher than before. Thus, collapse increases the stiffness of the lung increasing damage to alveoli and thus, effectively reducing the compliance. PEEP prevents or minimises this impairment, maintaining the FRC at the end of expiration at a healthier level and thus preserving recruitment.

Tidal volume is the second major parameter setting in MV therapy. It determines the volume of air delivered to the lung per breath and is typically determined by the patient's condition. If tidal volume is set too high, it can over inflate the lung and cause VILI [Carney et al., 2005, Dreyfuss and Saumon, 1998, Moloney and Griffiths, 2004, Pavone et al., 2007, Ricard et al., 2003]. If tidal volume is too low, then this can result in inadequate oxygenation and atelectasis [Hauber et al., 2010].

If the ventilator is operating under pressure controlled mode, the PEEP and PIP are set, with the air flow the resulting parameter. In contrast, if volume controlled mode is used, PEEP and tidal volume are set, with the pressure increasing as a result. In both cases, the inspiration phase is actively controlled by the ventilator, which then typically allows passive deflation to PEEP as controlled by the lung's own elastic recoil and compliance.

1.5 THE QUEST FOR GOLD

The use of a gold standard method of ventilation is the ultimate clinical goal, but it is often difficult to determine the optimal parameters. In normal conditions, V_t provides maximum gas exchange for minimum breathing effort [Otis et al., 1950]. However, for the ARDS lung, which is both stiffer and smaller in volume, normal amounts of V_t may be too high and lead to over-inflation and induce further injury. Finally, there is no standard measurement or assessment that defines an optimal state, which could be assessed or targeted.

1.5.1 TIDAL VOLUME

The application of tidal volume also implies that there is a level of strain occurring or being induced within the lung. Lung strain over the entire organ can be defined as the ratio of V_t /FRC [Chiumello et al., 2008]. Thus, for patients with severe ARDS, who have lower

FRC due to alveolar collapse, the lung stress and strain may be higher compared to healthier patients who have more healthy alveoli units available. Therefore, having a larger tidal volume, which results in a higher strain, may result in added risk of VILI for the ARDS patient [Ricard et al., 2003].

Because the ARDS lung is described to be heterogeneously distributed [Rouby et al., 2002, Gattinoni et al., 2001], some regions of lung are affected more than others. This strain distribution is particularly important for ARDS patients where the damaged alveoli are surrounded by healthy alveoli and local strains may vary. Thus, the use of low tidal volume has been investigated as an optimisation parameter to provide safe, so called lung protective, MV strategies.

Early interest in low tidal volume ventilation was spurred by Hickling and colleagues in an observational study [Hickling, 1998]. Animal studies also showed that large tidal volumes resulted in the development of ALI characteristics [Dreyfuss et al., 1985, Gajic et al., 2004]. The results of animal trials provided researchers with the justification that low tidal volumes would be beneficial to patients, and in the late 1990's four controlled trials were conducted to evaluate the effect of low versus high tidal volumes [Brochard et al., 1998, Amato et al., 1998, Stewart et al., 1998, Brower et al., 1999].

Out of these four studies, only Amato et al showed a significant decrease in outcome mortality using lower tidal volumes. The remaining three studies by [Brochard et al., 1998, Stewart et al., 1998, Brower et al., 1999] showed minimal and statistically insignificant differences in mortality between patients on low and high tidal volumes. However, a later randomised trial [Parsons et al., 2005] showed that low V_t reduced the inflammatory response, which are associated with mortality in ARDS and VILI.

To conclusively determine the effect of low tidal volume ventilation, a study was conducted by the ARDS Network on 861 patients in 2000 [The ARDS Network, 2000]. This study showed that patients with lower tidal volumes (6.2 ± 0.8 ml/kg) had a higher number of days free of mechanical ventilation and lower mortality rates than those with higher tidal volumes (11.8 ± 0.8 ml/kg). The result of this study has significantly improved ARDS therapy and provided a means of advancing patient management by choosing the appropriate tidal volume. However, these results and conclusions have also been criticised due to the impractically high tidal volume used (12 ml/kg, compared to normal practice of

8-10 ml/kg) during the trials for comparison [Eichacker et al., 2002] and for ignoring some negative aspects of low V_t [Kacmarek, 2005] , suggesting that the result was skewed.

However, with all these studies regarding the optimal tidal volume, the tidal volume was fixed for a given patient during the course of the MV therapy. Therefore, this methodology does not consider the lung strain, as strain is a function of lung size, time, and the patient-specific state of ARDS as it evolves [Jia et al., 2008, Johnston et al., 2003, Manzano et al., 2005]. Nor does it consider evolution of therapy as the condition evolves. Finally, it does not consider or account for variability in the individual patient response to therapy. Thus, to properly optimise the lung strain, an ideal tidal volume must regularly be re-evaluated based on patient-specific condition and response with a goal of minimising lung strain induced by V_t.

Although the debate of high vs low tidal volume continues, the use of low tidal volumes of 300 – 500 ml is becoming widely accepted and common place among ICU's. However, the second major setting, PEEP, is still widely debated. In particular, the level of PEEP required, regardless of tidal volume, is not standardised at all and requires further investigation.

1.5.2 PEEP

PEEP represents the pressure that the lung experiences during the end of expiration and is also set by the clinician. The objective of applying PEEP is to increase the level of oxygenation by increasing the number of recruited alveoli. This is achieved by lifting the lung pressure at the end of expiration so that alveoli remain open. This retention also reduces damage to alveoli due to repetitive opening and collapse during subsequent breaths.

The application of PEEP throughout the respiratory cycle has been shown to greatly improve oxygenation in patients with ARDS, as shown in early animal and human models [Hickling, 1998]. As a result, the outcomes of these early studies have led to the widespread use of PEEP in MV therapy. However, the appropriate level of PEEP over a given cohort has never been properly established, despite a very large amount of research in the area [Levy, 2002].

PEEP comes with tradeoffs and risks to a heterogeneous, injured lung. Too much PEEP risks injuring healthy lung units. In contrast, not enough PEEP results in continuous recruitment and de-recruitment of ARDS affected alveoli, which is also harmful [Brochard et al., 1998]. Thus, PEEP also has a risk of VILI, and an optimal value balances these risks.

Several trials have been conducted to evaluate the benefit of high PEEP in the treatment of ARDS. Higher PEEP would, it was hypothesised, maintain recruitment of these units preventing repetitive collapse. Amato et al showed that patients with high PEEP had significantly lower mortality [Amato et al., 1998]. Villar et al showed similar results for high PEEP [Villar et al., 2006]. However, others have shown that increased PEEP results in increased systemic inflammatory response [Miranda et al., 2005, Ranieri et al., 1999]. The problem with these studies was that the lower mortality rate could either be attributed to high PEEP or low tidal volume because of the trade-off between these two variables in setting MV [Jonson and Uttman, 2007]. No study has controlled both variables to date, nor accounted for their potential to vary patient-specifically, both in general and over time.

A study by the ARDS Network was conducted to determine the effect on mortality solely attributed to PEEP [Brower et al., 2004], by using only low tidal volumes. The study used low tidal volumes (6 ml/kg) and concluded that high PEEP increases oxygenation. However, there was no significant difference in mortality rates or length of MV. Thus, the result of this and other studies [Amato et al., 1998, Villar et al., 2006], provide no conclusive evidence on a set level of PEEP to be used to optimise recruitment across heterogeneous ICU cohorts.

Although higher PEEP can improve oxygenation, the risk of alveoli over-inflation is also increased at high PEEP for healthy alveoli in particular [Ricard et al., 2003]. Thus, using the highest PEEP possible is not the best solution for optimum ventilation therapy as it may cause more harm than good and contribute to VILI. However, if the PEEP is too low, then injury is induced by the repetitive opening and closing of alveoli units [Pavone et al., 2007, Schiller et al., 2003]. Therefore, the predicament lies in choosing an optimal value of PEEP by maximising recruitment and minimising additional damage to the lung and understanding that it might change or evolve over the time course of the disease.

1.6 PROBLEM SUMMARY

The major problem in MV lies in the lack of standard clinical protocols for treating patients with ARDS. Because ARDS implies a heterogeneous distribution of healthy and damaged alveoli, and can significantly change over time, a new patient-specific method of choosing PEEP is required. Currently, the clinical methodology is to use a low tidal volume and then to choose an appropriate PEEP based on the patient's condition, as assessed by the clinician. However, an optimal solution would be to choose initial parameters that would then vary over clinically relevant timeframes to continually optimise the therapy for each patient. This approach would thus account for heterogeneity of the disease and variability in response by patients.

To achieve this goal, patient-specific models need to be developed that can incorporate the various MV metrics. The specific objective of a model-based approach is to allow rapid patient-specific parameter identification and thus enable ready optimisation of MV with respect to the risk of VILI or lung injury and lung strain. This approach could thus potentially reduce the length of MV by providing more optimised care. Patient-specific model parameter identification and the resulting patient-specific models would, as a result, also enable model-based methods of monitoring disease progress and response to therapy.

This goal can be achieved by a mixture of engineering and physiological principles, which can be utilised to develop mathematical models that describe patient condition and allow optimal MV metric selection. In particular, a model that captures patient-specific recruitment and lung strain, relative to clinically available measurements, can provide weight into otherwise un-measureable metrics of lung status. Thus, such a model would capture what would otherwise be available only via computed tomography scans or other invasive measurements. In simpler terms, it would convert clinical pressure volume measurements into a physiological picture of patient-specific condition to aid clinical decision making.

The first goal of this thesis is to introduce a model of lung mechanics that captures the characteristics of the mechanically ventilated lung. The model, based on simplified physiology and lung mechanics has the capability of identifying patient-specific response to PEEP without invasive measurements. The model uses clinically obtainable pressure volume (PV) curves and estimates the recruitability of the lung for a given patient. In

addition, a second model is introduced, which looks at the changes in lung volume due to PEEP depending on lung stress and strain and estimates how responsive the lung is to pressure changes.

The second goal is to clinically validate these models, and, as a result, be able to determine the optimal patient-specific PEEP level for each patient. The validation process will consist of data acquisition, data processing and analysis, with the results being presented in a clear and clinically interpretable way. The criteria for such a validation is that the model should be readily adoptable without any costly pieces of added equipment and should be measurable in real time.

1.7 PREFACE

Chapter 2 of this thesis presents the background and basic theory of lung mechanics that the model will use. In addition, the chapter also introduces the concept of model-based approaches to managing ventilation therapy, and discusses various model-based approaches that have been developed. This discussion leads to the premise of this thesis; the development and application of a model-based method to optimise PEEP selection in the mechanically ventilated patient.

Chapters 3 and 4 introduce the models used in this thesis. Chapter 3 focuses on a model of lung mechanics and recruitment, as well as some initial validation performed. Chapter 4 introduces a model to estimate dFRC using lung stress and strain as a proxy as well as an initial validation.

Chapters 5, 6 and 7, analyse the results of full scale clinical trials used in this thesis. In particular, Chapter 5 discusses how the study was designed, and the ethics application and approval process. Chapter 6 presents the results of these trials and discusses the clinical implications of the recruitment model, and Chapter 7 further validates the lung stress strain model.

Chapter 8 introduces a third model, which begins to make a link between the pulmonary system and the cardiovascular system. The model provides a proof of concept approach to combine the theory of gas exchange and recruitment to evaluate changes in cardiac output.

Chapter 9 and 10 present the conclusions derived from this research then focus on the work that is needed to continue this research and look at what the future holds for ventilation therapy.

Chapter 2 - Lung Mechanics and Models

The heterogeneous nature of the ARDS lung makes patient treatment difficult, as each patient can exhibit significant heterogeneity in the distribution of ARDS affected units and in the response to changes in MV parameters. A given MV setting for one patient may not produce the same effect for another similar patient. This heterogeneity implies that a more patient-specific treatment methodology is required to better optimise patient care. In particular, what is needed is an approach that can be clinically implemented in real time, while simultaneously providing relevant information on the condition of the lung and how to treat it.

The idea of using model-based approaches to solve this problem provides a new methodological approach that combines engineering and medical principles. Model-based approaches can provide clinicians with rapid diagnostic capabilities, while simultaneously allowing a patient-specific treatment therapy to be delivered. In particular, model-based therapies use mathematical principles to model a given patient's physiological system, and outputs clinically relevant parameters to guide diagnosis and therapy selection. This overall model-based therapeutic method has been validated in other physiological systems related to critical care [Chase et al., 2008, Hann et al., 2010].

This chapter introduces a modern theory of lung mechanics on which the models used in this research is based. It then shows how ventilation settings can be selected based on current and prior theories of lung mechanics. In addition, the chapter also looks at past and present attempts to use model-based approaches in MV and how these prior works differ from the model presented in this thesis.

2.1 LUNG MECHANICS

Traditionally, the expansion of the lung was thought to be due to the isotropic balloon-like expansion of alveoli units. This expansion was often interpreted using a measured static or dynamic PV curve based on the lower inflection point (LIP) and upper inflection point (UIP). The LIP was thought to be a single point where massive, simultaneous recruitment of alveoli occurred, which was then followed by balloon-like expansion of all these alveoli.

This process is analogous to a balloon, which requires an initially high pressure to overcome elastic forces before it suddenly starts to expand. In contrast, the UIP represented the point where alveoli begin to overstretch and in effect begin to plastically deform, resulting in a sudden decrease in compliance.

However, this theory does not correspond well to clinical observations [Schiller et al., 2003, Hickling, 2002]. Rather, it is the recruitment and de-recruitment phenomenon that is now thought to contribute to the hysteresis observed in PV curves [Cheng et al., 1995]. Furthermore, research has observed that recruitment is continuous and occurs throughout the inspiratory PV curve and especially between the LIP and UIP [Albaiceta et al., 2004, Jonson et al., 1999, Maggiore et al., 2001, Mergoni et al., 2001].

These early ideas failed to hold because, for example, if the LIP was a point of massive recruitment, and PEEP was set above the LIP, clinicians should then have observed minimum hysteresis. In addition, both inflation and deflation PV curves should then overlap. However, this behaviour does not occur [Bersten, 1998]. Furthermore, if LIP indicated a point of massive recruitment, then further alveolar recruitment cannot occur at pressures above LIP. However, clinical data has shown that as PEEP increases, volume can increase for a given pressure [Hickling, 2002, Bersten, 1998], thus indicating that significant additional recruitment occurs above LIP.

2.1.1 RECRUITMENT & DE-RECRUITMENT

Thus, the current school of thought suggests that recruitment and de-recruitment greatly influence and define the shape of the PV curve. In particular, once healthy alveoli have been recruited, they undergo minimal isotropic expansion [Schiller et al., 2003]. This result leads directly to the conclusion that balloon-like expansion is not the correct mechanism of lung volume change.

When lung volumes at a given pressure are compared under zero end expiratory pressure (ZEEP) and PEEP conditions, there is an increase in volume as PEEP is increased [Jonson and Svantesson, 1999]. This increase is evident even when PEEP is set above the LIP and indicates that significant recruitment still occurs above the LIP. This result was directly confirmed, as above the LIP, studies have observed recruitment using computed tomography (CT) scans [Albaiceta et al., 2004, Gattinoni et al., 2001].

Other studies have looked at the energy required to recruit collapsed alveoli [Cheng et al., 1995]. Cheng et al used excised rat lungs and progressively increased the end inspiratory pressure, while simultaneously decreasing the end expiratory pressure. The study showed that additional energy was required to recruit alveoli. However, once recruited, less energy was required to keep them inflated. The study thus concluded that recruitment and de-recruitment are strongly dependent on end expiratory pressure.

Studies have correlated the continuous alveoli recruitment along the inspiratory PV curve limb with CT scans. Crotti et al [Crotti et al., 2001] proved that recruitment occurred throughout the inflation limb continuously and correlated well with the traditional super syringe PV curve. Hence, this study, and others [Pelosi et al., 2001], found no correlation between recruitment and the PV curve inflection points.

At the alveolar level, in vivo microscopy studies have captured alveolar dynamics. These studies have shown that once recruited, there is no significant increase in alveolar volume for healthy and some ARDS affected alveoli [Schiller et al., 2003, Carney et al., 1999]. In particular, the studies highlight that recruitment and de-recruitment, as opposed to balloon-like expansion, are the primary causes of volume change. Because normal, healthy alveoli are effectively open [Halter et al., 2003], recruitment is only observed with damaged alveoli. Thus, recruitment and de-recruitment are much more relevant in MV therapy when treating ARDS.

All of these studies examined recruitment at both the micro and macro levels and via different approaches. All of them lead to the conclusion that recruitment and de-recruitment occur continuously throughout the breathing cycle. In addition, once alveoli are recruited, the unit volume does not change significantly. Thus, volume change seen in the lungs during MV is not due to balloon-like expansion, but, predominantly, due to recruitment and de-recruitment. Therefore, managing and optimising PV curves in mechanically ventilated patients directly concerns the management of recruitment and de-recruitment of lung units.

2.1.2 PRESSURE DISTRIBUTIONS

The pressure at which an alveoli will recruit is known as the Threshold Opening Pressure (TOP). Similarly, it de-recruits at a Threshold Closing Pressure (TCP). Because

recruitment and de-recruitment is a continuous process, the TOP and TCP can take on a range of values over an entire ARDS lung. The shape of the distribution reflects the patient condition with respect to ARDS or lung damage, and thus reflects physical characteristics such as oedema, inflammation, ARDS and others.

The shapes of these pressure distributions have been studied extensively [Crotti et al., 2001, Pelosi et al., 2001]. An experiment using dog models concluded that the TOP and TCP were normally distributed and are affected by physical factors, such as superimposed pressures [Pelosi et al., 2001]. Similarly, another study looked at the difference in TOP and TCP distributions [Crotti et al., 2001]. This study also verified that TOP and TCP were normally distributed. Further, it found that the TOP distribution was higher in pressure than the TCP distribution, indicating more energy was required to recruit alveoli than to retain them. Thus, it reflected the results of other studies previously discussed [Cheng et al., 1995].

The TOP and TCP distributions can give an indication of the severity of the disease state and patient condition. Because ARDS results in alveoli being inflamed, filled with fluid or collapsed completely, the pressures required for recruitment are much higher as compared to healthy patients. In addition, because ARDS is heterogeneously distributed in the lungs, the distribution of TOP and TCP pressures is also much broader than in healthy lungs. Thus, the severity of ARDS can be quantified by the shape of the pressure distributions and their breadth in particular.

Because alveolar recruitment occurs continuously, the problem lies in determining what level of PEEP produces the maximum level of recruitment while retraining the greatest number of alveoli at the end of expiration. The recruitment and de-recruitment theory puts to rest the concept of titrating PEEP based on the LIP and UIP. Hence, a new method of selecting PEEP must be developed to capture and optimise patient-specific responses to ventilation therapy.

2.2 CLINICAL SELECTION OF PEEP

Choosing an appropriate level of PEEP is dependent on the clinical objective of MV therapy. Depending on the patient's condition, the objective is a combination of maximising recruitment and gas exchange, while minimising lung stress. If the goal was to

only maximise gas exchange at a given moment, then a very high PEEP would be appropriate. However, if lung stress and over-inflation are to be minimised, then a lower PEEP is more appropriate. Thus, the problem is defined as achieving a balance between these criteria with respect to the PEEP selected, and then optimising this trade-off as the patient-specific disease state evolves.

Several studies have evaluated the relationship between PEEP and lung stress. One primary conclusion is that the stress index is a good indicator on which to titrate PEEP [Grasso et al., 2004, Grasso et al., 2007]. The stress index describes the shape of the pressure time curve and describes how the rate of change of pressure reflects changes in lung elastance. In these studies, PEEP titration was performed for each patient based on the value of the stress index. The main objective was to minimise damage to alveoli and mitigate the risk of VILI from excessive lung stress. However, the stress index is only used when a constant flow waveform is used.

However, PEEP has also been selected focusing on the potential for lung recruitment [Barbas et al., 2005, De Michele and Grasso, 2006, Gattinoni et al., 2006]. These studies highlighted the effect on recruitment as a function of PEEP. A major conclusion of these studies is that the amount of potentially recruitable lung is strongly linked with the patient-specific volume recruitment response to PEEP [Gattinoni and Pesenti, 2005]. In particular, if a patient was highly responsive to PEEP, then the patient is more likely to have additional lung to recruit. Because of this strong correlation, clinicians try to choose PEEP based on how much potentially recruitable lung is available. However, this approach may not always be the most appropriate method, as it does not directly allow for minimising lung hyperinflation. In addition, determining the amount potentially recruitable lung is not practical in the ICU.

2.2.1 COMPUTED TOMOGRAPHY

The use of CT scans has provided researchers with a gold standard on measuring PEEP induced lung recruitment with ARDS [Rouby et al., 2003, Gattinoni et al., 2001, Albaiceta et al., 2004]. In these studies, a full lung spiral CT is obtained at both a fixed PEEP and at ZEEP. Comparison and image processing thus directly define the volume of recruited lung.

The CT scan method utilises the attenuation of individual pixels of the scan to determine if the alveoli are recruited, de-recruited or overinflated. This status is evaluated by assigning each pixel within the CT scan a Hounsfield unit (HU) attenuation value. The HU measures the radiodensity of the concerned medium and describes the level of x-ray radiation that passes through completely (ie – Air HU = -1000) or is completely absorbed (ie – Bone HU = 400). To measure the level of recruitment, a recruited lung unit is assigned a range between [900, -500] HU, a hyperinflated lung between [-1000, -900] HU, poorly aerated lung is between [-500, -100] HU, and non recruited lung is between [-100, 100] HU [Rouby et al., 2003]. Thus, a visual interpretation of the recruitment behaviour is presented for a given PEEP level.

Because the CT method distinguishes between overinflated and recruited units, the method also provides a tool to predict a more optimum PEEP to mitigate VILI or lung damage at any given time. By choosing the PEEP where the level of overinflated, and thus potentially damaged lung units is minimal compared to recruitment, clinicians can choose an appropriate setting for individual patients that recruit lung and minimises over-inflation damage and maximising the efficacy of the therapy. Hence, if clinically practicable, one could define, at a given time in the patient's stay and evolution, a relationship between recruitment and over-inflation versus PEEP. This trade-off curve could then be optimised as clinically desired.

However, CT methods have obvious clinical limitations that reduce the viability of this method in regular, everyday clinical use. First, CT scanning requires the patient to be transported from the ICU to a radiology unit, which has several attendant risks. In particular, many MV patients are less effectively ventilated in the CT scanner due to the extension tubing required to reach the mask, potentially skewing results. Second, the CT scanner provides additional radiation doses that might otherwise be avoided in normal care, which is generally avoided where possible [Brenner and Hall, 2007, Tubiana et al., 2008]. Finally, CT scans are time consuming, costly and heavily dependent on other clinical resources or demand for radiological service, potentially reducing access for patients who urgently need scans.

Hence, although CT scans provide exact and valuable information, it is not clinically practical or viable, and is thus limited to use as a research tool. In particular, it is not a bedside tool by any means. This last point clearly illustrates the need to have a simpler

approach to minimise clinical burden and cost that can be located with the ventilator at the bedside.

2.2.2 PRESSURE VOLUME CURVES

The static pressure volume (SPV) curve provides a bedside method of obtaining an appropriate PEEP level. The SPV curve is generally measured by three different methods [Harris, 2005]:

- The super syringe technique,
- The constant flow method,
- The multiple occlusion method.

SPV curves measure the steady state lung volume above the FRC for a given PEEP and pressure in patients with ARDS on MV [Lichtwarck-Aschoff et al., 2000, Lu and Rouby, 2000]. SPV curves are obtained at a rate slower than a breath so no hysteresis is observed from ZEEP to maximum pressure. These curves can be obtained directly from some ventilators [Harris, 2005] or from sensors on the mask or tracheal end of the ET tube. SPV curves provide a diagnostic tool that has been extensively used in the treatment and management of patients with ARDS [Albaiceta et al., 2003, Fernández et al., 1990, Servillo et al., 2000], and directly avoids the issues associated with using CT.

A SPV curve resembles a sigmoidal curve with no hysteresis, and is distinctly unique for each patient. The SPV is generally characterised by an UIP and LIP. Examining Figure 2.1, it is clear that along the SPV curve, compliance (slope of the curve) varies significantly. The physiological explanations of the UIP and LIP have been thoroughly studied [Jonson and Svantesson, 1999, Albaiceta et al., 2003, Maggiore et al., 2003] as previously discussed, which has led to better understanding of alveoli recruitment behaviour as a function of PEEP.

Although the conventional theory of lung mechanics, using balloon-like expansion, suggested that PEEP be set slightly above the LIP, this was not appropriate as recruitment is a continuous process and occurs above the LIP. Using the SPV as a tool for PEEP titration meant that clinicians selected PEEP, such that it was above the LIP, but below the UIP to prevent over-inflation within the linear portion of the curve. Hence, the LIP & UIP

were still used as markers for guiding therapy with SPV curves [Maggiore et al., 2003, Mergoni et al., 2001, Pelosi et al., 2001].

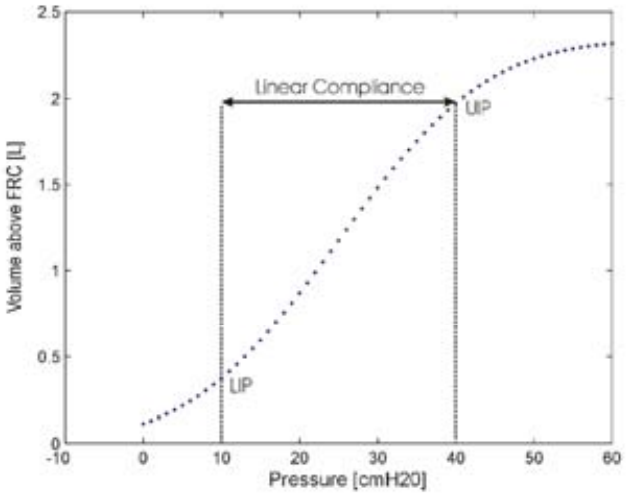

Figure 2.1 - Static Pressure Volume Curve showing LIP and UIP

However, continued investigation into the use of these inflection points to determine or optimise PEEP yielded two distinct problems. First, PEEP is applied primarily to prevent de-recruitment, as much as, to allow recruitment [Maggiore et al., 2001, Lu et al., 2006]. Thus, using the LIP to determine a minimum PEEP may not yield the best method [Hickling, 2002]. Second, although PEEP should be set between the LIP and UIP, the linear portion of the curve offers a very large range of PEEP values. Hence, this approach with SPV curves still does not offer one unique setting, even though it clearly characterises these inflection points.

Thus, the use of inflection points as anything more than a guide has been generally discredited [Hickling, 1998, Mergoni et al., 2001]. In particular, current understanding views the ARDS lung as:

- Heterogeneous in lung units and types (normal or ARDS affected)
- Heterogeneous in the effect of ARDS on any given alveoli or lung unit
- Heterogeneous in response to PEEP, with respect to the pressure (above PEEP) required to open or recruit the alveoli.

However, equally importantly, no other methods or approach has risen to replace the use of such SPV curve points.

One final problem with all these methods based on SPV curves is that the patient is temporarily disconnected from the ventilator [Lu and Rouby, 2000]. Although it is possible to measure SPV curves without disconnection, only certain ventilators have the functions required to measure this curve directly [Macnaughton, 2006, Piacentini et al., 2009]. It also takes a fixed amount of time (10 to 15 minutes) if done via a super syringe, which may not be available for clinical staff and requires specialised training to implement. Because not all hospitals will necessarily have these advanced ventilators, and the super syringe approach can be time consuming, intensive and problematic, the SPV curve is not an ideal method for regular monitoring of patient status and resulting PEEP selection.

Thus, the problem still lies in determining PEEP while addressing alveolar heterogeneity. More generally, for any type of lung unit, a given pressure may not recruit a certain alveoli, whereas at a higher PEEP it may be recruited at the same pressure [Hickling, 1998, Mergoni et al., 2001]. As a result, the problem can thus be defined by noting:

- Recruitment and de-recruitment can occur at any pressure, regardless of PEEP, and is continuous over the PV curve
- PEEP and pressure values that recruit some alveoli may equally overstretch normal alveoli creating a trade-off between recruitment and over distension/ damage, as noted earlier.

Therefore, the MV PEEP setting optimisation problem becomes one of needing to know or estimate two primary values:

- Recruitment status of the MV lung at a given PEEP
- Potential recruitment or volume change expected from a change in PEEP, which include changes in the volume of alveoli retained at the end of expiration, as well as new alveoli retained during inspiration.

Because these values would preferably be known before making that change, it would be therefore ideal to create patient-specific lung mechanics models that can capture and predict these changes. In particular, the ability to safely and accurately estimate the potential volume change in recruitment by changing PEEP before making the change could

allow this setting to be best optimised with minimal risk. Finally, these values should be available at the bedside and preferably with no interruption to the MV therapy, requiring then to be identified from measurements that are already available at the bedside and preferably automated.

2.3 MODEL-BASED APPROACHES

Because no ideal method exists to easily, effectively or accurately manage the problem of PEEP selection, researchers have been motivated to seek alternative methods. The overall goal is to determine the appropriate PEEP level in patients without the complications or other issues associated with the SPV curve or CT scans. By doing this task, clinicians can thus measure recruitment and de-recruitment in an optimal, patient-specific fashion.

To minimise clinical burden and cost, an optimal solution would introduce no significant new hardware or systems nor require excessive cost, clinical time or effort. Thus, some researchers have strived to develop mathematical models to help aid clinical decision making. Models can be used to turn readily available data, such as PV curves, from strings of data or plots, into a clear physiological picture required to enable clinicians to readily monitor and guide therapy.

Models of lung mechanics can be categorised into finite element models or lumped parameter models. Each type has distinct advantages and limitations. Finite element (FE) models of pulmonary recruitment and/or gas flow offer significant understanding of the underlying physiology and offer detailed resolution of complex systems [Burrowes et al., 2005, Swan et al., 2008, Tawhai et al., 2004]. FE models also offer the advantage of allowing a patient-specific solution as each model can represent a unique geometry for a given patient. However, the main barrier for FE models as a clinical tool is the cost associated with computational power and length of time to run a simulation. In addition, a patient-specific geometry would require a CT scan with additional costs and risk. Finally, identifying recruitment status with a model of such high resolution would be problematic and computationally very expensive. Thus, although FE models are very well suited to helping understand the underlying physiology, they are limited to being a research tool and do not provide a suitable bedside method for modelling patient-specific lung mechanics.

Although very simple models based on this approach would not necessarily be precluded, they have not been tried to date.

2.3.1 LUMPED PARAMETER MODELS

In contrast, lumped parameter models offer a simple and relatively inexpensive method of assessing lung mechanics and/or gas exchange, and thus for capturing essential dynamics. Lumped parameter models do not necessarily require excessive computational power. Hence, they can be utilised directly at the bedside in clinically realistic time frames.

A significant limitation of these types of models is the lack of physiological detail compared, for example, with FE models. Lumped parameter models can be made to be more physiologically complex, but the direct clinical benefit of the complex model must be compared with the computational power and costs associated with this added complexity. In contrast, such lumped parameter models represent the same external "view" the clinician has, and are thus defined in terms of readily available measurements.

Lumped parameter models, used for MV or similar therapeutic situations, can be broadly classed into gas exchange models and recruitment models. Both types of models can be used to assist in ventilation support and are used to model the effects of PEEP. Gas exchange models are used to study the effect on gas exchange in the airways and alveoli. In use, gas exchange models tend to be based on the perspective that MV therapy is about maximising gas exchange, matching the fundamental physiological and clinical goal of providing MV support. In contrast, recruitment models take a more mechanical view and are typically used to evaluate the effect on alveoli recruitment. Hence, these models take on a perspective that recruitment drives gas exchange or is proportional to it, turning the physiological and clinical problem into one of recruitment.

GAS EXCHANGE MODELS

Gas exchange models are used in conjunction with MV to determine how various parameters affect the oxygenation status of the blood. Ranging through different mathematical complexities, gas exchange models offer detailed descriptions of the diffusion process of oxygen using principles of mass balance. Ben-Tal reviewed these models extensively noting up to three different types of gas models [Ben-Tal, 2006]. Though not directly related to recruitment, the models respond to PEEP changes by

evaluating the impact of diffusion and gas exchange based on changes in recruitment and alveolar pressure status. Thus, they can give a broad indication of recruitment status. The use of clinical gas exchange models has been developed, but they often provide different model outputs for use in patients with different clinical goals and prognosis [Goode, 2003, Kwok, 2003, Rees et al., 2002].

The ALPE model (preceded by the INVENT system [Rees et al., 1999]) uses clinical measurements available in the ICU to help determine parameters, such as ventilation perfusion mismatch and pulmonary shunt [Rees et al., 2002, Rees et al., 1999, Rees et al., 2001]. Although the model uses clinical measurements from the ventilator, such as PEEP, and inspiratory and expiratory ratios, it does not determine the effect of MV on recruitment. In addition, the models were tested on patients with Chronic Obstructive Pulmonary Disease (COPD) or cardiac injuries, where gas exchange in the primary goal. Thus, it did not specifically target ARDS patients where recruitment is the primary clinical goal. However, the ALPE system provides a quick and easy estimate of gas exchange impairments, which could be used to optimise ventilation parameters.

Another method used to evaluate gas exchange parameters is the SOPAVENT model [Kwok, 2003, Goode, 2003, Wang et al., 2010]. The SOPAVENT model uses the concept of fuzzy logic to evaluate blood gas parameters and the estimation of pulmonary shunt fractions. The original SOPAVENT model provided an invasive means to estimate steady state blood gas predictions using ventilator inputs and was then further developed to incorporate other parameters, such as pulmonary shunt [Kwok, 2003, Goode, 2003]. However, the original models required an invasive measurement of oxygen consumption and cardiac output and also proved to be computationally expensive [Wang et al., 2010]. More recently, the SOPAVENT models have been further developed to provide a continuous real-time non-invasive prediction of blood gas parameters, which has been validated in the ICU setting [Wang et al., 2010].

Gas exchange models provide a useful clinical diagnostic to aid clinicians to set ventilation parameters. By examining how successfully gas is exchanged in the lungs, the models provide a tool for clinicians to then choose additional ventilation settings. However, these models fail to address the mechanism of recruitment, which is common in patients with damaged lungs. Thus, patients who have ARDS may experience improved gas exchange, but may still have plenty of additional recruitment available, which, as noted earlier, is not

ideal [Gattinoni and Pesenti, 2005]. Therefore, models of alveolar recruitment are also required to help optimise ventilation, particularly in ARDS where recruitment is crucial [Gattinoni et al., 2006].

RECRUITMENT MODELS

Mathematical models of lung mechanics have driven new areas of research in the hope of being able to choose the most appropriate PEEP setting for patients. Although gas exchange models provide a means of finding optimal gas exchange with respect to a given PEEP, this approach may not result in increasing alveolar recruitment which is the end objective when treating ARDS patients [Ranieri et al., 1991]. In addition, gas exchange models do not indicate the potential for recruitment, which is currently the primary clinical goal [Gattinoni et al., 2006], and gas exchange is thus presumed to proportionally follow recruitment.

Models of lung mechanics have been developed with the aim of studying the recruitment behaviour of alveoli. A mathematical model developed by Hickling aimed to simulate and understand the shape of the PV curve in an ARDS lung [Hickling, 1998]. The model confirmed that recruitment occurs above the LIP, and that the fundamental shape of the PV curve changes with recruitment. Although this paper did not adequately predict the volume change resulting from a change in PEEP, it provided information on the effect of the recruitment behaviour on the static PV curve. Although Hickling's model readily predicts the static PV curve during a recruitment manoeuvre, it has only been used as a research tool to date.

One of the earliest contributions to mathematically model the PV curve, and thus recruitment in general, was the Venegas equation [Venegas et al., 1998] which modelled the PV curve as a sigmoid function. This equation allows the SPV to be obtained based on geometric properties of the curve, while still maintaining good physiological accuracy as defined by its ability to capture vital capacity, maximal inspiratory volume, compliance at different inflation pressures, inflection pressure, and upper and lower corner pressures, by fitting the sigmoid equation parameters to measured data. The Venegas equation has shown very tight correlation with clinical data and has been validated in its ability to match or fit data in several studies [Gattinoni et al., 2005, Luecke et al., 2003, Harris et al., 2002]. However, its predictive value for guiding therapy has not been shown or tested.

More recently, animal studies [Schiller et al., 2003, Bickenbach et al., 2010] using in vivo microscopy showed that ARDS affected alveoli can be characterised into three distinct groups, with each group exhibiting different compliance and recruitment behaviour. Although, mathematical models that account for all unit types have been developed [Yuta, 2007, Yuta et al., 2004], these models contained too many parameters for unique identification from measurements readily available at the bedside. Hence, they are not uniquely identifiable with the limited data available and are very time consuming to model, rendering them ineffectual for clinical use in guiding therapy.

Thus, there is strong motivation to develop a model-based approach to specifically evaluate the patient-specific response to PEEP. In particular, the effect on recruitment, and retention at end expiration due to PEEP, a very is important clinical parameter to evaluate in a real-time basis. Most of the models described lack predictive power to guide therapy. Although the models accurately capture lung mechanics, the predictive value for guiding therapy have not been shown.

2.4 SUMMARY

The selection of optimal PEEP has been shown to be ineffective. Conventional methods which examine the LIP and UIP provide a guide to select PEEP. However, the LIP and UIP can take on a range of values and do not offer one unique setting. The introduction of model-based approaches provides an alternative method for selecting PEEP.

Model-based approaches use readily available data to capture lung dynamics. Although models can be classified as finite element models and lumped parameter models, only lumped parameter models are clinically viable. The two main lumped parameter models describe gas exchange and recruitment. Clinical models using gas exchange have been developed, but in patients with ARDS, recruitment is the major concern.

Most current recruitment models lack the power to guide therapy, and have only been created as research tools. Thus, there is strong motivation to create models that capture recruitment which can be used in a clinical setting. The following chapters discuss models that have been developed to select PEEP using lung mechanics and the clinical implications of such models.

Chapter 3 - Recruitment Model

This chapter introduces the lung recruitment model utilised in this study developed by Yuta [Yuta, 2007]. The model components are described along with their physiological relevance. In addition, a preliminary validation is shown [Sundaresan et al., 2009, Yuta, 2007] using clinical data obtained from Bersten [Bersten, 1998].

3.1 MODEL SUMMARY

The recruitment model is based on the work by Hickling [Hickling, 1998], which models the lung as a collection of multiple lung units. A unit represents sets of distal airways and attached alveoli. The lung is divided into several "horizontal" compartments to capture the different levels of superimposed pressure. The compartment at the bottom experiences higher superimposed pressure than the ones above due to the weight of the lung. Figure 3.1 shows the fundamental components of the modelled lung.

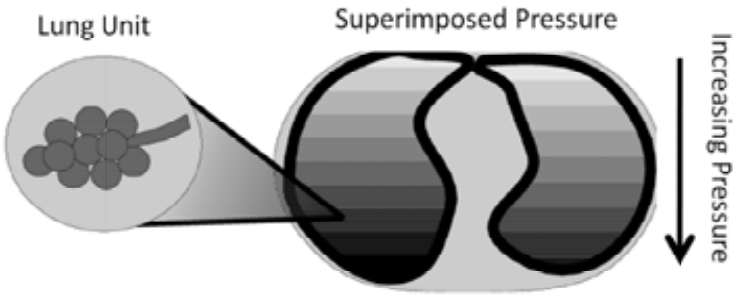

Figure 3.1 - Lung modelled as a collection of units, evenly divided into compartments of different superimposed pressure [Sundaresan et al., 2009].

Any given lung unit has only two possible states at any given pressure: (1) recruited or (2) de-recruited. The mechanism of volume change is based on the hypothesis that it is caused predominantly by recruitment and de-recruitment of lung units, especially in ARDS affected lung. In particular, it is based on the in vivo studies by Schiller et al [Schiller et al., 2003] that showed that the recruitment and de-recruitment of alveoli occurred even in healthy lungs and that once a unit was recruited, it did not change its size significantly. This result suggested that recruitment and de-recruitment is the dominant cause of volume

change, rather than isotropic “balloon like”, expansion of alveoli, as discussed in detail with significant supporting studies in Chapter 2.

3.1.1 THRESHOLD PRESSURES

The recruitment and de-recruitment of the modelled lung units are controlled by the distribution of Threshold Opening Pressure (TOP) and Threshold Closing Pressure (TCP), respectively. TOP is the critical pressure at which a previously collapsed unit is recruited during inspiration. Similarly, TCP is the critical pressure where a previously recruited unit collapses during expiration.

The work by Crotti et al and Pelosi et al [Crotti et al., 2001, Pelosi et al., 2001] indicated that pressure distributions were normally distributed. TOP and TCP distributions can therefore be modelled by a normal density (Gaussian) function. The shape of each distribution is defined by two unique variables: standard deviation (SD) and mean. The total number of lung units in the model is distributed according to these variables within a defined physiological pressure range, as well as across superimposed pressure compartments.

The TOP is distributed broadly from minimum to maximum pressure and simulates the continuous recruitment of lung units during inspiration. In contrast, the TCP distribution is significantly narrower compared the TOP, and concentrated at lower pressure. Physiologically, these distributions represent a continuous recruitment of lung units over a range of pressure during inflation and a more sudden, or faster, de-recruitment at lower pressure during deflation. This trend of consistent recruitment throughout inspiration and the relatively fixed point of de-recruitment has been evidenced in several clinical studies [Albaiceta et al., 2004, Jonson et al., 1999].

The shapes and the values of the distributions are also unique to the condition of the patient and the state of disease. These parameters therefore change as the state of disease and the condition of a given patient evolve. Thus, they can be used as a model-based marker to describe the level of recruitment, and thus oxygenation, in the lung, and indicate changes in patient condition over time.

3.1.2 UNIT COMPLIANCE

Once a lung unit is opened, it assumes a volume defined by a unit compliance curve. The shape and values of the curve are based on the work of Venegas [Venegas et al., 1998] and is described by the equation:

$$V = a + \frac{b}{1 + e^{(-P+c)/d}} \tag{3.1}$$

where the volume, V, is defined at each pressure increment, P, by a, a minimum volume [ml], b, the maximum volume [ml], c, the midpoint [cmH_2O] and d, the curvature [cmH_2O] as seen in Figure 3.2.

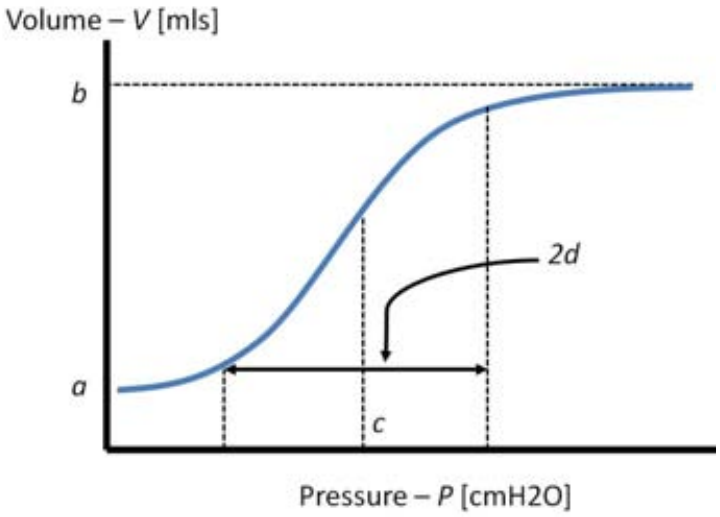

Figure 3.2 - Unit compliance curve using the Venegas equation

Equation (3.1) describes the volume at every pressure value. However, the model only uses a range of specified pressures. Venegas et al used a similar equation to describe the entire PV curve in this model based on a balloon-like expansion hypothesis. However, this model uses Equation (3.1) to describe the individual unit compliance curve, which represents visco-elastic effects of recruited alveoli and distal airways. It thus provides the model with slightly more flexibility to match observed clinical behaviour. Hence, it is important to note that this curve considers expansion only after recruitment, which is a limited, added fractional expansion from the opened state.

Thus, this model is based on the hypothesis that volume change is predominantly caused by recruitment and de-recruitment, and that the size of alveoli does not change significantly once recruited. Hence, this curve has relatively small effect on the total PV curve. The shape and values for the curve can therefore be fixed during the fitting process, significantly simplifying the analysis and reducing potentially redundant variables.

3.1.3 MODEL SIMULATION

As pressure changes during a breathing cycle, the model calculates the volume of the lung using the threshold pressure distributions and unit compliance curve. At each pressure increment, the model evaluates the number of recruited units in each compartment, using appropriate superimposed pressures and threshold pressure distributions. The number of recruited units is then multiplied by the appropriate unit volume according to the unit compliance curve to produce a volume of the compartment. Total lung volume at a specific pressure is the sum of all the compartment volumes. This solution process is shown schematically in Figure 3.3.

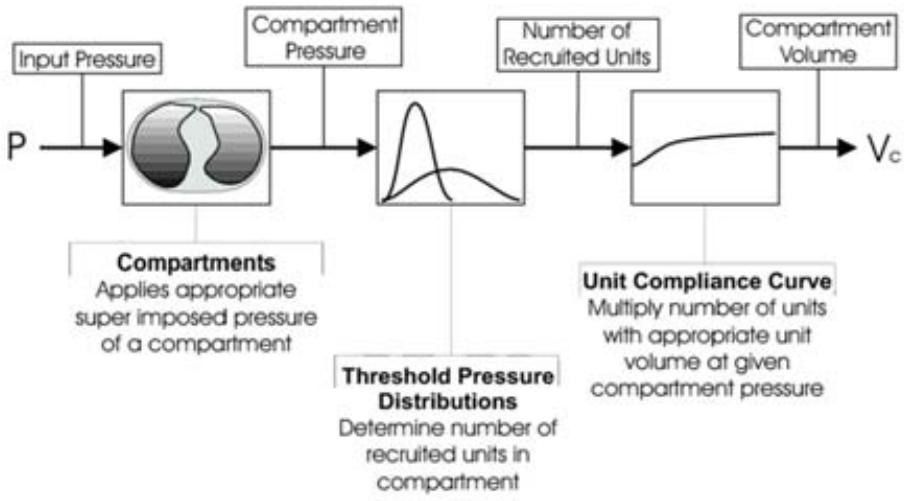

Figure 3.3 - A schematic of the model solution process. It shows each step of the process for calculating one compartment volume. The total lung volume of a given pressure is the sum of all the compartment volumes modelled.

Given data from clinical PV loops, the process can be readily inverted to find the threshold pressure distribution parameters. In other words, the model is uniquely and readily identifiable. Equally importantly, the model is effectively quasi-static, which is a

significant simplification over almost all models in the pulmonary mechanics modelling [Ben-Tal, 2006].

3.2 PARAMETER IDENTIFICATION

Early recruitment models developed by Yuta were validated and fitted to clinical data [Yuta, 2007, Yuta et al., 2004]. However, the models included four different types of lung units, based directly on work by Schiller et al [Schiller et al., 2003]. Each different type of unit thus required unique unit compliance and threshold pressure distributions. The model therefore required as many as 42 patient specific parameters to be identified [Yuta et al., 2004].

Most of those model parameters were impractical, if not impossible, to obtain clinically, especially with the limited time, data, and resources in a typical ICU. Hence, it was effectively not identifiable from available data. However, the model in [Yuta et al., 2004] was much more physiologically representative. Thus, its relationship to the model presented here is used to define this minimal model's physiological relevance, and ability to equally capture physiological data.

The model of [Yuta et al., 2004] was thus modified to create the model presented here, requiring only 2 parameters per breathing limb to make it clinically applicable. Reducing the number of unit types to just one and using the hypothesis that most of the volume change is caused by recruitment and de-recruitment (e.g. [Carney et al., 1999, Hickling, 2002]), the unit compliance has a relatively smaller contribution to the overall PV curve shape. As a result, the unit compliance curve defined in Equation (3.1) can be fixed at generic population values.

The minimum and maximum threshold pressures are fixed at 0 and 60 cmH_2O respectively, to cover the range of typically used ventilation pressures. The total number of parameters is thus reduced to just four:

- TOP distribution mean − Inspiratory limb of breathing curve
- TCP distribution mean − Expiratory limb of breathing curve
- TOP standard deviation − Inspiratory limb of breathing curve
- TCP standard deviation − Expiratory limb of breathing curve

Therefore, there are effectively two parameters for describing each of the inflation and deflation limbs. Other clinical MV related variables, such as PEEP, PIP, and tidal volume are assumed known, as they are set by the clinician or can be obtained directly from ventilator.

Hence, the changes made in reducing 42 parameters to four do not remove any significant physiological representation. What is lost is the level of physiological detail in the number and the types of ARDS affected and healthy lung units. However, these values were not uniquely identifiable without as many as 20 unique PV curves, which was not clinically practical.

In their place, there is now a single unit which takes on two states; recruited and de-recruited. However, these two states can, at a given pressure, represent the level of ARDS by the level of recruitment available at a given pressure. More specifically, as ARDS progresses, there is less recruitment at a given pressure and PEEP, which is effectively captured by the four (2 each) parameters describing TOP and TCP. Hence, alveoli-specific TOP and TCP, summarised by the mean and SD distribution parameters, can effectively capture this level of ARDS.

As a result, the parameter identification is greatly simplified and importantly, is unique, given a reasonably discretized measured PV curve. The main requirement is a minimum of 2 complete PV loops to provide enough data to identify the two parameters for the inflation (TOP distribution) and deflation (TCP distribution) limbs. A second requirement is that these loops be obtained at clinically different PEEP values. TOP and TCP parameter identification is readily done by iteratively modifying the threshold pressure distribution variables to minimize the sum squared error between the model and clinical data for each limb of the PV loops.

Since the inflation and deflation limbs are generated by different independent parameters, each limb can be fitted separately. The PEEP value sets the minimum pressure for the PEEP to PIP breathing cycle. The standard deviation of the TOP or TCP distribution primarily controls the slope of the curve and the mean value primarily controls the location along the pressure axis of the respective curves.

The TOP and TCP distribution parameters are effective for capturing both inter-patient and intra-patient variability. Inter-patient variability is accounted for by the difference in

distribution mean values between patients. Each patient may have a different TOP and TCP mean for a given PEEP and the mean is also reflective of the overall level of lung damage. In particular, suppose a patient had PV loops at 3 different PEEP values, then each PEEP would have an associated, patient-specific TOP and TCP mean. However, for a given PEEP, there will almost certainly be different distribution mean values across different patients, indicating the condition-specific level of lung damage in a patient. Intra-patient variability is similarly seen in the different mean values obtained for TOP and TCP at different PEEP in a given patient, where these are obtained at different points in time. These differences indicate the effect of PEEP on recruitment in the patient, as well as their patient-specific evolution of disease state.

Finally, the SD is held constant across all PEEP levels during each trial. The SD represents the compliance of the lungs, and is thus representative of the ARSD state. As SD changes, the severity of the ARDS affected lung changes. More specifically, a lower SD represents a more diseased lung state, while a higher SD indicates a more compliant lung. The SD is held constant across all PEEP as it represents the underlying disease state which does not change for a given trial. Rather, SD can vary over time as the patient condition deteriorates or improves.

3.3 PRELIMINARY MODEL VALIDATION

A preliminary model validation was performed by fitting to clinical PV data at different PEEP levels from 10 patients as reported by Bersten [Bersten, 1998] with two additional patients not reported. The datasets were recorded from patients with various levels of lung injuries, detailed in Table 3.1. Each dataset included recordings of at least 3 different PEEP levels with the deflation to FRC. The data was sampled for 60 seconds at 100 Hz for each PEEP level, with the last 15 to 20 seconds used for the dFRC measurement.

For this validation analysis, PV loops at different PEEP levels from the same patient were fit to the model by shifting the distribution mean value while other parameters, including the SD, remain fixed. This shift represented the effect of the dynamic mechanism of lung units at different PEEP values. More specifically, once a collapsed lung unit is recruited, it does not necessarily collapse again at the same pressure at which it was recruited. Instead, it stays recruited at a lower pressure [Maggiore et al., 2001] as discussed in Chapter 2. This

effect is especially significant in the ARDS lung because of the reduced number of functional lung units and lower compliance of the overall lung. In particular, the benefit of recruitment manoeuvres on ventilated patients is explicitly based on this dynamic mechanism [Foti et al., 2000]. The same effect results from increasing the PEEP, while keeping the tidal volume the same, causing higher PIP.

Table 3.1 - Characteristics of study patients from Bersten [Bersten, 1998]

Sex	Age [years]	Cause of lung injury
Male	74	Ruptured abdominal aortic aneurysm
Male	24	Lung contusion
Female	72	Legionnaire's disease
Male	48	Pancreatitis
Female	68	Pulmonary embolus
Male	54	Aspiration
Male	73	Aspiration
Male	72	Pneumonia
Male	81	Aspiration
Male	47	Liver transplant

This behaviour results in a shift in threshold pressure distributions in the model. Therefore, as PEEP is increased, the centre of the TOP distribution shifts to lower pressure, indicating that more units are kept recruited during the breathing cycle. Hence, the application of PEEP begins to recruit lung units that were collapsed at lower PEEP settings. Again, this physiological dynamic has been observed in several clinical studies (e.g. [Halter et al., 2003, McCann et al., 2001]).

Similarly, the TCP distribution mean shifts to higher pressures indicating unit instability at relatively higher pressures for these newly recruited lung units. The higher PEEP recruits more units in regions with higher superimposed pressure and injured units. These newly recruited units are inherently unstable, and thus, are likely to be de-recruited at relatively higher pressures. Hence, the higher PEEP increases the recruitment of previously collapsed units at a given pressure, increasing the number of functional units. However, some of those units are unstable and collapse at relatively higher pressure.

The amount of the shift in both distributions is dependent on the individual patients' condition and state of disease. More specifically, PEEP is modified to increase recruitment and optimize oxygenation, as well as to prevent de-recruitment at the end of expiration. Therefore, tracking the number of recruited units at a given pressure and PEEP over time is a measure of recruitment that effectively tracks the state of ARDS or lung disease using the level of recruitment. Hence, it can be used as a key parameter to describe the characteristics of a patient specific lung, track the level of recruitment, and quantitatively determine the impact of therapy.

The method for fitting the data is based on simulating the entire inspiratory capacity of the lung. For a given recruitment status of the lung, Figure 3.4 shows an example of a typical PV curve as obtained from either standard volume controlled ventilation (VCV) or pressure controlled ventilation (PCV) [Bersten, 1998]. Also shown is the tidal volume, PEEP and PIP.

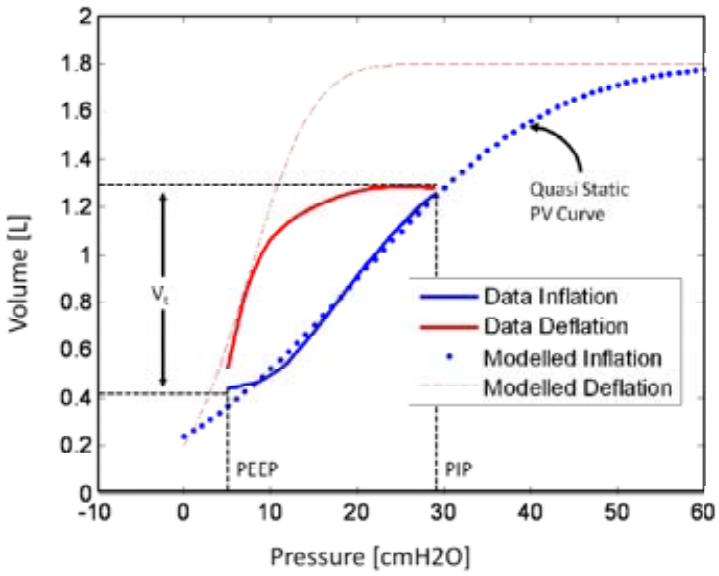

Figure 3.4 - An example of the model fit. The plot shows the modelled inflation, modelled deflation and the data for inflation and deflation. The model fits the entire lung capacity

The lower dotted curve represents the inflation curve which is dependent on the type of ventilation used. The upper dashed curve represents the quasi-static PV curve, which is ventilator independent and represents the steady state volume obtainable for each pressure increment from 0 to 60 cmH_2O when the patient expires. Again, note that the figure is only valid for a specific recruitment status of the lung. In practice, the alveoli recruitment

dynamics can change if different settings of PEEP are used for sufficiently long periods. The result of this physiological effect would be a change in the curves of Figure 3.4, and a shift in the mean of the corresponding TOP and TCP distributions over time at the same constant PEEP level. The upper dashed curve also represents the limiting behaviour of the deflation phase of the PV relationship for the given recruitment status, and in principle could be obtained experimentally by a sequence of pressure holds from 0 to 60 cmH_2O.

For example, in Figure 3.4**,** the limiting behaviour is constrained by the given PEEP value. In other words, during the passive expiratory phase of VCV, the pressure drops very quickly and stays close to PEEP, so that the volume must eventually settle onto the quasi-static PV curve. Therefore, the last, almost vertical part of this deflation curve is effectively equivalent to a pressure hold at PEEP. Another way of describing the upper expiratory dashed curve is that it is the asymptotic behaviour of the deflation curve from PIP to PEEP. Similarly, the lower dotted line represents the asymptotic behaviour of the inflation period.

Hence, at the start of inflation and end of deflation there is a transient period where the PV curve is seeking to settle on the global asymptotic curves shown in Figure 3.4. This period represents real lung mechanics. However, it does not significantly reflect the volume responsiveness described by dFRC and PIP, which are important clinical variables.

This transient behaviour is also evident in the PV data of Figure 3.5, where the sparse point distributions indicate this rapid transition, resulting in a reduced amount of sampled data. The use of a normal distribution to model TCP and TOP is hence justified as the data dense steady state part of the curve resembles a normal cumulative distribution. Similarly, the quasi-static asymptotic curve in Figure 3.4 corresponding to the deflation part of the PV curve has also been shown to be close to a normal distribution [Venegas et al., 1998]. The result of [Venegas et al., 1998] combined with the studies of [Crotti et al., 2001, Pelosi et al., 2001] further justifies the use of a normal distribution to model TCP and TOP.

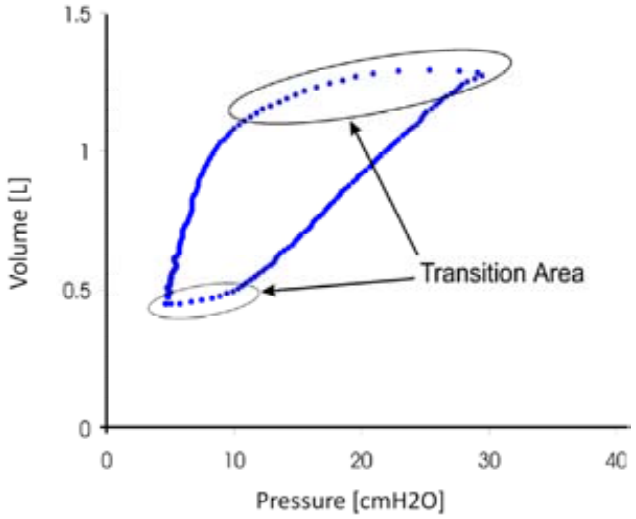

Figure 3.5 - PV loop showing the transient behaviour during inflation and deflation

Figure 3.4 and Figure 3.5 thus motivate a fitting procedure that uses the last approximately 60% of the inflation curve and the densely sampled 70% (by volume) of the deflation curve. These numbers were chosen empirically and are essentially arbitrary.

Figure 3.6(A) and Figure 3.6(B) show the model fit for two clinical PV data sets from [Bersten, 1998].The dotted lines show the clinical data and the solid lines show the model fit across the densely sampled non-transitional regions. The model was fitted to all the PV loops shown. However, only one model fit per dataset is shown here for clarity.

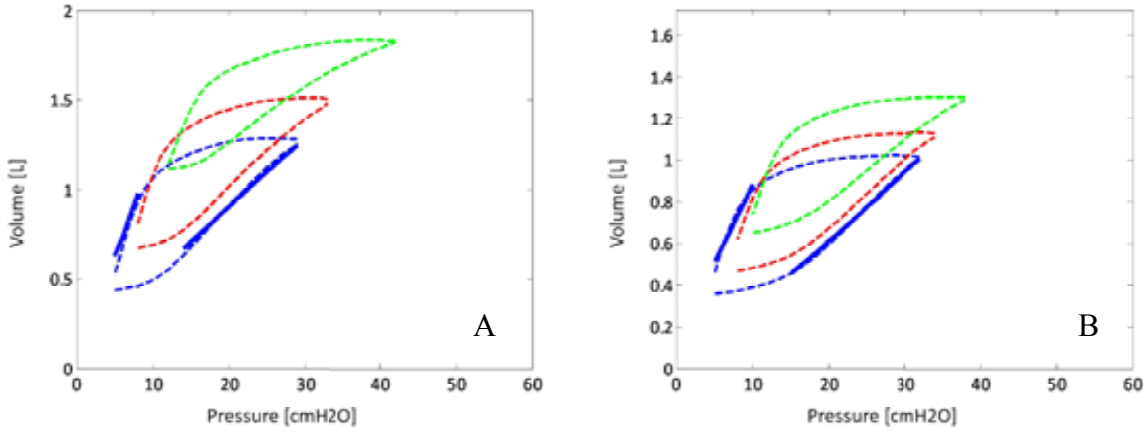

Figure 3.6(A) & (B) - Dataset 1 & 2. Dotted line shows the clinical data and solid line shows the model fitted to the clinical data [Bersten, 1998]. The model fit is for PEEP = 5 cmH_2O, as shown.

The identification and fitting error was calculated using the percentage difference between the model and the data in the inflation and deflation limb for each PV loop dataset. These results are shown in Table 3.2. Overall, the loops in Figure 3.6 show minimal deviation and indicate a good match to the measured data. Table 3.2 shows these results are relatively tight. Also shown are the range of mean and standard deviation for both the inflation and deflation limb across all patients and PEEP values in Table 3.3.

Table 3.2 - Summary of model errors

		PEEP [cmH$_2$O]			
		5	*7*	*10*	
Dataset 1	*Inflation*	1.71%	0.48%	0.34%	
	Deflation	12.33%	4.25%	0.92%	

		PEEP [cmH$_2$O]			
		5	*7*	*10*	
Dataset 2	*Inflation*	1.74%	0.53%	0.59%	
	Deflation	3.99%	2.59%	2.36%	

		PEEP [cmH$_2$O]			
		5	*7*	*10*	*12*
Dataset 3	*Inflation*	3.03%	0.79%	0.58%	0.63%
	Deflation	10.02%	7.49%	5.59%	3.09%

		PEEP [cmH$_2$O]			
		5	*7*	*10*	*12*
Dataset 4	*Inflation*	3.47%	1.24%	1.03%	0.48%
	Deflation	9.83%	2.48%	1.12%	0.75%

		PEEP [cmH$_2$O]			
		5	*7*	*10*	*12*
Dataset 5	*Inflation*	1.86%	0.58%	0.40%	0.33%
	Deflation	7.09%	2.87%	0.53%	0.24%

		PEEP [cmH$_2$O]			
		5	*7*	*12*	
Dataset 6	*Inflation*	2.50%	1.16%	0.85%	
	Deflation	5.15%	1.86%	1.02%	

		PEEP [cmH$_2$O]			
		10	*12*	*15*	
Dataset 7	*Inflation*	0.78%	0.47%	1.01%	
	Deflation	1.19%	0.78%	0.82%	

		PEEP [cmH$_2$O]			
		5	*7*	*10*	*12*
Dataset 8	*Inflation*	2.59%	0.54%	0.05%	0.54%
	Deflation	9.39%	4.04%	2.19%	1.07%

Table 3.2 - Summary of model errors(Cont)

		PEEP [cmH_2O]		
		5	*7*	*10*
Dataset 9	*Inflation*	1.62%	1.24%	0.62%
	Deflation	10.59%	5.34%	2.48%

		PEEP [cmH_2O]		
		5	*10*	*15*
Dataset 10	*Inflation*	2.30%	3.60%	0.93%
	Deflation	8.05%	5.17%	1.57%

		PEEP [cmH_2O]		
		0	*5*	*10*
Dataset 11	*Inflation*	24.31%	2.88%	1.16%
	Deflation	51.86%	1.25%	0.28%

		PEEP [cmH_2O]		
		5	*7*	*10*
Dataset 12	*Inflation*	1.48%	2.52%	0.45%
	Deflation	3.85%	2.96%	2.11%

Table 3.3 - Range of mean and SD across all datasets

	Range	**Median**
Inflation Mean	[7.79, 32.43]	19.99
Inflation SD	[12, 25]	17.5
Deflation Mean	[7.42, 15.83]	9.89
Deflation SD	[5, 10]	7

3.4 MODEL PREDICTION

The main objective of this research is to develop a minimal model that is also clinically useful in selecting a clinically appropriate PEEP value. One approach is to provide an objective method of determining optimal ventilator settings or PEEP for an individual patient. Another is to provide constant monitoring for a patient's level of lung recruitment, and thus the level of ARDS and the impact of therapy as patient condition evolves.

The data that the model requires can be directly obtained from the ventilator during normal operation and clinical adjustment. All the analysis can be done at bedside and be immediately applied. Furthermore, it does not require additional equipment or tests. Thus, additional cost and risk to the patient are mitigated. The ventilator setting optimization

procedure is done in 3 steps: (1) parameter identification, (2) simulation of a change in PEEP, and (3) analysis.

Because the model can identify lung mechanics over an entire pressure range, it can be used to predict the lung mechanics at different ventilator settings. Thus, the model allows the clinicians to see the result before it is actually applied to the patient, and decide on whether to apply the changes. The model also allows predictions about multiple results to be made quickly. Quick turnaround eliminates the need for clinical trial and error procedures. Hence, optimum PEEP and ventilator settings can be obtained via simulation if the model predictions are accurate.

Therefore, for patients with data at 3 PEEP settings in this data set, 2 PEEP settings are used to fit the model and the mean shift trend. The fitted model is then tested to predict the results of the remaining PV loop. If 4 PEEP settings are available, then the model is fitted with 3 loops. Any combination of 2 in 3 or 3 in 4 can be used to test the ability of the model trend to accurately predict the remaining unused PEEP value and PV curve.

Specifically, if 2 PV loops are obtained at higher PEEP values, then the model can predict a PV loop for a lower PEEP. Prediction of a lower PEEP is useful in the clinical setting as it means that alveolar collapse can be avoided as a result of PEEP reduction. Similarly, predicting higher PEEP level responses allows evaluation of the clinical impact in recruitment of changing PEEP.

The model was able to predict the missing mean shift and PV curve for the PEEP level with relatively small errors. The error metric chosen is the average relative percentage error, computed over the densely sampled portions of the PV loops used in the identification process. This approach avoids the transient period, as previously discussed and shown in Figure 3.4 and Figure 3.5.

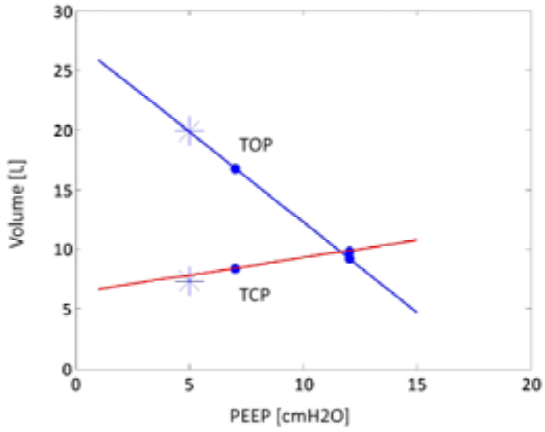

Figure 3.7 - A fitted mean shift for prediction for Dataset 1. PEEP = 7 and 12 cmH_2O were used to predict PV data at PEEP = 5 cmH_2O. The linear lines for mean shifts (solid lines) are identified from the 2 given datasets (solid dots). The * shows the true mean for PEEP = 5 cmH_2O.

Figure 3.7 illustrates the fitted mean shift and actual mean for PEEP of 5 cmH_2O in Dataset 1. This prediction was done by fitting the data to PEEP of 7 and 12 cmH_2O. The true mean value is marked with an asterisk (*) with predicted mean shown on the solid line. Figure 3.8 shows the resulting PV curve prediction, where the dashed lines are the original clinical data for the predicted PV loop. Because the model was not fit in the highly dynamic transition area, the prediction was also only made for the steady portion of the curve, as illustrated by the dots in the figure.

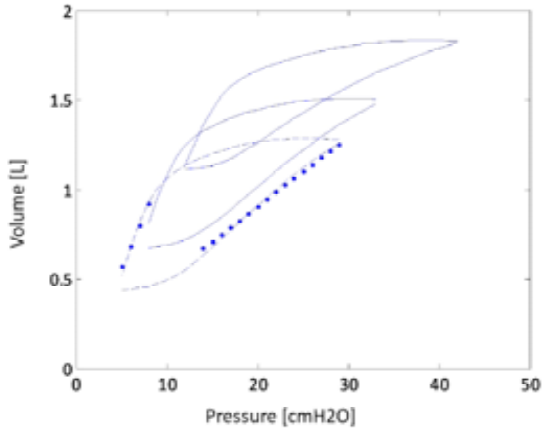

Figure 3.8 - A prediction result for PEEP = 5 cmH_2O of Dataset 1. The PV data was predicted by fitting 2 known PEEP levels (solid lines). The dots show the predicted data and the dashed lines show original data.

Figure 3.9 illustrates the same prediction method for a PEEP of 5 cmH_2O in the larger Dataset 5. In contrast to Dataset 1, the slope of these patient specific mean shift values is

lower, indicating a patient that is much less responsive to changes in PEEP. More specifically, this patient experiences far less of an increase in recruited lung volume for a given increase in PEEP, indicating less clinical effect in modifying therapy. Similar to the results for Dataset 1, all the predicted PV curves show clinically insignificant levels of error in their predictions based on mean shift.

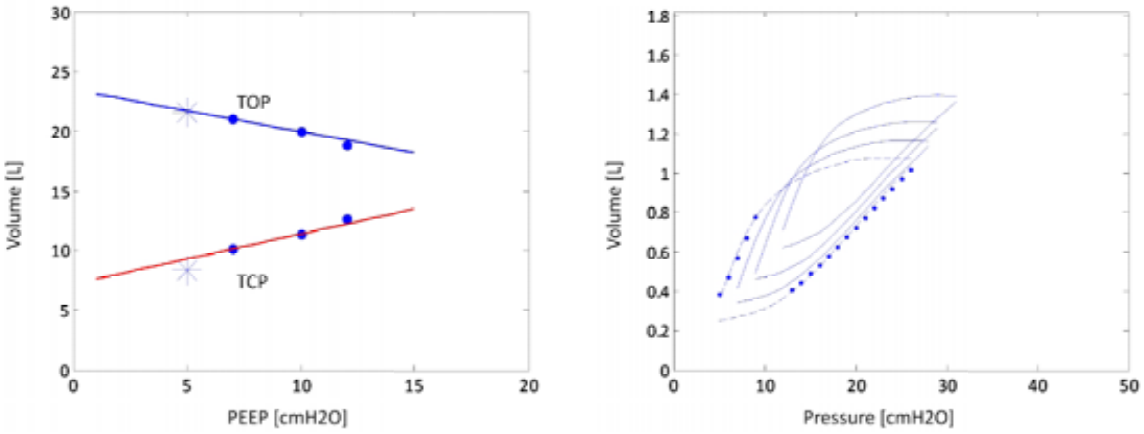

Figure 3.9 - Predicted mean shift for PEEP of 5 cmH_2O for Dataset 5

The results of this model show that as PEEP increases, the TOP distribution mean decreases, while the TCP distribution mean increases. These shifts indicate the change in recruitment and de-recruitment characteristics of lung units as PEEP is altered [Halter et al., 2003, McCann et al., 2001, Sundaresan et al., 2009]. In the model fit, inflation SD for Dataset 1 was calculated to be 18, while inflation SD for Dataset 5 was 14. This implies that Patient 5 is more compliant and is evident by the steeper slope of the PV curve from Figure 3.9 compared to Figure 3.8. Thus, the assumption of holding SD constant does not affect the predictive capability of the model.

The overall average pressure point error for Dataset 1 was 14.31 ml (1.40%) and 60.35 ml (6.36%), for inflation and deflation respectively. For Dataset 5, the average absolute error was 24.85 ml (1.61%) and 42.70 ml (3.33%), for inflation and deflation respectively. Table 3.4 summarises the prediction errors for these 2 data sets for each predicted PEEP value.

Table 3.4 - Summary of PV prediction errors for two data sets

		PEEP [cmH$_2$O]			
		5	*7*	*10*	
Dataset 1	*Inflation Error [ml]*	16.13	9.98	16.83	
	Error [%]	2.23	0.89	1.10	
	Deflation Error [ml]	49.26	67.16	64.65	
	Error [%]	7.58	6.71	4.78	
		PEEP [cmH$_2$O]			
		5	*7*	*10*	*12*
Dataset 5	*Inflation Error [ml]*	31.87	35.09	21.82	10.63
	Error [%]	2.52	2.33	1.11	0.48
	Deflation Error [ml]	35.60	112.82	13.33	9.06
	Error [%]	3.32	8.89	0.72	0.40

Table 3.5 summarises the overall prediction for all 12 datasets. This table shows the maximum and average percentage absolute error for inflation and deflation at each predicted PEEP level. The inter-quartile range of errors is also shown to provide the range of errors.

Table 3.5 - Summary of PV prediction percentage errors for all datasets. The errors are listed according to predicted PEEP levels

PEEP [cmH$_2$O]	**Inflation**				**Deflation**			
	Avg	*IQR*	*90% CI*	*Max*	*Avg*	*IQR*	*90% CI*	*Max*
5	7.46	2.29 - 7.74	1.89 - 24.16	29.32	10.02	5.13 - 11.46	2.64 - 23.60	33.77
7	4.60	1.29 - 7.41	0.88 - 13.39	15.40	11.06	6.71 - 14.91	5.12 - 21.45	24.43
10	5.41	1.11 - 5.41	0.71 - 18.24	29.32	9.72	3.63 - 9.90	1.25 - 28.89	43.85
12	3.90	0.75 - 2.55	0.47 - 12.96	16.34	3.61	0.91 - 4.94	0.48 - 8.18	9.26
15	3.47	2.65 - 4.28	1.99 - 4.95	5.10	7.37	5.73 - 9.00	4.41 - 10.31	10.64

The model requires a minimum of two PV loops at different PEEP settings to obtain all the required parameters. However, more data will increase the accuracy of the parameters and resulting simulation, particularly in presence of noise. The values of PEEP used do not need to be predetermined or specified, but should be within a safe range determined by medical staff for that specific patient and be reasonably different. Once a best fit is achieved, the model records those parameter values for prediction and simulation.

The model can simulate the lung for any combination of PEEP and tidal volume, including the extreme values that may not be safe to test on an actual patient. Since the model is based on a reduced number of parameters and simplified mechanics, the simulation can be done in matter of minutes. This produces real-time feedback and a condition specific result.

The volume shifts between different PEEP levels are captured by the shifting distribution means. In general, the TOP mean decreased as PEEP increased, and the TCP mean increased as PEEP increased. Physiologically, this behaviour indicates the varying nature of TOP and TCP under this therapy.

Since the model identifies essential parameters representing lung recruitment, it can be used to track patient recruitment and oxygenation, while the patient is on the ventilator. Thus, when the patient's condition improves or worsens, these parameters change accordingly. By tracking the changes in parameter values over time, the condition of the patient can also be tracked. This approach can be used to aid clinical decisions and evaluate the effect of treatment.

3.5 MODEL LIMITATIONS

The model has some potential limitations that need to be addressed. First, the fitting method requires data with deflation to FRC. This data is not typically obtained during current protocols for ventilator treatment. However, this measurement can be obtained by deflating the lung to atmospheric pressure and measuring dFRC. Once the airway is opened to atmospheric pressure, the lung assumes FRC rapidly, and the entire measuring process can be completed in a matter of seconds [Bersten, 1998]. This value might have to be obtained once every 1–2 days.

This process requires intervention from the ICU staff and interruption of the patient's breathing pattern, both of which may be clinically unavailable or undesirable. Furthermore, a typical ventilator is only designed to record data on tidal ventilation, so that recording the deflation to FRC would require either a specialised ventilator or a separate data acquisition system. In this case, clinical model validation will employ external sensor systems.

Similarly, the mean shift trend and prediction of PV loops are primarily based on the relative change of the PV loops with respect to the first PV loop. In other words, for PV predictive purposes, the initial volume or FRC is essentially arbitrary and could be set to 0. All that is required is the change in FRC (ΔFRC) after each PEEP intervention. This ΔFRC can be easily obtained by a pressure hold at each required increasing PEEP. For example, the change in volume occurring from increasing PEEP from 0 to 5 cmH_2O in a pressure hold manoeuvre is precisely ΔFRC. This process could even be integrated into the ventilator to measure ΔFRC automatically [Rees et al., 2002].

The mechanics of the lung at the missing PEEP values are readily predicted by linearly fitting the mean shift to identify the impact of this change. It also allows a simple method for predicting the mean at a new PEEP level. However, some of the mean values obtained are not perfectly fitted as the dots are not exactly on the predictive linear line for this relatively extreme PEEP setting. This inaccuracy causes the relatively larger error of the predicted PV curve. Importantly, this error is still within clinical expectations.

The prediction method shown utilizes just a single parameter TOP and TCP (mean shift) to predict between different PEEP settings. Thus, it is simple and easy to use, and can predict an important patient specific response to the change in primary therapy of PEEP.

The model does not directly account for other ventilator settings, such as ventilator mode, flow pattern and maximum inspiratory flow. Since the modelling approach can capture any changes in the TOP and TCP distributions from their impact on the measured PV curves, any PV changes that occur from different ventilator settings are therefore implicitly accounted for. Therefore, the model potentially provides the framework for correlating different ventilator settings with respect to their effect on TOP and TCP distributions.

That all said, such drastic ventilator changes are not typically part of standard ventilator therapy, which focuses more on gradual evolution of settings [Rouby et al., 2002]. In addition, more detailed models could potentially manage such changes, but at a cost of much greater data requirements to create clinically useful patient specific models. Hence, it might be best noted that the model is limited to evolutionary prediction and changes typical of critical care.

This model has the ability to fit and follow the trend of any data including those from a ventilator. Thus, it can reproduce the shape and values of the particular PV curves. For

example, if the model was used to identify the parameters for ventilator data, then the model can predict the ventilator data at different settings. Similarly, if carina measurements like those of Karason et al [Karason et al., 2000] are used, then the model can be used to predict the PV curve at the carina for different settings. Thus, the model can be very generally applied to any dataset that may be available.

It may also be possible to use this model to assess the true lung mechanics, if the ET tube and proximal airway resistances were better known or estimated empirically at the bedside. This approach would require a smarter, more automated ventilator and/or excessive clinical time. However, such smarter ventilators are being developed [Rees et al., 2002], and may appear in future.

The patient specific mean shift parameter identified by this model is a direct result of analysing raw proximal PV data, which includes dynamic and resistive effects. Therefore, the parameter identified may not directly represent true lung mechanics. However, because the model is based on the fundamental mechanics, the slope of the mean shift and its clinical relevance can be readily related to the true lung mechanics. One such method to show this relation is to use the estimated carina measurement, which require measurements of the air flow rates and fluid dynamics based estimates of intubation tube resistance, and integrate this aspect in the model.

3.6 SUMMARY

The validation performed in this section is done with limited clinical data from the literature. Although this data contained PV loops at different PEEP levels, the range of PEEP used is still small. In a typical recruitment manoeuvre, patients may exhibit PEEP levels at much higher ranges which may lie outside the linear portion of the static pressure volume curve. Therefore, further validation using more extensive clinical data is required. Such data would also enable more direct study of clinical application and patient outcomes. More features may need to be included in the model to be fully clinically practical. Such features could include automated data acquisition, parameter identification, airway resistance estimates, and more efficient analysis. However, the overall goal of a clinically useful minimally complex model has been proven in concept.

In addition, the limitation of measuring dFRC at each PEEP provides another problem that needs to be addressed. The process of measuring dFRC could be harmful to the patient, as it requires a deflation to ZEEP. Although a change in dFRC can be easily measured, absolute dFRC values need to be calculated for the recruitment model to be effective. Chapter 4 introduces a model to estimate dFRC at various PEEP levels as an alternative to the invasive measurement.

Chapter 4 - Model-Based dFRC

The recruitment model detailed in Chapter 3 requires a deflation to FRC to measure the level of dFRC at a given level of PEEP. This measurement when typically done is invasive, and, in MV patients, can cause sudden de-recruitment which can prove harmful. In addition, the recruitment model does not evaluate the effect that PEEP has on pulmonary volume, in that it does not capture it. This chapter introduces a model-based method to estimate the patient-specific dFRC as a function of PEEP using lung stress and strain as a proxy for pressure and volume.

4.1 MODEL INTRODUCTION

The level of FRC represents the pulmonary gas volume at the end of expiration at atmospheric pressure. One objective of MV is to maximise FRC, thus increasing the amount of recruited alveoli. Hence, there is significant motivation to track and measure FRC as the patient undergoes MV therapy and as their condition evolves.

Currently, there are few methods of measuring FRC at the bedside. Gas washin/washout techniques are one type of method [Heinze et al., 2007], but are not readily available on most ventilators. A further limitation of this type of measurement is that only an absolute value of FRC is measured. Hence, no information on the potential for new recruited lung volume is given, which is critical in setting PEEP to gain maximum recruitment with minimum added injury.

Figure 4.1 shows a schematic of the lung. When FRC is measured using a washin/washout technique, it cannot be determined how many potential recruitable units are available. Therefore, as shown in the schematic, a lung with an FRC of 1.4 litres could be a result of a lung with 1.4 litres of fully recruited healthy lung units or 1.0 litre of recruited lung plus an additional amount of lung (0.4 L) that was recruited due to additional PEEP. In both cases, one gets the total recruited lung volume, not the recruited volume as a function of PEEP.

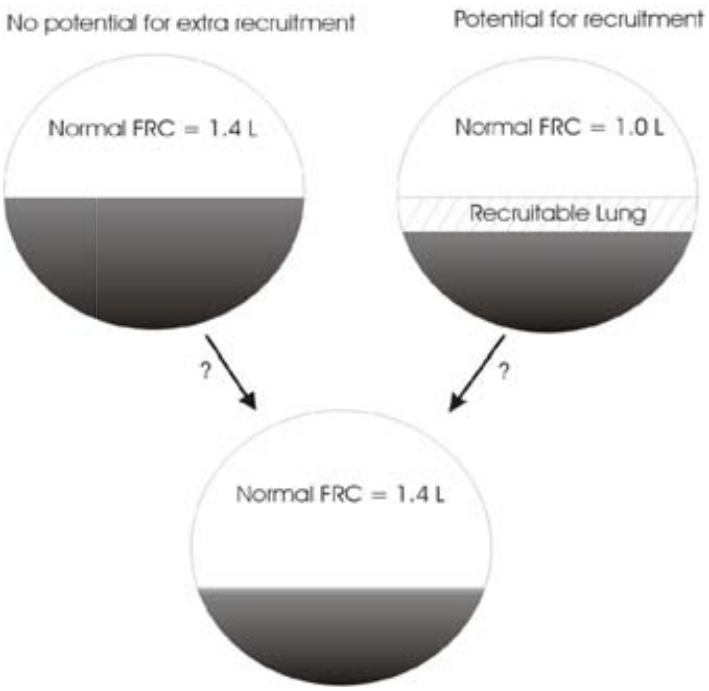

Figure 4.1 - Schematic of lung showing the limitation of an absolute FRC measurement as used in gas washin/washout methods

FRC can also be measured by using CT scans [Malbouisson et al., 2001]. Timed at the end of expiration, the gas volume can be assessed at each slice and summed across all the slices in the lung to calculate FRC. However, this type of measurement is unrealistic for regular use or monitoring in the ICU, due to its invasiveness, radiation dose, difficulty and cost.

Although specialised ventilators may have FRC measurements and can re-estimate FRC due to PEEP changes (GE ventilators [GE Healthcare, 2006]), most standard ventilators do not measure FRC and do not give the appropriate information required for optimal ventilator treatment. In addition, measuring FRC using standard ventilators requires transportation of the patient (CT scanning). Due to the currently limited availability of specialised ventilators, not all ICU's are equipped with them. Thus, in these situations, there is no practical bedside method that can be used to estimate recruitable lung. In addition, most current methods need the aid of the clinician and cannot be automated. Therefore, there is a motivation to be able to estimate the level of potential recruitment in the lung to help clinicians optimise MV treatment without the availability of advanced ventilators.

The ability to use standard ventilator data to estimate dFRC as a function of PEEP, which includes recruited lung, would be a potential enhancement in ventilation management.

Dynamic FRC is the level of additional lung volume that is achieved in the lung due to an additional level of applied PEEP [Amir et al., 1995] and is shown schematically in Figure 4.2. Although dFRC cannot by itself estimate the potential of lung recruitment, used with the recruitment model from Chapter 3 and gas measurements, it can provide the clinician with useful information on lung recruitability.

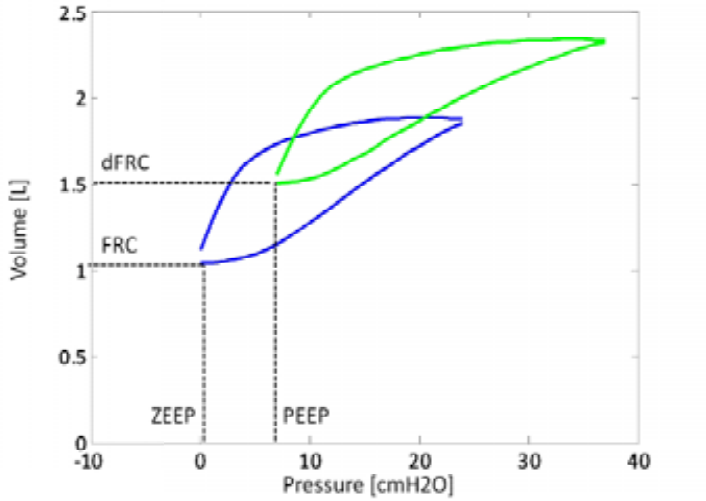

Figure 4.2 - Schematic showing the difference between FRC and Dynamic FRC

Thus, the dFRC value represents an aspect of the clinical endpoint in ventilation management, with the potential to be continuously tracked with changes in patient condition. This chapter develops a tool to estimate the level of additional pulmonary volume of collapsed alveolar units that can be recruited resulting from changes made to the applied inspiratory and expiratory airway pressures during MV. The method is based on identifying global parameters using a stress strain approach and estimating the level of additional lung volume obtained due to PEEP. The potential for the model to be used in a clinical setting is explored based on the measurements required.

4.2 MODEL SUMMARY

The stress strain model introduced here is based on the work of Chiumello et al [Chiumello et al., 2008], which studied the relationship between global stress and strain during MV in ARDS patients. They defined the clinical equivalent of stress as the transpulmonary pressure (ΔP_L), while the strain was defined as the ratio of change in volume (ΔV) to the

volume at the relaxed state of the lung or FRC. They also defined the specific lung elastance (E_{Lspec}) as the transpulmonary pressure at which FRC effectively doubles. The relationship between stress and strain was defined [Chiumello et al., 2008]:

$$\Delta P_L(stress) = E_{Lspec} \times \frac{\Delta V}{FRC}(strain) \tag{4.1}$$

where $\Delta V/FRC$ is the strain. The values of the specific lung elastance E_{Lspec} in Chiumello's study were reported as 13.4 ± 3.4 for surgical control subjects, 12.6 ± 3.0 for medical control subjects, 14.4 ± 3.6 for ALI subgroup and 13.6 ± 4.1 cmH_2O for the ARDS subgroup. This indicates that E_{Lspec} does not vary significantly within different groups and has a tight range of values.

The general relationship between the change in plateau airway pressure (ΔP_{aw}), when the airflow is zero and the corresponding transpulmonary pressure is also defined [Chiumello et al., 2008]:

$$\Delta P_L(stress) = \Delta P_{aw} \times \alpha \tag{4.2}$$

$$\alpha = \frac{E_L}{E_L + E_{CW}} \tag{4.3}$$

where α represents the static lung elastance and represents the ratio of the lung elastance (E_L) to the combined elastance of the lung and chest wall (E_{CW}).

It is critical to understand the importance of α in MV therapy. When a given airway pressure is applied, part of the pressure is used to inflate the lungs. The remainder is used to inflate the chest wall. The aim of MV is to ventilate patients, while simultaneously trying to minimise the stresses exhibited in the lungs.

Figure 4.3 shows the effect of different elastance values for the lungs and chest wall. Although in both cases, the total elastance is the same, Figure 4.3(A), typical of an ARDS patient, would experience a higher lung stress than Figure 4.3(B) as the lung is stiffer due to the higher elastance. Thus, α gives an indication of the severity of the ARDS affected lung, and is seen in Figure 4.3 in the relative contributions of E_L and E_{CW} versus Equation (4.3), where ARDS patients have higher α values.

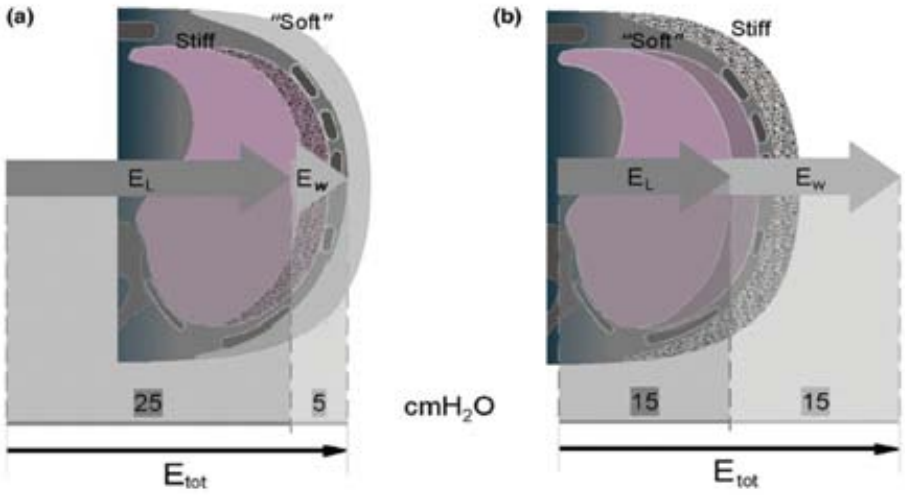

Figure 4.3 - Effect of different lung and chest wall elastance. An equal total elastance may arise from different combinations of lung and chest wall elastance [Gattinoni et al., 2004], where (a) is typical of ARDS patient and (b) healthier patient. Thus, α is higher in (a)

The values of α in [Chiumello et al., 2008] varied from 0.69 ± 0.15 for surgical control subjects, 0.74 ± 0.16 for medical control subjects, 0.64 ± 0.15 for the ALI subgroup, and 0.71 ± 0.16 for the ARDS subgroup. As with strain, α remained relatively constant across all patients with little deviation. Hence, a population value of α is possible.

The equation of motion describes the total airway pressure ($\Delta P_{aw_{tot}}$) as a function of the resistive and elastic components of the respiratory system, and is defined as:

$$\Delta P_{aw\_tot} = V \times E + Q \times R + P_0 \tag{4.4}$$

where V is the lung volume, E is the respiratory elastance, Q is the airflow rate, R is the respiratory resistance, and P_0 is the offset pressure, which is a combination of applied PEEP and intrinsic PEEP [Carvalho et al., 2007, Eberhard et al., 1992]. As resistance and elastance increase, the equation shows the airway pressure increasing, as expected, to overcome the respiratory resistance and the increased elastic recoil of the respiratory system.

In the case of no flow, the resistive term in Equation (4.4) is zero. In this case, the airway pressure is purely a function of the respiratory elastance and is known as the plateau airway pressure, as shown in Equation (4.5).

$$\Delta P_{aw} = V \times E + P_0 \quad (4.5)$$

Typically, if the pressure is measured, it is done at the ventilator or near the mask. Hence, all the PEEP data in this study represents plateau airway pressures, which are measured at zero flow at end expiration. Because transpulmonary pressure is not typically measured at the bedside, it is estimated using the PEEP. Thus, rather than using the transpulmonary pressure ΔP_L, the airway pressure is used as an estimate based on the relationship in Equation (4.2).

At the beginning of inspiration, when the airway pressure is equal to PEEP, there is a point of zero flow, when the airflow reverses between expiration and inspiration. At this point in time, the volume is measured as the dFRC. Because plateau airway pressure occurs during zero flow, this justifies the use of PEEP and the corresponding dFRC as a substitute for plateau airway pressure and lung volume. Thus, measured at this time, $\Delta P_{aw} = PEEP$ and $V = dFRC$ in Equation (4.1) and (4.2).

Combining Equations (4.1) and (4.2) yields a formula for FRC involving the two easily measured quantities ΔV and $\Delta P_{aw} = \Delta PEEP$ assumed here:

$$FRC = \frac{\Delta V}{\Delta PEEP} \times \frac{E_{Lspec}}{\alpha} \quad (4.6)$$

Equation (4.6) represents the FRC as a function of the specific lung elastance and the volume responsiveness (compliance) of the patient. The data provided by Bersten [Bersten, 1998] did not include any FRC measurements. However, it did include the dFRC measurements measured by the deflation to ZEEP. These values are graphically represented in Figure 4.4, where FRC is shown as the baseline volume at ZEEP, and dFRC is thus measured relative to an unknown FRC value.

Figure 4.4 shows the dFRC for a low and a high PEEP setting for a given patient. The dFRC is composed of FRC and the additional volume due to PEEP. As PEEP increases from $PEEP_1$ to $PEEP_2$, there is an increase in dFRC. In a recruitment manoeuvre, additional PEEP is applied to re-inflate collapsed alveoli. Once the additional PEEP is removed, some of the re-inflated alveoli remain open and hence dynamic FRC is increased at the original PEEP value. Therefore, physiologically, the change in dFRC represents the ΔFRC plus the change in alveolar recruitment due to PEEP.

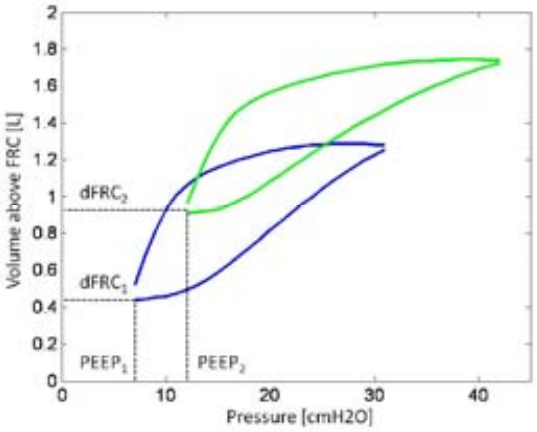

Figure 4.4 - PV curve showing two PEEP levels and the corresponding dFRC level relative to FRC

In this model, the FRC is not known. The effect on FRC from the recruitment manoeuvre is also not known, and typically is quite intensive or difficult to measure in a typical clinical situation. Hence, the aim of this model was to estimate the increase in dFRC due to PEEP.

Thus, this model hypothesises that the dFRC follows similar mathematical form to Equation (4.6). The given PEEP and dFRC in Figure 4.4, correspond to $\Delta V = \Delta dFRC$ and $\Delta P_{aw} = \Delta PEEP$.

$$FRC + dFRC = \frac{\Delta dFRC}{\Delta PEEP} \times \frac{E_{Lspec}}{\alpha}(1 + x) \tag{4.7}$$

Therefore, the dynamic FRC takes the form:

$$dFRC = \frac{\Delta dFRC}{\Delta PEEP} \times \frac{E_{Lspec}}{\alpha} \times x \tag{4.8}$$

where x is a function of the PEEP level at which dFRC is estimated. Because E_{Lspec} and α are relatively constant values [Chiumello et al., 2008], it suggests that these parameters can be lumped into a single parameter β, but of unknown value. Therefore, an alternative model for estimating dFRC is developed:

$$dFRC = \frac{\Delta dFRC}{\Delta PEEP} \times \beta \tag{4.9}$$

where β is a function of the PEEP level, and is labelled as the PEEP stress parameter . It must be noted, the assumption that α remain constant only holds for the linear portion of the static PV curve when elastance does not change significantly. Re-arranging Equation (4.6) to solve for $\Delta dFRC/\Delta PEEP$ (patient compliance), and substituting into Equation (4.9), we can solve for β:

$$\beta = \frac{E_{Lspec}}{\alpha} \times \frac{dFRC}{FRC} \tag{4.10}$$

Equation (4.10) shows β as a function of E_{Lspec}, α, $dFRC$ and FRC. At a given point in time, FRC remains constant. In addition, as discussed previously, E_{Lspec} and α are relatively constant. Thus, at a given point in time, β is only a function of dFRC. Because dFRC is a function of PEEP, this implies that β is a function of PEEP. Thus, the hypothesis used for this model is that for a single value of PEEP, β can be assumed to be constant for all patients.

With PEEP increasing, the dFRC also increases as more recruitment occurs, as seen in Figure 4.4. Thus, β represents the potential for additional recruitment based the given level of PEEP, and also accounts for the level of damage to the lung by taking into account the elastances of the lung and chest wall via E_{Lspec} and α.

In the clinical setting, the dFRC is a parameter that is not normally measured and it is this variable that the model estimates. Because dFRC is a function of PEEP, and β is a function of dFRC, it is possible to combine parameters further, such that β is a function of PEEP. This further manipulation then provides a method to estimate dFRC using a known β and PEEP.

Because FRC was not known for any patient in the clinical data available, β was analytically solved based on Equation (4.9) using the measured dFRC value from the data. Once β values were calculated for each patient at each PEEP value, a median β over all patients was then evaluated for each PEEP level. This median value was then used as a generic population β value for a given PEEP across the entire population. The dFRC was then estimated using this median β value. The overall process is summarised in Figure 4.5.

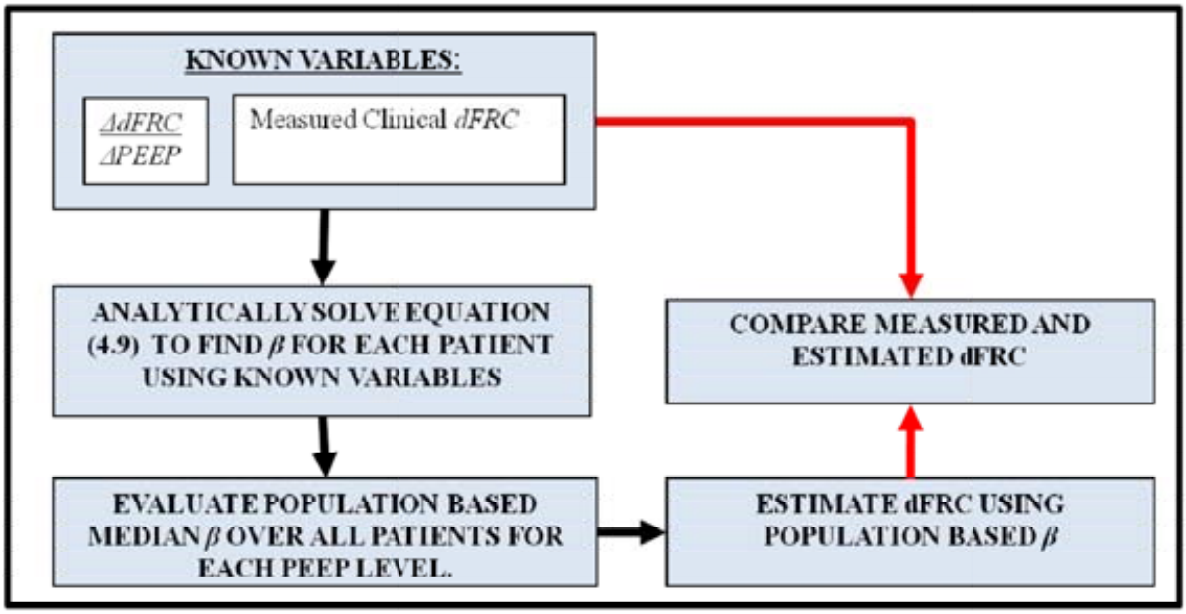

Figure 4.5 - Flow Chart showing the process of dFRC estimation

4.3 ANALYSIS & STATISTICS

The median and interquartile range non parametric statistics were chosen to be the summary statistics to report. Because of the limited number of data points available (N = 39 PV loops to predict from), the distribution of errors was non-Gaussian. In such situations it is better to present the median which is a true representation of the central tendency and the 50th percentile [Micceri, 1989]. As the number of data points increases, the mean value would tend to converge to the median value if the distribution was Gaussian.

The dFRC values that were estimated using the median β value were compared with the actual measured dFRC values to assess the estimate error over the method and the impact of the assumed population constant value of β. A cross correlation test was performed as a preliminary validation with the measured clinical dFRC. The data provided 40 different dFRC measurements at various PEEP levels. Thus, 80% of the data (32 data points) were randomly selected without replacement and the median β value found for each PEEP along with the gradient of β vs PEEP, or $m\beta$.

Using these calculated parameters (β, $m\beta$) from only 80% of the data, the dFRC was then estimated for the remaining 20% of the data. A linear regression was performed by comparing the estimated dFRC with the measured dFRC for the tests sets comprising the

remaining 20% of the data (8 data points). This process was then repeated 100,000 times and summary statistics reported.

This repetition (100,000 iterations) ensures a wide and reasonably exhaustive coverage of possible test (n = 8) and validation (n = 32) sets being examined. This approach eliminates or reduces the potential that random chance or specific patient data sets skewed the results. The overall analysis using test and validation sets serves to statistically validate the general modelling and analysis approach presented.

4.4 PRELIMINARY MODEL VALIDATION

The model was validated using the 12 datasets obtained from Bersten [Bersten, 1998], with the data acquisition process detailed in Chapter 3. Table 4.1 shows the analytical solution of β for each PEEP level over all 12 patients. The median and IQR are shown. The dFRC for each PEEP value was then estimated using the median value of β at that PEEP value, over all patients.

Table 4.1 - Exact and Median Values of β for different PEEP for all patients

PEEP [cm H_2O]		*0*	*5*	*7*	*10*	*12*	*15*
PATIENT	*1*		4.67	7.14		11.79	
	2		6.1	7.96	11.09		
	3		4.96	6.75	9.12	12.23	
	4		2.07	3.58	6.79	8.98	
	5		4.49	6.51	9.5	11.49	
	6		3.15	5.67		10.28	
	7				10.13	12.44	15.17
	8		4.73	7.23	9.75	11.94	
	9		3.85	5.95	8.86		
	10		2.43		6.88		12.43
	11	0.48	5.31		10.48		
	12		2.96	5.25	8		
Median		**0.48**	**4.49**	**6.51**	**9.31**	**11.79**	**13.8**
IQR			**[3.06, 4.85]**	**[5.67, 7.14]**	**[8.22,10.04]**	**[10.89,12.09]**	**[13.12,14.49]**

Table 4.2 shows the percentage error between the clinically measured dFRC and the dFRC estimated with the model-based method and population constant β value. Figure 4.6 shows the general trend of clinical dFRC vs predicted dFRC for a PEEP of 5 cmH_2O across all

patients, yielding $R^2 = 0.712$ (R = 0.845). This relatively low linear trend is attributed to the limited number and range of data points at this one particular PEEP level.

Table 4.2 - Percentage Error of actual dFRC and predicted dFRC for all patients at all PEEP levels

PEEP [cm H_2O]		*0*	*5*	*7*	*10*	*12*	*15*
PATIENT	*1*		3.93	8.86		0.01	
	2		26.44	18.19	16.02		
	3		9.5	3.54	2.13	3.62	
	4		116.52	81.97	37.14	31.24	
	5		0.02	0	2	2.58	
	6		42.65	14.75		14.7	
	7				8.1	5.19	9.02
	8		5.11	9.98	4.53	1.24	
	9		16.69	9.42	5.07		
	10		84.95		35.27		11.04
	11	0.52	15.41		11.19		
	12		51.55	24.06	16.4		
	Median	**0.52**	**16.69**	**9.98**	**9.64**	**3.62**	**10.03**
	IQR	**N/A**	**[7.31, 47.10]**	**[8.86, 18.19]**	**[4.66, 16.30]**	**[1.91, 9.94]**	**[9.52, 10.54]**

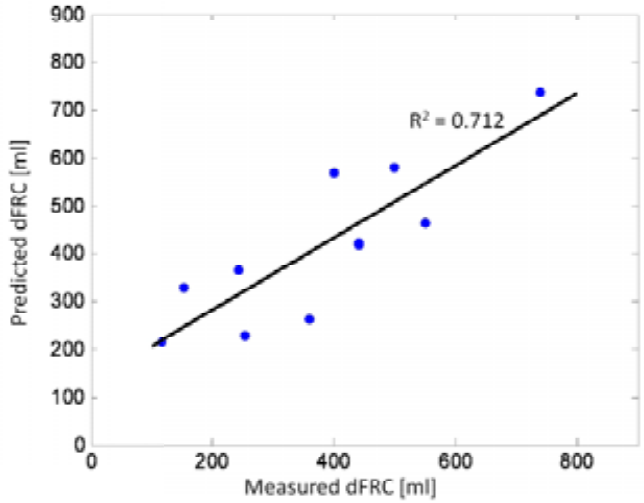

Figure 4.6 - Plot of Clinical dFRC vs Predicted dFRC for all patients with a PEEP of 5 cmH_2O

Figure 4.7, which shows the predicted dFRC versus the measured dFRC across all patients at all PEEP levels shows greater linearity over all PEEP values with $R^2 = 0.947$ (R = 0.973). The relatively lower R^2 value in Figure 4.6 could thus also be attributed to the relatively low range of dFRC values compared to Figure 4.7. Hence, the linear trend in

clinical vs predicted dFRC is sustained over all PEEP values and a very wide range of dFRC.

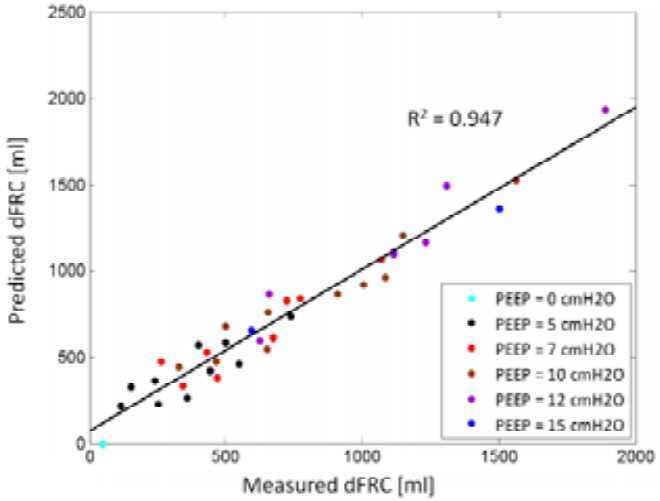

Figure 4.7 - Plot of Clinical dFRC vs Predicted dFRC for all patients for all PEEP values

To show the range of errors for the predicted dFRC, Figure 4.8 shows a Bland Altman plot with a 90% confidence. Although a few points exist outside the interval, the majority of the points are within a 90% confidence interval of the mean indicating that the maximum deviation from measured dFRC is around 200 ml.

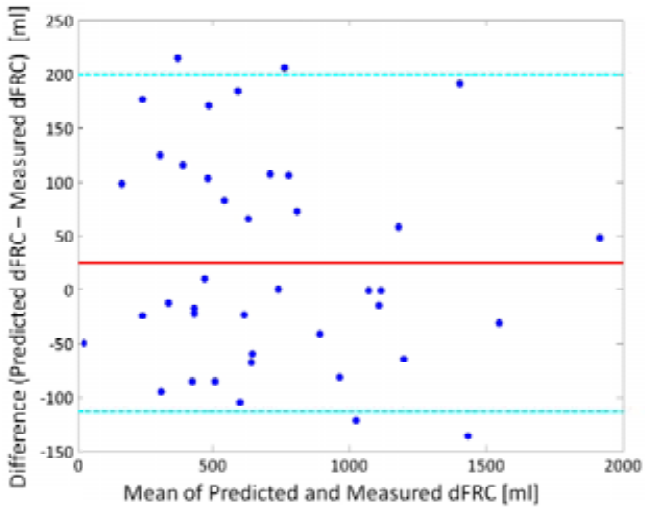

Figure 4.8 - Bland Altman plot of predicted dFRC and measured dFRC. Solid red line is the mean difference and dashed lines represent the 90% confidence interval

The summary statistic and results in the cross validation test are shown in Figure 4.9 and Table 4.3. Figure 4.9 shows the median β across all patients and PEEP levels and clearly shows a linear relationship with PEEP. At a PEEP = 0 cmH_2O, the dynamic FRC value should be zero, and hence the linear relationship between β and PEEP is described as:

$$\frac{\beta}{PEEP} = m\beta \tag{4.11}$$

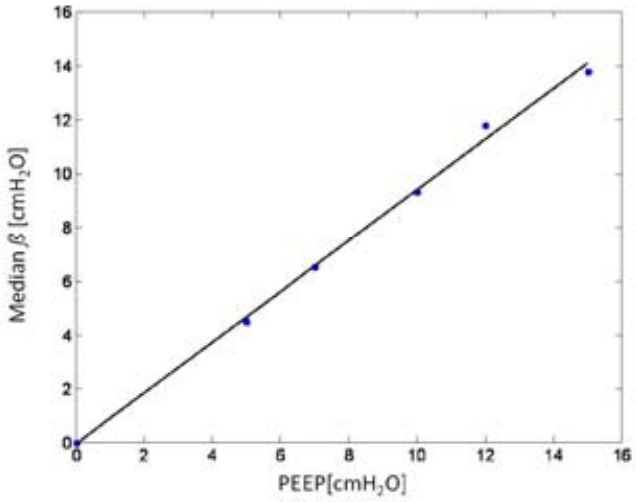

Figure 4.9 - Plot of median beta vs PEEP taken across all data points

Table 4.3 - Median, IQR and 90% Confidence Interval of R^2 correlation coefficient, mβ and β at every level of PEEP

	Median	***IQR***	***90% CI***
R^2 Coefficient	0.944	[0.933, 0.952]	[0.910, 0.960]
Beta Gradient (mβ)	0.953	[0.877, 1.046]	[0.804, 1.164]
Beta at PEEP = 5 cmH_2O	4.065	[3.695, 4.458]	[3.057, 5.020]
Beta at PEEP = 7 cmH_2O	6.257	[5.823, 6.680]	[5.122, 7.233]
Beta at PEEP = 10 cmH_2O	9.074	[8.628, 9.520]	[7.883, 10.190]
Beta at PEEP = 12 cmH_2O	11.371	[10.873, 11.887]	[10.235, 12.230]
Beta at PEEP = 15 cmH_2O	13.8	[12.512, 15.170]	[12.430, 15.170]

Table 4.3 shows the statistical results for the R^2 correlation coefficient between the estimated and actual dFRC. It also shows the value of $m\beta$ across all PEEP values as per Figure 4.9 and the β for each PEEP level. As shown, a 90% confidence interval still produces a very high correlation coefficient. The low variability in $m\beta$ and β indicates the

potential to label them as global population parameters that can be used to describe any patient at a given level of PEEP.

4.4.1 FRC PREDICTION

Equation (4.9) shows that β incorporates *dFRC*, *FRC*, E_{Lspec} and α. One of the potential outcomes of this equation is the ability to calculate FRC. Rearranging Equation (4.9) yields a new equation with FRC as a function of β, *dFRC*, E_{Lspec} and α, and shown below:

$$FRC = \frac{E_{Lspec}}{\alpha} \times \frac{dFRC}{\beta} \tag{4.12}$$

Equation (4.12) provides a new method of estimating FRC provided all other parameters are known. In the model presented in this chapter, β was assumed to be a constant population value for a given PEEP, which provided a value dFRC at that PEEP level. In addition, Chiumello et al reported that ARDS patients have an FRC value of 1013 ± 593 ml, where $\alpha = 0.7 \pm 0.15$ and $E_{Lspec} = 13.6 \pm 4.1$ cmH_2O [Chiumello et al., 2008].

For Patient 1, when $\alpha = 0.7$ and $E_{Lspec} = 13.6$ cmH_2O, the estimated FRC was calculated to be 1833 ml. Chiumello reported that ARDS patients had FRC of 1013 ± 593 ml [Chiumello et al., 2008]. Although the estimated FRC for Patient 1 is slightly higher than the one standard deviation value reported by literature, this could be attributed to the values of α and E_{Lspec} chosen. In addition, 1833 ml is 1.38 standard deviations above the mean, implying that is approximately the 92nd percentile value and within the two standard deviation range of a Bland-Altman plot. Hence, it is an outlying, but not unexpected value.

It must also be noted that the values reported by Chiumello et al are more likely to resemble a log normal distribution. More specifically, the values of 1013 ± 593 ml were reported as the mean and one standard deviation. This would imply that the range of possible FRC values when using two standard deviations, which represents 95% of all the data, would be between -119 and 2199 ml. Because lung volumes cannot take on negative values, the use of a normal distribution is not justified, and the true distribution is more likely to be log normal skewed with a multiplicative standard deviation.

To convert an assumed normal distribution to log normal, the normal mean (μ') and standard deviation (σ') need to be logtransformed to lognormal mean (μ) and standard deviation (σ) using Equations (4.13) and (4.14).

$$\mu = \exp\left[\ln(\mu') - \frac{1}{2}\ln\left[1 + \left(\frac{\sigma'}{\mu'}\right)^2\right]\right] \tag{4.13}$$

$$\sigma = exp\left[\sqrt{\left[\ln\left[1 + \left(\frac{\sigma'}{\mu'}\right)^2\right]\right]}\right] \tag{4.14}$$

When the FRC values of Chuimello et al are transformed (μ' = 1013 ml, σ' = 593 ml), then μ = 874 ml and σ = 1.72. Thus, using a lognormal distribution, the expected range of FRC values within one standard deviation is between 508 and 1504 ml.

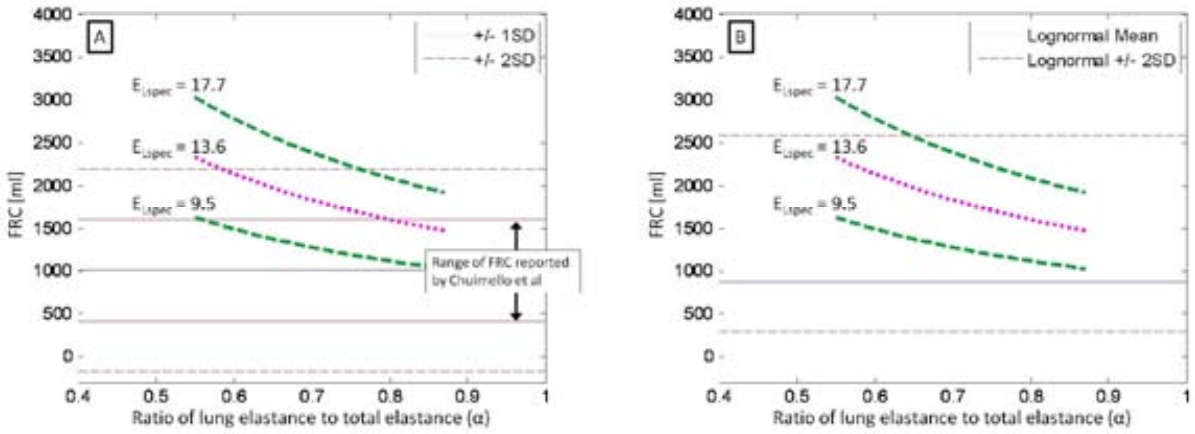

Figure 4.10 - FRC as a function of varying α for Patient 1. Thick dotted line indicates estimated FRC when mean E_{Lspec} is used. (A) Normal distribution range - Thin lines show the +/- 1 and 2 SD from mean as reported by Chiumello et al [Chiumello et al., 2008]. (B) Lognormal distribution range - Thin dotted lines show the +/- 2 SD using lognormal distribution

Figure 4.10(A) and (B) show the effect of varying α and E_{Lspec} on the estimated FRC using a normal and lognormal distribution. Although using the mean values of α and E_{Lspec} yielded an FRC of 1833 ml, Figure 4.10 shows the sensitivity of FRC estimations to the initial estimates of α and E_{Lspec}. For Patient 1, Figure 4.10 indicates that there are a range of values where the estimated FRC fall within the reported range in literature. Thus, the

estimation of FRC is sensitive to the estimate of α and E_{Lspec}. Table 4.4 shows the estimated FRC for all patients when the mean values of α and E_{Lspec} are used, and also shows the number of standard deviations away from the normal and log normal mean. Plots of estimated FRC when α and E_{Lspec} are varied are shown in Appendix A.

Table 4.4 - Estimated FRC for all patients when α = 0.7 and E_{Lspec} = 13.6 cmH_2O, and the number of standard deviations using a normal and log normal distribution.

			Number of SD's away from Mean	
		Estimated FRC [mls]	Mean = 1013 ml (Normal)	Mean = 874 ml (Lognormal)
PATIENT	*1*	1833	1.38	1.37
	2	1141	0.22	0.49
	3	989	-0.04	0.23
	4	1426	0.70	0.90
	5	3193	3.68	2.39
	6	2470	2.46	1.92
	7	1923	1.53	1.45
	8	1811	1.35	1.34
	9	2520	2.54	1.95
	10	931	-0.14	0.12
	11	2010	1.68	1.54
	12	1591	0.97	1.10
	Median	1822	1.36	1.35

4.5 MODEL DISCUSSION

The ability to use lung stress and strain as a proxy produces a reasonable estimate of dFRC. For the clinical data set used, the results indicated that β increased linearly as a function of PEEP. Chiumello et al [Chiumello et al., 2008] indicated that the ratio of lung elastance to total respiratory elastance (α) varied between 0.33 and 0.95 over various PEEP settings. Gattinoni et al showed that the respiratory mechanics may vary significantly in patients depending on whether the ARDS originated from pulmonary or extrapulmonary disease [Gattinoni et al., 1998]. They concluded that, depending on the origin of ARDS, the total respiratory elastance could increase or decrease as a function of increasing PEEP. However, interestingly, no significant changes for β occurred in this study, as in [Chiumello et al., 2008], implying that E_{Lspec} and α are interdependent on each other, but constant in that ratio.

In this analysis, β incorporates the dFRC, FRC, E_{Lspec} and α according to Equation (4.10). Hence, as β increases, the value of dFRC also increases linearly, which means that β can be used as a potential metric to track dFRC. Another implication of this model is the potential ability to estimate true FRC. According to Equation (4.12), FRC is related to the value of β, α, E_{Lspec} and dFRC at a given PEEP. When the mean of α = 0.7 and E_{Lspec} = 13.6 cmH_2O are used to estimate FRC, the median value across all patients is 1822 ml. Although this was slightly higher than what is reported in the literature, it is still within two standard deviations.

In reality, the value of α and E_{Lspec} vary and FRC can thus also take on a range of values. This was shown for Patient 1 in Figure 4.10, and highlighted the sensitivity of the estimated FRC with regard to α and E_{Lspec}. Although the estimations of FRC may not be accurate, measuring the change in FRC can still yield useful information. In particular, by tracking estimated FRC daily, or more frequently, the clinician can use the changes in FRC as an indicator of when to begin weaning a patient from ventilation.

Chiumello defined the specific lung elastance as the transpulmonary pressure at which FRC doubles [Chiumello et al., 2008] and measured E_{Lspec} using the supersyringe technique and inflating the lungs with an additional volume equal to FRC. Using the dFRC estimation model, when dFRC equals FRC, the volume of the lung has essentially doubled (total lung volume equalling FRC plus dFRC), and this results in a β value of 19.4 cmH_2O (using average values for α = 0.7, E_{Lspec} = 13.6 cmH_2O). Using the median value for $m\beta$ shown in Table 4.3 and Equation (4.11), the PEEP that produces this β value is calculated to be 20.4 cmH_2O. According to Equation (4.2), this corresponds to an equivalent transpulmonary pressure of 14.3 cmH_2O. In this study, the value of E_{Lspec} is therefore evaluated to be 12.9 cmH_2O which falls within the limits found by [Chiumello et al., 2008], as a form of further validation.

Although this is not the exact value, the difference in specific lung elastance values could arise from the fact that different data sets were used. This study used data from Bersten [Bersten, 1998] with patients who had severe ARDS. In Chiumello's study, the specific lung elastance in ARDS patients had a range from 9.5 to 17.7 cmH_2O. The value obtained in this study falls within this reported range for ARDS patients. Secondly, Bersten reported P_aO_2/F_iO_2 values as low as 66. However, the ranges reported by Chiumello for ARDS patients had a minimum value of 83. This difference could also cause the specific lung

elastance to be slightly higher, as the more significant the ARDS, the more applied pressure required for doubling the FRC.

4.6 MODEL LIMITATIONS

Although the method predicts dFRC, there are some significant limitations to its predictive capability. At lower PEEP, the error for predicted dFRC was shown to be as high as 120%, as shown on Table 4.2. As PEEP increased, the percentage error dropped, but some patients still exhibit a difference of about 200 ml between measured and predicted dFRC. At lower PEEP, a difference of 200 ml and can cause the predicted dFRC to be very different than true dFRC. Despite a high R^2 value shown in Figure 4.7, the predicted value either over states or understates the amount of potential lung volume that is being recruited. In the case of the lower PEEP settings, a large prediction error therefore can limit the potential estimator method. However, even though an estimate of dFRC can have an error of up to 120%, the model still more accurately identifies the relative changes on dFRC due to PEEP. With respect, to Table 4.1, Patient 6 yielded the highest error in estimated dFRC. Examining Figure 4.11, both the estimated and measured dFRC for this patient respond in the same way to PEEP, implying that although absolute volume measurements are inaccurate, the trends are still evaluated.

Another limitation with this model is the assumption E_{Lspec} and α being constant. This assumption only holds during the linear portion of the static PV curve. The linear portion of the static PV curve is where most of the data points occur on any measured dynamic PV loop. The PV curves obtained from Bersten [Bersten, 1998] indicated that over 90% of the data points occurred in the linear portion of the static PV curve. The non-linear portions at PEEP and PIP are actually high flow regions and thus do not account for or include the majority of the data. This point is further highlighted by assuming that $\Delta dFRC/\Delta PEEP$, effectively the compliance, does not change as a function of PEEP. An estimate of the static PV curve was plotted using the points of zero flow from each of the PV loops, and is shown in Figure 4.12. A linear line of best fit was plotted and the R^2 coefficient was computed to show if the estimated static PV curve was linear or non linear showing there, and in Table 4.5, that the linear assumptions and data points used hold almost exclusively.

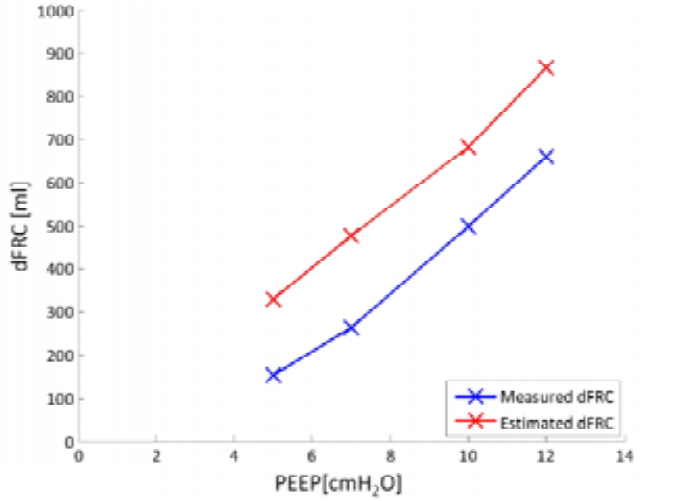

Figure 4.11 - Measured and estimated dFRC for Patient 6. Although the percentage error is high, the estimated dFRC can still pick up the trend due to PEEP application

Table 4.5 - Linearity of static PV curve for each patient

Patient	R^2	Patient	R^2
1	0.9977	**7**	1
2	0.9998	**8**	0.9971
3	0.9995	**9**	0.9978
4	0.9981	**10**	0.9972
5	0.9885	**11**	0.9998
6	0.9975	**12**	0.998

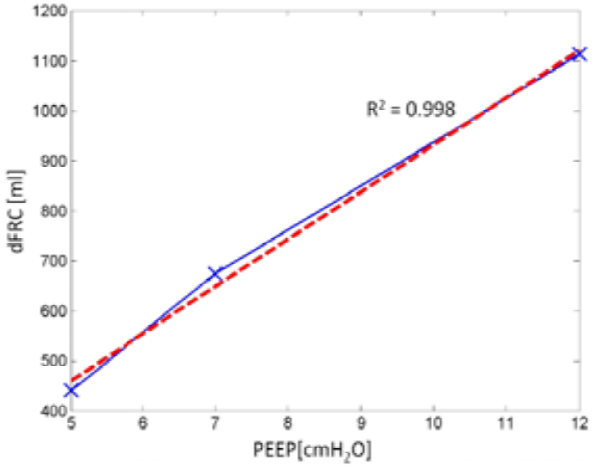

Figure 4.12 - Estimate of the static PV curve for patient 1 using points of zero flow

Finally, the data used in this study is idealised. In each case, the PEEP is held for 30 minutes before any sampling was done. In a clinical setting, holding two or three PEEP

settings for 30 minutes to measure *ΔdFRC/ΔPEEP* is not practical. Thus, the model may be limited in clinical use Therefore, for clinical application, the *ΔdFRC/ΔPEEP* would have to be estimated without the 30 minute hold on PEEP, and can be achieved if a recruitment manoeuvre is used.

4.7 SUMMARY

The model uses 2 parameters to estimate the dFRC for a given PEEP. The parameters are β and $m\beta$, where $m\beta$ is the gradient of the line of β vs PEEP. Cross correlation and validation showed very tight ranges for each value of R^2 over PEEP. This result implies that β and $m\beta$ can be used as universal population parameters across all PEEP levels to estimate the dFRC and its change for a given PEEP, as well as for any ARDS patient.

However, the limited number of datasets used in this validation implies further validation is required to justify β and $m\beta$ as population constants. To ensure that the parameters are true population constants, a larger dataset is required. In addition, the potential for the model to predict FRC must also be similarly further investigated. Thus, there is a requirement for further clinical trials to investigate this model. The following chapters examine the study design for a series of clinical trials and will examine the clinical viability of the recruitment model and the dFRC model.

Chapter 5 - Study Design

Prior to any intervention within the ICU, ethics approval is required to ensure that the protocols used in clinical trials are safe. To develop adequate protocols, the objectives of the clinical trials need to be fully clarified. The purpose of the trials was to validate the models of lung mechanics developed and presented in this thesis. More specifically, the trials aim to examine the clinical viability of the recruitment and dFRC estimation models.

5.1 TRIAL OBJECTIVES

The general objective of the trials was to use clinical data to validate mathematical models. However, to ensure that the trials were effective, a more specific set of objectives were required. The goal was to ensure that any protocol developed was optimised to provide the most clinical information possible.

5.1.1 RECRUITMENT MODEL

The recruitment model discussed in Chapter 3 highlighted the importance of PEEP as a clinical parameter to optimise. In particular, the problem of how much PEEP is the primary motivation to develop these model-based approaches. The recruitment model requires PV curves as inputs to determine the recruitability of the patient.

The preliminary validation performed using data obtained from Bersten [Bersten, 1998] used PV loops from PEEP values ranging from 5 to 15 cmH_2O. At most, a patient did not have more than four PV curves to fit in the model. In addition, the study did not use a recruitment manoeuvre to obtain PV curves. Rather, 30 minutes of sustained PEEP was applied with the resulting PV data obtained at each level.

The first objective of these clinical trials was to examine how individual patient's responded to a given level of PEEP in a clinically realistic setting. In addition, the effect of different PEEP values on a patient's recruitability, or ability to recruit with PEEP, was required to examine how a patient-specific response could be determined. These criteria led to the development of the first part of the study. It was decided that the first part of the

study would use a recruitment manoeuvre to obtain PV curves at various levels of PEEP. The use of the recruitment manoeuvre would ensure that the process of obtaining PV loops could be done in a more clinically realistic and shorter timeframe than Bersten [Bersten, 1998]. Simultaneously, multiple PV loops could be recorded to allow the model to evaluate the effect of recruitment at different PEEP values.

The initial model validation performed in Chapter 3 indicated that the recruitment model has the ability to predict and quantify alveolar recruitment. Because the model captures the total lung capacity (TLC) for a patient, the effect of PEEP on alveolar recruitment can be quantified. In effect, the model calculates the total number of alveolar units recruited with respect to the TLC.

Various studies have shown that recruitment can be accurately measured using CT scans [Gattinoni et al., 2001, Lu et al., 2006, Malbouisson et al., 2001, Rouby et al., 2003]. Thus, a second objective is to correlate the recruitment measured from CT scans with the model output if possible. In particular, CT scans at various PEEP levels will be required to correlate the recruitment at different PEEP, where patient consent and ethical considerations do not prohibit them.

5.1.2 DYNAMIC FRC (DFRC) MODEL

The dFRC estimation model introduced in Chapter 4 examined the effect of PEEP on pulmonary volume. In particular, the model used a population constant, the PEEP stress parameter (β), and used an estimate of static linear compliance to estimate dFRC for a given patient at a set level of PEEP. As discussed previously, the data used in the initial validation only ranged from 5 to 15 cmH_2O. Although the model showed high linearity between β and PEEP, two major problems need to be addressed. First, for β to be a true population constant, a larger dataset is required for validation. Second, the low levels of PEEP in the validation do not indicate how β behaves at higher levels of PEEP.

The third objective is to examine the effect of higher PEEP on dFRC and increase the size of the population on which β is based on. Thus, to provide further validation of the dFRC model, the recruitment manoeuvre needs to include true dFRC measurements and also include higher PEEP values. Finally, the dFRC model was also shown to have the ability to potentially predict FRC non-invasively. Because FRC can be measured using CT scans

[Gattinoni et al., 2001, Malbouisson et al., 2001, Gattinoni et al., 1995], the CT scans obtained will also be used to validate the FRC prediction, where possible.

The four objectives discussed form the basis of the study and provide a platform to design a set of clinical trials. Essentially, the trial consists of two parts; (1) a specialised recruitment manoeuvre, and (2) CT scanning with a recruitment manoeuvre occurring simultaneously. The trial objectives are outlined in Table 5.1. It is important to note that ethical considerations limit CT scans in some patients, so the CT scan correlation will not occur for all patients.

Table 5.1 - Study objectives and corresponding clinical trial required

Study Objective	Trial Required
1 *- Examine patient recruitability using the lung mechanics model*	Recruitment Manoeuvre
2 *- Correlate alveolar recruitment between recruitment model and CT scans*	CT Scan Correlation
3 *- Validate dFRC model and increase dataset for population constant*	Recruitment Manoeuvre
4 *- Correlate predicted FRC with measured FRC*	CT Scan Correlation

5.2 PROTOCOL DEVELOPMENT

While meeting the objectives for the study, the clinical trial protocols must also be safe. All protocols developed must be approved by the New Zealand Upper South Island A or B Regional Ethics Committee. The following section discusses the evolution of the protocols developed both for the recruitment manoeuvre and the CT scanning parts of the study, and the ethics considerations encountered.

5.2.1 RECRUITMENT MANOEUVRES

For patients involved in the study, it was decided that a recruitment manoeuvre would be required. This would allow clinicians to recruit an already ill patient, while simultaneously acquiring data for the study. The primary objective of a recruitment manoeuvre is to re-inflate collapsed alveoli. This outcome is achieved by using periodic higher pressure manoeuvres with moderate levels of PEEP to change the visco-elastic strain state of ARDS affected alveoli so they will subsequently open at lower pressures, aiding recruitment [Gattinoni et al., 2006, Lapinsky and Mehta, 2005, Moran et al., 2003]. The overall, clinical result of this additional recruitment is a beneficial effect on oxygenation with the

presence of adequate PEEP, as well as preventing the de-recruitment of existing lung units [Lapinsky and Mehta, 2005].

Various forms of recruitment manoeuvres exist [Lapinsky and Mehta, 2005]. A common method of recruiting patients is by using sustained high pressure inflation with airway pressures between 35 and 50 cmH_2O for a duration of 20 to 40 seconds [Amato et al., 1998]. However, this method does not apply incremental PEEP during the manoeuvre and may not result in beneficial outcomes.

The intermittent sigh method is also used as a method to recruit patients [Pelosi et al., 2003]. A sigh is a breath with higher tidal volume than conventional breaths. In practice, the method uses 3 intermittent sighs, which produces sufficient pressure to recruit alveoli. However, any beneficial effect on oxygenation was shown to be short term [Pelosi et al., 2003]. In addition, the sigh method does not reflect PEEP changes.

Finally, intermittent increases in PEEP can be used as a recruitment manoeuvre with peak airway pressures of up to 45 cmH_2O [Gattinoni et al., 2006]. In this method, PEEP is increased for a few breaths and peak airway pressure is increased. Because this method involves the direct application of PEEP, this type of manoeuvre is appropriate for this study.

Conventional PEEP recruitment manoeuvres use a single intermittent PEEP value. The primary data required for this study comprises of PV data at different PEEP levels. Thus, the recruitment manoeuvre was modified to allow an incremental PEEP trial that would allow multiple PV curves to be obtained at different levels of PEEP.

5.2.2 CT SCANS

The use of CT scans in quantifying alveolar recruitment and measuring FRC have been shown to be an important research tool. Several studies have used CT scans with success [Gattinoni et al., 2001, Gattinoni et al., 1995, Lu et al., 2006, Malbouisson et al., 2001, Rouby et al., 2003]. More importantly, they have successfully correlated alveolar recruitment to CT scans, as well as providing the ability to measure FRC.

FRC MEASUREMENT

The analysis of CT scans utilises the attenuation of individual pixels, as discussed in Chapter 1. Each pixel is assigned a particular attenuation or Hounsfield Unit (HU) [Vieria et al., 1999]. Performing an analysis on a scan and interpreting the HU attenuation can yield information on the level of gas in the lung. To measure the FRC of a lung, a full lung CT scan is required starting from the apex to the diaphragm at ZEEP [Gattinoni et al., 2001, Malbouisson et al., 2001]. Typically, a high resolution spiral CT scanner is used to obtain a full lung CT, which is both highly invasive, radiation intensive, and time and resource intensive.

In a full lung CT, the entire image is made up of several slices of CT scans of known thickness. Each slice is made up of voxels, a unit of volume measurement. Because individual voxels have different HU attenuation, it is possible to determine if the voxel contains gas or lung tissue. In a given slice, the total number of voxels can be calculated, and then multiplied by the slice thickness to determine the volume of gas in a slice. This process is then repeated across all the CT slices, and the total gas volume is summed to determine the FRC [Gattinoni et al., 2001, Malbouisson et al., 2001]. Hence, using enough slices, a highly accurate assessment of FRC and recruitment can be made, even for a highly heterogeneous ARDS lung.

ALVEOLAR RECRUITMENT

The analysis of voxel attenuation can also be used to determine the level of PEEP induced alveolar recruitment. Currently, two different approaches are used to quantify recruitment using CT scans [Gattinoni et al., 2006, Malbouisson et al., 2001]. The method by Malbouisson et al [Malbouisson et al., 2001] uses a similar approach as the FRC measurement. A full spiral CT is obtained at PEEP conditions and the resulting gas volume is compared to FRC to evaluate the PEEP induced recruitment.

In contrast, alveolar recruitment can also be evaluated using single slice scans. The study by Gattinoni et al used a single slice CT located 1 cm above the diaphragm [Gattinoni et al., 2001]. The change in non-aerated lung volume between PEEP and ZEEP conditions for a given slice is then used to evaluate alveolar recruitment.

The single slice method and the full lung CT method each have unique advantages and disadvantages. Obtaining a high resolution full lung CT scan can provide a more accurate estimation of alveolar recruitment [Malbouisson et al., 2001], and also provide a measurement of FRC. However, the high resolution scanner may expose patients to unnecessarily high radiation doses. In addition, such scans are also very time and resource intensive.

In comparison, a single slice need not be high resolution and provides a less intensive dose of radiation. However, the single slice method cannot measure FRC. In addition, it is by nature less accurate, particularly in a heterogeneous lung, and thus can underestimate or overestimate the level of recruitment. These issues are fundamentally due to the fact that the single slice does not consider recruitment across an entire, heterogeneous ARDS lung.

The specific research objectives of a study decide what CT course should be used. For this research, the use of an appropriate CT protocol depends on the following criteria:

- Measurements required for validation (Performance Factor)
- Resolution of measurements required (Performance Factor)
- Acceptable level of radiation exposure for patient (Safety Factor)

These three metrics thus balance the performance required from the measurement, and patient safety or risk. To satisfy the three criteria for patients receiving a CT scan, it was decided that a full lung CT scan would be obtained at ZEEP, followed by three single slice scans at various PEEP values. This approach would allow the measurement of FRC that was required, while also allowing the scans to assess PEEP induced recruitment. With respect to patient safety, avoiding four full high resolution lung CT scans, the radiation dose delivered to the patient is minimised, while still being able to achieve the objectives of the study outlined in Table 5.1.

5.2.3 ETHICAL CONSIDERATIONS

The study was submitted for consideration by the New Zealand Upper South Island A Regional Ethics Committee. Although the study was split into two sections, the ethics committee was satisfied with the safety and recruitment manoeuvre, as they are well documented in the literature [Amato et al., 1998, Lapinsky and Mehta, 2005, Moran et al.,

2003, Pelosi et al., 2003]. The primary concern from the ethics committee was with regard to the radiation dose and risks associated with the proposed CT scans.

The main objection from the ethics committee revolved around a study published by Brenner and Hall [Brenner and Hall, 2007]. The study examined the effects of radiation doses from CT scans on the future of public health in the United States. In particular, the study compared the radiation dose delivered from CT scans compared to conventional x-rays and concluded that although the individual risks are minimal, the aggregate effect on the population will cause a public health problem in the future. The study also argued that due to the increased risk of cancer, clinicians should avoid unnecessary CT scans whenever possible.

Because the research study presented in this thesis was the first of its kind in New Zealand, and only a few have been done elsewhere [Gattinoni et al., 2001, Malbouisson et al., 2001], there was no set standard for the ethics committee to determine how much radiation is too much. The committee thus requested the following information:

- A comprehensive analysis on the science of radiation dosage from CT scan systems
- An experimental method to limit the exposure from radiation to patients

THE SCIENCE OF RADIATION

A common measure of effective radiation dose is the millisieverts (mSv). This measure of radiation is used when the distribution of radiation is not homogeneous, as the case with CT scans. The effective dose allows for a rough comparison between different CT scenarios, but provides only an approximate estimate of the true risk.

The effective dose from the four CT scans proposed in this study, as estimated by the Medical Physics & Bioengineering Department at Christchurch Hospital, was calculated as 10.2 mSv. The International Commission on Radiological Protection (ICRP), an advisory board providing recommendations and guidance on radiation protection, approximates that the increase in fatal risk of cancer is 5% per 1000 mSv [ICRP, 2008]. Thus, the doses delivered in this study would, linearly analysed, attribute to a 0.05% increase in cancer risk.

The main problem with the methods of examining risk through radiation is the ongoing debate between the uses of the linear no threshold model (LNT) [NCRP, 2002, Preston,

2003] and radiation hormesis model [NCRP, 2002, Feinendegen, 2005, Feinendegen and Pollycove, 2001, Tubiana, 2005]. The two models are different ways of approximating the damage caused by ionising radiation. The LNT model suggests that the damage by ionising radiation is linear and directly proportional to the dose. In contrast, the radiation hormesis model suggests that below a certain threshold, radiation exposure can be beneficial or have no harm [Cohen, 2008, Feinendegen, 2005, Tubiana, 2005], which is a non-linear, dose dependent approach. More specifically, low dose radiation may cause positive genetic traits to develop and protect against cancer [Feinendegen and Pollycove, 2001], while extremely higher doses could cause harm. This model is shown schematically in Figure 5.1.

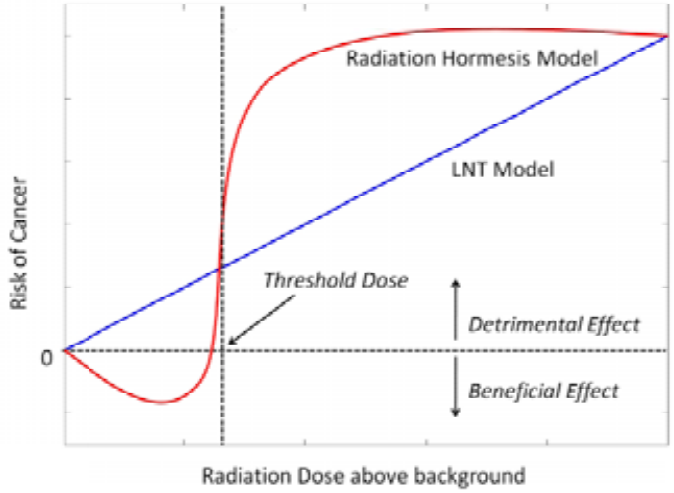

Figure 5.1 - Risk of Cancer vs Radiation Dose for LNT (blue) and Radiation Hormesis model (red). Radiation hormesis shows beneficial impact of low dose radiation

These conflicting models are a result of a lack of data with respect to radiation damage. The majority of evidence comes from studies looking at the effects of Hiroshima and Nagasaki bomb survivors, from patients who have received large doses for medical purposes, and miners exposed to high levels of radiation [Preston, 2003]. These studies support the LNT model but are, importantly, limited to high dose cases where the 2 models might well be similar in prognosis. Crucially, studies examining the effects of low dose radiation at a cellular level [Feinendegen and Pollycove, 2001] support the hormesis model.

IMPACT ON STUDY DESIGN

Although the LNT model is widely accepted, there is still a strong push in the field to adopt the radiation hormesis model [Cohen, 2008]. Because of the conflicting evidence from the two models, the ethics committee approved the CT study, with the following restrictions:

- Only patients who were scheduled for a CT scan for other clinical reasons were eligible for the CT part of the overall study
- Patients who had a cumulative radiation exposure greater than 20 mSv per annum (for the current year) or 100 mSv over 5 years prior to the study were excluded.

The value of 20 mSv per annum was defined to be the upper limit of exposure that a patient could receive. This is the value recommended by the ICRP [ICRP, 2008], and adopted by the New Zealand Ministry of Health [NRL, 2009], on the maximum allowable dose for occupational radiologists and medical radiation technologists (MRT).

Because no similar study using CT had been previously performed in New Zealand, this application and resulting limit on radiation exposure was the first to set a standard on radiation dose. The Upper South Island A Regional Ethics Committee approved this study with these amendments.

5.3 METHODOLOGY & PROTOCOLS

The goal of this research was to recruit up to 10 MV patients receiving treatment in the Christchurch Hospital ICU. All patients enrolled in the study underwent a recruitment manoeuvre over different levels of PEEP. If eligible, patients were then transported to the CT scanner for four lung CT's. The following sections discuss the inclusion and exclusion criteria for patients, and specific protocols used to adjust PEEP.

5.3.1 PATIENT SELECTION CRITERIA

INCLUSION CRITERIA

1. Patients on MV therapy.
2. All recruited patients were to be over the age of 16.

3. Patients were included in trial if PF ratio was between 150 and 300 mmHg on the day of consent. Patients who have a PF ratio, partial pressure of arterial oxygen (P_aO_2) divided by the fraction of inspired oxygen (F_iO_2), between 200 – 300 mmHg are defined as ALI. PF ratios below 200 mmHg are defined as ARDS. Patients with a PF ratio less than 150 mmHg were deemed too unwell for inclusion.

EXCLUSION CRITERIA

1. Patients who were likely to be discontinued from MV therapy in 24 hours.
2. Patients who were moribund and/or not expected to survive for greater than 72 hours
3. Patients who were not disorientated in time, place or person. These patients were excluded as they would have required additional sedation, which may have prolonged their length of stay.
4. Patients with asthma were excluded.
5. Patients who had significant brain injury. The application of high airway pressures can increase blood pressure in the brain that could have proved harmful.
6. Women less than 45 years were excluded for the CT part of the study to mitigate any added risk of breast cancer
7. Patients who had already received 20 mSv through medical radiation in the last twelve months or would receive a cumulative radiation dose of ≥ 20 mSv (over a 12 month period) as a result of the additional study scans, were excluded from the CT section of the study.
8. Patients who had already received 100 mSv through medical radiation in the last five years or would receive a cumulative radiation dose of ≥ 100 mSv (over a 5 year period) as a result of the additional study scans, were excluded from the CT section of the study.

5.3.2 TRIAL SETUP

Because patients were sedated, consent was obtained on behalf of the patient by immediate family members only. If patients recovered later, then they would provide final consent on the use of the data. Consented patients were sedated, or sedated and paralysed using muscle relaxants, to prevent spontaneous respiratory efforts. The patient's initial ventilator

settings, plateau pressure at end expiration, tidal volume, and initial PEEP setting were all recorded.

All patients were ventilated using volume controlled mode, synchronised intermittent mandatory ventilation (SIMV) while the study was conducted. SIMV sets the tidal volume, with the airway pressure dependent on the patient's condition. The tidal volume was selected by the clinician treating the patient and was not changed for the duration of the measurements. However, if the patient was already on a volume controlled mode, then tidal volume was not directly set by the clinician. If a patient was on pressure controlled ventilation, they were switched to SIMV. The measured tidal volume of the pressure controlled mode was then used to set the mandatory tidal volume of the SIMV mode.

Patients who were spontaneously breathing were put on SIMV mode and given additional sedation to synchronise their respiratory efforts with the ventilator. In addition, muscle relaxants were used if the patient was unaware of their surroundings. Patients were sedated with propofol and rocuronium bromide (ROC) was the preferred relaxant.

All patients in the study underwent a protocolised recruitment manoeuvre with the airway pressure and the volume data collected. Heart rate, blood pressure and body temperature were also recorded. Before the recruitment manoeuvre and 30 minutes post manoeuvre, an arterial blood gas was taken to measure the PF ratio. This measurement was used to evaluate any changes on blood oxygenation.

Patients were ventilated using a Puritan Bennett PB840 ventilator (Covidien, Boulder, CO, USA) in the Department of Intensive Care, Christchurch Hospital, New Zealand. A Hamilton Medical flow sensor (Hamilton Medical, Switzerland) was attached to the y-piece of the tubing and connected to a calibrated pneumotachometer. The pneumotachometer was used to obtain the pressure and flow measurements, and could capture the volume changes due to PEEP. A standard Dell™ (Dell, Austin, TX, USA) laptop was used in conjunction with the software Labview Signal Express (National Instruments, Austin, TX, USA) to obtain the raw measurements and store it in a text file. Raw data was then processed with the aid of Matlab 2009 (The Mathworks, Natick, Massachusetts, USA) for use with the model.

5.3.3 STUDY PROTOCOLS

The protocol used in this study was based on the work by Gattinoni et al [Gattinoni et al., 2006], but was modified to satisfy the objectives of this study. The protocol involved a PEEP trial, with PEEP incremented in steps of 5 cmH_2O and peak airway pressure limited to 45 cmH_2O. Two individual protocols were developed for the recruitment manoeuvre without and with the added CT scans. In addition, an expiratory and inspiratory hold was performed to measured auto-PEEP and inspiratory resistance respectively. Once the maximum PEEP was achieved, PEEP was decremented in steps of 5 cmH_2O until PEEP was back to the initial setting.

PROTOCOL 1 – RECRUITMENT MANOEUVRE ONLY

In this protocol, once all the equipment was connected to the patient's breathing circuit, the clinician deflated the patient to ZEEP. Next PEEP was incremented by steps of 5 cmH_2O and PV curves obtained. Once maximum PEEP ($PEEP_{max}$) was achieved, such that airway pressure was equal to 45 cmH_2O, the clinician then decremented PEEP in steps of 5 cmH_2O until the ventilation settings was restored back to the patient's initial settings. Table 5.2 summarises this protocol.

Table 5.2 - Recruitment manoeuvre protocol

	Process
1 -	Pneumotachometer is attached to the 'Y' connector of the patient's ventilation circuit. System is tested
2 -	Deflate to ZEEP, and then carry out 5 more PV loops.
3 -	Hold ventilation in end expiration for 20 seconds to determine Auto-PEEP for the final breathe
4 -	Hold ventilation in end inspiration for 20 seconds to determine circuit resistance for the final breathe
5 -	Apply 5 cmH_2O PEEP and carry out 5 PV loops with tidal volume of 500ml (or set to the patient's previous setting, whichever is the lesser). This data will be captured. *This tidal volume will remain constant for the duration of the study.*
6 -	Apply an additional 5 cmH_2O PEEP to the last PEEP value used and carry out 5 PV loops.
7 -	Repeat step 6 until peak airway pressures reach 45 cmH_2O and $PEEP_{max}$ is thus found
8 -	Decrement PEEP in steps of 5 cmH_2O until initial PEEP setting is achieved

PROTOCOL 2 – RECRUITMENT MANOEUVRE WITH CT SCAN

This part of the study included a set of CT scans, while simultaneously performing a recruitment manoeuvre. Thus, at least three and a maximum of four, CT scans were to be obtained. Because each patient exhibited a different $PEEP_{max}$, the level of PEEP where CT scans could be obtained was different for each patient. Thus, a patient who has a $PEEP_{max}$ of 15 cmH_2O may have CT scans at different levels of PEEP compared to a patient who has a $PEEP_{max}$ of 35 cmH_2O. Depending on the value of $PEEP_{max}$, the PEEP where CT scans were obtained would vary. Table 5.3 shows the PEEP levels where CT scans are to be obtained depending on the $PEEP_{max}$.

The PEEP values where CT scans needed to be obtained had to be determined before the patient was transported to the radiology department, ensuring no time was wasted while in the CT scanner. Prior to moving the patient, the clinician would determine $PEEP_{max}$ by increasing PEEP until peak airway pressure was 45 cmH_2O. For example, if the clinician determined that $PEEP_{max}$ was 18 cmH_2O, then CT scans would be obtained at PEEP values of 0, 5, 10 and 18 cmH_2O according to Table 5.3.

Table 5.3 - PEEP level where CT scans are obtained depending on $PEEP_{max}$

$PEEP_{max}$	PEEP level of CT scan			
6 to 10	0	5		10 or $PEEP_{max}$
11 to 15	0	5	10	15 or $PEEP_{max}$
16 to 20	0	5	10	20 or $PEEP_{max}$
21 to 25	0	10	15	25 or $PEEP_{max}$
26 to 30	0	10	20	30 or $PEEP_{max}$
31 to 35	0	15	25	35 or $PEEP_{max}$
36 to 40	0	20	30	40 or $PEEP_{max}$

Once $PEEP_{max}$ was determined, the patient was transported to radiology, positioned in the scanner, and the protocol outlined in Table 5.2 was performed. The only modification was when the patient was deflated to ZEEP, during the expiratory hold, a full lung CT would be performed from the apex to the diaphragm. Additionally, single CT scans would be

obtained at the predetermined PEEP levels. At the completion of all scans, the patient was then transported back to the ICU for regular care.

5.4 SUMMARY

This chapter discussed the evolution of the study design and related ethical considerations. In particular, until now, no formal benchmarking has occurred when subjecting patients to additional CT scans. However, the research presented in this chapter indicated that the current theories regarding radiation risk are divergent and far from conclusive. This result has lead to the first formal benchmark dose that patients are allowed to receive in New Zealand. This formal upper limit is a step in making CT and other radiation related studies a more standardised practice in New Zealand.

The recruitment manoeuvres and protocols described provide a platform to analyse PV curves and validate the models structure and its clinical function as well. The recruitment manoeuvres used were based on prior, well regarded studies of lung function. These study protocols were modified only to optimise this study to validate the model-based methods presented.

Chapter 6 - Recruitment Model Validation

Ten patients were recruited to take part in this study, of which two patients underwent multiple clinical trials on different days. This chapter examines the results of the clinical trials and discusses the clinical implications of model-based approaches to help select patient-specific ventilation settings. In specific, the recruitment model was tested on patient data and a process of optimal PEEP selection is discussed.

Although the initial validation performed in Chapter 3 showed the behaviour of threshold opening pressure (TOP) and threshold closing pressure (TCP) as a function of PEEP, that study did not specifically address how these metrics can be used to select optimal PEEP. It was seen that the shape of the mean shifts can give an indication as to which level of PEEP to use in ventilation therapy. In essence, the TOP and TCP mean shifts can yield information on patient recruitability and how patients respond to PEEP. However, no specific approaches were put forward on that data.

In addition, the study in Chapter 3 was highly linear. TOP and TCP showed strong linear trends with respect to PEEP. However, the linear trend could be attributed to the small range of PEEP used. To completely validate the recruitment model, and create a robust means of determining PEEP, a larger range of PEEP is required to be tested.

6.1 METRICS

6.1.1 METRICS FOR PEEP DECISION SUPPORT

TOP

To optimise PEEP, the clinician must have the ability to assess how recruitable a patient is with respect to PEEP. The slope of the TOP mean shift yields information on the patient-specific level of alveolar recruitability. If the TOP mean shift is flat with little or no change in TOP with PEEP, then the application of PEEP does not yield recruitment. However, if an increase PEEP yields a large decrease in mean TOP, it implies that additional PEEP produces additional recruitment of new alveoli units. Based on this change, the TOP can be

used as a metric for PEEP selection. Thus, PEEP can be selected on the basis of how TOP changes with PEEP.

In particular, following this idea, if TOP decreases, then the clinician should continue to increase PEEP. If no change in TOP is observed, implying no recruitment, then no additional PEEP is should be applied. A third case, which is counter intuitive, occurs when TOP can increase with PEEP. This result can occur when there are leaks in the circuit or the lung compliance suddenly increases for some reason. In this situation, applying additional PEEP is sub-optimal.

TCP

The clinician must also consider the de-recruitment behaviour of the patient. In this situation, the TCP mean shift can be used to titrate PEEP. Similar to the way TOP behaves, TCP can either increase as a function of PEEP or remain constant. If TCP increases, then the application of PEEP continues to prevent de-recruitment of unstable units. In contrast, if TCP remains constant, then added PEEP yields no positive benefit to monitoring the recruitment status or recruited alveoli units of the lung. Thus, if TCP increases, then the clinician should continue to increase PEEP to prevent de-recruitment maintaining recruited alveoli. If little or no change in TCP is observed, PEEP should not be increased.

As discussed in Chapter 2, the application of PEEP can risk inducing VILI [Ricard et al., 2003, Carney et al., 2005, Gajic et al., 2004, Adams et al., 2003]. Although in some cases TCP could continue to increase with PEEP, the risk of VILI can be mitigated by setting a benchmark PEEP value. When the mean TCP is greater than PEEP, then more than 50% of alveoli will de-recruit during expiration. Thus, the point where PEEP and TCP mean are equal represents the PEEP at which no more than 50% of alveoli de-recruit. This value represents a somewhat arbitrary trade-off. Although a higher PEEP could prevent further de-recruitment, it could increase the risk VILI. Hence, it represents a turning point in the return on increased PEEP, and thus, this PEEP setting should be used when the objective is to prevent de-recruitment.

TOP and TCP shifts with PEEP could take on the four possible cases shown in Figure 6.1. In the best case, the mean shifts would exhibit the combination shown in Figure 6.1(A), where TOP decreases and TCP increases (with high slope). This combination indicates that more recruitment occurs as PEEP is increased, while a larger proportion of alveoli also

remain recruited during expiration. Figure 6.1(B) shows the case where the patient is not highly recruitable, but the application of PEEP prevents de-recruitment. In contrast, Figure 6.1(C) shows a patient who exhibits high recruitability, but struggles to keep alveoli recruited during expiration. The worst clinical situation for an ARDS affected lung is shown in Figure 6.1(D). In this case, the patient exhibits limited alveoli recruitability as shown by the flat TOP curve, and also does not retain recruited alveoli during expiration. This scenario would be associated with almost zero net recruitment with increasing PEEP and thus with increased risk of VILI, regardless of PEEP, due to repetitive opening and closing of alveoli [Carney et al., 2005, Ricard et al., 2003]. This situation is also most reflective of a health patient. As a patient's condition improves, the TOP and TCP gradients should become flatter.

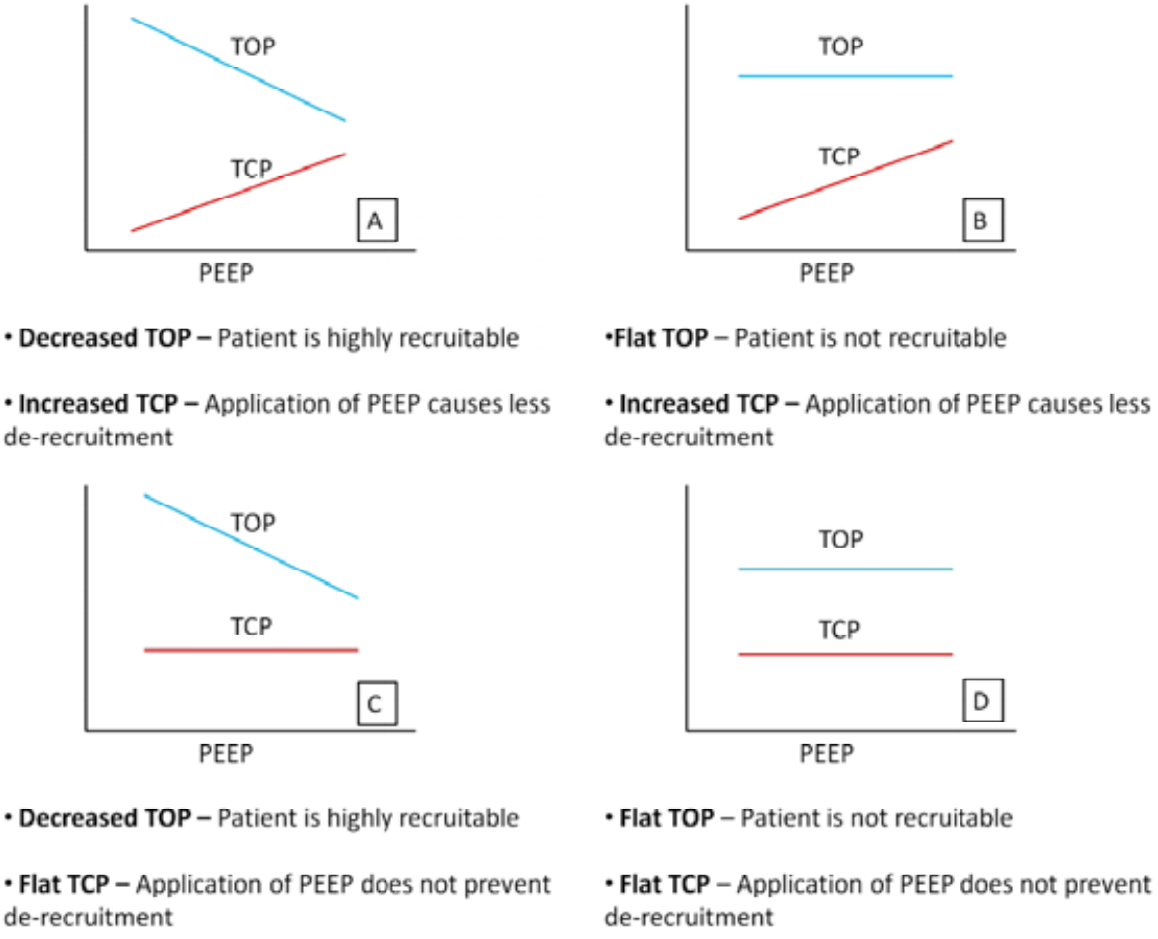

Figure 6.1 - Combinations of TOP and TCP mean shift

NET RECRUITMENT

Although TOP and TCP can be used individually to evaluate optimal PEEP, it is possible to evaluate the net effect of recruitment and de-recruitment together. Because the primary objective of MV is to maximise recruitment and minimise de-recruitment, a third metric may be used to choose PEEP by examining the difference between the amounts of alveoli recruited at certain PEEP during inspiration and the amount remaining at the end of expiration.

Figure 6.2 shows a static PV curve with total lung capacity (TLC). When an airway pressure of P_{crit} is applied, the volume during inflation is represented by the volume V_{inf}. However, during the deflationary portion of the static curve, the lung experiences a level of hysteresis and results in much higher lung volume for a given pressure, V_{def}. The percentage of lung recruited at a given pressure is the lung volume divided by the TLC. Thus, during inflation for a given pressure, the percentage recruited volume is V_{inf} divided by the TLC. Simultaneously, during deflation, the percentage alveoli remaining recruited at expiration is the V_{def} divided by TLC. The difference between the percent of alveoli remaining recruited at expiration and percent recruited during inflation is the net level of recruitment and varies as a function of pressure.

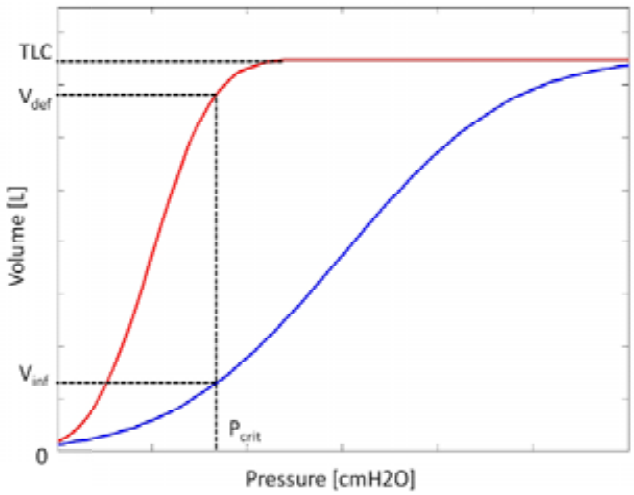

Figure 6.2 - Static PV curve during inflation and deflation. Hysteresis is shown, with the volume at inflation, V_{inf}, much lower than volume during deflation, V_{def}, for a given pressure, P_{crit}

Though the mechanism of hysteresis is still not fully understood, studies have shown that the larger the hysteresis, the higher the recruitability of the lung [Bernard et al., 1994,

Henzler et al., 2005, Hickling, 1998, Hickling, 2002]. Thus, the airway pressures should be increased to provide additional recruitment. However, as airway pressure increases, a point of maximum net recruitment occurs at a pressure P_{crit}, shown in Figure 6.3. At pressures below P_{crit}, the alveoli de-recruit faster than new alveoli recruit. As recruitment begins, the net recruitment increases until it reaches a maximum. At pressures above P_{crit}, recruitment and de-recruitment begin to slow, causing net recruitment to drop. Thus, this metric provides the clinician with the pressure required where to keep the process of recruitment and de-recruitment in balance, and provide the best trade off with respect to PEEP.

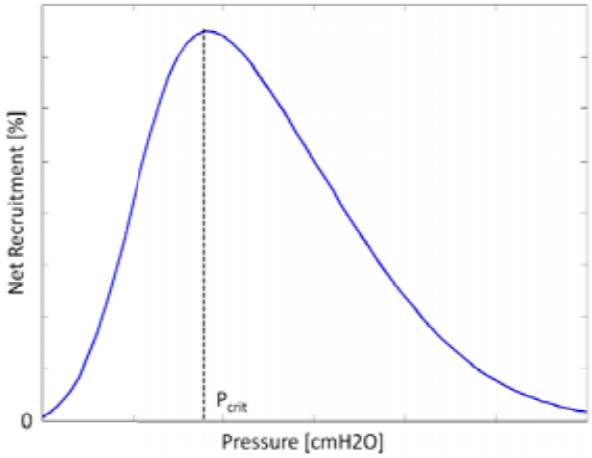

Figure 6.3 - Net recruitment as a function of pressure. P_{crit} indicates pressure where net recruitment is maximised. At pressures below P_{crit}, the rate of de-recruitment increases, while pressures above P_{crit}, the rate of recruitment decreases.

This net recruitment parameter is only valid when TOP is decreasing. If TOP increases with PEEP, then additional PEEP causes alveoli overstretching and a TCP metric would be more useful. In particular, although net recruitment may increase mathematically in this situation, it is not due to true recruitment. Hence, net recruitment should only be used if the TOP continues to decrease with PEEP.

CHOICE OF METRIC

The choice of metric depends on the particular requirements of the patient. Although all the metrics will be used in the clinical validation, the use of a given metric in the clinic should be rated on performance versus clinical expectation. Thus, the three metrics used are:

- TOP mean
- TCP mean
- Net rate of recruitment

The level of accuracy in selecting PEEP is dependent on the range of values predicted by the three metrics. However, the three metrics provide multiple means of selecting patient-specific PEEP.

Each parameter provides useful information to the clinician. If the primary objective is to maximise alveolar recruitment, then the TOP provides information on how PEEP affects recruitability. In contrast, if the objective is to ensure PEEP maintains recruitment, or prevent de-recruitment, then the TCP should be used to guide PEEP selection. Finally, the net recruitment is useful when examining the combined effects of recruitment and de-recruitment.

6.1.2 DISEASE STATE METRICS

In addition to PEEP selection metrics, four other parameters are introduced to illustrate how the ARDS disease state varies and can be assessed with time. The primary outputs of the model are the TOP / TCP mean and SD. While the level of recruitability is described by the TOP and TCP mean, the level of compliance is described by the SD. Although SD and compliance reflect the ARDS condition and the TOP mean represents the recruitability, they are both not unrelated.

MEAN – TIME METRIC

The first metric to evaluate the evolution of disease state uses the TOP mean shift. As a patient's condition changes, the magnitude of the TOP for a given PEEP also changes. Monitoring how the TOP varies with time can give an indication as to how stiff the lung is. If the TOP increases, it indicates that alveoli have de-recruited over time or become less recruitable at a given pressure, and a higher pressure is required to re-recruit them. Similarly, a decrease in TOP implies that overall, more, new lung units are available at a given pressure, and the lung has become less stiff. The trend of TOP can take on three possible scenarios as shown in Figure 6.4, and tracking this metric on a regular basis can indicate whether new alveoli have recruited. In specific, this implies a worsening, static or improving disease state in the lung.

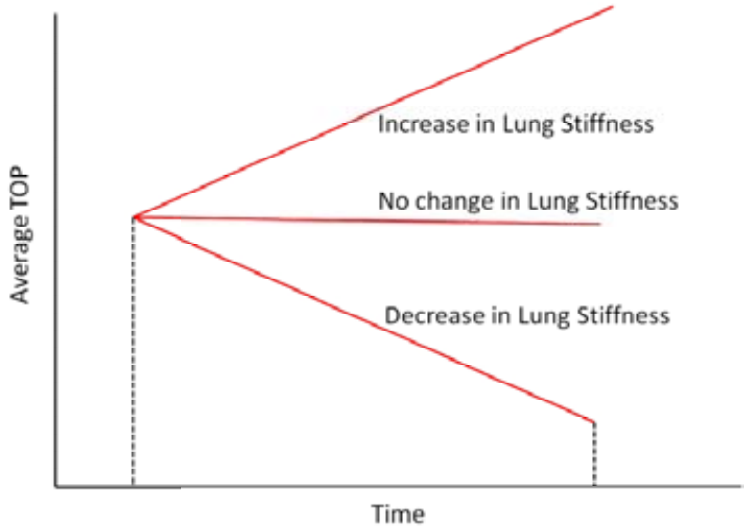

Figure 6.4 - Change in TOP as a function of time. Metric provides information with a change in lung condition and stiffness, and also provides information to the overall disease state

COMPLIANCE – TIME METRIC

The second metric uses the SD to assess how the compliance of the lung changes with time. The change in SD could give information as to how the condition of the lung has changed, as shown in Figure 6.5. As the study by Schiller et al [Schiller et al., 2003] showed, alveoli with various levels of injury appear in the same region of the lung, and even in the same microscopic field, because the ARDS lung is highly heterogeneous [Ashbaugh et al., 1967, Bernard, 2005, Gattinoni et al., 1998, Hudson and Steinberg, 1999, Maggiore et al., 2003, Ware and Matthay, 2000, Zilberberg and Epstein, 1998]. However, injured units recruit at higher pressures, while healthier units recruit at lower pressures. Therefore, changes in SD could evaluate how healthy and damaged units are distributed as their relative percentages and compliance change.

In particular, over time, an increase in SD could be interpreted as more injured lung units being present in the lung. Similarly, a decrease in SD could be attributed to a reduction and a corresponding improvement in disease state. More specifically, the increase or decrease of ARDS as in Figure 6.5 implies an increase or decrease in heterogeneity seen in the model by SD.

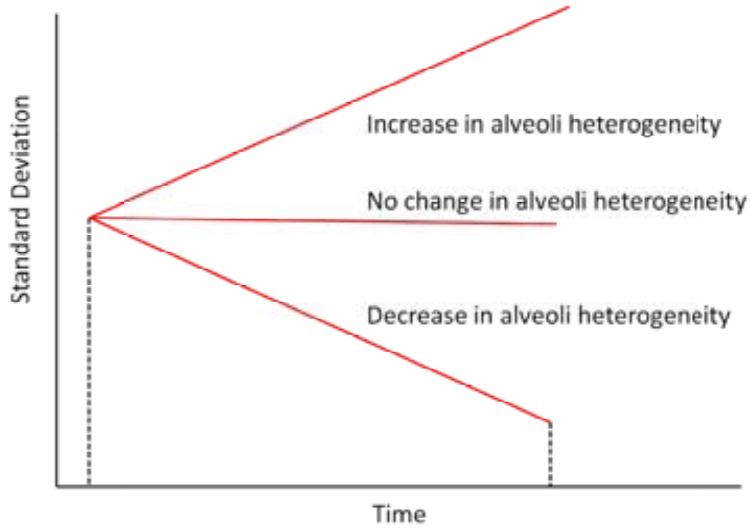

Figure 6.5 – Model standard deviation as a function of time.

TOP GRADIENT METRIC

A third metric to evaluate the evolution of disease state uses the gradient of the TOP mean shift. As a patient's condition changes, the gradient of the TOP curve also changes. The gradient of TOP represents the patient's recruitment response to PEEP. More specifically, if the TOP curve is steep, the patient is highly recruitable. In contrast, if the TOP gradient is shallow, then the patient is non-responsive to PEEP, and will not experience additional PEEP induced recruitment.

When evaluated over time, the gradient examines how the recruitability response varies. An increase in magnitude of the TOP gradient implies that the patient is becoming more responsive to PEEP. Similarly, a decrease in the magnitude of the TOP gradient suggests that that patient is becoming less responsive to PEEP.

TCP GRADIENT METRIC

The fourth metric examines the gradient of the TCP mean shift as a function of time. Similar to the TOP gradient, the TCP gradient assesses how PEEP affects the de-recruitment behaviour of alveoli. A steep TCP curve suggests that additional PEEP can prevent de-recruitment. Alternatively, a flat TCP suggests that applying additional PEEP does not prevent more de-recruitment.

By evaluating the gradient of TCP over time, it is possible to see how de-recruitment status of alveoli vary. An increase in the gradient over time suggests that fewer alveoli are de-

recruiting as a function of PEEP. In contrast, if the gradient of TCP drops, then the application of PEEP does not prevent de-recruitment. Patients who are healthy will have all available alveoli recruited. Thus, these healthy patients will exhibit flat TOP and TCP gradients. However, this analysis only considers mechanically ventilation of very ill patients where the TOP and TCP gradient can vary significantly.

6.1.3 METRIC SUMMARY

Seven metrics have been developed that will be used in the validation process. Three metrics have been developed as a means to guide PEEP selection, with the remaining four used as a metric to track disease state over time. The model was fitted using PV loops above the auto-PEEP, with the results presented in the following section. The latter four metrics are tracked only in patients undergoing multiple trials.

6.2 CLINICAL RESULTS

The trial protocols developed in Chapter 5 described the process of acquiring PV curves from patients in this study. Although PV curves were obtained from ZEEP to a maximum PEEP, an expiratory hold was performed to measure auto-PEEP. Auto-PEEP is a common phenomenon in patients who are mechanically ventilated, and represents the pressure that is already in the lung without any external ventilation.

When auto-PEEP is present, an obstruction or collapsed airway causes gas to be trapped within alveoli [Fernández et al., 1990, Mughal et al., 2005], as shown in Figure 6.6(A). As the pressure in the airway is increased during inflation or with increased PEEP, the airway opens up and the compliance suddenly increases. This is due to the sudden added volume from these pre-recruited alveoli due to the presence of auto-PEEP, shown in Figure 6.6(B). The presence of auto-PEEP can also be detected by examining the PV curves for different PEEP levels and noting that they have the same peak airway pressures, shown in Figure 6.7. Because the presence of auto-PEEP does not accurately reflect the underlying ARDS/ALI disease state or overall recruitability and compliance of the lung, the model was re-fitted in these cases without including PV loops below auto-PEEP.

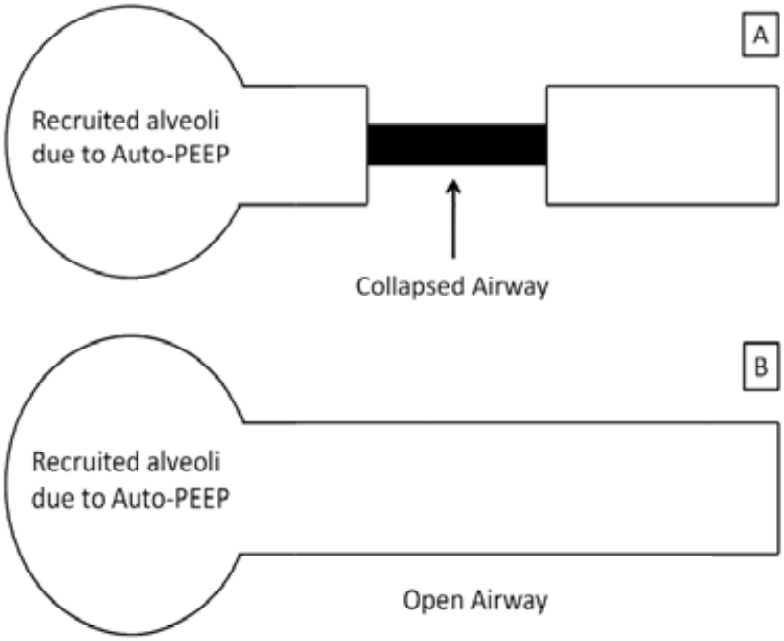

Figure 6.6 - Schematic highlighting concept of Auto-PEEP. Figure (A) shows the presence of a collapsed airway, with recruited alveoli causing a level of auto-PEEP. Figure (B) shows the collapsed airway opening up when additional PEEP is applied

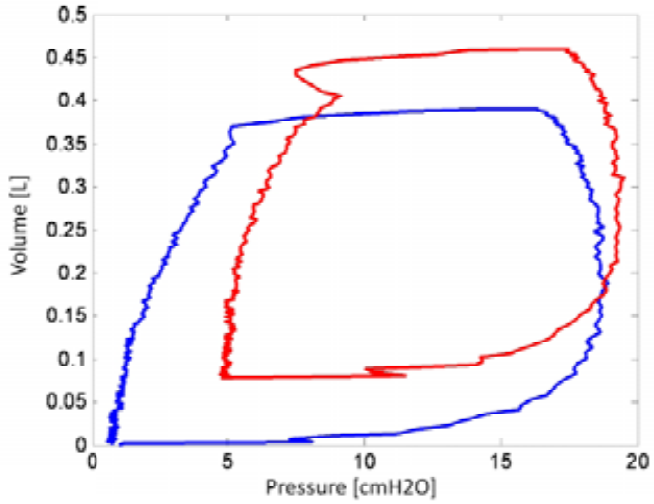

Figure 6.7 - PV curves for Patient 1 at PEEP below auto-PEEP. Auto-PEEP was equal to 7 cmH_2O

6.2.1 MODEL-BASED OPTIMAL PEEP

The model was able to fit the clinical data well. Ten patients were enrolled in the study, with the cause of their lung injury highlighted in Table 6.1. As expected, the standard deviation and the mean were significantly higher for the TOP distribution than the TCP distribution across all patients. All the data showed a linear increase in TCP, and a decrease in TOP as a function of PEEP. Table 6.2 summarises the best fit threshold pressure distribution parameters and the average fitting errors for Patient 1 and excludes

PV curves with PEEP levels below the auto-PEEP. Tables of fitting errors for all patients are shown in Appendix B and summarised in Table 6.3. In all cases, the model was unmodified from what was presented in Chapter 3, with patient-specific standard deviation held constant for each patient across all PEEP values in a given trial. The fitting errors are presented as average absolute volume fitting errors and as percentage errors.

Table 6.1 - Characteristics of trial patients

	Sex	**Age [years]**	**Cause of lung injury**
Patient 1	Femle	61	Peritonitis
Patient 2	Male	22	Trauma
Patient 3	Male	55	Aspiration
Patient 4	Male	88	Pneumonia
Patient 5	Male	59	Pneumonia
Patient 6	Male	69	Trauma
Patient 7	Male	56	Legionnaires
Patient 8	Female	45	Aspiration
Patient 9	Male		H1N1
Patient 10	Male		Legionnaires

Table 6.2 - Model fitting error for Patient 1

PATIENT 1

Number of Units	144000
Inflation SD	15
Deflation SD	7
Auto-PEEP [cmH_2O]	10

	Inflation			Deflation		
PEEP [cmH_2O]	Mean	Error [ml]	Error [%]	Mean	Error [ml]	Error [%]
10	30.97	22.17	7.86	15.57	15.48	4.61
15	28.07	22.50	4.44	17.68	5.61	1.02
20	27.12	22.27	3.11	19.88	5.72	0.63
25	26.41	21.71	2.05	22.43	7.47	0.68
27	26.18	15.11	1.34	23.39	2.73	0.24

Table 6.3 - Summary of fitting errors for all patients

	Inflation		**Deflation**	
	Error [ml]	**Error [%]**	**Error [ml]**	**Error [%]**
Median	19.47	2.50	6.96	0.82
IQR	[12.36 – 22.79]	[1.56 – 4.62]	[4.51 - 13.22]	[0.54 - 2.34]
Range	[1.73 - 55.09]	[0.63 - 151.80]	[1.39 - 58.17]	[0.11 - 116.89]

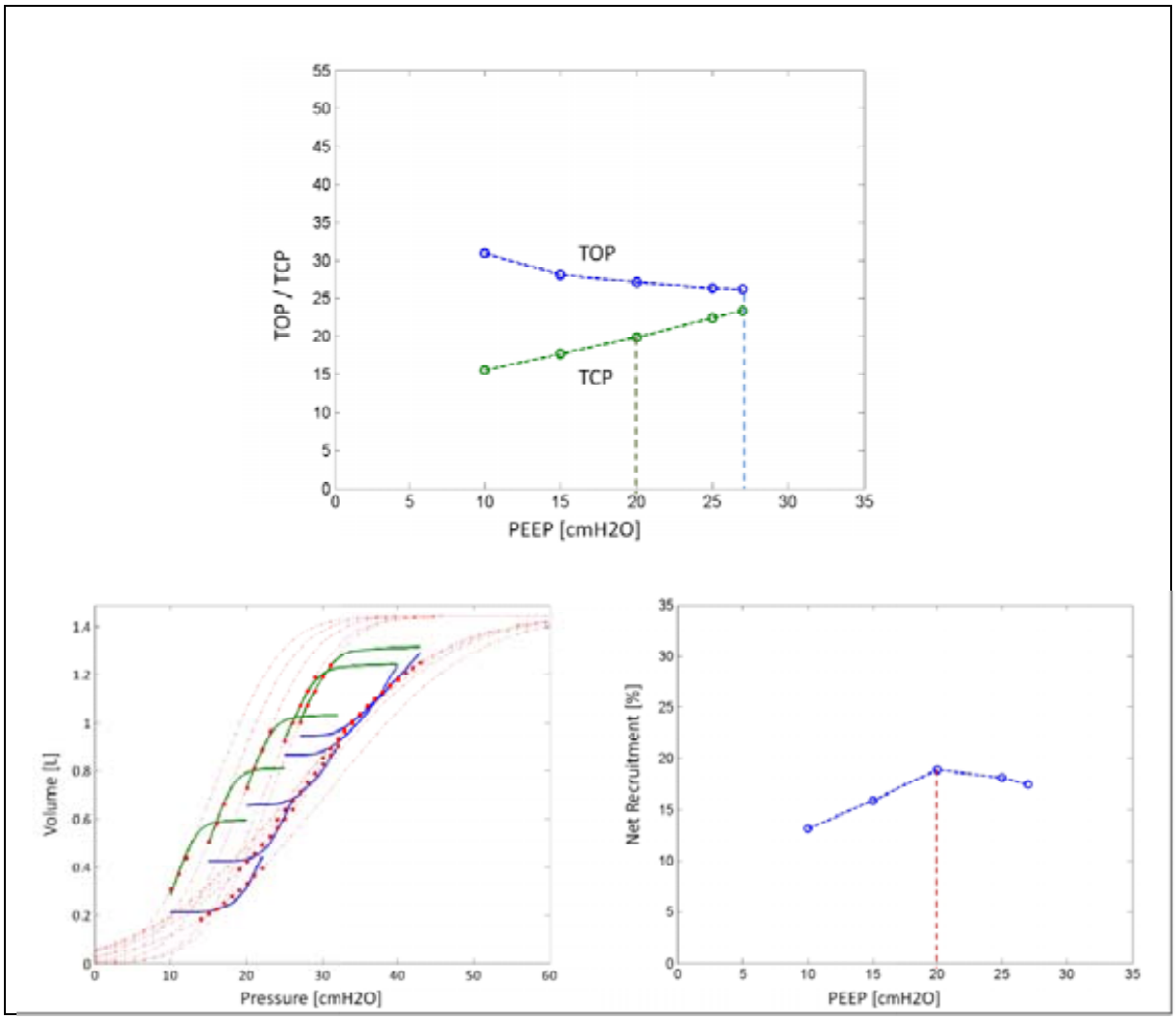

Figure 6.8 - Main plot shows TOP and TCP as a function of PEEP for Patient 1. Bottom left plot is the model fit. Bottom right indicates net recruitment

Table 6.4 – Clinically selected PEEP and Optimal PEEP indicated by TOP, TCP and net recruitment for Patient 1

Method	Optimum PEEP [cm H_2O]	Reason
TOP	27	Recruitment maximised - but could pose risk of VILI
TCP	20	Higher PEEP results in less de-recruitment but can risk VILI
Net Recruitment	20	Lower PEEP does not maximise recruitment, while higher PEEP does not minimise de-recruitment
Clinical Setting	10	Clinician selected

Figure 6.8 illustrates the TOP and TCP curves for Patient 1. In addition, the model fit and net recruitment curves are also shown. The main plot shows the effect of PEEP on mean

TOP and TCP. Patient specific optimal PEEP was determined by using the three metrics described in Section 6.1.1 . Finally, the optimal patient-specific PEEP depending on the TOP, TCP and net recruitment are also evaluated and compared to the clinical PEEP setting on Table 6.4. TOP and TCP curves for all patients are shown in Appendix C.

The results of the model-based approach are summarised in Table 6.5, as well as the auto-PEEP each patient experienced. The clinical PEEP setting is also shown for comparison.

Table 6.5 – Summary of auto-PEEP and model-based PEEP selection metrics for all patients.

	Auto-PEEP [cmH_2O]	Clinically Selected PEEP [cmH_2O]	Inflation SD	Model-Based PEEP Selection [cmH_2O]		
				TOP	TCP	Net Recruitment
Patient 1	10	10	15	27	20	20
Patient 2	2	12	11	15	15	15
Patient 3	0	10	12	10	15	20
Patient 4	9	10	25	20	20	30
Patient 5 - Trial 1	13	12	16	20	25	25
Patient 5 - Trial 2	8	12	15	20	25	20
Patient 6 - Trial 1	10	11	11	15	20	20
Patient 6 - Trial 2	3	13	14	15	15	20
Patient 6 - Trial 3	2	10	14	10	20	15
Patient 7	2	7.5	10	5	10	10
Patient 8	0	12	15	15	20	30
Patient 9	12	10	15	25	20	29
Patient 10	3	10	16	15	20	15

6.2.2 MONITORING DISEASE EVOLUTION

Patients 5 and 6 had multiple trials and recruitment manoeuvres on different days. The purpose of these cases was to examine if the model could track the evolution of the disease state with time. Patient 5 had two trials, with the second performed three days after the first. Patient 6 had three trials, with the subsequent two manoeuvres performed 7 and 14 days later. The variations of TOP, SD, TOP gradient and TCP gradient are shown in Figure 6.9 for Patient 5 and Figure 6.10 for Patient 6.

PATIENT 5

The average TOP for patient 5 was calculated using the modelled TOP values at PEEP values of 15, 20 and 25 cmH_2O from Table B.1. Figure 6.9(A) shows the average TOP and SD over time for Patient 5, and shows that a significant drop in average TOP, and a negligible drop in SD. This result implies that Patient 5 has indeed recruited. However, the state of the ARDS affected lung has only slightly improved.

Figure 6.9(B) shows the variance of the TOP and TCP gradient over time. The TOP gradient shows no change over time, suggesting that the recruitment response to PEEP has not changed. In contrast, the TCP gradient shows a slight increase over time. This result implies that the effectiveness of PEEP to prevent de-recruitment has improved over time resulting in an improved condition overall.

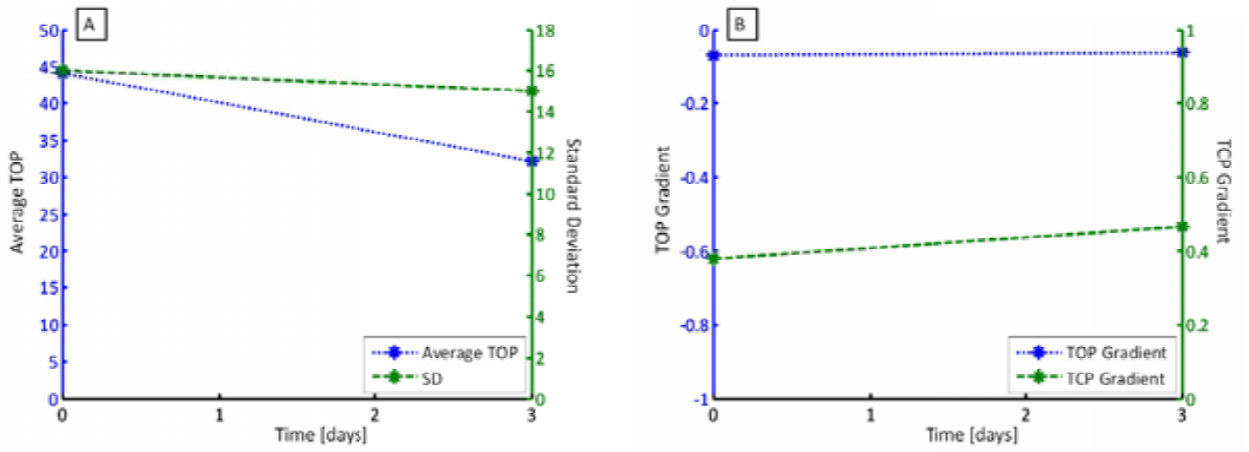

Figure 6.9 – (A) Average TOP and SD over time for Patient 5 and (B) TOP and TCP gradient over time

PATIENT 6

Figure 6.10 shows the state of the disease for Patient 6, with average TOP calculated using PEEP values of 10, 15 and 20 cmH_2O. Similar to Patient 5, Patient 6 exhibits a decrease in average TOP, indicating recruitment has occurred with time over the three trials. However, Figure 6.10(A) also indicates that between the first and second trial, SD has increased. This increase would imply that there is an increase in unhealthy alveoli and a loss of compliance. Prior to the trial, the clinician hypothesised that this patient had severe ARDS. Hence, the distribution of healthy to unhealthy alveoli was extremely heterogeneous and

there were potentially large numbers of affected alveoli. The increased level of recruitment could be attributed to marginally unhealthy units being recruited after sustained level of pressure. However, the increase in SD suggests that the condition of unhealthy alveoli was getting worse or that more alveoli were becoming ARDS affected. This patient later died due to severe respiratory failure, which supports this conclusion.

Figure 6.10(B) shows the gradient of TOP and TCP. Between the first and second trial, the magnitude of the TOP gradient seems to decrease, or become flatter, suggesting that the patient is becoming less responsive to PEEP induced recruitment. This lack of response becomes even more pronounced between the second and third trial. In particular, the TOP gradient begins to become positive indicating that the levels of PEEP used are sub-optimal. The TCP gradient shows a slight increase with time. This would imply, similar to Patient 5, that the effectiveness of PEEP to prevent de-recruitment has improved somewhat.

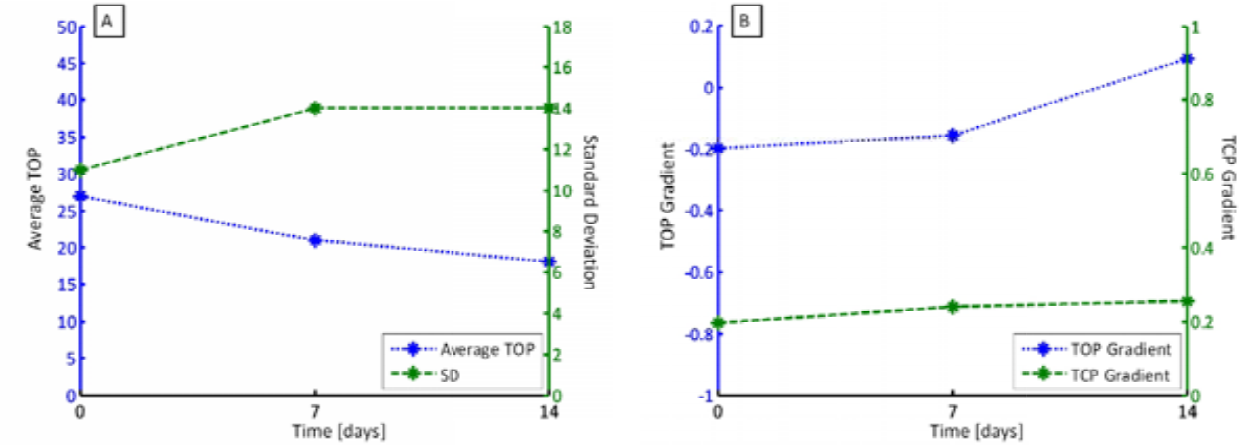

Figure 6.10 - (A) Average TOP and SD over time for Patient 6 and (B) TOP and TCP gradient over time

It is also interesting to note the difference in magnitude between TOP and TCP gradients between both patients. During the first trial, Patient 6 exhibited a much higher negative TOP gradient than Patient 5. This would suggest that Patient 6 was more responsive to PEEP than Patient 5. However, with time, Patient 6 become much less responsive, as shown in Figure 6.10(B) compared to Patient 5. Similarly, the magnitude of TCP gradient also indicates that PEEP was much more effective at preventing de-recruitment in Patient 5. This result can be inferred by examining Figure 6.9(B) and noting that the gradient of TOP is much steeper when compared to Patient 6.

Tracking the evolution of the disease provides useful information into how the patient is reacting to ventilation therapy overall, as well as how they are progressing in the ICU. The use of four metrics allows insight into the different objectives of ventilation. In particular, the metrics potentially allow the clinician to examine whether the patient recruited, the state of the ARDS affected alveoli, the response on recruitment through PEEP and the response to prevent de-recruitment through PEEP.

6.3 DISCUSSIONS & LIMITATIONS

6.3.1 PEEP SELECTION

Based on the results of these clinical trials, the model highlighted aspects of MV that are clinically important in determining optimal PEEP. First, the model evaluates waveforms to assess recruitment and de-recruitment, thus determining the recruitability of the patient's lungs. By examining how recruitable a patient is with respect to TOP, TCP, and net rate of recruitment, the model evaluates the point where additional PEEP does not cause additional recruitment or retention of alveoli.

The model uses the TOP to assess the impact on recruitability using PEEP. The clinical data suggested that Patients 1, 3 and 4 were highly recruitable. These patients showed a significant drop in TOP as PEEP increased. In contrast, Patients 2, 6, 7 and 8 showed negligible or no change in TOP as PEEP increased, with PEEP resulting in minimally additional or no recruitment. Patient 5 underwent two trials, and in trial 1, was not very recruitable due to the minimal changes seen in TOP. However, during the second trial, Patient 5 had a much stronger recruitment response to PEEP, with the TOP dropping much more rapidly as PEEP was applied.

The model also uses TCP to evaluate optimal PEEP. Rather than aiming to maximise recruitment, using TCP as a metric, the aim is to prevent de-recruitment or maintain recruited alveoli. All ten patients showed an increase in TCP as PEEP increased. This suggests that continual increases in PEEP will at least minimise de-recruitment, and PEEP should be maximised. However, because high PEEP can result in VILI [Adams et al., 2003, Carney et al., 1999, Gajic et al., 2004, Ricard et al., 2003], the PEEP where no more than 50% of alveoli de-recruit was chosen as the optimal PEEP in this analysis. Although

this is an arbitrary value, it represents a trade off between patient safety and ventilation efficacy.

Finally, the model also used the net recruitment as a metric to select PEEP. This metric is only valid when the TOP decreases. Patients 2, 5 (trial 2), 6 (trials 1 and 3) and 7 showed an increase in TOP at high levels of PEEP, as shown in Figure 6.11(A) and Appendix C. Based on alveolar recruitability, an increase in TOP would imply that high PEEP results in volume lost. Physiologically, this outcome would imply that there are more alveoli being destroyed (due to over inflation) than being recruited. However, this sudden change of patient condition is highly unlikely due to the relatively low pressures that were used in this trial.

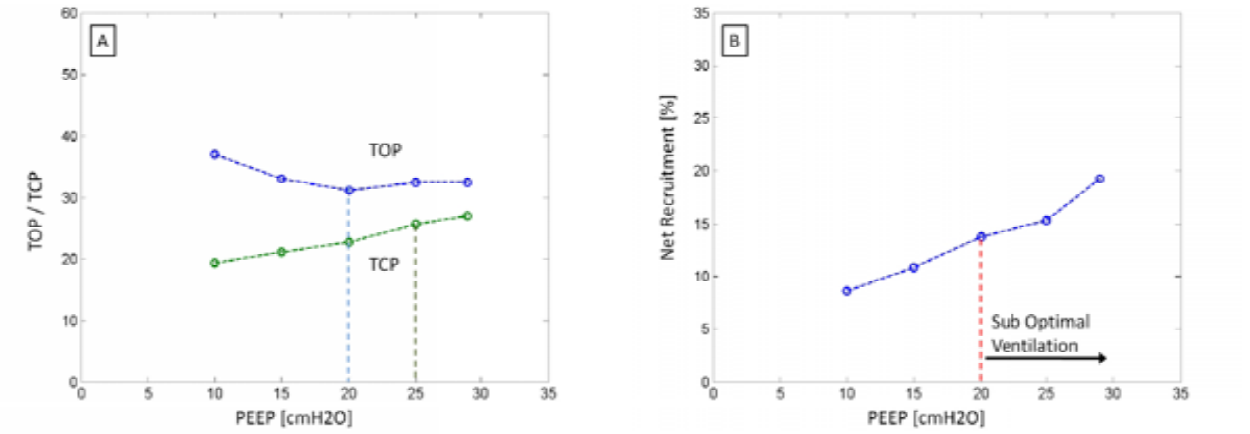

Figure 6.11 - (A) TOP and TCP vs PEEP for Patient 5, Trial 2. (B) Net recruitment for Patient 5, Trial 2 indicating sub-optimal ventilation beyond 20 cmH_2O.

The clinical data showed this increase in TOP occurred when the compliance of the dynamic PV curve decreased markedly. When the compliance of the lung decreases, the pressure required to deliver a given volume of air increases. This result can occur when alveoli are maximally recruited and begin to over-inflate [Schiller et al., 2003]. Thus, an increase in PEEP results in alveolar over-inflation rather than additional recruitment, and ventilating at higher PEEP is similar to ventilating above the upper inflection point (UIP). Therefore, the increase in TOP is an indication of alveolar over-inflation thus justifying the conclusion that it results in sub-optimal ventilation, as can be seen in Figure 6.11(B).

6.3.2 COMPLIANCE CHANGES

The model used a constant SD across PEEP and within a given trial to reflect the disease state of a patient, as fitted to the largely linear portion of the dynamic PV curve. When the model was applied to the clinical data, it was evident that the standard deviation is not necessarily constant across all PEEP values considered in this study. At low and high PEEP, the compliance is significantly different compared to PEEP in the linear portion of the static PV curve [Harris, 2005]. The variation in compliance is shown in Table 6.6 for the patients in this study. The unusually high compliance values could be attributed to the presence of auto-PEEP in patients. Regardless of this limitation, it still reflects the recruitment response to PEEP indicating the robustness of the model.

Table 6.6 - Variation in compliance across all patients

	Compliance [ml/cmH_2O]
Patient 1	[34.92 - 60.47]
Patient 2	[58.34 - 103.91]
Patient 3	[25.70 - 107.96]
Patient 4	[21.82 - 75.19]
Patient 5 - Trial 1	[24.40 - 55.57]
Patient 5 - Trial 2	[26.94 - 62.21]
Patient 6 - Trial 1	[17.02 - 58.69]
Patient 6 - Trial 2	[33.70 - 63.12]
Patient 6 - Trial 3	[23.64 - 77.45]
Patient 7	[5.76 - 23.48]
Patient 8	[32.14 - 72.48]
Patient 9	[36.70 - 61.23]
Patient 10	[26.74 - 44.68]

The preliminary validation performed in Chapter 3 used PV curves obtained during 30 minutes of sustained pressure [Bersten, 1998] and showed similar compliance across the different PEEP. Recruitment manoeuvres applying sustained pressure for relatively long periods of time have been shown to improve recruitability [Lapinsky and Mehta, 2005]. This approach may have resulted in the very constant compliance in the data used in the initial validation on the Bersten data [Bersten, 1998]. The model required multiple PV loops to assess the recruitability of the patient. From a practical perspective, if multiple PV loops are required, it is not feasible to hold the PEEP for 30 minutes as part of a clinical protocol for everyday use. Thus, in this situation, a short recruitment manoeuvre would be

more appropriate clinically, as used in these clinical trials. However, it may result in slightly different compliances across various PEEP levels.

Figure 6.12(A) shows PV curves from the Bersten dataset and Figure 6.12(B) from the clinical dataset. Figure 6.12(A) shows the linear compliance not varying significantly in the three curves. In contrast, Figure 6.12(B) shows compliance varying at extreme PEEP, but remaining relatively constant in the linear region. Thus, although 30 minutes of sustained PEEP is not performed for the clinical dataset, the relatively constant compliance within the linear region is still obtained, which still incorporates the clinically acceptable PEEP ranges. In addition, the data from Bertsen used a maximum PEEP of 15 cmH_2O, and did not push PEEP to higher values compared to the trials used in this study. Thus, the relatively constant compliance seen by Bersten could have also been attributed to the fact that PEEP was not tested at extreme values.

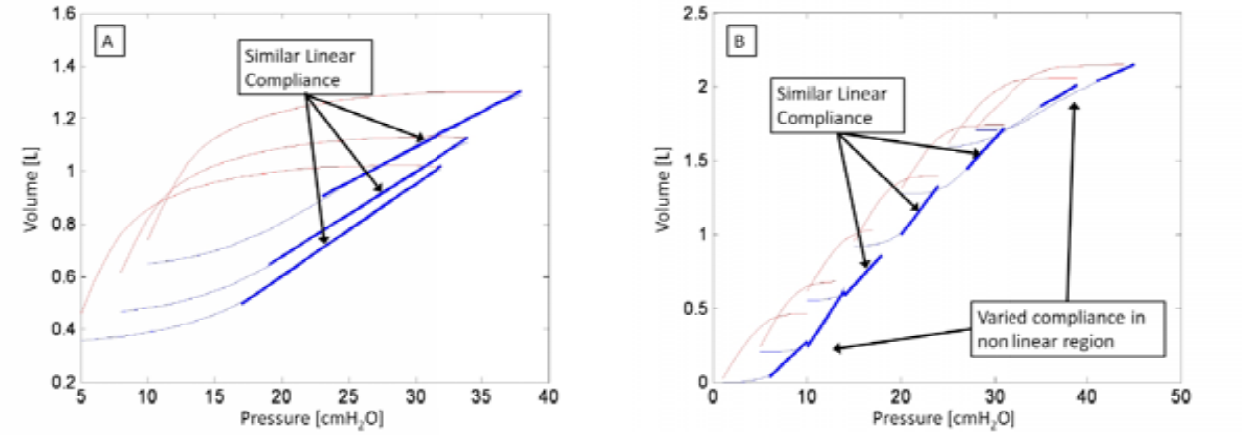

Figure 6.12 - (A) PV curves for a dataset from Bersten et al showing similar linear compliance. (B) PV curves from clinical data. Similar compliance is exhibited in the linear portion, but compliance significantly varies at low and high PEEP.

6.3.3 SD & COMPLIANCE

Compliance in the linear portion of the static PV curve has been reported to be between 20 and 61 ml/cmH_2O for patients with ALI and ARDS [Amato et al., 1998, Brower et al., 2004, Gattinoni et al., 2006, Gattinoni et al., 1998, Jonson and Svantesson, 1999]. Table 6.7 summarises the inflation SD and the corresponding compliance of the linear portion of the static PV curve, with the results plotted in Figure 6.13. The aim of this analysis was to examine the strength of the correlation between SD and compliance.

Table 6.7 - SD and linear compliance for each clinical patient. Compliance was normalised to allow correction for varying TLC.

	Inflation SD	Linear Compliance [ml/cmH_2O]	TLC [mls]	Normalised Linear Compliance [ml/cmH_2O]	TLC [mls]
Patient 1	15	37.79	1440	26.25	1000
Patient 2	11	60.52	1710	35.40	1000
Patient 3	12	71.66	2200	32.48	1000
Patient 4	25	34.94	2200	15.88	1000
Patient 5 - Trial 1	16	48.80	1980	24.61	1000
Patient 5 - Trial 2	15	42.26	1610	26.25	1000
Patient 6 - Trial 1	11	33.92	960	35.36	1000
Patient 6 - Trial 2	14	47.97	1710	28.02	1000
Patient 6 - Trial 3	14	43.21	1540	28.04	1000
Patient 7	10	25.11	650	38.57	1000
Patient 8	15	46.20	1760	26.23	1000
Patient 9	15	49.58	1890	26.23	1000
Patient 10	16	36.17	1470	24.60	1000

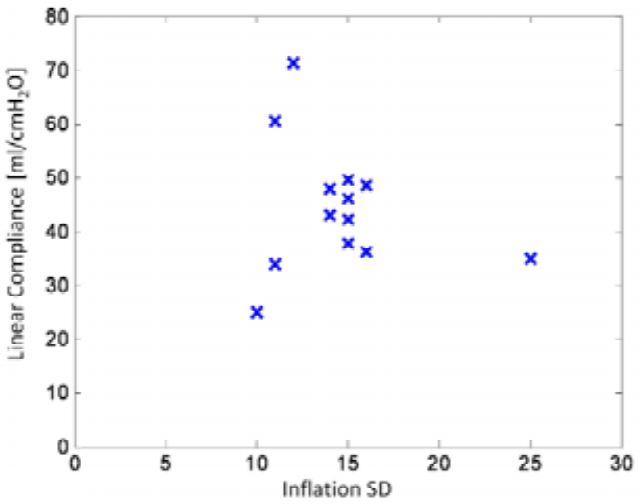

Figure 6.13 - SD vs linear compliance for all patients

Figure 6.13 suggests that there is no strong correlation between inflation SD and the linear compliance. However, this result could be attributed to the fact that the TLC varies significantly between patients. For example, Patient 1 and Patient 8 exhibit the same SD, but the linear compliance is different, as shown in Figure 6.14.

Figure 6.14 shows the quasi-static inflation PV curve for Patient 1 and 8. Although both patients have the same SD, the linear compliance is different due to the difference in TLC. To correct for the varying lung capacity, the compliance was normalised, such that all patients exhibit a TLC of 1 L. This normalization effectively scales the static PV curve,

and thus, modifies the compliance. The normalised compliance values are shown in Table 6.7, and plotted in Figure 6.15.

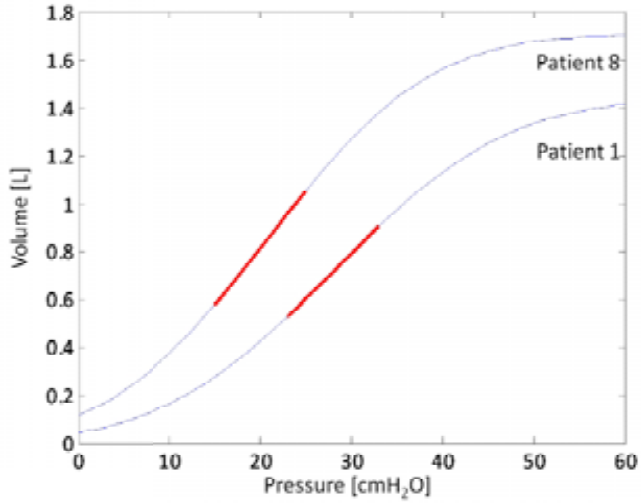

Figure 6.14 - Static PV curve for Patient 1 and Patient 8. Red solid lines show the linear compliance for both patients. SD is identical for both patients, but TLC is different, causing linear compliance to vary.

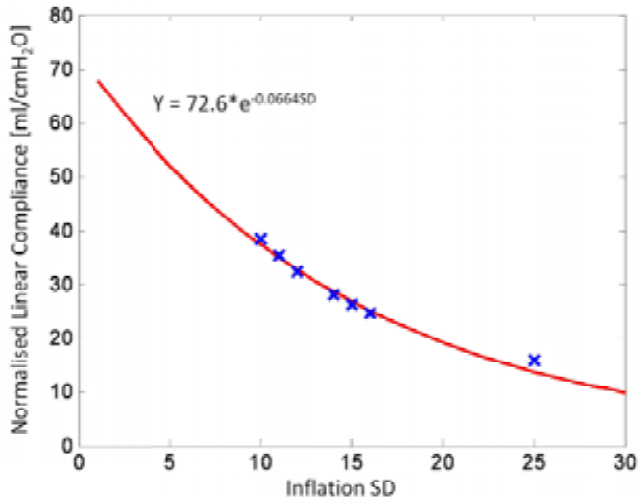

Figure 6.15 - SD vs normalised linear compliance for all patients

Figure 6.15 shows the normalised compliance as a function of SD and a very strong exponential relationship. In essence, the SD captures the effect of compliance. Although numerically, SD may not accurately represent true linear compliance, these results show that SD can be effectively used as an indicator of the diseased state. More specifically, SD can be used to determine the normalised linear compliance, which accounts for varying TLC between patients.

6.3.4 MECHANICAL FAILURE

Patient 2 showed an increase in TOP when PEEP was set above 15 cmH_2O, seen on Figure 6.16(A). In this particular case, the increase in TOP could also be attributed to a leak in the circuit. To prevent leaks from the circuit, an endotracheal cuff is used to seal the tube. When a patient is ventilated and intubated, the cuff is set by filling it with air and inflating it within the trachea. This causes a pressure build up in the cuff and ensures it is less susceptible to leaks. The cuff pressure generally set in the Christchurch Hospital ICU was between 30 and 40 cmH_2O. For this patient, the cuff was set to 30 cmH_2O.

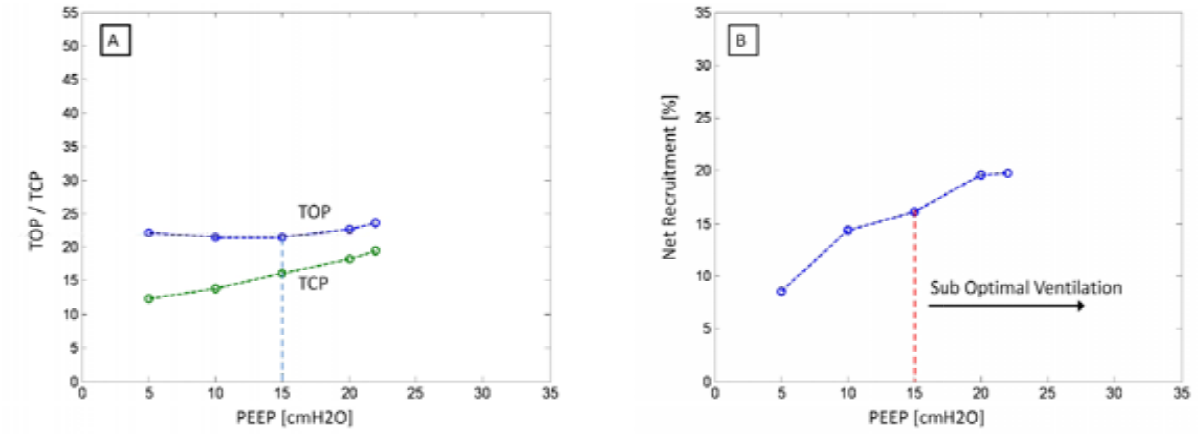

Figure 6.16 - (A) TOP and TCP vs PEEP for Patient 2. (B) Net recruitment for Patient 2 indicating sub-optimal ventilation beyond 15 cmH_2O.

The increase in TOP begins to occur at a PEEP of 15 cmH_2O where the peak airway pressure approaches 30 cmH_2O, as shown on Figure 6.16(A). As the airway pressure approaches and exceeds the cuff pressure, the cuff begins to slip and cause a slight leak. The leak was detected after the trial was completed when the cuff pressure was shown to have dropped, implying that a leak did in fact occur.

In this case, the application of higher PEEP is indicative of the leak resulting in sub-optimal ventilation. Thus, the increase in TOP could potentially also be used as a method to determine mechanical failures in the circuit which could lead to sub-optimal ventilation. If an increase in TOP is observed, then the clinician could check the cuff to ensure no leaks are present. If the TOP continues to increase, then this could be attributed solely due to over-inflation resulting in applied PEEP being reduced.

6.3.5 EFFECT OF INSPIRATORY RESISTANCE

The effect of endotracheal tube resistance was evaluated by performing an inspiratory hold during the deflation to ZEEP and measuring plateau pressure. The difference in peak pressure and plateau pressure was attributed to the pressure loss of the tube. Patients 1 - 4 did not have this measurement taken as this was a modification to the original study approved. Because a known decelerating flow waveform was used, the inspiratory resistance could be calculated. By correcting for resistive pressure, the PV curves takes on a narrower shape, as shown in Figure 6.17.

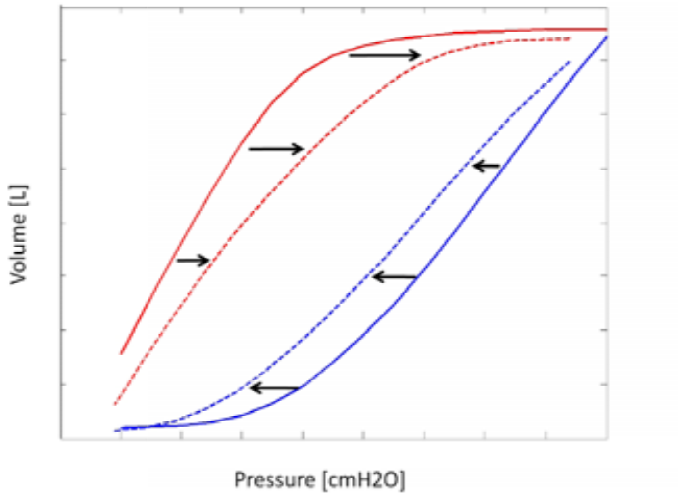

Figure 6.17 - PV curve takes on a narrower shape when corrected for resistive pressure

The model was re-fitted with the corrected PV curves, and the resulting TOP and TCP calculated. Figure 6.18 shows the TOP and TCP plot for Patient 5, trial 1. As shown in the plot, the overall magnitude of the TOP drops, while the TCP increases. This result is as expected, as the pressure to overcome resistance has been compensated for. In particular, the pressure required to recruit alveoli is lower. Similarly, the pressure required to de-recruit alveoli is higher. It must be noted that in both cases, the overall trend of the TOP and TCP is still similar, and thus, the results, which are based on trends are unchanged.

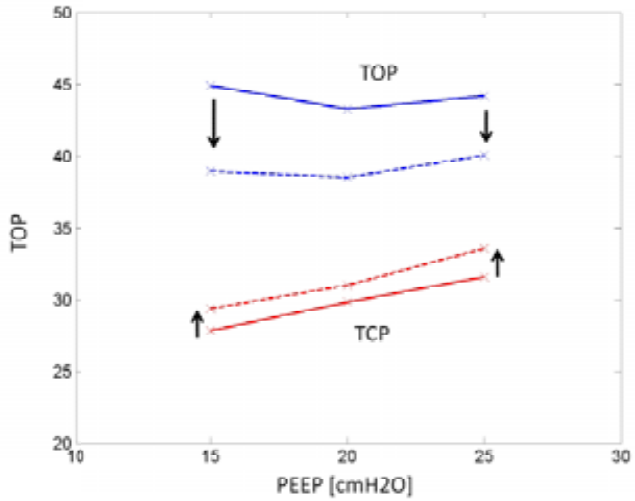

Figure 6.18 - TOP and TCP magnitude change when model is fitted to PV loops with resistive pressure removed for Patient 5, Trial 1

The inspiratory hold is an additional step when obtaining the PV curves. Although the magnitude of TOP and TCP changes when corrected for resistive pressure, the trend is similar, and still produces the same patient-specific PEEP response. Thus, from a practical perspective, not measuring the flow resistive component still yields similar responses. By avoiding this measurement, an additional measurement step can be avoided when obtaining the PV loops.

6.3.6 AIRWAY OBSTRUCTIONS

One of the major limitations of this model is the reliance on the quality of the PV curve. In particular, the model does not work when patients exhibit severe airway obstructions, was the case with Patient 4. Patient 4 exhibited very high auto-PEEP of 9 cmH_2O and, as a result, the model was only fitted to PV curves with PEEP above 10 cmH_2O.

Figure 6.19 shows the flow and pressure waveforms. The waveforms highlight an interesting scenario where airway pressure begins to decrease even though the ventilator is still delivering positive flow. More specifically, the volume of the lung continues to increase even though there is a pressure drop.

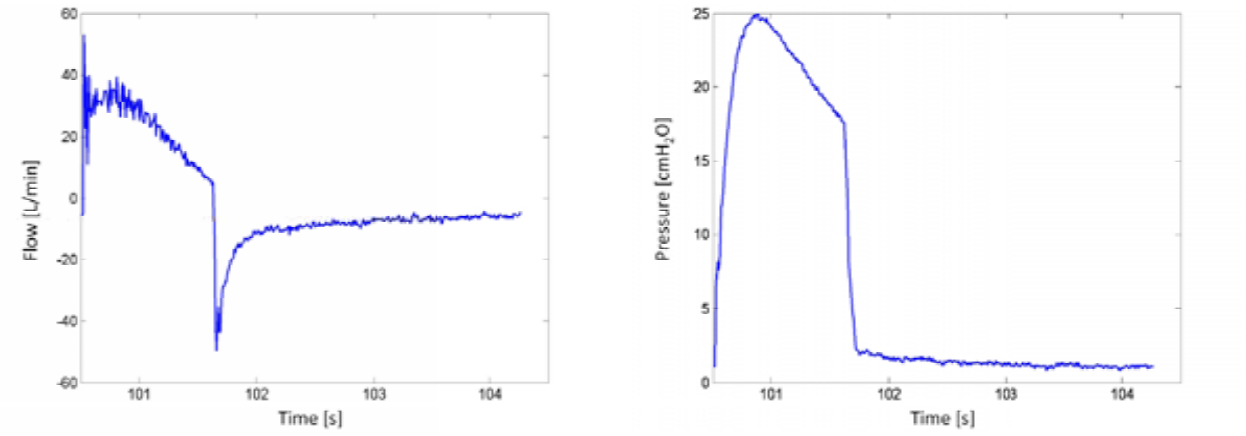

Figure 6.19 - Raw Flow vs Time and Pressure vs Time for Patient 4

In patients with ARDS and ALI, the lung is very heterogeneous. Some areas of the lung are compliant and healthy; while other portions of the lung can be extremely stiff [Gattinoni et al., 2005]. In addition to a heterogeneous distribution of alveoli, an ARDS lung can exhibit significant airway resistance due to the presence of fluid secretions within the airway. The drop in pressure can be explained when one considers this heterogeneous nature of the ARDS lung.

When the ventilator delivers air to the lungs, the pressure in the airway increases. As more air flows into lungs, the airflow takes the path of least resistance and begins to fill the highly compliant and healthy alveoli, A, as shown in Figure 6.20. However, the volume of alveoli A is limited by its compliance and the size cannot expand any further. The continual flows delivered by the ventilator means that there is still a pressure build up in the airways. As this pressure increases at point 1, the flow then overcomes the resistance blocking alveoli B and causes more volume to be opened up.

In this trial, the flow waveform used was a decelerating flow pattern. When the pressure difference at point 1 overcomes the resistance, flow begins to enter alveoli B. However, because the flow is decelerating, the newly available volume is not being filled fast enough by the decelerating airflow. Thus, although lung volume is still increasing, the pressure drops due to the lack of flow.

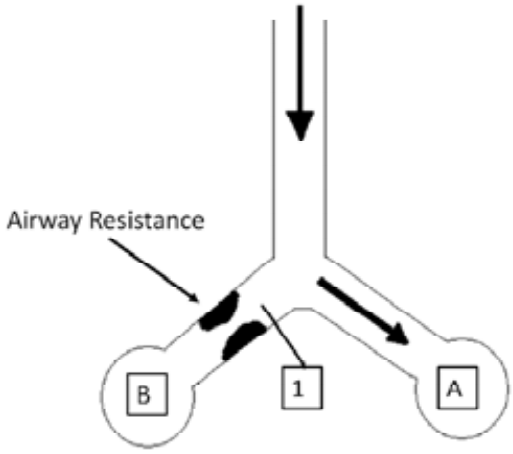

Figure 6.20 - Schematic highlighting the decreasing pressure phenomena

This pressure drop could also be indicative of the severity of the disease state. Patient 4 was the only one who exhibited this drop in pressure. This point implies that this patient has severe airway restrictions, similar to what a COPD patient experiences. The pressure drop indicates that there are severe resistances to the airflow and highlight that the lung may be heterogeneous to the point of being critically ill. Patient 4 later died due to advanced respiratory failure further highlighting that a drop in pressure could be attributed to the level of critical illness of ARDS.

Although Patient 4 showed such a pressure drop, the true compliance for this patient is when the pressure and volume increase (ie – when alveoli A is filling). Hence, the model is fitted to the regions of PV loops where pressure and volume are increasing. However, the problem with fitting to this region is that there are not many data points available. Hence, although the model can still fit to the PV curves, it may not give an accurate representation of patient recruitability.

6.3.7 H1N1

Patient 9 was admitted to the ICU with the H1N1 virus. Patient 9 was in the ICU for six days before consent was obtained and the patient was included in the trial. The patient exhibited similar compliance to other ARDS affected patients, with optimal PEEP selected as 25, 20 and 29 cmH_2O through TOP, TCP and net recruitment respectively. The use of high PEEP in H1N1 patients has proven to be beneficial [Ramsey et al., 2010, Peris et al., 2010], and the model-based optimal PEEP correlates well with current observations.

However, the metrics calculated using this model may not highlight the true mechanics observed in H1N1 patients as the patient was under ventilation for several days before the trial began. During this time, the H1N1 became less acute and more ARDS-like as patient condition improved in response to therapy.

6.4 SUMMARY

The clinical trials have highlighted the potential for clinical use for the recruitment model. Although the model was not modified from what was described in Chapter 3, this chapter introduced the three metrics used to select an optimal patient-specific PEEP. Although the TOP, TCP and net recruitment provide three difference methods to evaluate the PEEP, they provide a set of values that can be used in the clinic as a guideline.

This chapter also introduced four additional metrics to help with assessing how the disease state evolves with time. Tracking the TOP with time yields information on the recruitability of the patient, and how this changes with time. In addition, tracking the SD provides information on how compliant the patient is and the state of the disease with time. Finally, tracking the gradient of TOP or TCP with time, provides information on how the patient's response to PEEP has changed.

The model has shown to be limited when patients experience severe airway obstructions. This may limit the use of the model when trying to ventilate COPD patients and patients with airway obstructions. In addition, the model is also limited by the assumption of constant SD across all PEEP. The clinical data shows that there is significant compliance change at different PEEP. However, even when assuming constant SD, the model still gives a reasonable estimation of recruitability. In particular, the model shows an increase in TOP at high PEEP, when compliance decreases, indicating the beginning of sub-optimal ventilation.

Chapter 7 - dFRC Estimation Validation

Chapter 4 introduced a model to estimate dynamic FRC (dFRC) as a function of PEEP. In particular, the model introduced the PEEP Stress parameter (β) as a means to estimate dFRC, given that the compliance of the patient is known. The initial validation, as per chapter 4, was performed with data from 12 patients where each patient had an associated dFRC measurement. The results suggested that β was a function of PEEP, and could be assumed constant across all patients. In essence, β was assumed to represent a population stress constant as a function of PEEP, which a surprising result for a diverse patient group.

The purpose of this chapter is to further validate the use of β as a population constant. The clinical data obtained, from the trials performed per Chapter 5, had dFRC measurements for ten additional patients. In addition, the data also included measurements at much higher PEEP levels than were used compared to the first dataset from Bersten [Bersten, 1998].

7.1 CLINICAL RESULTS

During the recruitment manoeuvre performed on the clinical group, the deflation to ZEEP ensured that dFRC could be measured. During ZEEP, the volume of the lung is recorded as zero. Because the pneumatachometer measures changes in volume due to pressure, when PEEP is applied, dFRC can be measured. Thus, dFRC at a given PEEP is defined as the change in volume between ZEEP and PEEP. All ten patients were deflated to ZEEP, with the only exception being Patient 6, Trial 1. Figure 7.1 shows a plot of PEEP vs clinically measured dFRC for Patient 1, which effectively represents the static PV curve. Static PV curves for all patients are shown in Appendix D.

The estimation of dFRC for the clinical data was performed via two methods using Equation 4.9. The initial estimation of dFRC was performed using the median β from the initial validation in Table 4.1, Chapter 4. A second estimation was performed by evaluating the median β for all twenty patients, comprising of 12 patients from the initial validation of Chapter 4 (Group 1) and the ten clinical patients from the new trials of Chapter 5 (Group 2). Because Equation 4.9 requires a compliance term to estimate dFRC, compliance was evaluated in the linear portion of the static PV curve shown in Figure 7.1 by the solid line.

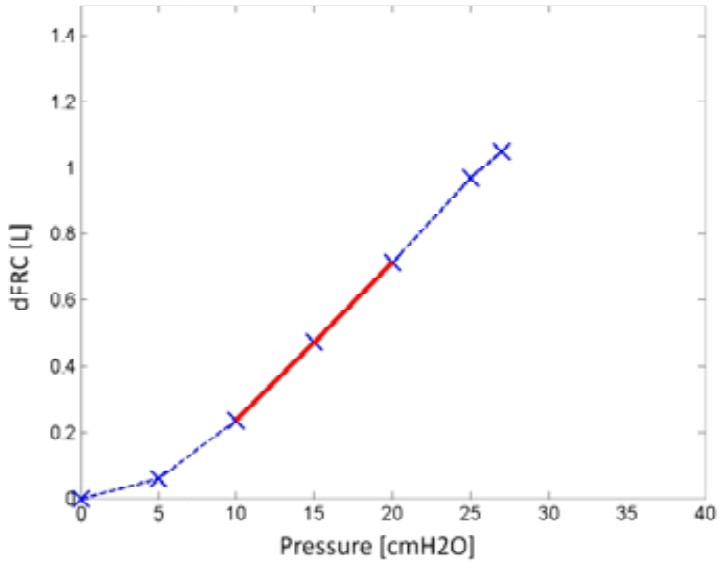

Figure 7.1 - PEEP vs dFRC for Patient 1. Red thicker solid line indicates the linear portion of the static PV curve

Table 7.1 shows the median β for Group 1, as reported from Chapter 4. Although Group 1 only contained PEEP values of 5, 7, 10, 12 and 15 cmH_2O, linear extrapolation was used to calculate median β at higher PEEP values. The median β from Group 1 was used to evaluate dFRC on Group 2, with the percentage error between calculated and measured dFRC shown in Table 7.2. Table 7.3 shows the median β when Group 1 and 2 are combined. It thus includes the median β from the 12 patients from Group 1 ([Bersten, 1998]), as well as from the ten clinical patients in Group 2. Table 7.4 shows the percentage error between the measured and calculated dFRC of Group 2 using the values from Table 7.3.

Table 7.1 - Median β from initial validation using data from Group 1 [Bersten, 1998], as per Chapter 4

PEEP [cmH_2O]	5	7	10	12	15
Median β	4.49	6.51	9.31	11.79	13.8

Table 7.2 -Percentage Error of actual dFRC and predicted dFRC for all patients in Group 2 at all PEEP levels using median ß from Table 7.1

PEEP [cmH_2O]		5	10	15	16	20	22	25	27	28	29	30
PATIENT	1	263.01	91.04	43.32		26.73		17.11	16.79			
	2	38.63	11.28	5.10		2.55	4.45					
	3	36.36	12.25	4.02		2.95		5.74		7.86		
	4	986.83	329.40	105.22		55.06		41.37				35.35
	5 - Trial 1	280.45	341.36	174.46		55.81		13.26				
	5 - Trial 2	2399.16	343.20	114.33		55.93	34.81				32.54	
	6 - Trial 2	35.84	21.79	11.65		6.76		13.47				
	6 - Trial 3	0.20	11.79	11.91		8.40						
	7	23.23	25.75	11.72	9.05							
	8	47.91	27.12	15.29		8.74		2.48				1.27
	9	95.49	196.54	77.84		43.54		26.57			27.61	22.10
	10	96.16	47.98	28.74		15.66		12.49	11.66			
	Median	**72**	**38**	**22**	**9**	**16**	**20**	**13**	**14**	**8**	**30**	**22**
	IQR	**[36.23, 267.37]**	**[19.41, 229.76]**	**[11.70, 84.68]**	**N/A**	**[7.58, 49.30]**	**[12.04, 27.22]**	**[10.76, 19.47]**	**[12.89, 15.51]**	**N/A**	**[28.84, 31.31]**	**[11.69, 28.73]**

Table 7.3 - Median *β* from all patients, comprising of data from Group 1 [Bersten, 1998] and data from Group 2

PEEP [cmH$_2$O]	5	7	10	12	15	16	20	22	25	27	28	29	30
Median *β*	3.33	6.85	8.38	11.79	12.34	16.58	16.33	19.91	20.84	22.38	25.90	21.12	23.27

Table 7.4 - Percentage Error of actual dFRC and predicted dFRC for all patients in Group 2 at all PEEP levels using median ß from Table 7.3

PEEP [cmH$_2$O]		5	10	15	16	20	22	25	27	28	29	30
PATIENT	1	192.71	83.24	37.69		23.62		19.32	11.80			
	2	11.79	6.74	0.96		0.03	3.17					
	3	9.96	7.66	0.07		0.42		7.74		10.37		
	4	776.37	311.86	97.15		51.25		44.05				39.56
	5 - Trial 1	206.78	323.33	163.66		51.98		15.40				
	5 - Trial 2	1915.20	325.09	105.90		52.10	37.36				23.25	
	6 - Trial 2	9.53	16.82	7.26		4.13		15.62				
	6 - Trial 3	19.53	15.39	15.37		10.66						
	7	38.10	28.78	15.19	2.68							
	8	19.27	21.93	10.76		6.07		4.42				4.42
	9	57.63	184.43	70.84		40.01		28.96			18.66	25.90
	10	58.18	41.94	23.67		12.82		14.62	6.89			
Median		**48**	**35**	**20**	**3**	**13**	**20**	**16**	**9**	**10**	**21**	**26**
IQR		**[17.40, 95.33]**	**[16.46, 216.29]**	**[9.88, 77.42]**	**N/A**	**[5.10, 45.63]**	**[11.72, 28.81]**	**[12.90, 18.96]**	**[8.12, 8,73]**	**N/A**	**[19.81, 22.10]**	**[15.16, 29.31]**

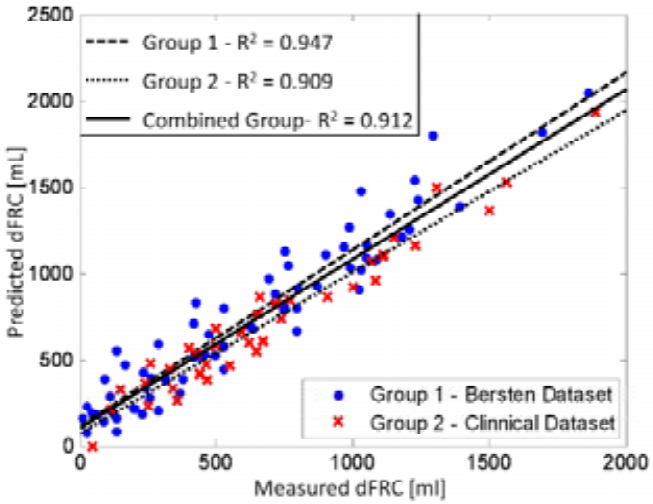

Figure 7.2 - Plot of Measured vs Predicted dFRC for all datasets. Red crosses indicate data points from Group 1 and blue dots indicate data points from Group 2. Dashed line is regression line for Group 1, dotted line for Group 2 and solid line for combined data set.

Figure 7.2 shows the predicted dFRC versus the measured dFRC for both Group 1 and 2. The plot shows strong linearity across all PEEP for Group 2 with an R^2 value of 0.909 (R = 0.9534). This linear relationship agrees with the results from Chapter 4, where Group 1 showed an R^2 value of 0.947. In addition, by combining the both Group 1 and 2, R^2 remained high with a value of 0.912.

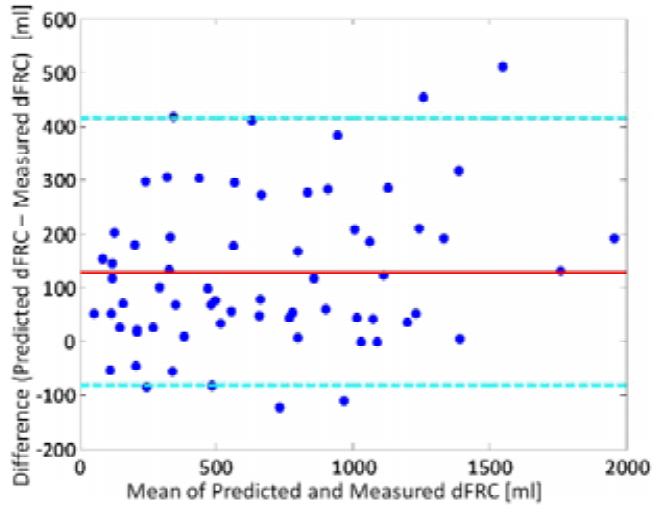

Figure 7.3 - Bland Altman plot of predicted dFRC and measured dFRC for clinical patients. Solid red line is the mean difference and dashed lines represent the 90% confidence interval

Figure 7.3 shows the Bland Altman plot with a 90% confidence. Compared with the results of Figure 4.8, Chapter 4, the 90% interval for the clinical data suggests much higher differences between predicted and measured dFRC. In addition, the mean difference is also much higher. However, this large difference can be attributed to some limitations of the model.

One of the implicit assumptions of the model is that the specific lung elastance (E_{Lspec}) and α are constant, where α represents the static lung elastance and represents the ratio of the lung elastance (E_L) to the chest wall elastance (E_{CW}). The assumption of α being constant is only valid during the linear portion of the static PV curve. Therefore, as discussed in Chapter 4, the dFRC estimation model may not accurately predict dFRC when there are significant changes in compliance. Figure 7.4 shows the static PV curves for Patient 4 and 5, which include these significant changes occurring at very low and very high PEEP.

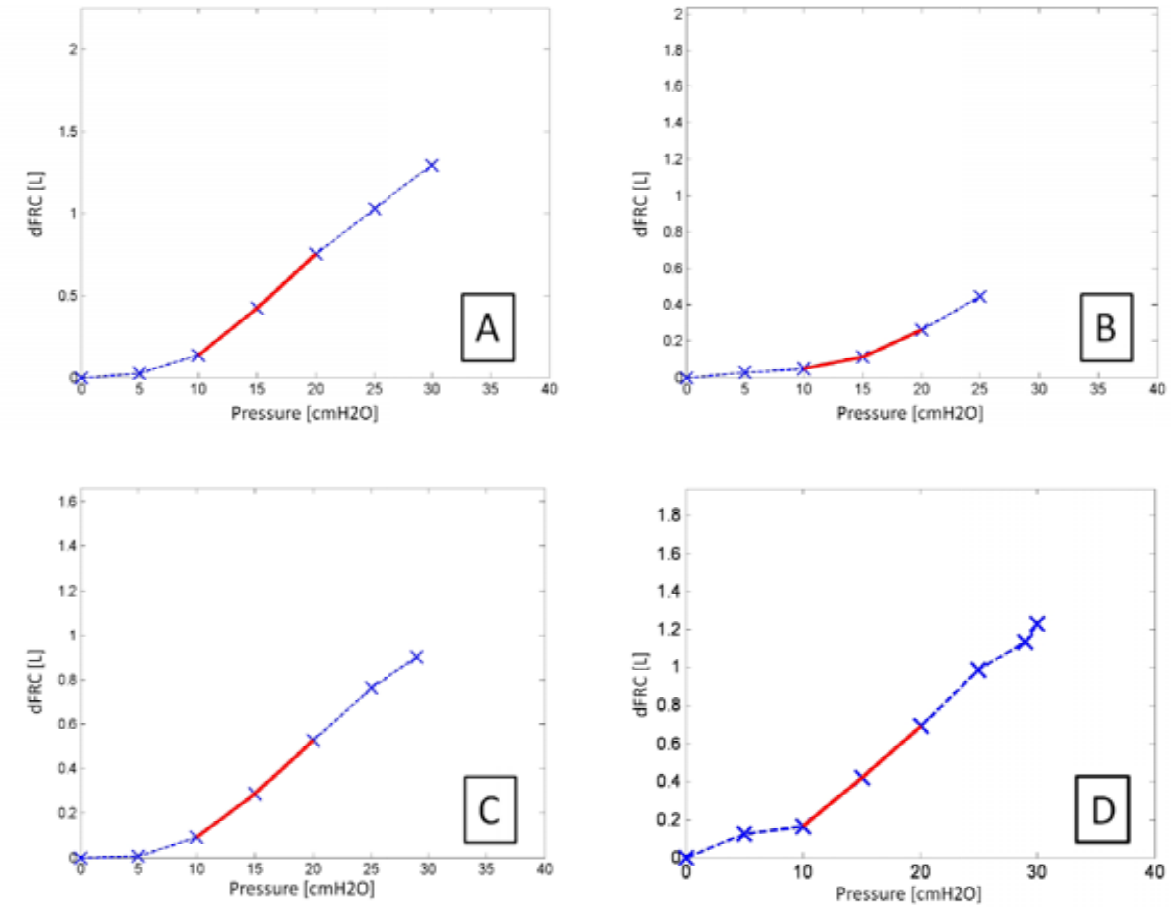

Figure 7.4 - PEEP vs dFRC for (A) Patient 4, (B) Patient 5, Trial 1, (C) Patient 5, Trial 2 and (D) Patient 9. Plots show very low compliance at low PEEP highlighting a limitation to the dFRC estimation model across wide PEEP ranges. However, this variation in compliance occurs at PEEP outside clinically reasonable range

As shown in the plots, there is a significant change in compliance across the range of PEEP. In particular, compared to other patients, Patients 4, 5 and 9 showed extremely low compliance at low PEEP. Patients 4, 5 and 9 showed extremely high errors when comparing predicted and measured dFRC, shown in Table 7.4. This result implies that the model may not be valid in regions where large compliance changes occur. When Patients 4, 5 and 9 are removed from the dataset, the Bland-Altman plot is modified and is shown in Figure 7.5.

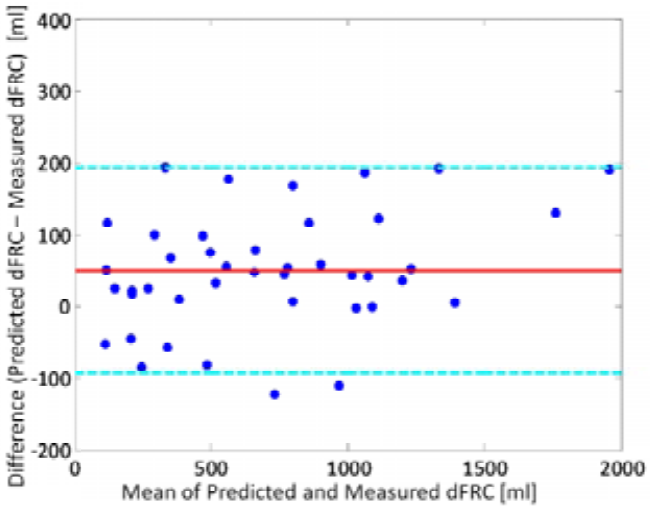

Figure 7.5 - Bland Altman plot of predicted dFRC and measured dFRC for clinical patients without Patients 4, 5 and 9. Solid red line is the mean difference and dashed lines represent the 90% confidence interval

When Patients 4, 5 and 9 are excluded from the analysis, the mean and 90% confidence interval changes significantly. Figure 7.5 indicates that maximum deviation, within 90% confidence, from measured dFRC is between 100 and 200 ml. These values correspond well with the values obtained during the preliminary analysis of Chapter 4, where the 90% interval was between 120 and 200 ml, shown on Figure 4.8.

Table 7.5 shows the percentage and absolute errors between predicted and measured dFRC for all datasets for PEEP values of 5, 10 and 15 cmH_2O. This includes the datasets from the initial validation of Chapter 4 (Group 1), along with the clinical data obtained during the new trials presented (Group 2). Although the inter quartile range (IQR) for a PEEP of 5 cmH_2O reaches as high as 45%, the low median percentage error may suggest that β is, in fact, a useful population constant.

Table 7.5 - Percentage error between predicted and measured dFRC across all data sets using median β. Absolute error in brackets

PEEP [cmH_2O]		5	10	15
GROUP 1 - BERSTEN DATASET	1	3.93 (17.41)		
	2	26.44 (94.81)	16.02 (104.38)	
	3	9.5 (24.06)	2.13 (9.80)	
	4	116.52 (177.30)	37.14 (184.92)	
	5	0.02 (0.00)	2 (31.62)	
	6	42.65 (170.55)		
	7		8.1 (81.36)	9.02 (134.62)
	8	5.11 (22.62)	4.53 (41.32)	
	9	16.69 (83.17)	5.07 (58.03)	
	10	84.95 (98.80)	35.27 (116.25)	11.04 (65.68)
	11	15.41 (84.71)	11.19 (121.53)	
	12	51.55 (124.97)	16.4 (107.23)	
GROUP 2 - CLINICAL DATASET	1	192.71 (117.38)	83.24 (195.77)	37.69 (178.16)
	2	11.79 (23.18)	6.74 (33.55)	0.96 (7.66)
	3	9.96 (24.47)	7.66 (48.40)	0.07 (0.77)
	6 - Trial 2	9.53 (19.19)	18.82 (76.73)	7.26 (54.46)
	6 - Trial 3	19.53 (44.65)	15.39 (80.95)	15.37 (122.06)
	7	38.10 (52.28)	28.78 (83.00)	15.19 (55.57)
	8	19.27 (25.78)	21.93 (69.38)	10.76 (56.59)
	10	58.18 (51.99)	41.94 (100.96)	23.67 (98.79)
Median IQR		**19 (52) [9.64 (23.62) , 47.10 (96.81)]**	**16 (81) [6.97 (50.81), 27.07 (106.51)]**	**11 (61) [7.70 (54.74), 15.33 (116.24)]**

7.2 DISCUSSION & LIMITATIONS

7.2.1 COMPLIANCE CHANGES

One of the major limitations that the clinical trials have highlighted is the effect of large compliance changes. As discussed in Section 7.1 and Chapter 4, the model assumes that the static lung elastance, α, remains constant across the range of PEEP. This assumption is only valid in effectively the linear portion of the static PV curve. At low and high PEEP levels, the lung and chest elastance can vary significantly, and this variation can contribute to significant compliance changes.

Patients 4 and 5 exhibited very large compliance changes as PEEP varied. More specifically, an increase from ZEEP to 5 cmH_2O PEEP yielded almost no volume change,

indicating very low compliance. However, a further increase in PEEP resulted in larger volume changes. For both patients, this variable compliance change implies that elastance is not constant across PEEP. Hence, the large errors between predicted and measured dFRC for some estimates based on these patients can be attributed to this variable compliance, highlighting a significant limitation with the model. In contrast, patients who exhibited largely linear compliance across all measured PEEP seemed to show small errors between measured and predicted dFRC.

It must be noted that the regions where there is significant compliance change occur outside the clinically useful range of PEEP. More specifically, compliance is very low at extremely low and high PEEP, which is generally not used when attempting to recruit patients. Thus, although some patients did not exhibit constant compliance, compliance remained linear in the clinically applicable segment of the static PV curve. In addition, although there may be large errors between measured and estimated dFRC, the relative changes of dFRC in the linear portion still show similar trends. Thus, although these errors are large, general trends remain the same.

This sudden compliance change is also attributed to the large percentage error for Patient 2 when PEEP was 5 cmH_2O, as shown on Table 7.2 and Table 7.4. The extremely low compliance meant that the true measured volume was close to zero. Thus, when calculating the percentage error, the denominator approaches zero yielding an extremely large percentage error, for an absolute change in volume that is not necessarily clinically significant.

7.2.2 COMBINED DATASET

To ensure that β is truly a population constant, the size of the dataset was increased. Data from Group 1 (12 datasets – 39 data points) was added to Group 2 (ten datasets – 54 data points) and the median β was calculated. The median β calculated across the combined dataset, shown in Table 7.3, still showed a linear trend as seen in Figure 7.6. In addition, extending the data set also indicates that β remains linear even at high PEEP.

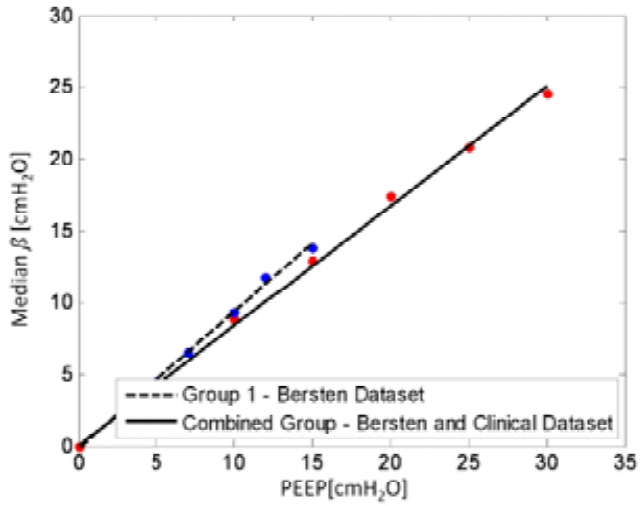

Figure 7.6 - Median *β* across combined dataset compared with the median *β* of Group 1

The difference between the median *β* for the initial validation on Group 1 and the combined dataset (Group 1 & Group 2) shows a small difference, as shown in Figure 7.6. However, this difference is assumed to occur due to the limited size of the dataset of Group 1. Hence, there is a strong indication of a global population constant. As the size of the dataset increases, *β* should also change. More specifically, as the number of data points increase, the assumption of *β* representing a population constant will become more valid.

7.2.3 DFRC & RECRUITMENT MODELS

To accurately apply the recruitment model, the patient requires a deflation to ZEEP so that dFRC can be measured. In reality, the deflation to ZEEP can prove to be harmful to patients who are severely ARDS affected, as it may cause sudden de-recruitment. During the clinical trials, all patients were deflated to ZEEP with the exception of the first trial for Patient 6. For this trial, the lowest PEEP was set at 10 cmH_2O, with PEEP being incremented to 15, 20 and 25 cmH_2O, shown in Figure 7.7.

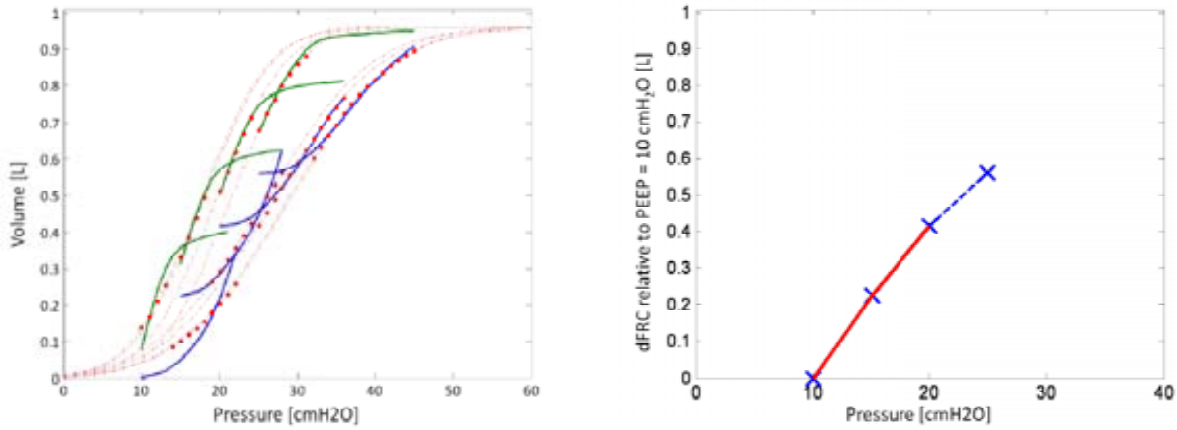

Figure 7.7 - PV curves for Patient 6, Trial 1. No measurements of dFRC were taken as patient was not deflated to ZEEP

Although the recruitment model can be fitted to these PV loops, the model works best when dFRC measurements are known. If the deflation to ZEEP is deemed unsafe for the patient, then estimating dFRC could be used as an alternative to actual measurements. Figure 7.8 shows dFRC being estimated and the corresponding PV curves being shifted for Patient 6, Trial 1. The re-calculated PV curves can be fitted to the recruitment models to evaluate new threshold opening (TOP) and threshold closing pressure (TCP) parameters, which are shown in Figure 7.9. This process is only valid when β is a population constant, which is a function of PEEP.

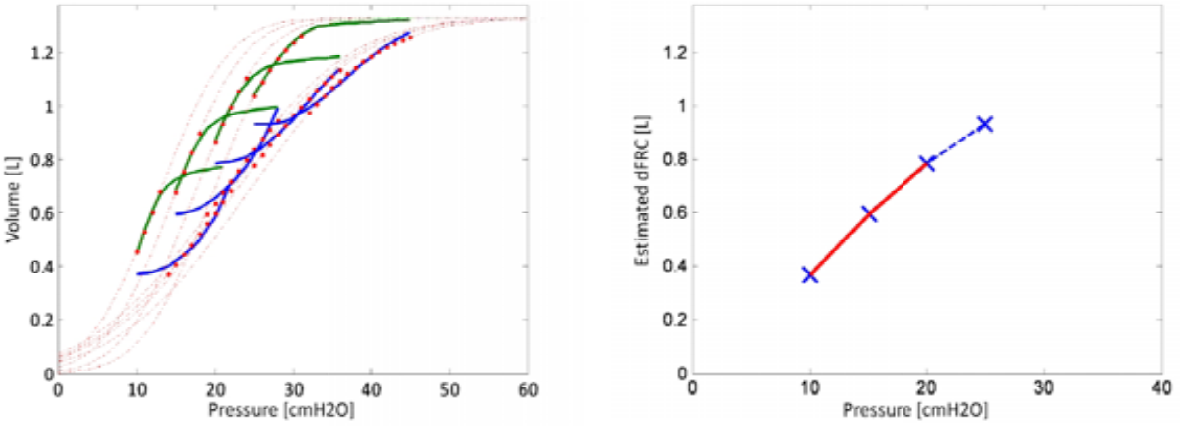

Figure 7.8 - PV curves for Patient 6, Trial 1. dFRC is estimated using the linear compliance for Patient 6, Trial 1.

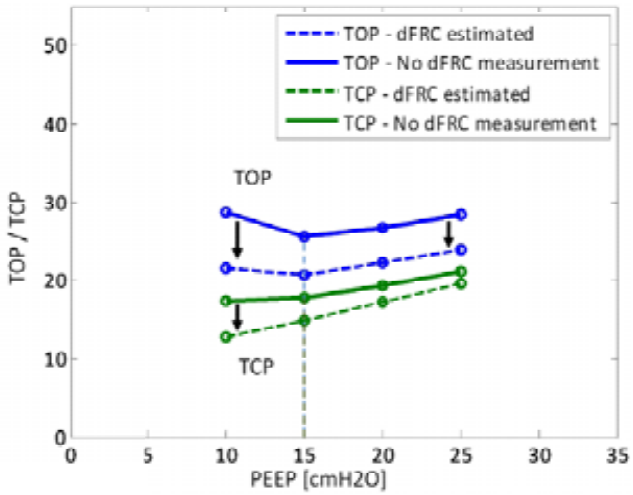

Figure 7.9 - Comparison of TOP and TCP when dFRC is estimated for Patient 6, Trial 1

Figure 7.9 shows the TOP and TCP when dFRC is estimated in this way for that patient. Although there is a decrease in absolute values of TOP and TCP, the trend of both seems to remain relatively constant. In addition, when dFRC is not measured, TCP predicts optimum PEEP at 20 cmH_2O. In contrast, when dFRC is estimated, TCP selected PEEP is 15 cmH_2O.

7.3 SUMMARY

The results discussed in this chapter further highlight the potential for β to be used as a global population constant (as a function of PEEP) for estimating dFRC. The preliminary validation performed in Chapter 4 provided evidence on the variation in β when PEEP was varied between 5 and 15 cmH_2O, and showed a linear relationship between PEEP and β. By increasing the dataset, the linear relationship was also shown to hold at higher PEEP values up to 30 cmH_2O.

The increased dataset has also highlighted a limitation to the dFRC estimation model. For a given patient, when compliance changes significantly with PEEP, the model fails to accurately estimate true dFRC. Thus, the model is primarily valid when compliance is constant across all PEEP for a given patient. For patients where compliance did vary significantly at low and high PEEP, this limitation may not necessarily pose a major problem as these PEEP values are outside the clinically useful range. In addition, although

predicted and measured dFRC may show high percentage errors, within the linear region, the trends are still the same.

The dFRC model can be used in conjunction with the recruitment model when dFRC measurements are not available. When the deflation to ZEEP is deemed to hazardous to the patient, estimating dFRC provides a means to improve the results of the recruitment model and provide a more accurate set of PEEP results and potentially improved decision support.

Chapter 8 - Cardiac Output Estimation

Hitherto, the models presented in this thesis use lumped parameter models as a means to optimise ventilation therapy. More specifically, the models presented are classified as recruitment models, where recruitment is the primary objective for mechanical ventilation. The models introduced in Chapters 3 and 4 examine the effect of PEEP on lung recruitment and lung volume. However, as discussed in Chapter 2, gas exchange models are an alternative lumped parameter model which can be used to help select PEEP based on oxygenation.

This chapter introduces a third mathematical model that combines the effect of recruitment and gas exchange. The combination of these two principles leads to additional information being available to the clinician. More specifically, by combining gas exchange and recruitment models, it is possible to examine the effects of PEEP on thoracic cavity pressures, and thus on the cardiovascular system and circulation, which are also very important clinical variables in the ICU.

8.1 INTRODUCTION

Patients diagnosed with ARDS often experience pulmonary shunt or gas exchange abnormalities due to lack of recruited alveoli. Shunt also occurs when there is an increased thoracic pressure that restricts blood flow, thus reducing gas exchange in the lung. The primary objective of MV is to improve the condition of the patient by increasing alveoli recruitment and thus also improving or optimising gas exchange.

As discussed in previous chapters, the application of sub-optimal PEEP can cause repetitive opening and closing of alveoli. In addition, the application of PEEP can also decrease cardiac output (CO) [Cournand et al., 1947, King et al., 1973]. The decrease in CO from high PEEP is due to the reduction in stroke volume of the heart. As PEEP increases, the intrathoracic pressure increases, which increases cardiac afterload and thus restricts the venous flow into the thorax resulting in a lowered CO. Any decrease in CO lowers oxygen consumption, as determined by Fick's law, and describes the inability of the heart to pump enough blood to meet the metabolic requirements of the body. Reduced CO

can also have an impact on circulation management and therapeutics used. Hence, the application of PEEP to improve recruitment may have unintended negative impacts on the cardiovascular system.

Current methods to measure CO, such as thermodilution and pulse pressure methods, are clinically invasive, requiring the use of catheters [Forrester et al., 1972, Leibowitz and Oropello, 2007]. These catheters carry some added risks of infection [Lorente et al., 2004], and are thus used only in an increasingly limited subset of critically ill patients receiving MV. More specifically, for critically ill patients, the benefits from CO measurements may not offset the dangers associated with invasive tools. In addition, these methods take time and effort, are not performed regularly and cannot be monitored in clinical real time. Hence, significant motivation exists to develop non-invasive, real-time tools to track CO, independent of the need to monitor and manage MV

MV patients treated for ARDS may not have CO measurements readily available. However, the changes in CO due to changes in applied PEEP are important as it may also help indicate an optimal level of PEEP. In particular, if a change in PEEP causes a large drop in CO, it may more than offset its benefit on recruitment. Alternatively, if the drop in CO is minimal, then the benefits of PEEP induced recruitment may offset the detrimental effects of an insignificant drop in CO. Hence, the ability to model changes in CO due to PEEP may also prove beneficial for optimizing the setting of PEEP, which can itself be controversial [Levy, 2002].

This chapter aims to combine the effects of two individual models to estimate changes in CO due to PEEP. The recruitment model, developed in Chapter 3, is combined with the oxygen diffusion model of Andreassen et al [Andreassen et al., 1996]. The diffusion model estimates pulmonary shunt and oxygen diffusion resistance by measuring variations in fraction of inspired oxygen (F_iO_2) and arterial oxygen saturation (S_pO_2). The diffusion model takes inputs of cardiac output, F_iO_2 and other ventilation data, and estimates pulmonary shunt and diffusion resistance as outputs.

8.2 DIFFUSION MODEL

A detailed explanation of the recruitment model is presented in Chapter 3. The following section introduces the diffusion resistance model developed by Andreassen et al [Andreassen et al., 1996] and the mathematics behind it.

Current methods of describing gas exchange abnormalities, such as arterial oxygen saturation, alveolar arterial oxygen pressure gradient or venous admixture [Wandrup, 1992, Wandrup, 1995] are insufficient. In particular, these parameters lump the effects of oxygen diffusion and true pulmonary shunt into a single parameter. This single parameter is typically inadequate as it is difficult to interpret which mechanism causes the gas exchange abnormality.

Pulmonary shunt occurs when the alveoli in the lung are perfused with blood, as desired, but not adequately ventilated. In patients with ARDS, alveoli collapse occurs as a result of fluid build up, which results in the ARDS lung not being ventilated. Thus, as ARDS severity increases, pulmonary shunt also increases. Even if alveoli are recruited or do not collapse, if gas exchange does not occur it is considered to be part of the shunt volume. Similar abnormality or failure of gas exchange can occur when CO and minute ventilation are mismatched [Karbing et al., 2007].

In patients who are mechanically ventilated, the application of PEEP can increase alveolar recruitment. As more alveoli are recruited, there is an increase in alveolar ventilation and as a result, pulmonary shunt decreases. Using standard data, such as S_pO_2 and arterial oxygen pressure (P_aO_2), curves of S_pO_2 can be generated as a function F_iO_2. These curves can then be used to estimate the pulmonary shunt and diffusion resistance [King et al., 1974, Andreassen et al., 1999].

The model developed by Andreassen et al [Andreassen et al., 1996] uses a compartmental oxygen status model as shown in Figure 8.1. The net oxygen consumption by the alveoli (VO_2) is calculated by using known values of F_iO_2, fraction of expired oxygen (F_eO_2), respiratory frequency (f) and tidal volume (V_t), and where dead space (V_d) is the amount of air in the lungs that does not reach the alveoli, and thus is does not contribute to any gas exchange.

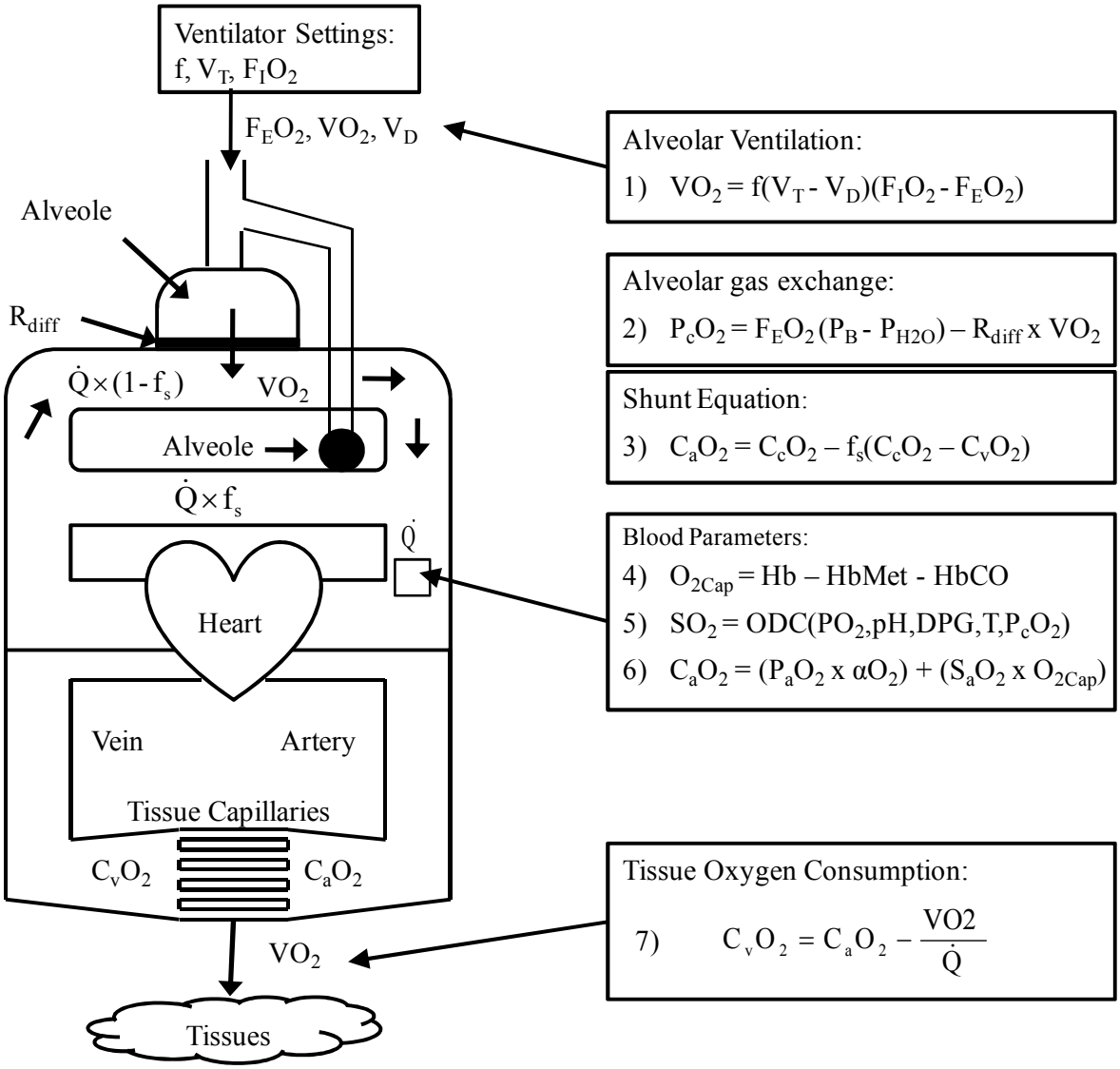

Figure 8.1 - Diffusion Model reproduced from Rees & Andreassen et al [Rees et al., 2002, Andreassen et al., 1996]

$$VO_2 = f(V_t - V_d)(F_iO_2 - F_eO_2) \quad (8.1)$$

Once the inspired gas reaches the alveolar compartments, oxygen begins the diffusion process across the alveolar membrane to the capillaries. The partial pressure of oxygen in the capillary (P_cO_2) is a function of the partial pressure in the alveoli minus the drop in partial pressure due to diffusion resistance (R), where P_b is the atmospheric pressure.

$$P_cO_2 = (F_EO_2 \times P_B) - (R \times VO_2) \quad (8.2)$$

After the oxygen has diffused through the alveolar wall, oxygen from the capillaries with high concentration (C_cO_2) mixes with venous blood, which has low concentration (C_vO_2). Depending on the level of pulmonary shunt (f_s), the arterial oxygen concentration can be evaluated (C_aO_2).

$$C_aO_2 = C_cO_2 - f_s(C_cO_2 - C_vO_2) \quad (8.3)$$

The oxygen carrying capacity of haemoglobin (O_{2Cap}) can be defined as a function of blood parameters such as haemoglobin (c*Hb*), methaemoglobin (c*MetHb*) and carboxyhaemoglobin (c*COHb*).

$$O_{2Cap} = cHb - cMetHb - cCOHb \quad (8.4)$$

The oxygen saturation curve (S_cO_2) can then be calculated based on the oxygen dissociation curve (*ODC*).

$$S_cO_2 = ODC(pO_2^c \times f_1(pH^c) \times f_2(BE^E) \times f_3(T^c) \times cf^c) \quad (8.5)$$

Finally, C_cO_2 can then be defined:

$$C_cO_2 = (S_cO_2 \times O_{2Cap}) + (P_cO_2 \times AO_2) \quad (8.6)$$

The net difference between the arterial concentration and the drop in oxygen consumption by the tissues then gives C_vO_2.

$$C_vO_2 = C_aO_2 - \frac{VO_2}{CO} \quad (8.7)$$

Table 8.1 shows the different parameters that are measured, estimated and calculated in this diffusion resistance model. First, the model requires a gas exchange analyser to measure the F_iO_2 and F_eO_2 values along with a pulse oximeter to measure the S_pO_2. Respiratory frequency and tidal volume are measured with a ventilator, while the haemoglobin concentrations are measured by taking a blood sample.

In the model developed by Andreassen et al [Andreassen et al., 1996], CO was estimated. However, it can also be measured using thermodilution techniques, although it is not clinically feasible in regular, repetitive fashion. Using all these measurements, and an estimate of dead space, it is then possible to calculate shunt and diffusion resistance by solving Equations (8.1) - (8.7).

Table 8.1 - Measured, estimate and calculated parameters in the diffusion resistance model

Directly Measured Parameters	Estimated Parameters	Calculated Parameters
Respiratory Frequency (*f*)	Dead Space (V_d)	Shunt (f_s)
Inspired Oxygen Content (F_iO_2)		Diffusion Resistance (*R*)
Expired Oxygen Content (F_eO_2)		
Tidal Volume (V_t)		
Atmospheric Pressure (P_B)		
Pulse or Arterial Oxygen Saturation (S_pO_2)		
Cardiac Output (*CO*)		
Haemoglobin (*cHb*)		
Methaemoglobin (*cMetHb*)		
Carboxyhaemoglobin (*cCOHb*)		

8.3 COMBINED MODEL DEVELOPMENT

8.3.1 DIFFUSION MODEL PARAMETERS

The diffusion model by Andreassen et al [Andreassen et al., 1996] was used to simulate responses to variations in the model parameters. In particular, the study examined how shunt and oxygen diffusion resistance varied under different F_iO_2. The simulations used the input parameters shown in Table 8.2**.**

Figure 8.2 shows the S_pO_2 varying as a function of F_iO_2 depending on the level of shunt with a diffusion resistance of zero. When no shunt exists, the S_pO_2 curve is identical to the oxygen dissociation curve. However, as shunt increases, then for a given F_iO_2, the level of oxygen saturation decreases.

Table 8.2 - Diffusion model parameters from Andreassen et al [Andreassen et al., 1996]

Respiratory frequency	f	14 min^{-1}
Tidal volume	V_t	0.5 L
Dead space volume	V_d	0.15 L
Cardiac output	CO	5 L/min
Oxygen consumption	VO_2	11.5 mmol/min
Haemoglobin	cHb	9 mmol/L
Methaemoglobin	$cMetHb$	0 mmol/L
Carboxyhaemoglobin	$cCOHb$	0 mmol/L
Oxygen solubility coefficient	AO_2	0.0102 mmol/(L kPa)
Arterial pH status	pH^a	7.4
Capillary pH status	pH^c	7.4
Arterial base excess	BE^a	0 mmol/L
Capillary base excess	BE^c	1 mmol/L
Arterial blood temperature	T^a	37 C
Capillary blood temperature	T^c	37 C
Barometric pressure	P_B	101.3 kPa

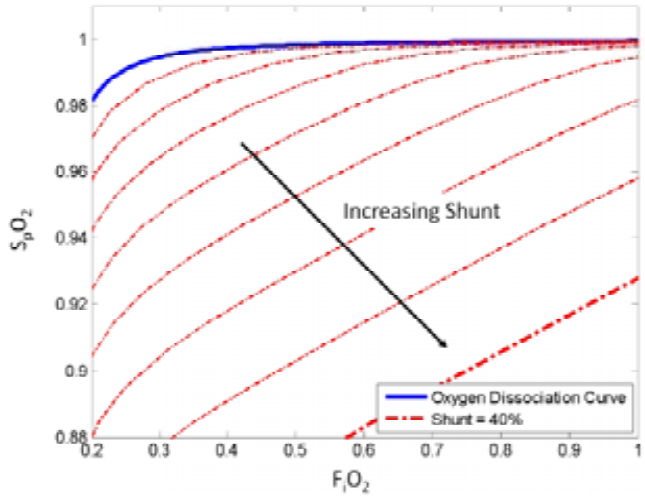

Figure 8.2 - Oxygen saturation curves changing as a function of F_iO_2 and various levels of shunt

Figure 8.3 shows the effect of varying the diffusion resistance instead of shunt. Similar to shunt, an increase in oxygen resistance also causes incomplete oxygenation. It is assumed that shunt is zero for all the curves in this figure.

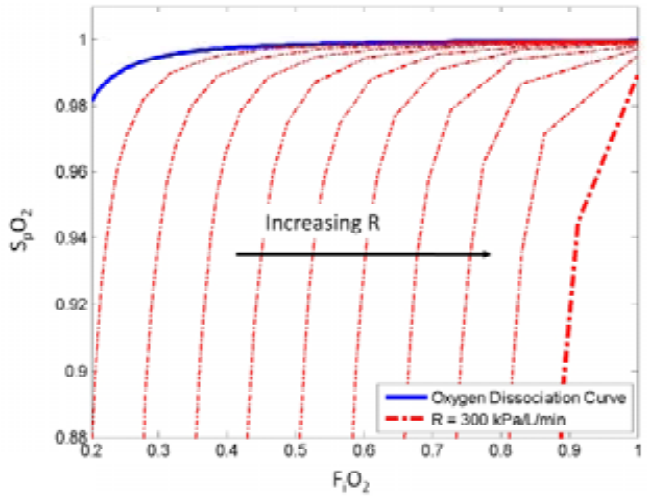

Figure 8.3 - Oxygen saturation curves at various levels of diffusion resistance and shunt = 0

Theoretically, if two different F_iO_2 measurements were taken and the corresponding S_pO_2 values measured and plotted, it is possible to evaluate the shunt and diffusion resistance by plotting the best fit S_pO_2 curve. However, in Figure 8.2 and Figure 8.3, the cardiac output is held at a constant value of 5 L/min. Unless measured, the value of CO is assumed to be 5.0 L/min in this analysis [Rees et al., 2002, Andreassen et al., 1996]. However, in patients with ARDS where PEEP is titrated based on clinical choice, the assumption of using a constant CO is not valid. In addition, as a result of MV therapy and other aspects of their condition, CO is much more variable, with a typical range of 2-8 L/min [Hoeper et al., 1999, Luecke and Pelosi, 2005, Vidal Melo, 1998].

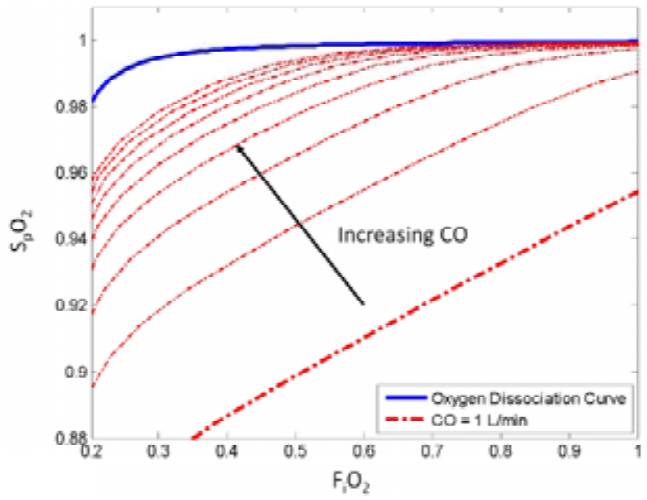

Figure 8.4 - Oxygen saturation curve varying as a function of cardiac output

While such changes in CO were not modelled by Andreassen et al, they are easily incorporated into this model. Figure 8.4 shows the effect of varying cardiac output given a shunt value of 10% and a diffusion resistance of 0 kPa/L/min. As shown in Figure 8.4, an increase in cardiac output causes a more complete oxygenation of the blood. Overall, it adds a third unknown variable, CO, to the shunt and diffusion resistance noted previously.

In Figure 8.2 – Figure 8.4, the lines of constant shunt, diffusion resistance and cardiac output are analogous to principles in thermodynamics, such as isotherms (lines of constant temperature), isobars (lines of constant pressure) and isochors (lines of constant volume). In particular, if two states are known, then it is possible to determine the third state of a gas as all variables are interrelated. Similarly, the lines of constant shunt, diffusion resistance and cardiac output are all interrelated.

8.3.2 ESTIMATING SHUNT CHANGES DUE TO PEEP – LINKING THE TWO MODELS

Because the current diffusion models use CO as an input, it is possible to estimate the shunt and diffusion resistance if a few measurements such S_pO_2 and F_iO_2 are taken. However, as PEEP increases, the level of alveoli recruitment also increases at the cost of decreased CO. Thus, unless the patient has a continuous measurement of CO, then an alternative method must be developed to generate the S_pO_2 curves and predict shunt.

The principle hypothesis behind the linked model is that any increase in PEEP directly causes a decrease in shunt. In ARDS affected lungs, collapsed alveoli do not contribute to the ventilation process. Although the capillaries around collapsed alveoli may be properly perfused they contribute to pulmonary shunt because they do not contribute to gas exchange and ventilation. As PEEP is applied, more alveoli are recruited, which means there is more aerated surface area for gas exchange, which causes a decrease in shunt [Acosta et al., 2007, Michelet et al., 2005]. Thus, if it is possible to estimate changes in shunt, theoretically, it should be possible to estimate CO, as all other parameters are assumed known.

If shunt decreases with increased recruitment, then it is possible to estimate shunt changes using the recruitment model from Chapter 3. Because the recruitment model has the ability

to estimate changes in recruitment, it is hypothesised here that the increase in recruited volume due to PEEP is directly related to the decrease in shunt. More specifically, changes in recruited volume are assumed equal to the corresponding reductions in shunt.

This novel method of linking up recruitment and gas exchange models provides a new insight into lung mechanics. In particular, using recruitment models to estimate shunt, and combining with gas exchange models provides a new method to track CO changes.

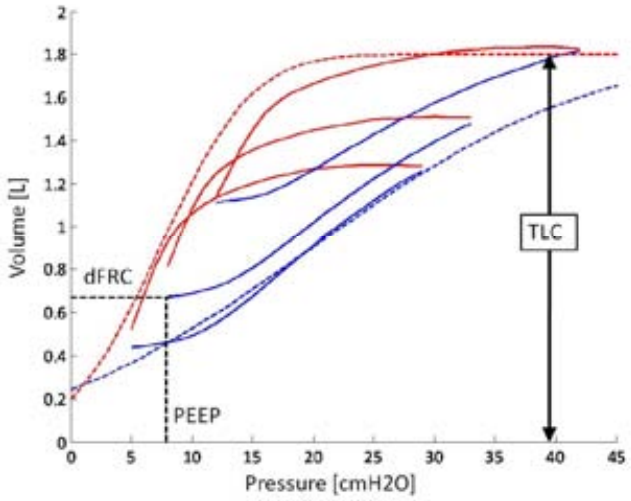

Figure 8.5 - Model fitting using measured PV loops - Dataset 1 from Bersten [Bersten, 1998]. dFRC is measured and then all PV loops fitted to maximum theoretical TLC

Figure 8.5 shows the PV curves for Dataset 1, from Bersten [Bersten, 1998], fitted to the recruitment model. If an initial shunt value is known or estimated, then to estimate a percentage change in shunt, the changes in dFRC can be examined with reference to the maximum theoretical TLC. Thus, using the stated hypothesis, the percentage change in shunt (Δf_s) for a given change in PEEP can be evaluated using Equation (8.8).

$$\Delta f_s = \frac{dFRC_1 - dFRC_2}{F_H - dFRC_1} \tag{8.8}$$

Although the recruitment model cannot predict absolute shunt fractions, it does have the ability to predict changes in shunt volume, which is the clinically critical aspect. Thus, for the first PEEP setting, a shunt fraction is measured using the diffusion model using a known or estimated CO. Once an initial shunt measurement is obtained, changes in PEEP induced recruitment can be used to estimate the shunt at a new level of PEEP by

calculating the percentage change in shunt from that initial value, using the stated hypothesis.

Given that result, subsequent measurements of F_iO_2 and S_pO_2 at the new PEEP, and fitting an S_pO_2 curve constrained by the new level of shunt allows the level of CO to be estimated working backwards to find the CO value that yields this curve. This overall process of evaluating the CO is summarised in Figure 8.6.

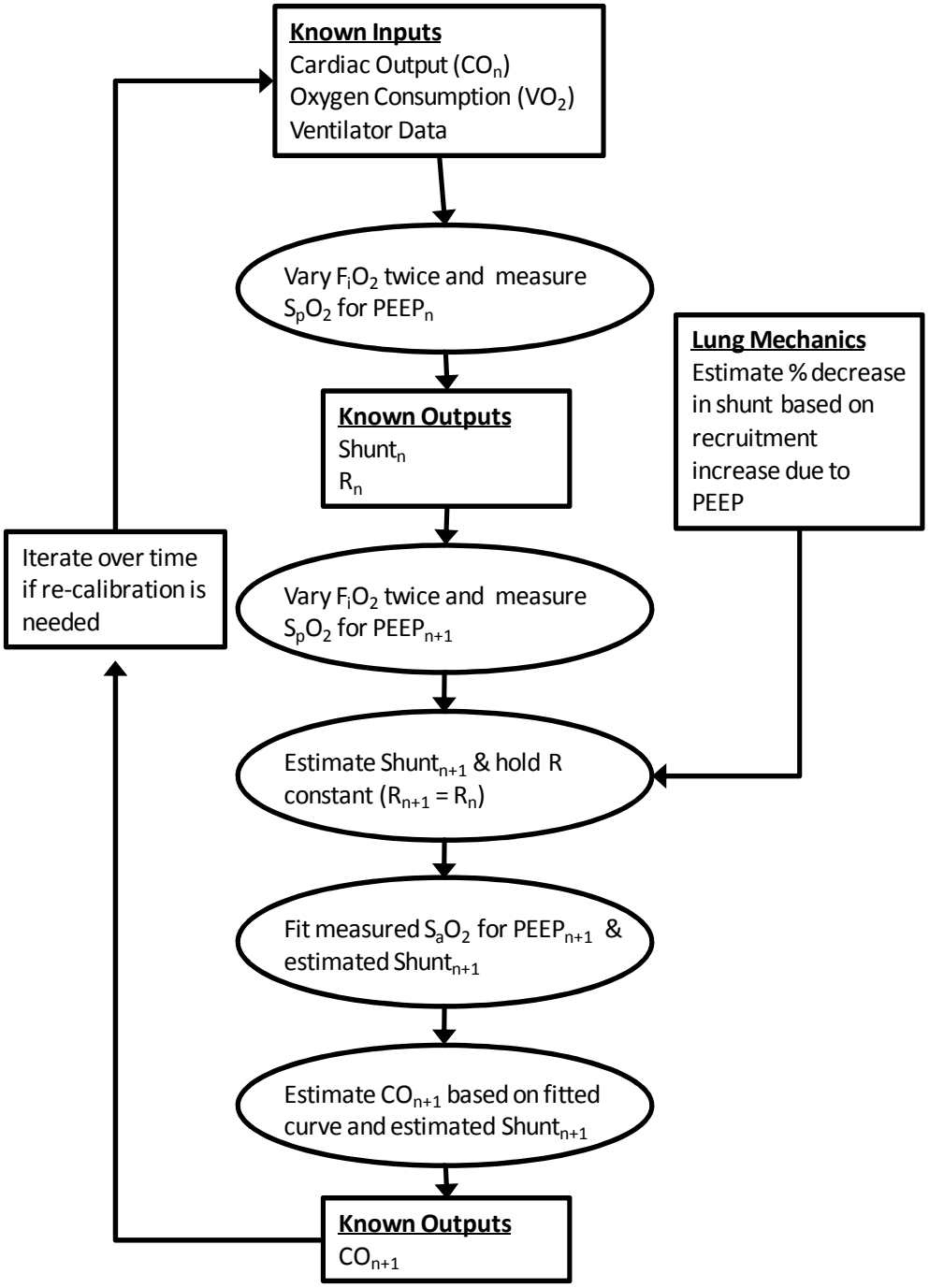

Figure 8.6 - Flow chart determining the process of estimating cardiac output at a higher PEEP level

In particular, Figure 8.6 shows the need for an initial measurement of CO. Once an initial measurement or a reasonable estimate is obtained, it is then possible to track changes in CO with changes to PEEP. As noted, such an initial or daily measurement is readily available via thermodilution if necessary catheters are not in place. Thus, over a given time period, the changes in CO are calibrated to the initial or regular CO measurements obtained through thermodilution, or if available, invasive catheters. Finally, large predicted changes in CO with this method could generate a new, confirmatory thermodilution measurement.

8.4 MODEL VALIDATION & ANALYSIS

8.4.1 PROOF OF CONCEPT

To test the concept of tracking changes in CO, a proof of concept (POC) model has been evaluated based on a mixture of simulated parameters and clinical data. The data used in the study uses one set of data containing PV loops obtained from Bersten [Bersten, 1998] and arterial blood gas measurements from Andreassen et al [Andreassen et al., 1996]. Although these measurements do not correspond to the same data set, the aim is to evaluate the utility of the POC model presented and the robustness of its underlying assumptions prior to further clinical validation.

Three PV loops were obtained from Bersten [Bersten, 1998] with the associated deflation to dFRC for dataset 1. The TOP and TCP were modelled using the recruitment model described in Chapter 3, with the PV loops shown in Figure 8.5 and in Table 8.3. Using Equation (8.8), it is then possible to evaluate the percentage change in shunt as PEEP increases.

Table 8.3 - Measured PV data for Patient 1 from Bersten [Bersten, 1998] fitted with the recruitment model

PEEP [cmH_2O]	dFRC [L]	TLC [L]	Δf_s
5	0.441		
7	0.674		-0.15
12	1.1125	1.98	-0.34

Because there is no initial measurement of shunt at the first PEEP level, it is not possible to estimate the shunt at higher levels of PEEP. The PV data from Bersten did not include any blood gas measurements. To simulate the POC model, the blood gas data from Andreassen [Andreassen et al., 1996] was used and is shown in Table 8.4. To fit the S_pO_2 curve, two measurements of F_iO_2 were required. These initial F_iO_2 and S_pO_2 measurements at t_1 and t_2 were assumed to occur at the initial PEEP setting of 5 cmH_2O. It was also assumed that the CO at the first PEEP was 5 L/min. These overall values and assumptions, while not from the same dataset, are clinically realistic. Measuring S_pO_2 at two different F_iO_2 values for a given PEEP is also readily achieved.

Table 8.4 - Measured values of varying F_iO_2 and S_pO_2 from Andreassen et al. These values are assumed to occur at the initial PEEP level

	Time t_1	**Time t_2**
F_iO_2 [%]	25	35
S_pO_2 [%]	90.9	95.1

Fitting the diffusion model to the data in Table 8.4 yields a shunt of 17% and a diffusion resistance of 36 kPa/L/min. For the purpose of this POC model, it is assumed that this is the true shunt at the initial PEEP. The raw data points and the best fit S_pO_2 curve are shown in Figure 8.7.

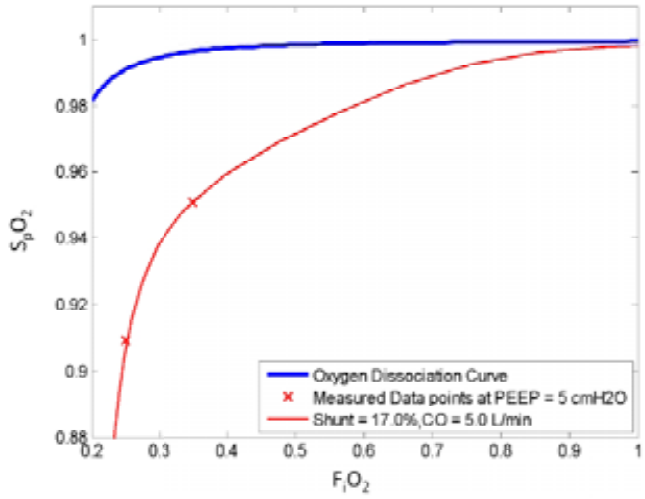

Figure 8.7 - Best fit oxygen saturation curve assumed to occur at the first PEEP. Shunt = 17% and diffusion resistance = 36 kPa/L/min with CO = 5 L/min

After evaluating the shunt at the initial PEEP level, it is then possible to evaluate the shunt at higher PEEP settings using the percentage change in shunt from the results in Table 8.3. For the higher PEEP values, the measured S_pO_2 is fit to an oxygen saturation curve by constraining the predicted shunt and thus, evaluating the new CO, which is shown in Figure 8.8.

Table 8.5 - Modified shunt and cardiac output as a function of PEEP. * indicates measured or known input values. + indicates estimated values

PEEP [cmH_2O]	F_iO_2 [%]	S_pO_2 [%]	Shunt [%]	R [kPa/L/min]	CO [L/min]
5	[25 35]*	[0.909 0.951]*	17*	36	5*
7	[25 35]*	[0.91 0.96]*	14.5^+	36	4.7^+
12	[25 35]*	[0.91 0.97]*	9.5^+	36	4.3^+

The shunt, CO and diffusion resistance for this POC model example are summarised in Table 8.5 along with the values of F_iO_2 and S_pO_2.

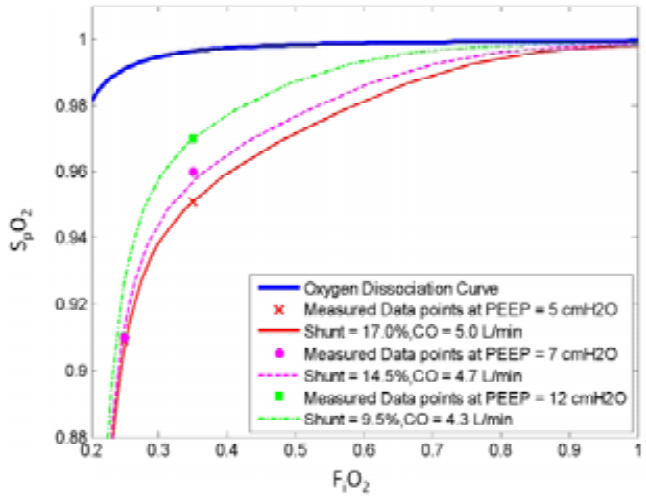

Figure 8.8 - Improved oxygenation as shown by the increase in oxygen saturation with the application of PEEP

8.4.2 OPTIMISATION OF PEEP & PATIENT CARE

In the POC model, the cardiac output was shown to drop from 5 to 4.3 L/min as PEEP increased from 5 to 12 cmH_2O. This drop agrees with current data showing that CO drops with increased PEEP [Cournand et al., 1947, King et al., 1973]. The POC model showed that the application of PEEP improved oxygenation. However, Figure 8.4 shows that any

decrease in CO should reduce oxygenation with all else equal and shunt at a constant value.

The results of the POC model thus confirm the trade off between the amounts of decreased shunt versus the decrease in cardiac output. To test this theory, the CO was set to drop from 5 to 1.5 L/min (corresponding to a drop of 0.5 L/min/cmH_2O) as PEEP increased, for the same shunt values shown in Table 8.5. The resulting oxygen saturation curves are shown in Figure 8.9 and it is evident that if the drop in cardiac output is too high, then the application of PEEP and resulting increased volume for gas exchange does not improve oxygenation, as seen by the minimal gap between curves in Figure 8.8 vs Figure 8.9. In addition, S_pO_2 curves in Figure 8.9 actually drop as PEEP is increased and the drop in CO is too high. Such a situation clinically would thus require increased F_iO_2, with its own risks [Register et al., 1987], to improve S_pO_2.

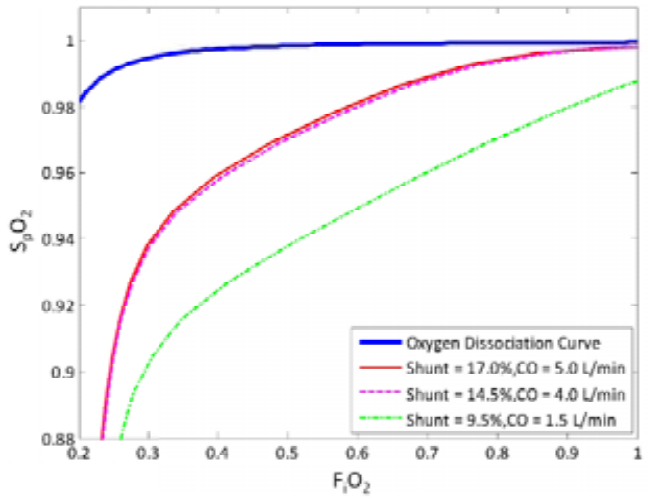

Figure 8.9 - Decrease/ negligible effect on oxygenation due to PEEP indicating that there is a tradeoffs between decreased shunt and decreased CO when PEEP is applied

Figure 8.9 shows that if the drop in CO is too high, it can have a detrimental effect on oxygenation even with decreased shunt. The decrease in CO offsets the positive effects of PEEP application and recruitment and causes decreased oxygenation, which is contradictory to the overall intention of applying PEEP. More importantly, the ability to capture this effect in this analysis suggests that this model can be used to evaluate oxygenation based on changes in cardiac output due to PEEP.

Figure 8.10 shows the effect on oxygenation depending on the magnitude of the cardiac output drop as PEEP is applied. The dashed curve represents the oxygenation change when PEEP is 7 cmH_2O and the shunt is estimated at 14%, while the dotted curve is for PEEP of 12 cmH_2O and shunt at 9%. The curves give an indication of the maximum allowable drop in CO for a given shunt that will not offset the benefit of increasing PEEP. Three distinct points are shown; labelled A, B and C in this figure.

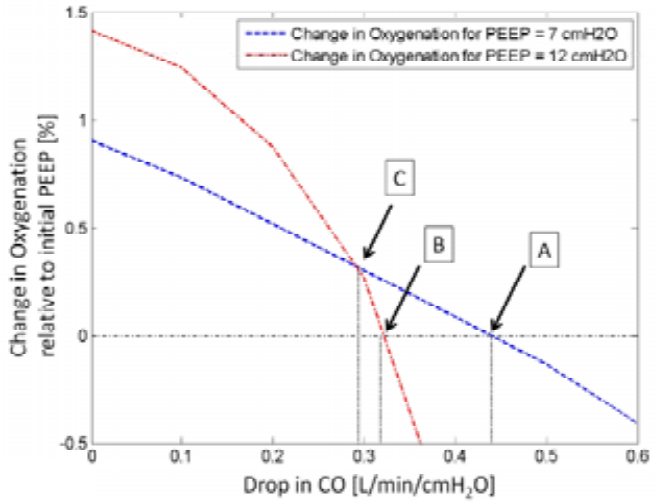

Figure 8.10 - Effect of drop in cardiac output on oxygenation

Point A represents the maximum allowable drop in cardiac output (approximately 0.43 L/min/cmH_2O) at which application of PEEP 7 cmH_2O will still yield beneficial oxygenation. However, at point A, if the PEEP is then raised to 12 cmH_2O, the oxygenation is worse. Thus, point B is the maximum allowable CO drop if a PEEP of 12 cmH_2O is to be applied (approximately 0.33 L/min/cmH_2O). Between points B and C, an applied PEEP of 12 cmH_2O will provide better oxygenation than the initial PEEP, but still not as good as provided by PEEP of 7 cmH_2O. Only if the drop in CO is less than 0.3 L/min/cmH_2O (Point C), then a PEEP of 12 cmH_2O is more beneficial than 7 cmH_2O.

Thus, based on the drop in CO as a function of PEEP, this model-based approach provides a means of optimising the PEEP setting in ventilation with respect to CO and oxygenation. In the case shown in Figure 8.10, the ideal PEEP levels are determined by the drop in CO and summarised in Table 8.6. Hence, during an initial recruitment manoeuvre, if the drop

in cardiac output can be estimated, then based on the rate of change of CO due to PEEP, an optimal PEEP can be selected. More importantly, the entire process requires only an initial estimate of CO or a minimum single invasive thermodilution measurement. From that point, it can noninvasively track changes in CO as required, although the need to recalibrate is not yet known and will require clinical verification.

Table 8.6 - Optimum level of PEEP depending on rate of cardiac output change

PEEP [cmH_2O]	Drop in cardiac output [L/min/cmH2O]
5	> 0.43
7	> 0.29 and < 0.43
12	< 0.29

8.4.3 ROBUSTNESS TESTING

In clinical practice, the need to initially measure the CO may not be viable due to the severity of the patient's condition, and an estimate for the CO at the base PEEP may be required. To test the validity of the initial CO estimate, a robustness test was conducted.

Cardiac output differs between patients and is typically reported to range from 2-8 L/min [Hoeper et al., 1999, Luecke and Pelosi, 2005, Vidal Melo, 1998]. For the initial PEEP level of 5 cmH_2O in Figure 8.8, the CO was varied between 2 and 8 L/min in steps of 0.5 L/min. Using the linear least squares method, a line of best fit was then plotted to fit through the 'measured' data points at a PEEP of 7 and 12 cmH_2O. The results of the robustness test are shown in Table 8.7, where the initial estimate of CO at PEEP = 5 cmH_2O is shown in the grey cells. The drop in CO and percentage drops in CO are shown for the different initial estimates on Figure 8.11 and Figure 8.12.

Figure 8.11 shows the effect of different initial estimates of CO on the absolute drop in CO at higher PEEP values. The graph illustrates the absolute drop on CO to be highly dependent on the initial estimate of CO. As the initial estimate of CO increases towards 8 L/min, the drop in CO also increases, and shows significant differences from the median CO drop.

However, from a percentage drop perspective, Figure 8.12 indicates that the percentage drop does not vary too much. The percentage drop of CO with the application of PEEP is

approximately constant and does not drop by more than 15%. It is also clear that all points are within close proximity to the median. Thus, given an arbitrary initial estimate between 2 and 8 L/min, it is possible to track percentage changes as a function of PEEP application, which is the clinically more important aspect when monitoring patients.

Table 8.7 - Initial estimate of CO at PEEP = 5 cmH_2O (grey cells). Drop in CO and percentage drop in CO shown for the different initial estimates

	PEEP [cmH_2O]			Drop in CO [L/Min]		Percentage Drop in CO [%]	
	5	7	12	PEEP 5 & 7	PEEP 7 & 12	PEEP 5 & 7	PEEP 7 & 12
Cardiac Output [L/min]	2	1.8	1.7	0.2	0.1	10	6
	2.5	2.4	2.2	0.1	0.2	4	8
	3	2.7	2.5	0.3	0.2	10	7
	3.5	3.3	3	0.2	0.3	6	9
	4	3.6	3.3	0.4	0.3	10	8
	4.5	4.2	3.8	0.3	0.4	7	10
	5	4.7	4.3	0.3	0.4	6	9
	5.5	5.1	4.6	0.4	0.5	7	10
	6	5.3	4.9	0.7	0.4	12	8
	6.5	6.1	5.5	0.4	0.6	6	10
	7	6.3	5.8	0.7	0.5	10	8
	7.5	6.8	6.1	0.7	0.7	9	10
	8	7.2	6.3	0.8	0.9	10	13
	Median			**0.4**	**0.4**	**9.3**	**8.5**
	Max			**0.8**	**0.9**	**11.7**	**12.5**
	Minimum			**0.1**	**0.1**	**4.0**	**5.6**

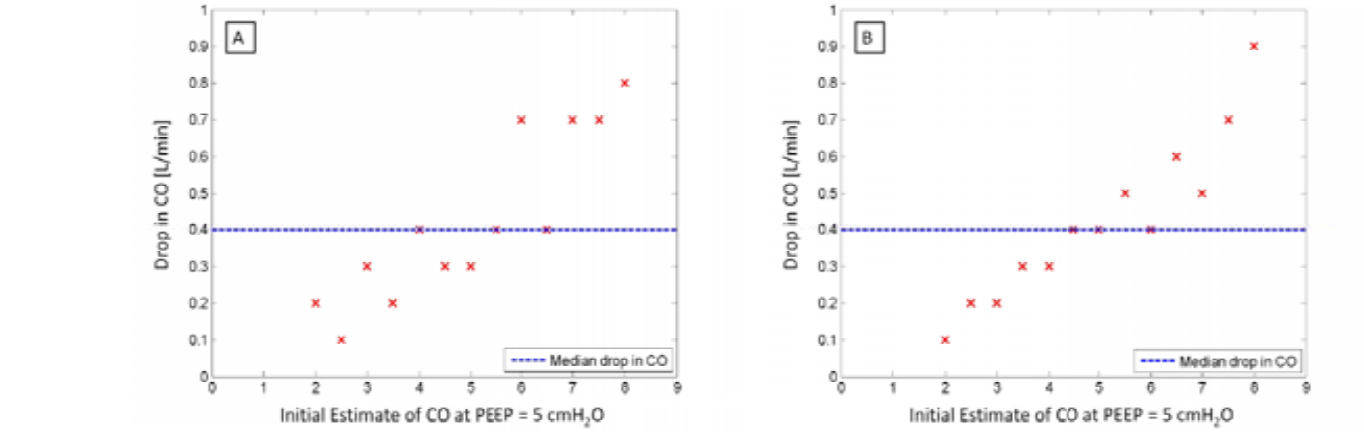

Figure 8.11- Scatter plot of drop in CO for different initial estimates of CO relative to median drop. (A) Drop from changing PEEP from 5 to 7 cmH_2O, (B) drop from changing PEEP from 7 to 12 cmH_2O

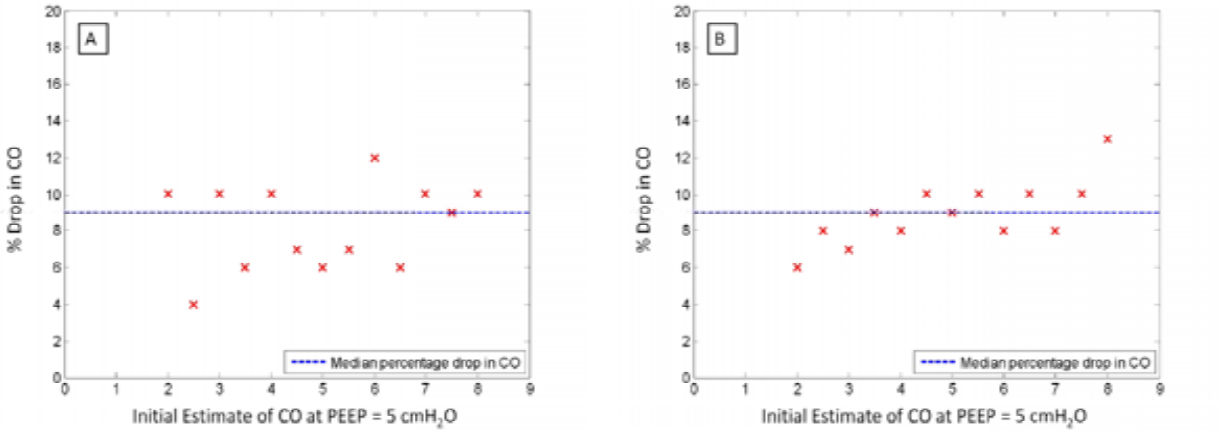

Figure 8.12 - Scatter plot of percentage drop in CO for different initial estimates of CO relative to median percentage drop. (A) Drop from 5 to 7 cmH_2O, (B) drop from 7 to 12 cmH_2O

8.4.4 SENSITIVITY TO LUNG MECHANICS

The estimation of percentage change in shunt is calculated using Equation (8.8), and is dependent on the maximum theoretical lung capacity, as determined by the recruitment model. However, the theoretical lung capacity is a value derived from the model fit and is not necessarily the exact value of true lung capacity. Thus, the estimation of shunt changes according to Equation (8.8) may have some error.

To test how the change in shunt is affected by different values of theoretical lung capacity, a sensitivity test was performed. By varying the theoretical lung capacity by 10%, the effect on the shunt at a PEEP of 7 cmH_2O and the percentage decrease in shunt between 5 and 7 cmH_2O was modelled to measure the sensitivity of these two parameters.

As shown in Figure 8.13, a 10% change in the theoretical lung capacity causes the percentage drop on shunt between PEEP of 5 and 7 cmH_2O to be between 10 and 15%. Although this is still within what is clinically tolerable, it indicates that the percentage drop is reasonably sensitive to the lung capacity.

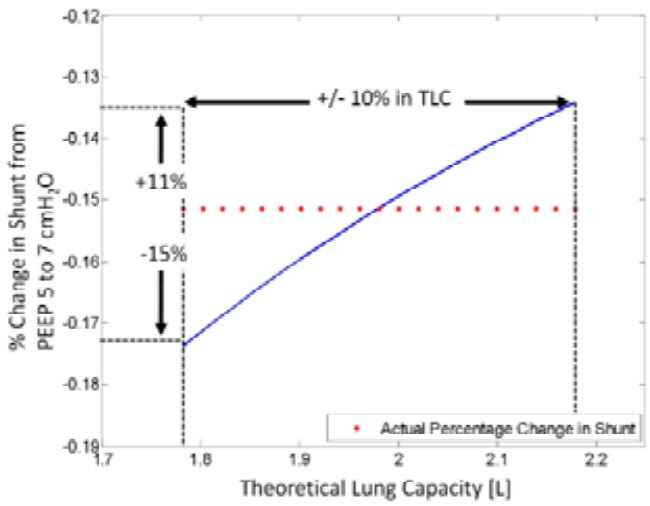

Figure 8.13 - Effect on the percentage drop in shunt from 5 to 7 cmH2O as the theoretical lung capacity is varied by 10%

However, if the absolute value of shunt is examined, then there is very minimal difference when the lung capacity is varied. Figure 8.14 shows that for a 10% change in lung capacity, the shunt evaluated at a PEEP of 7 cmH_2O only varies by a maximum of 3%. This apparent lack of sensitivity illustrates that even though the recruitment model does not estimate the true lung capacity, one can be relatively confident that the shunt at higher PEEP levels is reasonably accurate given the initial shunt measurement is known, or well estimated using the thermodilution delivered CO measurement.

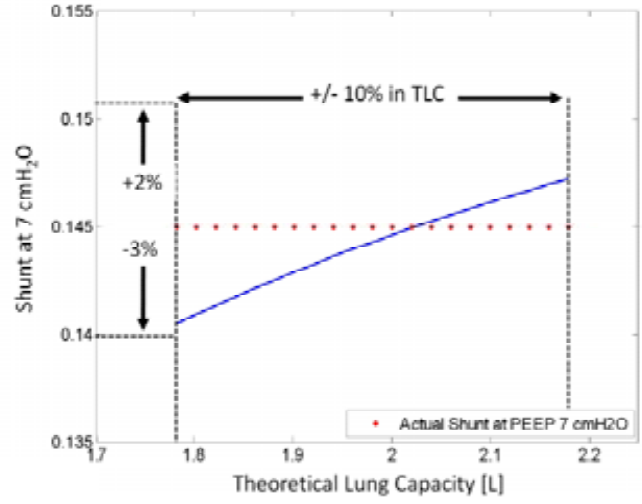

Figure 8.14 - Effect on shunt at PEEP 7 cmH_2O as the theoretical lung capacity is varied by 10%

8.5 MODEL LIMITATIONS & DISCUSSIONS

The model this chapter presents has some limitations that must also be discussed. The first major limitation is the lack of complete clinical data in validating this model. Although the aim of this chapter was only to describe the proof of concept, the combination of two different data sets does not give an accurate representation of true lung mechanics. For this model to be properly validated, a full set of clinical trials is required. These trials must capture both lung mechanics and gas exchange parameters, in addition to cardiovascular measurements, which was not possible with the originally designed trials of Chapter 5.

When evaluating the changes in shunt due to PEEP application, the CO model assumes that diffusion resistance does not change for the purpose of simplicity. It also considers and treats shunt as being homogeneous and responsive to PEEP, which is not always the case [Gattinoni et al., 1998]. These assumptions may or may not be accurate and will need to be tested with further clinical data.

The estimations of shunt changes according to Equation (8.8) are dependent on the total lung capacity as modelled by the recruitment model. In reality, this theoretical lung capacity could take on any value and thus, the estimation of shunt changes may not be entirely accurate. However, the data from the recruitment trials required a wide range of PEEP values. When higher PEEP PV curves are incorporated into the recruitment model, the accuracy of estimating maximum lung capacity increases.

Finally, the initial measurement of shunt requires a known value of cardiac output. In this study, the initial cardiac output for the PEEP of 5 cmH_2O was assumed to be 5 L/min. This measurement may require some invasive measurement that may not be ideal for all MV patients. Furthermore, without the use of clinical data, it is difficult to see how frequently the CO needs to be re-calibrated to the initial measurement from thermodilution. However, even if the initial cardiac output is estimated, the changes in CO are still tracked, which is the more important parameter. Thus, the initial measurement of the initial CO can be avoided if the changes in CO is all that is needed, provided that a reasonably accurate estimate is available.

8.6 SUMMARY

The combination of recruitment and gas exchange models presented in this chapter provide a tool that can be used in two applications. First, it can be used to monitor CO and assess the impact of changes in PEEP on the resulting CO. Hence, it can, secondly, potentially be used to optimise PEEP with respect to gas exchange and oxygenation, as well as its impact on circulation and its management.

More specifically, two models are presented and linked through a hypothesis that a change in shunt can be reasonably approximated by a change in lung volumes due to PEEP changes. It should be noted that this approximation is necessary as there is still no accurate measurement of shunt, including CT, available. A proof of concept case study based on clinical data is used to show the model's capability and validity. Finally, a sensitivity analysis is performed to illustrate the models potential robustness to its underlying assumptions.

Such linked physiological models offer the opportunity to move beyond simple clinical, model-based decision support to more complex cases including physiological interactions between systems. In particular, the ability to combine the pulmonary system to the cardiovascular system would allow a more complete and holistic picture of how different interactions occur within the body. Although the model is presented using a proof of concept, further clinical validation is required.

Chapter 9 - Conclusions

9.1 OVERVIEW

The use of mechanical ventilation for ICU patients has major implications for mortality and length of stay in the hospitals. The current approach to choosing ventilation settings does not provide patient-specific therapies and can often result in sub-optimal treatment, increasing length of MV, length of stay and mortality. Models of recruitment and lung stress are produced and tested in the clinic using readily available PV data to provide patient-specific information. The models provide clinically useful information to evaluate lung status, and show significant potential to be used at the bedside as a diagnostic tool. A third model is developed to highlight the link between the cardio and pulmonary system, enabling further potential model-based monitoring and diagnostic applications, as well as a more holistic approach to modelling.

9.2 SPECIFIC OUTCOMES & IMPLICATIONS

Mechanical ventilation is widely utilised in the ICU, but the costs for treatments can be high. Patients experiencing breathing difficulties are subjected to MV therapy to help assist breathing. In particular, when patients are diagnosed with ARDS and ALI, the resulting collapse of lung units can result in an effectively smaller lung volume, which interferes with the process of gas exchange. This outcome can be exacerbated when ventilation is sub-optimal resulting in increased lung damage, length of MV, length of stay, cost and mortality. The problem is worsened by the limited data available to clinicians at the bedside with respect to lung recruitment and status. Thus, there is significant motivation to develop more optimal ventilation therapies.

Although several studies have shown low tidal volumes to be an effective ventilation strategy, the selection of optimal PEEP is still debated. Conventional methods that examine the PV curve inflection points (LIP and UIP) provide a guide to select PEEP. However, the LIP and UIP can take on a range of values and do not offer one unique setting. The

introduction of model-based approaches provides an alternative method for selecting PEEP.

Model-based approaches use readily available clinical data to capture dynamics. Although models can be classified as finite element models and lumped parameter models, only lumped parameter models are clinically viable at the bedside for patient-specific therapy optimisation. The two main lumped parameter modelling approaches describe gas exchange and recruitment. In the past, clinical models using gas exchange have been developed, but in patients with ARDS, recruitment is the primary and dominant concern. However, current recruitment models lack the power to guide therapy, and have only been created as research tools. Thus, there is strong motivation to create models that fill this gap and capture recruitment in a manner that can be directly used in a clinical setting.

The recruitment model presented in this thesis is based on physiologically relevant and mechanically accurate components. It utilises newly hypothesised and clinically observed lung mechanics. It is the first clinically focused lung model to base its mechanics on the primary mechanism of recruitment and de-recruitment. Patient-specific and physiologically relevant model parameters are thus able to be directly identified using readily available clinical PV data. Hence, it can provide the necessary patient-specific identification of lung status and condition. The model was initially validated using retrospective clinical data consisting of 12 patients with various PEEP levels and the associated dFRC's. The initial results suggested a high level of clinical relevance, while capturing the recruitment effect through PEEP.

A second model was developed that described the effect of PEEP on dFRC using lung stress and strain as a proxy. The dFRC model developed and validated a generic population PEEP stress parameter, β, to estimate changes in dFRC at various levels of PEEP. The dFRC model was initially validated with the retrospective clinical data, the results of which suggested that β could be attributed as a population constant function of PEEP, a unique finding.

To validate the clinical viability of the recruitment and dFRC models, a series of ethics approved clinical trials was required. The study was to be split into two components. The first part of the study was to perform a specialised recruitment manoeuvre on ventilated patients and record PV data at various levels of PEEP. The second part of the study

involved the use of CT scans. By correlating the images from CT scans with the model output, it was hoped to provide further validation of the model output. Concerns that patients would be exposed to unnecessary doses of radiation were addressed by limiting the effective exposed dose to 20 mSv. Ethics was approved by the New Zealand Upper South Island A Regional Ethics Committee.

Real time clinical data was used to validate the recruitment model. Outputs of the model were the TOP and TCP mean as well as the net recruitment. These three metrics provided a means to select optimal PEEP depending on the selection criteria. If the aim was to maximise recruitment, then TOP was used to choose PEEP. In contrast, if the objective was to minimise de-recruitment, then the TOP would be used to guide therapy. Finally, the net recruitment was used when the combined effect of recruitment and de-recruitment was required. Although the TOP, TCP and net recruitment provided three different methods to evaluate optimal PEEP, they provided a set of values that could be used in the clinic as a guideline. These physiologically relevant parameters uniquely capture lung status from standard PV loops. They are the first such clinically used model parameters to guide ventilation therapy based on patient recruitability.

In addition to these physiologically based PEEP selection metrics, four additional metrics were developed to assess how disease state varies with time. More specifically, if a patient undergoes multiple trials on different days, then the model can track the TOP, SD, TOP gradient and TCP gradient which yield important information on the disease state of the patient. Tracking these metrics provide a clearer physiological picture of how the disease condition is changing using model-based parameters. The parameters represent a unique model-based approach to track disease state only using basic, non-invasive, real time clinical data.

The dFRC model was also validated with the same real time clinical data. This secondary validation indicated that β remained linear and a population constant, even with high PEEP values. This result strengthened the argument of the linear relationship between PEEP and β. However, the increased dataset also highlighted some limitations of the model. When patients exhibit very large changes in compliance, the errors between measured and estimated dFRC are large. However, this limitation may not pose a major problem, as the PEEP levels where compliances changes are large are generally well outside of the clinically acceptable range of PEEP. In addition, although predicted and measured dFRC

may show high percentage errors, within the linear region, the trends are still the same. The dFRC model can thus be used in conjunction with the recruitment model when dFRC measurements are not available providing valuable added insight. In particular, deflation to ZEEP is likely to often be deemed hazardous to the patient. Thus, model-based estimates of dFRC, even with some error, provide a means to improve the results of the recruitment model and provide a more accurate set of PEEP values, resulting in potentially improved decision support and added clinical insight that was not previously available.

Finally, the combination of lumped parameter models can yield additional information, rather than if each model was used by itself. By combining recruitment and gas exchange models, a third novel model is developed that yields information on the cardiovascular system. The models are linked on the hypothesis that a change in shunt can reasonably be approximated by a change in lung volume due to PEEP. The CO model can be used to monitor CO and assess the impact of changes in PEEP on the resulting CO. Hence, it can, secondly, potentially be used to optimise PEEP with respect to gas exchange and oxygenation, as well as its impact on circulation and its management. A proof of concept in silico analysis based on clinical data showed this models capability and a sensitivity analysis was performed to illustrate its robustness to its founding assumptions.

Overall, the models developed and tested in this research are based on fundamental physiology and lung mechanics of the ventilated patient. The models fit a variety of clinical datasets and showed the potential for clinical use at the bedside. Preliminary validation on retrospective data warranted full scale clinical trials. Although no CT data was obtained, the results of the clinical trials suggest that the models can potentially be used to assist therapies and guide clinicians as a diagnostic decision support tool and a continuous patient monitoring tool in critical care.

The models developed and tested in this research provide rapid parameter identification while retaining important physiological information and is obtained by using PV data more effectively. This research represents the first in such clinical trials where recruitment models are used to derive diagnostic information. In addition, the development of a dFRC stress model provides a unique population constant, β. The modelling approaches used in this research provide a novel way of guiding therapy and setting mechanical ventilation parameters.

Chapter 10 - Future Work

The models developed in this thesis combined with the clinical validation presented provide a platform to deliver optimised ventilation therapy. The models have shown good clinical viability and the results give an indication of the potential pathways of work that could be conducted in the future to further this research.

10.1 CLINICAL PATHWAY

The acquisition of additional datasets would require a more clinical focus. In particular, the development of new clinical trials would benefit new research objectives and allow the concept of model-based methods to progress.

10.1.1 CT SCANNING

The major limitation to this study was the lack of CT data. A limit of 20 mSv was set on patients who were asked to participate in the CT study. The total dose from the proposed CT scans was evaluated to be 10.2 mSv which was below the acceptable limit. However, patients coming into the ICU often require urgent CT scans, for other clinical reasons, upon admission. This initial scan, not related to the study, causes the total effective dose on a patient to be high. Thus, any additional scan from this study would exceed the limit of 20 mSv. Another way of incorporating CT scans into the study may be to use animal data. In particular, trials could be set up to induce lung damage in pigs or goats to mimic ARDS. These trials could then incorporate a set of recruitment manoeuvres in conjunction with CT scans. By using animal data, the dose limitations of CT scans for humans may not pose a major problem when used on animals.

10.1.2 N × N TRIALS

To evaluate the impact of the recruitment model on mortality and length of stay, an NxN trial would be required. During this sort of trial, two cohorts of N patients would be selected. One, non-interventional, cohort would be ventilated using conventional methods. In contrast, the second cohort would undergo a daily or regular recruitment manoeuvre and

be ventilated according to the recruitment model output. The mortality rates, length of mechanical ventilation and length of stay will be recorded to evaluate the utility of model-based recruitment models. Inflammatory markers associated with ARDS and ALI could also be measured to assess the impact of the therapy on patient condition.

10.1.3 NON-INTERVENTIONAL TRIALS

The recruitment model showed the ability to use model metrics to track the state of the disease and resulting lung condition as a function of time. However, the results in this thesis were limited to two patients. To test the efficacy of the tracking parameters, a larger cohort is required. Thus, a set of non-interventional trials could focus on acquiring PV data for each patient over time. By collecting data multiple times at regular intervals over several patients, and correlating disease state metrics with mortality, this trial could provide a validation to the usefulness of these new metrics.

10.1.4 CARDIAC OUTPUT MONITORING

The CO model introduced in Chapter 8 used a proof of concept to show the potential of such a model in the clinic. To thoroughly validate this model, a proper clinical trial is required with cardiovascular measurements occurring simultaneously with ventilation measurements. More specifically, the trial will need an intervention from the clinician to vary PEEP and inspired oxygen fraction while also recording continuous cardiovascular data. This will allow the CO model to be fully validated, and if successful, will allow a future pathway of non-invasive CO tracking with PEEP changes.

10.1.5 VARIATION IN VENTILATION MODE

In the clinical trials performed in this research, PV curves were obtained under constant volume conditions to ensure repeatability among different patients. However, obtaining PV loops under different ventilation modes would evaluate the robustness of the recruitment model. In particular, obtaining PV curves using pressure controlled ventilation or different flow waveforms would allow for more potential use. Because clinicians use different settings for various patients, by testing the model on other settings, the models use can be expanded.

10.1.6 SPONTANEOUSLY BREATHING PATIENTS

One disadvantage with the current recruitment model presented is that it does not account for spontaneously breathing patients. In this study, patients were sedated to prevent spontaneous breathing. Because a proportion of ventilated patients still breathe spontaneously, sedating all patients is not practical. Given current trends in providing MV, this proportion is likely to increase. Thus, the model should account for patients spontaneously breathing.

The primary difficulty when examining spontaneously breathing patients occurs when a measurement of transpulmonary pressure is required. For patients who are fully sedated, transpulmonary pressure should reflect airway pressure when an inspiratory hold is performed, as in these trials. However, for patients who spontaneously breathe, any sudden change in diaphragmatic movement can cause sudden changes in transpulmonary pressure. To measure transpulmonary pressure, the oesophageal pressure is required in conjunction with airway pressure. The difficulty arises when trying to measure oesophageal pressure with an oesophageal balloon, which is a very intrusive measurement and not feasible for regular clinical use. Thus, a means of circumventing this difficulty is required.

One possible set of clinical trials could focus on obtaining oesophageal pressure measurements simultaneously with airway pressure measurements in spontaneously breathing patients. During these trials, examining correlations between oesophageal and airway pressures could yield information as to the interaction between the two values in spontaneously breathing patients. Furthermore, if a useful physiological or empirical relationship exists between oesophageal pressure and airway pressure, it then may be possible to make estimates of transpulmonary pressure and account for spontaneously breathing patients without invasive manoeuvres, enabling model-based approaches for these patients.

10.1.7 DATASET SIZE

To further validate the use of β as a population parameter, a larger dataset is required. During all the potential types of trials described previously, an invasive measurement of dFRC may also be performed at various PEEP. Ultimately, for β to be used as a population constant in the clinic, the size of the tested dataset must be large enough to warrant it as a

population constant. Although the research presented here suggests it is a population constant, further trials must be carried on to confirm this.

Finally, the research showed variations in β across different patients. Although this variation was minimal across the majority of patients studied herein, some patient's β values varied significantly. Because β is a function of chest and lung elastance, another set of trials could focus on examining the elastance characteristics of different patients and correlating with β.

10.2 MODELLING PATHWAY

Although additional datasets may open the possibility of developing new research objectives, the acquisition of the clinical data in this research may open up the possibility of alternative models. In addition, the use of the recruitment model is currently limited to analysing the data after the trials. Thus, from an engineering perspective, there is potential for creating a real-time automated model.

10.2.1 ARDS DISTRIBUTION MODELLING

The current recruitment model assumes that alveoli are either recruited or de-recruited. The model does not consider the effect over-stretching. Although models have been developed that account for different type of alveoli, these are clinically impractical due to the excessive computational time. To overcome this limitation, a new modelling approach may be required.

Various works have shown the individual compliance curves of healthy and unhealthy alveoli. Using the individual compliance curves, it may be possible to estimate a distribution of healthy and unhealthy alveoli. More specifically, when the recruitment model is fitted to PV curves, an estimate of the total lung capacity (TLC) is given. Using an estimate of TLC, for a given pressure and unit compliance, the sum of the individual alveoli could then give the volume at that given pressure. This modelling approach may give a rapid indication as to the heterogeneity of the lung and could be correlated with lung CT scans to validate it.

10.2.2 INCREMENTAL STRESS STRAIN APPROACH

For a given increment in pressure, the lung experiences a combination of increased strain and alveolar recruitment. Increased strain is seen on alveoli that have already previously recruited, while collapsed alveoli begin to newly recruit. Theoretically, if there was an increase in volume for no increase in pressure, this would imply that all the volume change is attributed to increased recruitment and zero additional strain on existing alveoli (infinite lung compliance). Thus, this hypothetical situation would represent the zero strain case. In contrast, if the change in volume produced a disproportionately large change in pressure, then the level of additional recruitment is overshadowed by the increase in strain of existing recruited alveoli.

When PEEP is applied, every increment of PEEP produces a certain amount of stretch on already recruited lung units. Thus, although applying additional PEEP may cause additional recruitment, it may significantly overstretch existing alveoli which may cause more harm. Another potential modelling approach is to expand on this concept and examine how incremental strain of individual alveoli corresponds with the compliance of the PV curve.

More specifically, based on the compliance curves of individual alveoli, it may be possible to evaluate the strain on each alveoli. By comparing the alveolar strain with the compliance of the entire PV curve, it may be possible to develop a new metric that highlights the risks between applying PEEP and the stretch on previously recruited healthy alveoli.

10.2.3 COPD

The research presented in this thesis fitted the steady portion of the dynamic PV curve to get estimates of the patient recruitment behaviour. One of the limitations of such an approach is it discards the dynamic portion of the PV curve. In patients suffering from COPD, the initial dynamic deflationary portion can give an indication to the severity of the COPD. More specifically, COPD patients have a much faster initial passive deflation.

In reality, most patients will have some level of obstruction present. Thus, depending on the shape of the deflation PV curve, the recruitment model may be extended to quantify the level of the obstruction for each patient. This may prove useful when trying to ventilate

patients, as clinicians could quantify the severity of COPD and recognise that a new ventilation strategy is required.

10.2.4 AUTOMATION

The analysis of the data in this research occurred after the trials had been completed. To be viable in the clinical scenario, the model requires a full or semi automated system which would incorporate data acquisition, processing and analysis. In addition, the process must be easy to use for the intensive care staff, and should incorporate all the processes that were highlighted in the recruitment manoeuvre and have the option of correcting for endotracheal tube resistance. Finally, the data must be easy to read and implement if necessary.

Appendix A – FRC Sensitivity Plots

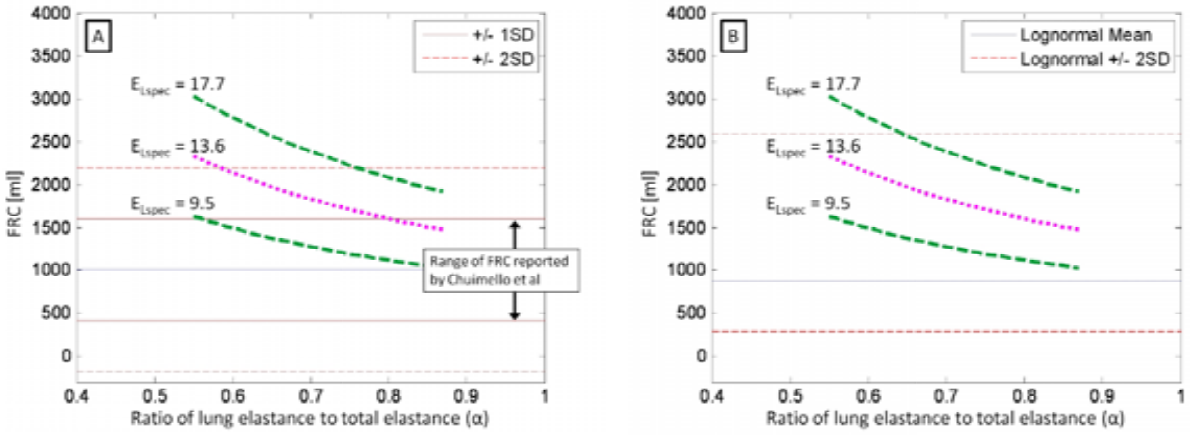

Figure A. 1 - FRC as a function of varying α for Patient 1. Thick dotted line indicates estimated FRC when mean E_{Lspec} is used. (A) Normal distribution range - Thin lines show the +/- 1 and 2 SD from mean as reported by Chiumello et al [Chiumello et al., 2008]. (B) Lognormal distribution range Thin dotted lines show the +/- 2 SD using lognormal distribution

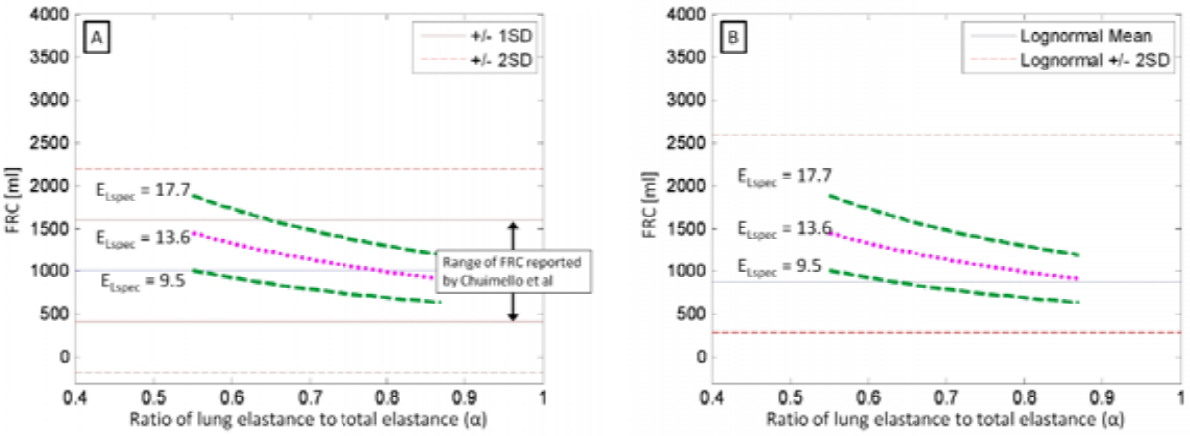

Figure A. 2 - FRC as a function of varying α for Patient 2

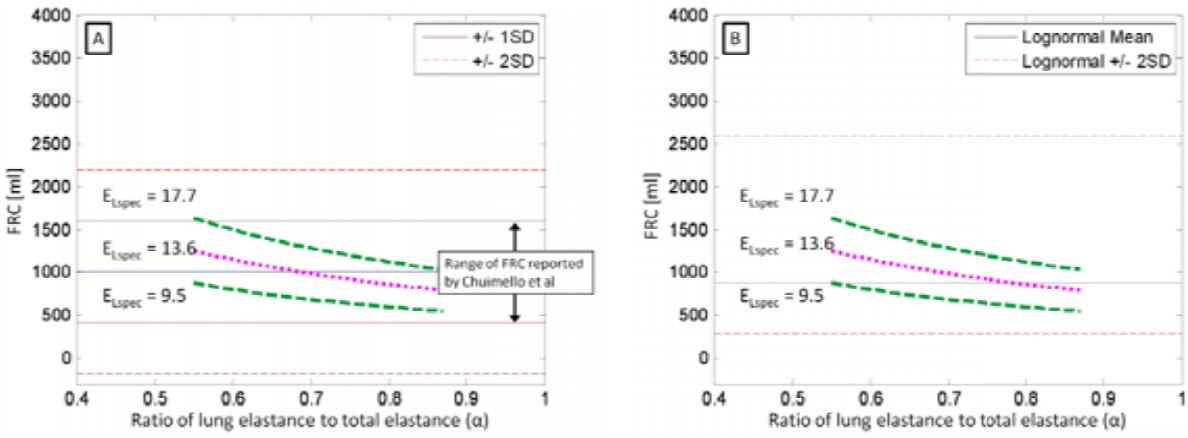

Figure A. 3 - FRC as a function of varying α for Patient 3

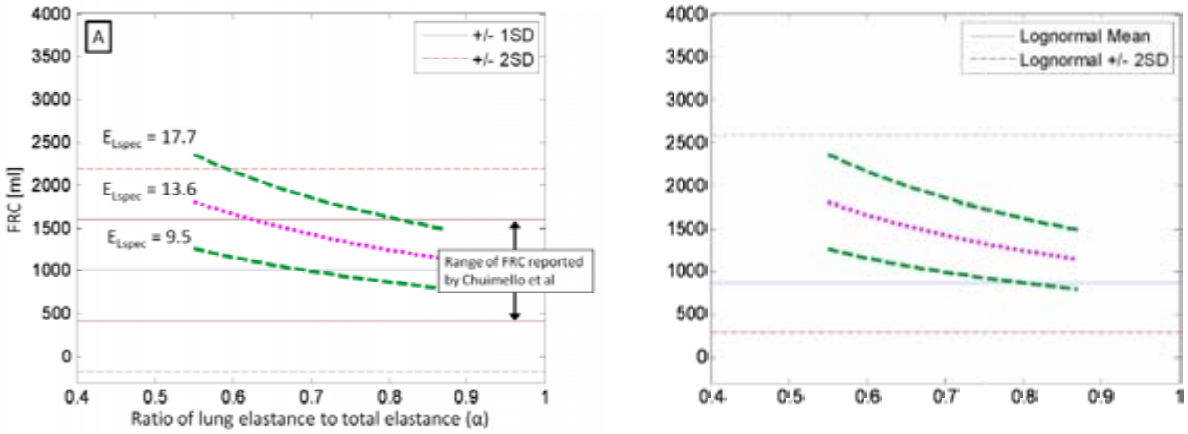

Figure A. 4 - FRC as a function of varying α for Patient 4

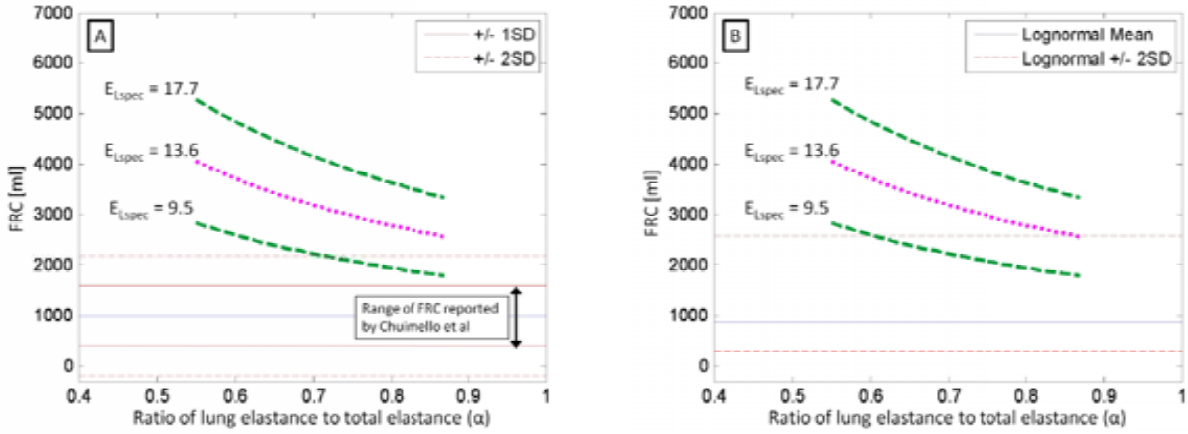

Figure A. 5 - FRC as a function of varying α for Patient 5

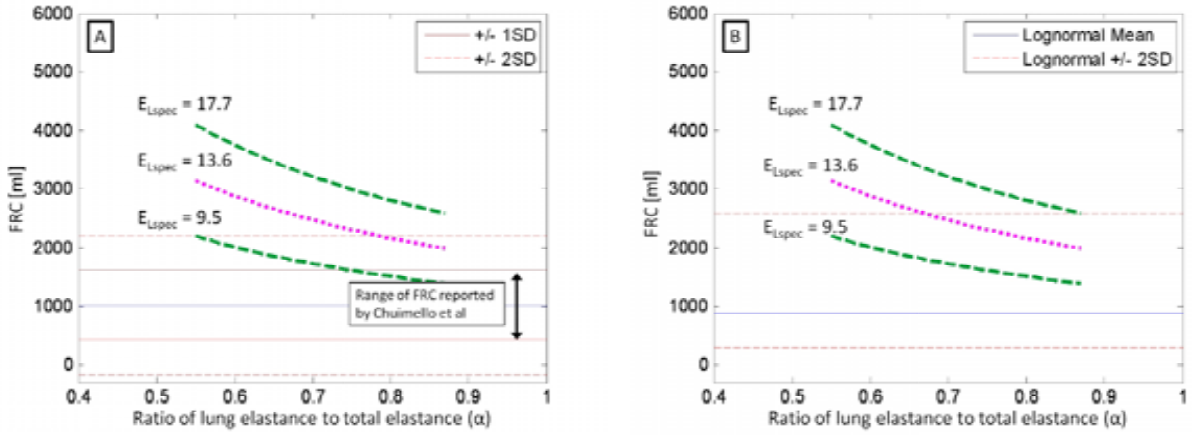

Figure A. 6 - FRC as a function of varying α for Patient 6

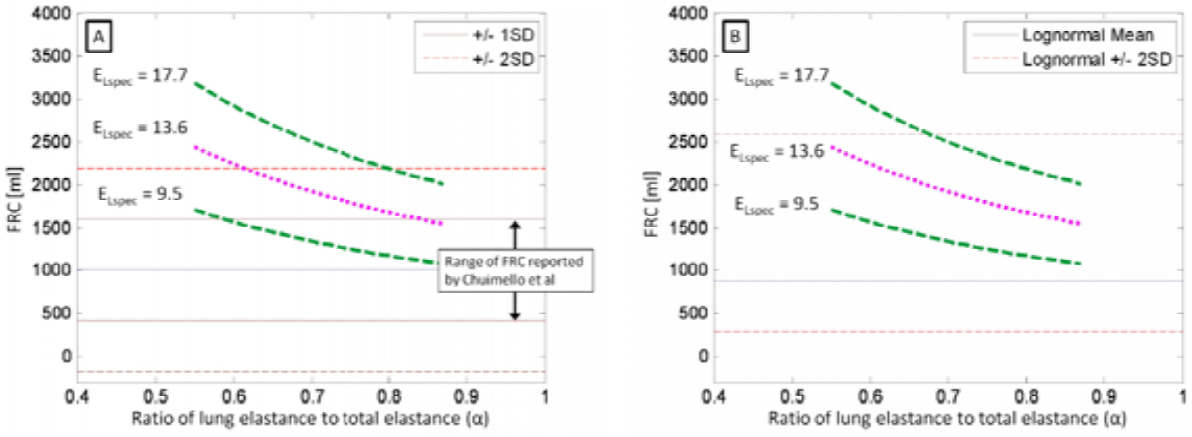

Figure A. 7 - FRC as a function of varying α for Patient 7

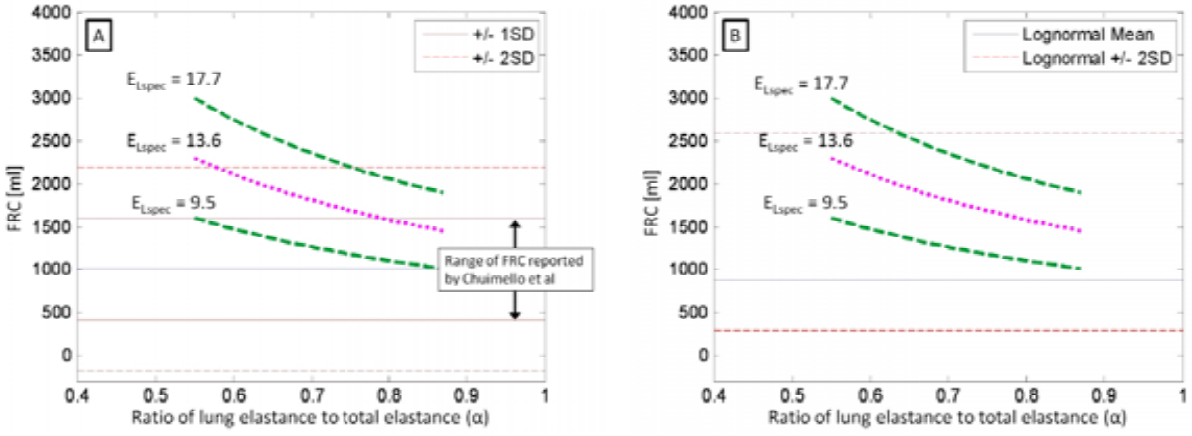

Figure A. 8 - FRC as a function of varying α for Patient 8

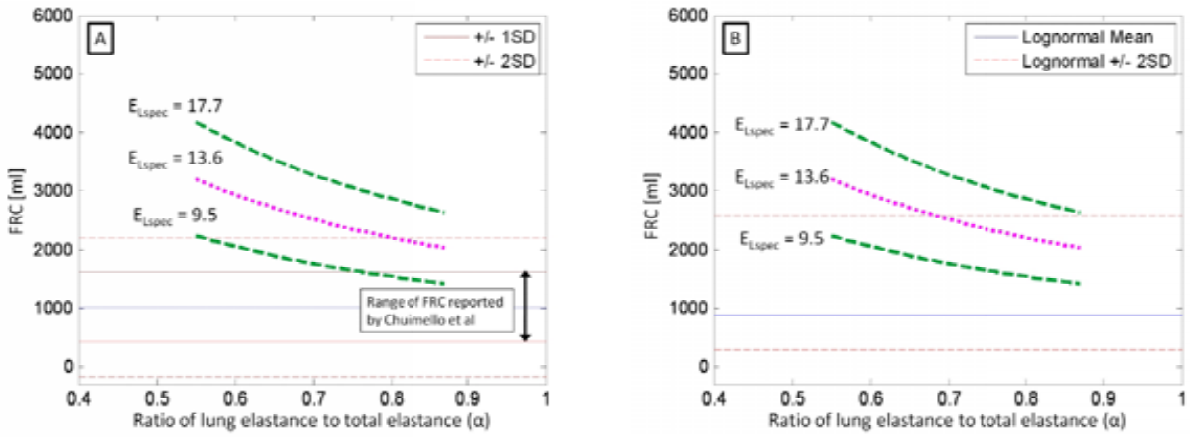

Figure A. 9 - FRC as a function of varying α for Patient 9

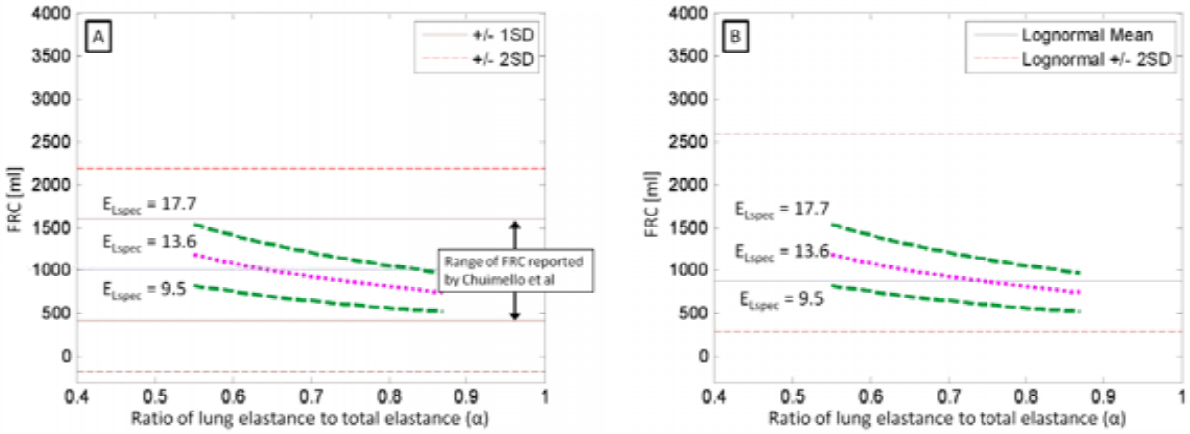

Figure A. 10 - FRC as a function of varying α for Patient 10

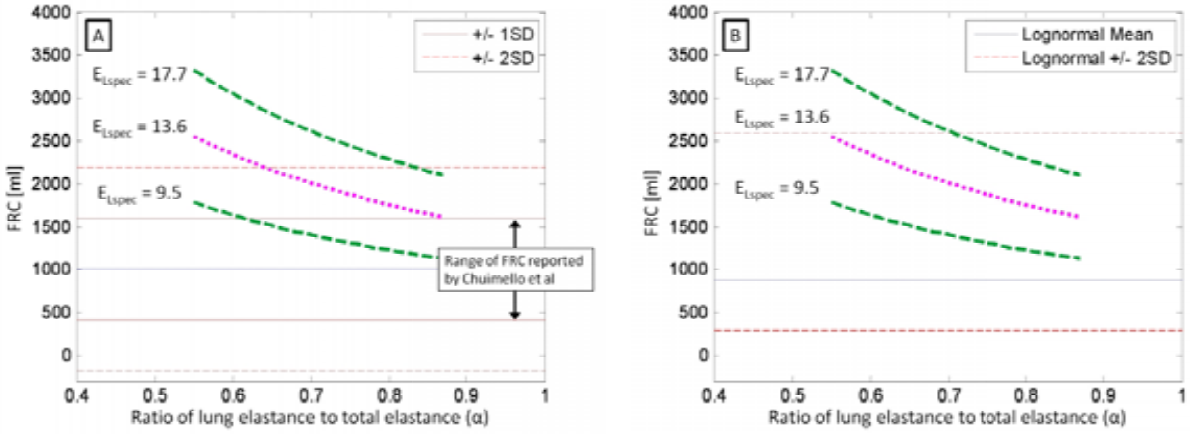

Figure A. 11 - FRC as a function of varying α for Patient 11

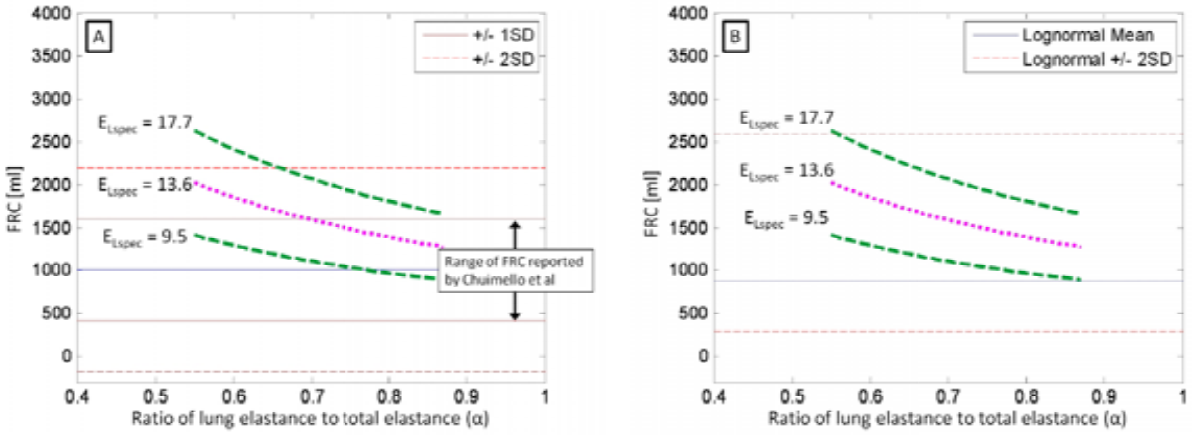

Figure A. 12 - FRC as a function of varying α for Patient 12

Appendix B – Model Fitting Errors

Table B. 1 - Model fitting errors for all patients

PATIENT 1

Number of Units	144000
Inflation SD	15
Deflation SD	7
Auto-PEEP [cmH_2O]	10

	Inflation			Deflation		
PEEP [cmH_2O]	Mean	Error [ml]	Error [%]	Mean	Error [ml]	Error [%]
10	30.97	22.17	7.86	15.57	15.48	4.61
15	28.07	22.50	4.44	17.68	5.61	1.02
20	27.12	22.27	3.11	19.88	5.72	0.63
25	26.41	21.71	2.05	22.43	7.47	0.68
27	26.18	15.11	1.34	23.39	2.73	0.24

PATIENT 2

Number of Units	171000
Inflation SD	11
Deflation SD	7
Auto-PEEP [cmH_2O]	2

	Inflation			Deflation		
PEEP [cmH_2O]	Mean	Error [ml]	Error [%]	Mean	Error [ml]	Error [%]
5	22.15	50.26	16.50	12.40	23.68	8.98
10	21.53	37.78	6.14	13.86	7.08	1.28
15	21.53	41.85	4.78	16.10	7.47	0.78
20	22.69	35.41	3.15	18.24	4.82	0.41
22	23.60	33.79	2.76	19.48	7.65	0.60

PATIENT 3

Number of Units	220000
Inflation SD	12
Deflation SD	8
Auto-PEEP [cmH_2O]	0

	Inflation			Deflation		
PEEP [cmH_2O]	Mean	Error [ml]	Error [%]	Mean	Error [ml]	Error [%]
0	26.07	51.08	151.80	14.38	45.59	116.89
5	22.54	55.09	16.17	13.97	40.19	11.08
10	21.25	12.79	1.97	14.57	18.31	2.76
15	21.25	25.68	2.43	16.34	20.53	1.92
20	21.25	36.99	2.49	18.11	23.34	1.58
25	21.25	48.72	2.65	19.98	13.26	0.76
28	22.37	32.58	1.69	21.86	12.88	0.69

PATIENT 4

Number of Units	220000
Inflation SD	25
Deflation SD	10
Auto-PEEP [cmH_2O]	9

	Inflation			Deflation		
PEEP [cmH_2O]	Mean	Error [ml]	Error [%]	Mean	Error [ml]	Error [%]
10	55.56	9.37	5.52	20.04	4.28	1.16
15	44.45	32.86	7.02	21.10	8.24	1.31
20	37.09	35.19	4.47	21.58	1.95	0.19
25	33.18	39.34	3.52	23.13	1.39	0.11
30	30.77	24.31	1.77	24.75	5.10	0.32

PATIENT 5 - TRIAL 1

Number of Units	198000
Inflation SD	16
Deflation SD	10
Auto-PEEP [cmH_2O]	13

	Inflation			Deflation		
PEEP [cmH_2O]	Mean	Error [ml]	Error [%]	Mean	Error [ml]	Error [%]
15	44.89	25.88	12.31	27.83	14.49	6.04
20	43.26	9.93	2.73	29.83	10.80	2.31
25	43.26	53.48	7.86	31.61	20.67	3.12

PATIENT 5 - TRIAL 2

Number of Units	161000
Inflation SD	15
Deflation SD	8
Auto-PEEP [cmH_2O]	8

	Inflation			Deflation		
PEEP [cmH_2O]	Mean	Error [ml]	Error [%]	Mean	Error [ml]	Error [%]
10	36.99	31.51	19.71	19.30	15.86	7.52
15	33.05	16.44	4.16	21.09	10.88	2.75
20	31.11	15.75	2.39	22.72	2.85	0.45
25	32.42	21.27	2.52	25.73	13.99	1.55
29	32.42	30.72	2.85	26.91	10.75	1.03

PATIENT 6 - TRIAL 1

Number of Units	96000
Inflation SD	11
Deflation SD	7
Auto-PEEP [cmH_2O]	10

	Inflation			Deflation		
PEEP [cmH_2O]	Mean	Error [ml]	Error [%]	Mean	Error [ml]	Error [%]
10	28.72	41.45	49.57	17.42	35.78	27.75
15	25.57	18.04	4.02	17.76	11.07	2.87
20	26.75	9.68	1.88	19.40	5.20	0.91
25	28.44	7.69	1.05	21.20	6.31	0.76

PATIENT 6 - TRIAL 2

Number of Units	171000
Inflation SD	14
Deflation SD	8
Auto-PEEP [cmH_2O]	3

	Inflation			Deflation		
PEEP [cmH_2O]	Mean	Error [ml]	Error [%]	Mean	Error [ml]	Error [%]
5	23.58	27.97	7.98	12.41	11.54	3.46
10	21.89	7.07	1.17	14.09	7.25	1.28
15	20.83	9.70	1.11	15.66	2.70	0.32
20	20.83	18.99	1.56	16.49	17.35	1.37
25	20.83	20.73	1.41	18.60	2.91	0.19

PATIENT 6 - TRIAL 3

Number of Units	154000
Inflation SD	14
Deflation SD	9
Auto-PEEP [cmH_2O]	2

	Inflation			Deflation		
PEEP [cmH_2O]	Mean	Error [ml]	Error [%]	Mean	Error [ml]	Error [%]
5	19.88	43.11	11.66	12.33	17.91	5.31
10	17.76	17.00	2.37	12.38	3.81	0.58
15	17.76	9.18	0.95	13.57	6.14	0.61
20	18.85	8.43	0.76	14.94	2.71	0.22

PATIENT 7

Number of Units	65000
Inflation SD	10
Deflation SD	5
Auto-PEEP [cmH_2O]	2

	Inflation			Deflation		
PEEP [cmH_2O]	Mean	Error [ml]	Error [%]	Mean	Error [ml]	Error [%]
5	15.89	1.73	0.63	8.70	4.51	1.93
10	15.89	17.74	3.77	11.29	3.28	0.66
15	19.09	11.95	2.16	14.39	3.09	0.56
16	19.50	19.96	3.37	14.79	4.86	0.83

PATIENT 8

Number of Units	176000
Inflation SD	15
Deflation SD	10
Auto-PEEP [cmH_2O]	0

	Inflation			Deflation		
PEEP [cmH_2O]	Mean	Error [ml]	Error [%]	Mean	Error [ml]	Error [%]
0	33.03	36.08	81.81	13.11	58.17	34.11
5	28.67	34.56	13.37	15.51	12.30	4.29
10	27.41	12.36	3.18	17.32	10.47	2.36
15	26.58	14.82	2.44	18.87	2.03	0.31
20	26.58	15.54	1.72	20.62	3.48	0.38
25	26.58	21.82	1.90	22.21	4.63	0.38
30	26.58	14.11	1.02	22.93	2.12	0.15

PATIENT 9

Number of Units	189000
Inflation SD	15
Deflation SD	9
Auto-PEEP	12

	Inflation			Deflation		
PEEP	Mean	Error [ml]	Error [%]	Mean	Error [ml]	Error [%]
15	29.53	13.22	2.04	20.37	5.27	0.84
20	29.14	12.09	1.45	21.97	3.88	0.44
25	28.61	17.32	1.56	23.36	8.29	0.66
29	28.60	15.40	1.17	24.41	2.12	0.15
30	28.49	11.20	0.79	25.00	6.85	0.47

PATIENT 10

Number of Units	147000
Inflation SD	16
Deflation SD	9
Auto-PEEP	3

	Inflation			Deflation		
PEEP	Mean	Error [ml]	Error [%]	Mean	Error [ml]	Error [%]
5	30.54	33.80	17.27	16.50	20.39	9.43
10	28.76	13.10	3.04	17.62	6.33	1.69
15	27.99	6.73	1.04	19.16	13.18	2.11
20	27.99	11.97	1.56	21.94	5.15	0.59
25	27.99	10.75	1.08	24.01	5.48	0.54
27	27.99	8.70	0.80	24.94	6.02	0.59

Appendix C – Recruitment Model Results

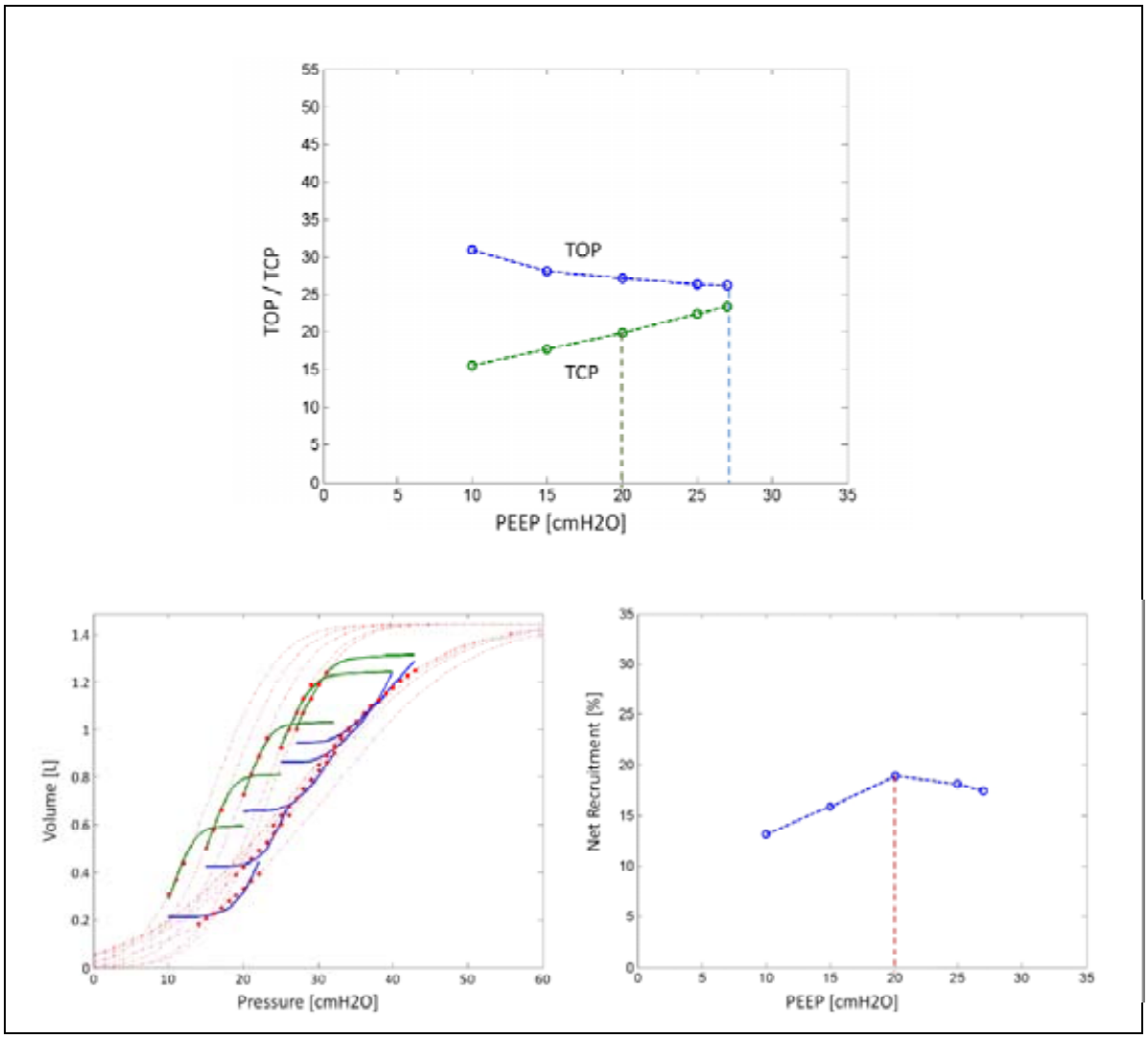

Figure C. 1 - Main plot shows TOP and TCP as a function of PEEP for Patient 1. Bottom left plot is the model fit. Bottom right indicates net recruitment

Table C. 1 - Clinically selected PEEP and Optimal PEEP indicated by TOP, TCP and net recruitment for Patient 1

Method	Optimum PEEP [cm H_2O]	Reason
TOP	27	Recruitment maximised - but could pose risk of VILI
TCP	20	Higher PEEP results in less de-recruitment but can risk VILI
Net Recruitment	20	Lower PEEP does not maximise recruitment, while higher PEEP does not minimise de-recruitment
Clinical Setting	10	Clinician selected

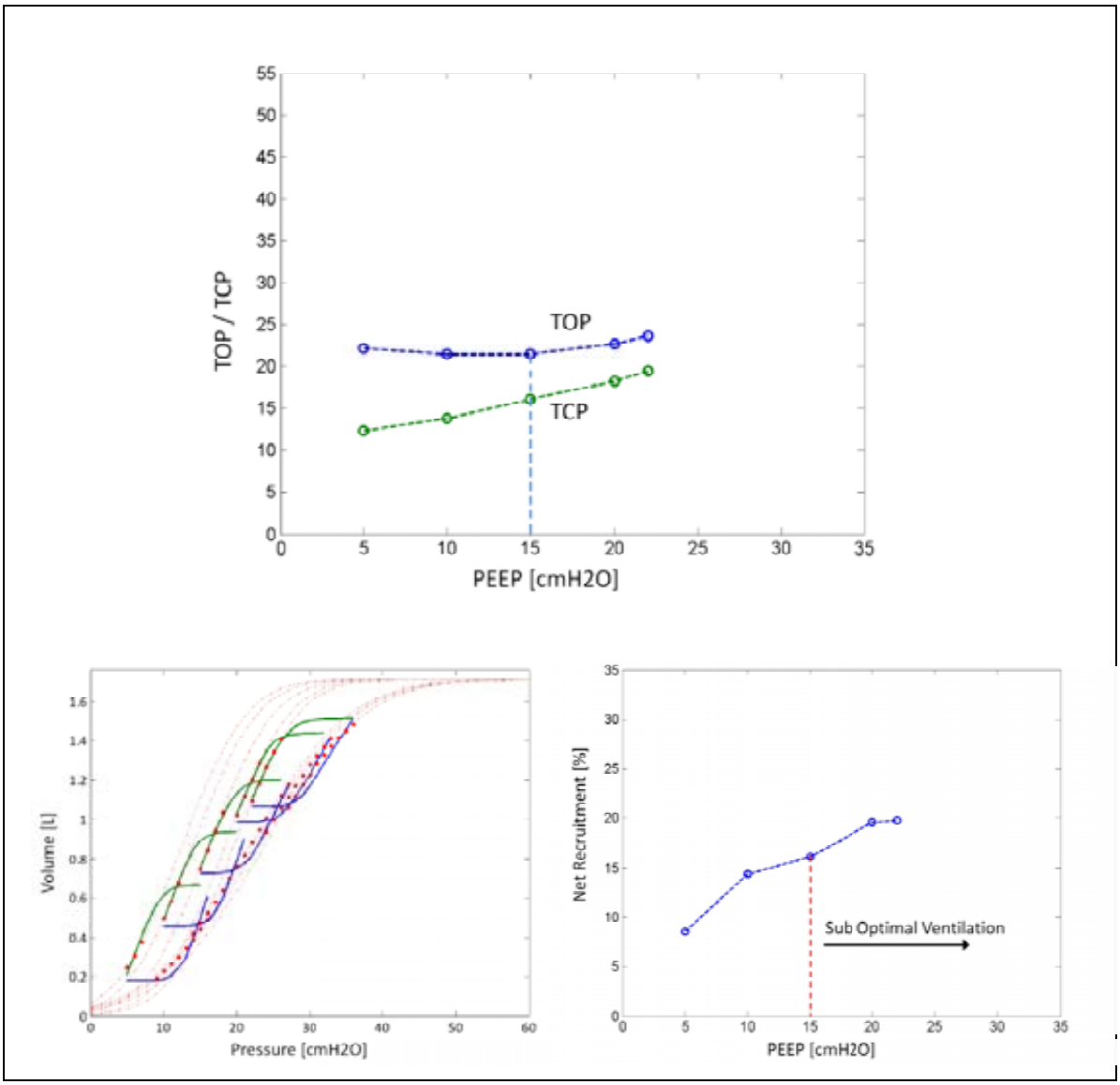

Figure C. 2 - Main plot shows TOP and TCP as a function of PEEP for Patient 2. Bottom left plot is the model fit. Bottom right indicates net recruitment

Table C. 2 - Clinically selected PEEP and Optimal PEEP indicated by TOP, TCP and net recruitment for Patient 2

Method	Optimum PEEP [cm H_2O]	Reason
TOP	15	Recruitment maximised - Higher PEEP resulted in circuit leak
TCP	15	Higher PEEP results in less de-recruitment
Net Recruitment	15	Lower PEEP does not maximise recruitment, while higher PEEP is sub-optimal
Clinical Setting	12	Clinician selected

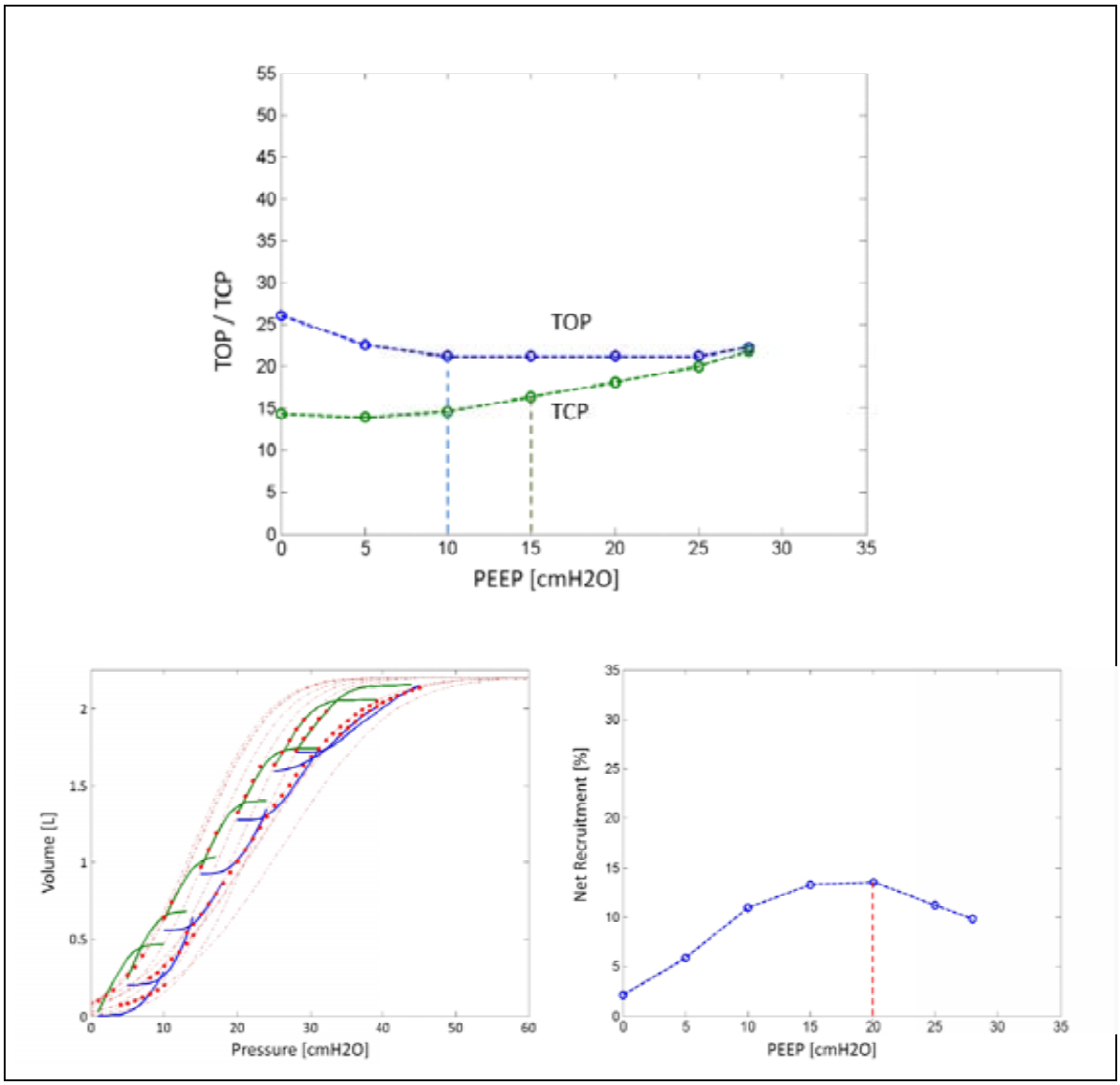

Figure C. 3 - Main plot shows TOP and TCP as a function of PEEP for Patient 3. Bottom left plot is the model fit. Bottom right indicates net recruitment

Table C. 3 - Clinically selected PEEP and Optimal PEEP indicated by TOP, TCP and net recruitment for Patient 3

Method	Optimum PEEP [cm H_2O]	Reason
TOP	10	Recruitment maximised - Additional PEEP does not cause additional recruitment
TCP	15	Higher PEEP results in less de-recruitment but can risk VILI
Net Recruitment	20	Lower PEEP does not maximise recruitment, while higher PEEP does not minimise de-recruitment
Clinical Setting	10	Clinician selected

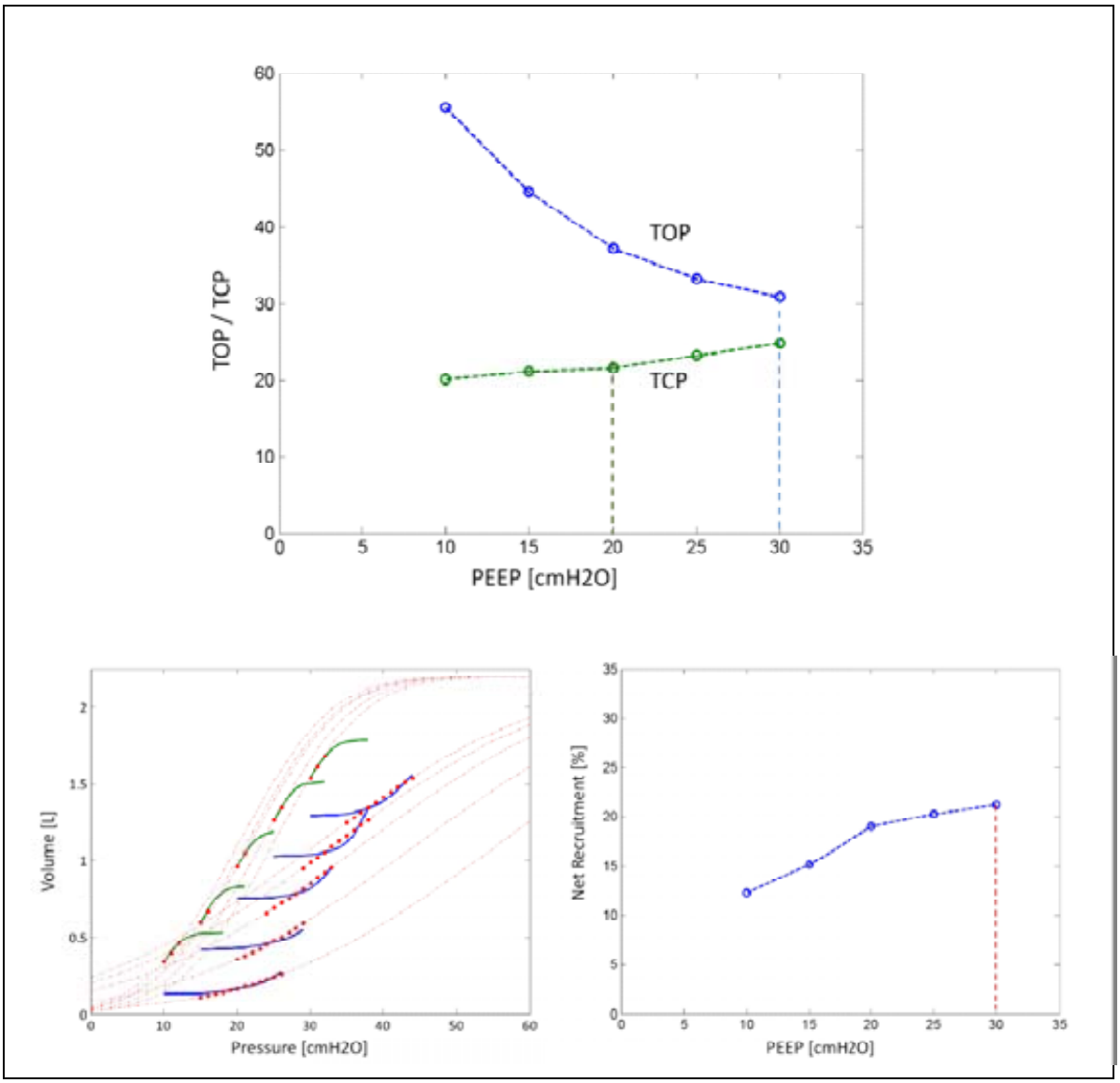

Figure C. 4 - Main plot shows TOP and TCP as a function of PEEP for Patient 4. Bottom left plot is the model fit. Bottom right indicates net recruitment

Table C. 4 - Clinically selected PEEP and Optimal PEEP indicated by TOP, TCP and net recruitment for Patient 4

Method	Optimum PEEP [cm H_2O]	Reason
TOP	30	Recruitment maximised - but could pose risk of VILI
TCP	20	Higher PEEP results in less de-recruitment but can risk VILI
Net Recruitment	30	Lower PEEP does not maximise recruitment
Clinical Setting	10	Clinician selected

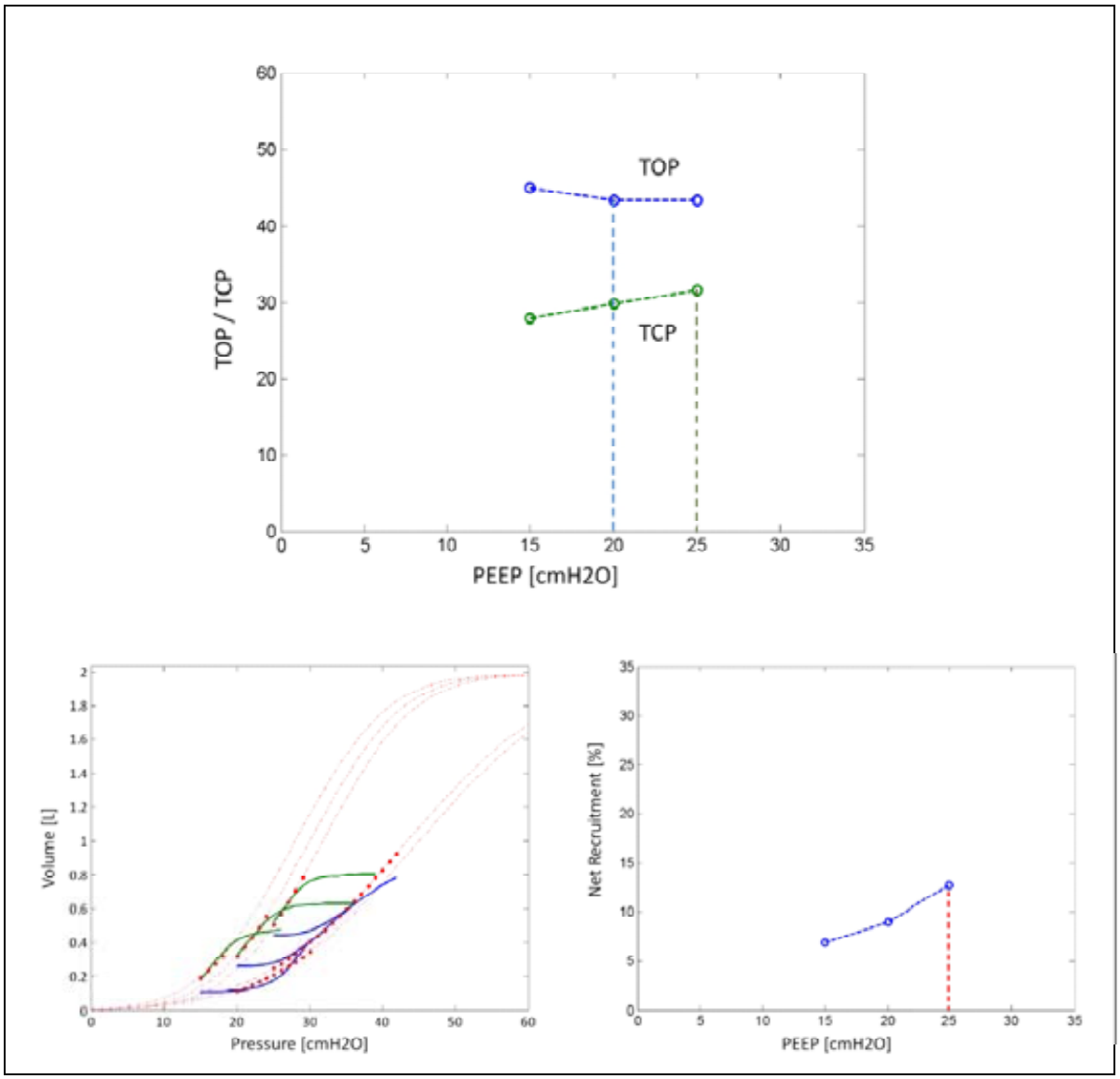

Figure C. 5 - Main plot shows TOP and TCP as a function of PEEP for Patient 5, Trial 1. Bottom left plot is the model fit. Bottom right indicates net recruitment

Table C. 5 - Clinically selected PEEP and Optimal PEEP indicated by TOP, TCP and net recruitment for Patient 5, Trial 1

Method	Optimum PEEP [cm H_2O]	Reason
TOP	20	Recruitment maximised - Additional PEEP does not cause additional recruitment
TCP	25	Higher PEEP results in less de-recruitment but can risk VILI
Net Recruitment	25	Lower PEEP does not maximise recruitment
Clinical Setting	12	Clinician selected

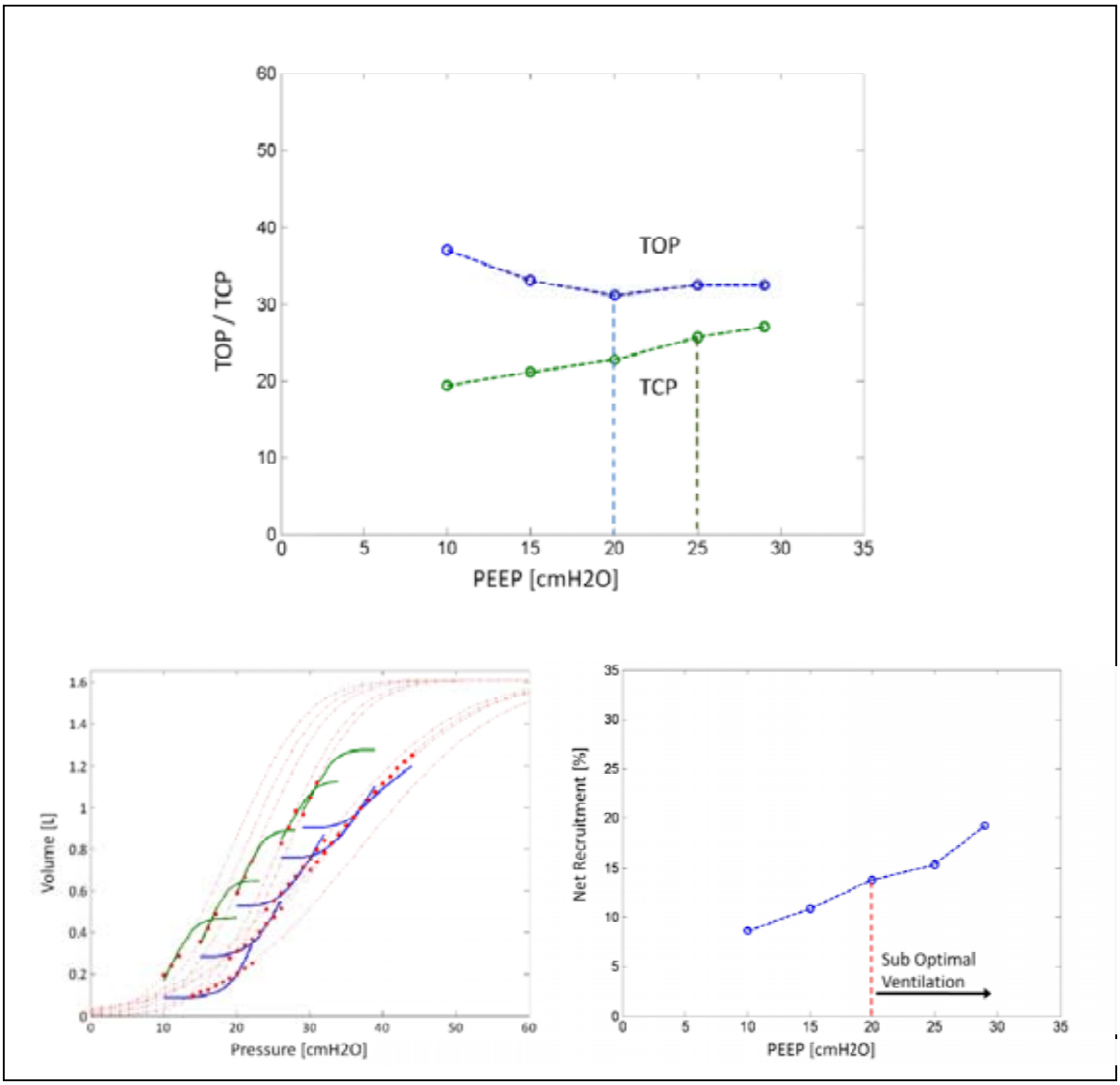

Figure C. 6 - Main plot shows TOP and TCP as a function of PEEP for Patient 5, Trial 2. Bottom left plot is the model fit. Bottom right indicates net recruitment

Table C. 6 - Clinically selected PEEP and Optimal PEEP indicated by TOP, TCP and net recruitment for Patient 5, Trial 2

Method	Optimum PEEP [cm H_2O]	Reason
TOP	20	Recruitment maximised - Additional PEEP is suboptimal and increases compliance
TCP	25	Higher PEEP results in less de-recruitment but can risk VILI
Net Recruitment	20	Lower PEEP does not maximise recruitment, while higher PEEP is sub-optimal
Clinical Setting	12	Clinician selected

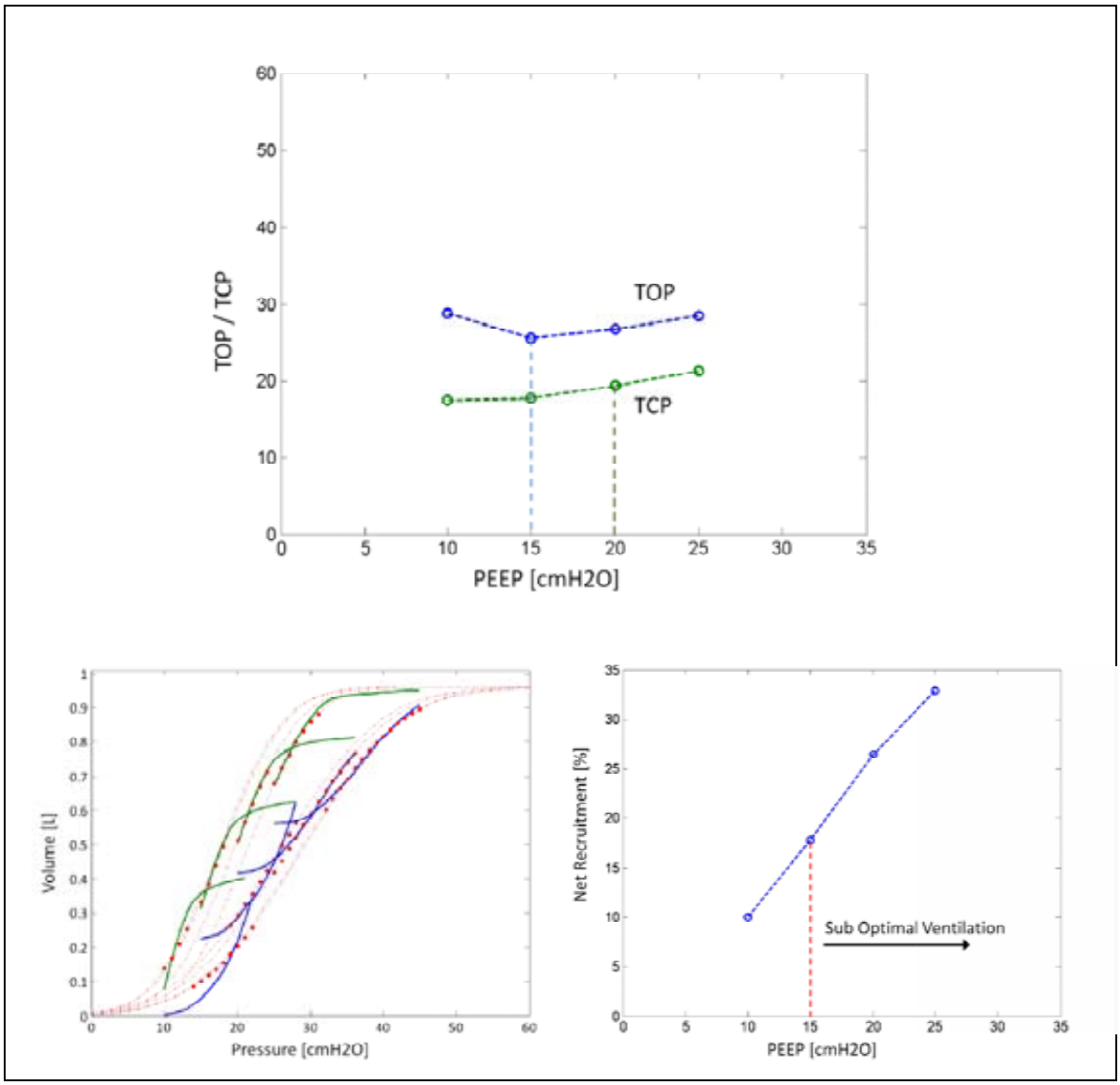

Figure C. 7 - Main plot shows TOP and TCP as a function of PEEP for Patient 6, Trial 1. Bottom left plot is the model fit. Bottom right indicates net recruitment

Table C. 7 - Clinically selected PEEP and Optimal PEEP indicated by TOP, TCP and net recruitment for Patient 6, Trial 1

Method	Optimum PEEP [cm H_2O]	Reason
TOP	15	Recruitment maximised - Additional PEEP is suboptimal and increases compliance
TCP	20	Higher PEEP results in less de-recruitment but can risk VILI
Net Recruitment	20	Lower PEEP does not maximise recruitment, while higher PEEP is sub-optimal
Clinical Setting	11	Clinician selected

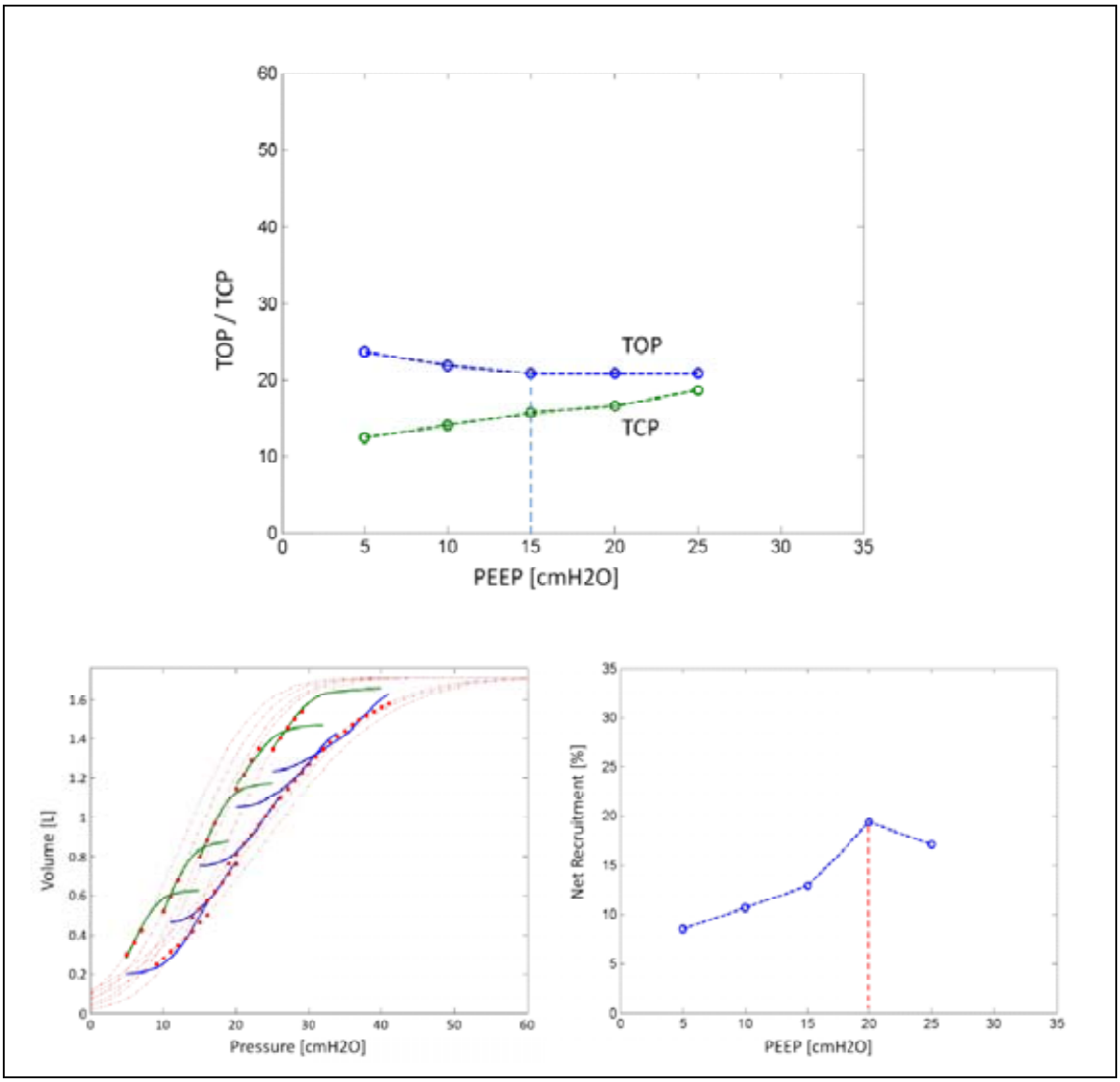

Figure C. 8 - Main plot shows TOP and TCP as a function of PEEP for Patient 6, Trial 2. Bottom left plot is the model fit. Bottom right indicates net recruitment

Table C. 8 - Clinically selected PEEP and Optimal PEEP indicated by TOP, TCP and net recruitment for Patient 6, Trial 2

Method	Optimum PEEP [cm H_2O]	Reason
TOP	15	Recruitment maximised - Additional PEEP does not cause additional recruitment
TCP	15	Higher PEEP results in less de-recruitment but can risk VILI
Net Recruitment	20	Lower PEEP does not maximise recruitment, while higher PEEP does not minimise de-recruitment
Clinical Setting	13	Clinician selected

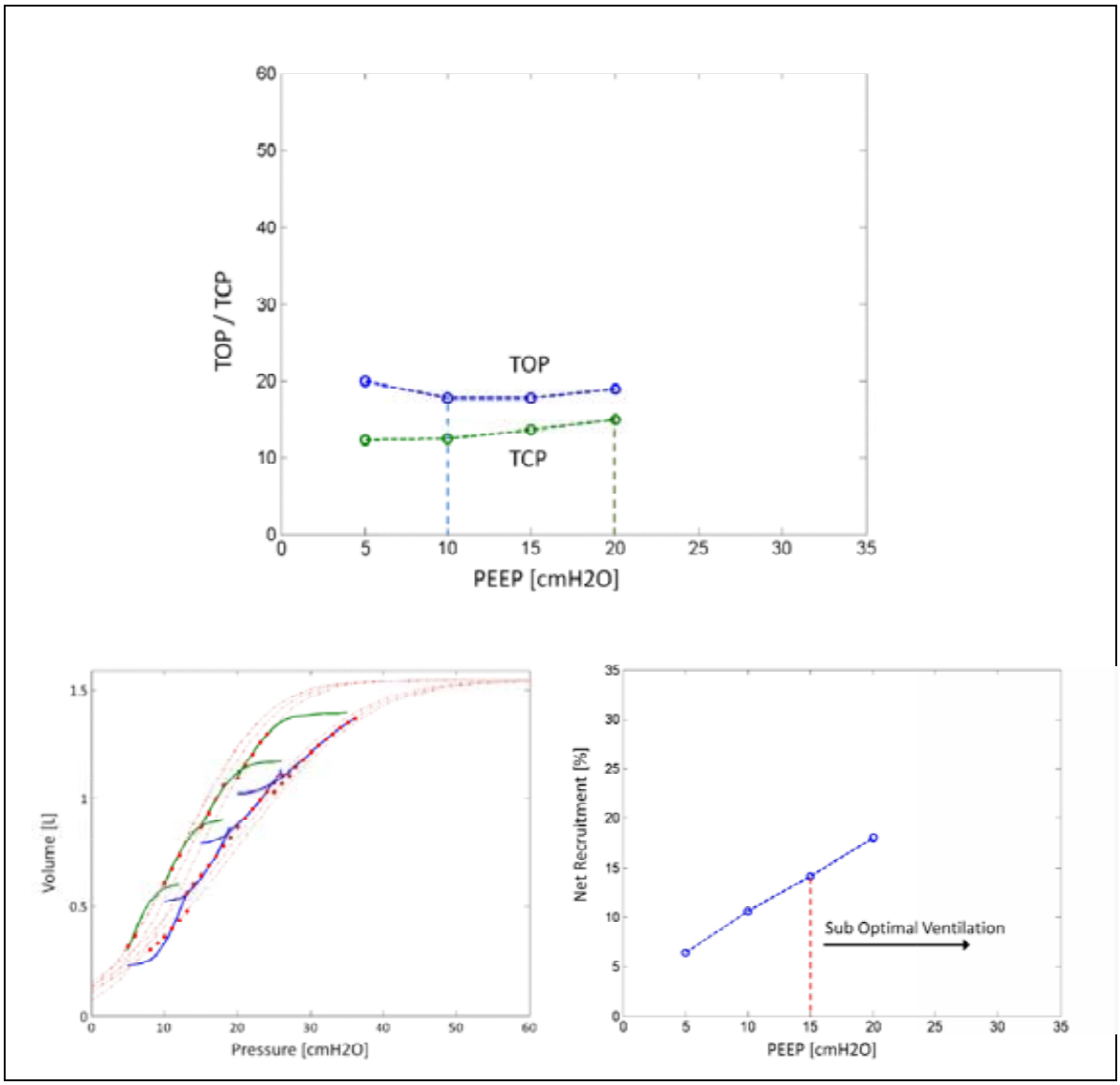

Figure C. 9 - Main plot shows TOP and TCP as a function of PEEP for Patient 6, Trial 3. Bottom left plot is the model fit. Bottom right indicates net recruitment

Table C. 9 - Clinically selected PEEP and Optimal PEEP indicated by TOP, TCP and net recruitment for Patient 6, Trial 3

Method	Optimum PEEP [cm H_2O]	Reason
TOP	10	Recruitment maximised - Additional PEEP does not cause additional recruitment
TCP	20	Higher PEEP results in less de-recruitment but can risk VILI
Net Recruitment	15	Lower PEEP does not maximise recruitment, while higher PEEP is sub-optimal
Clinical Setting	10	Clinician selected

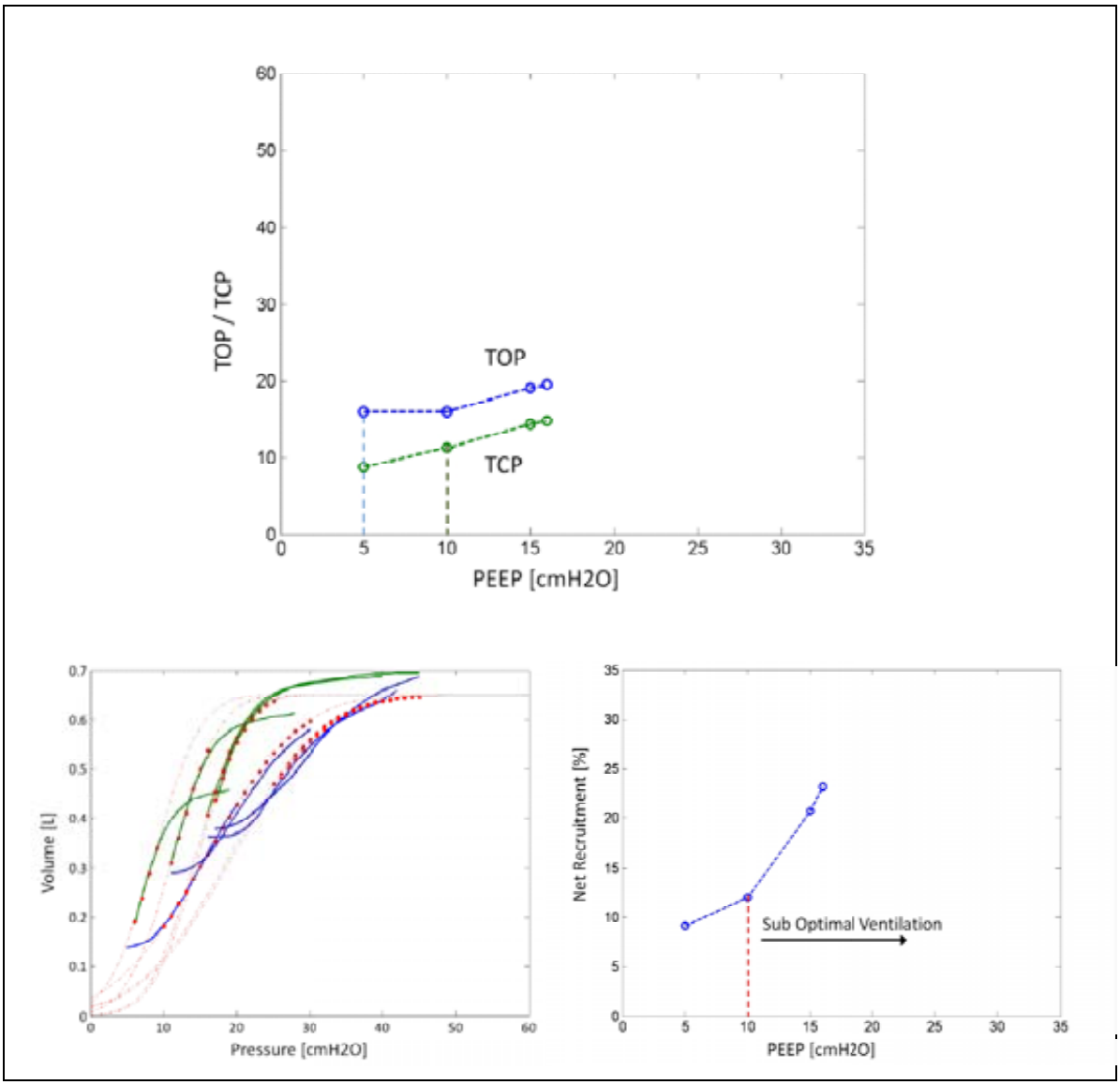

Figure C. 10 - Main plot shows TOP and TCP as a function of PEEP for Patient 7. Bottom left plot is the model fit. Bottom right indicates net recruitment

Table C. 10 - Clinically selected PEEP and Optimal PEEP indicated by TOP, TCP and net recruitment for Patient 7

Method	Optimum PEEP [cm H_2O]	Reason
TOP	5	Recruitment maximised - Additional PEEP does not cause additional recruitment
TCP	10	Higher PEEP results in less de-recruitment but can risk VILI
Net Recruitment	10	Lower PEEP does not maximise recruitment, while higher PEEP is sub-optimal
Clinical Setting	7.5	Clinician selected

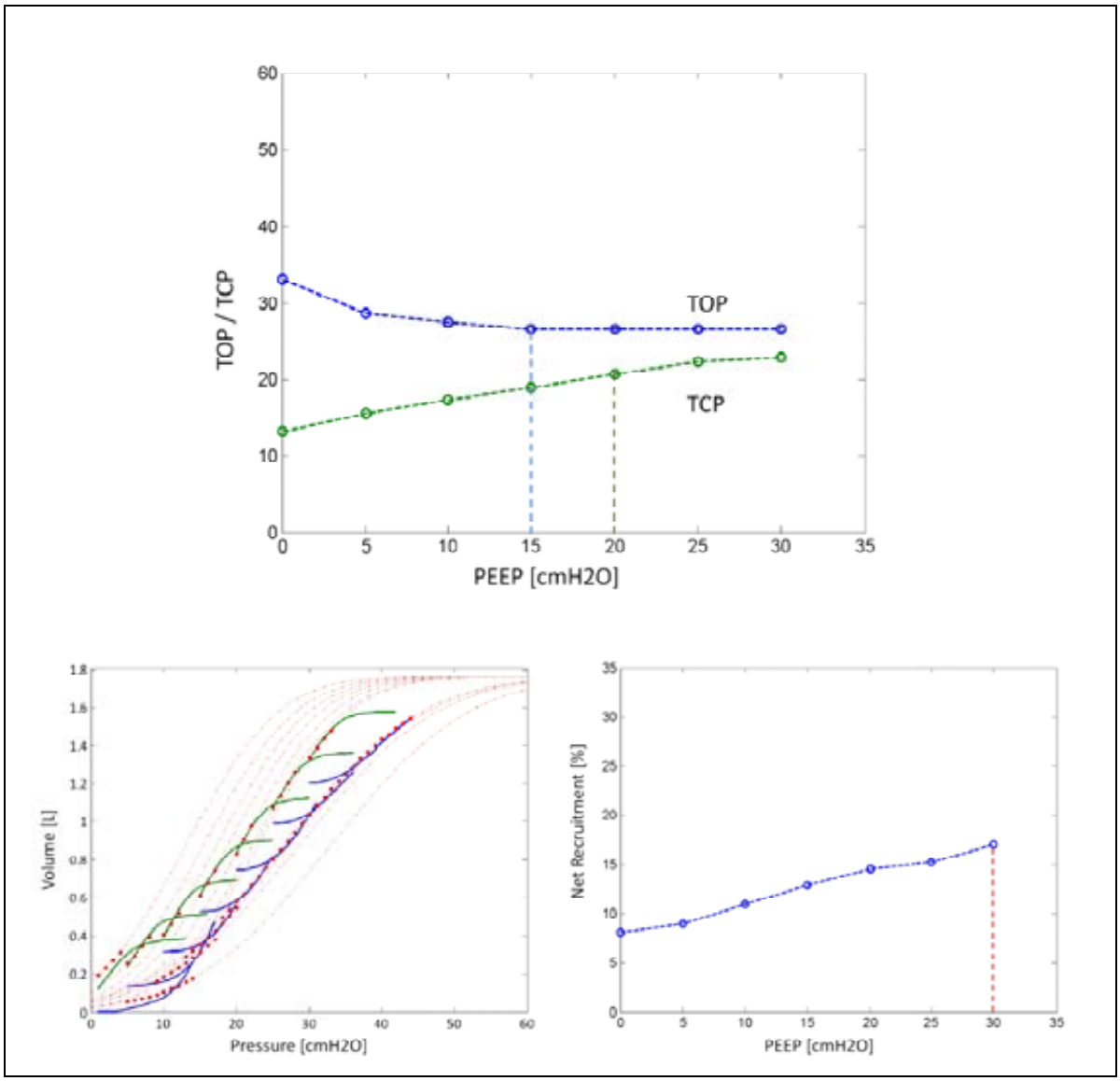

Figure C. 11 - Main plot shows TOP and TCP as a function of PEEP for Patient 8. Bottom left plot is the model fit. Bottom right indicates net recruitment

Table C. 11 - Clinically selected PEEP and Optimal PEEP indicated by TOP, TCP and net recruitment for Patient 8

Method	Optimum PEEP [cm H_2O]	Reason
TOP	15	Recruitment maximised - Additional PEEP does not cause additional recruitment
TCP	20	Higher PEEP results in less de-recruitment but can risk VILI
Net Recruitment	30	Lower PEEP does not maximise recruitment, while higher PEEP is sub-optimal. But may risk VILI
Clinical Setting	12	Clinician selected

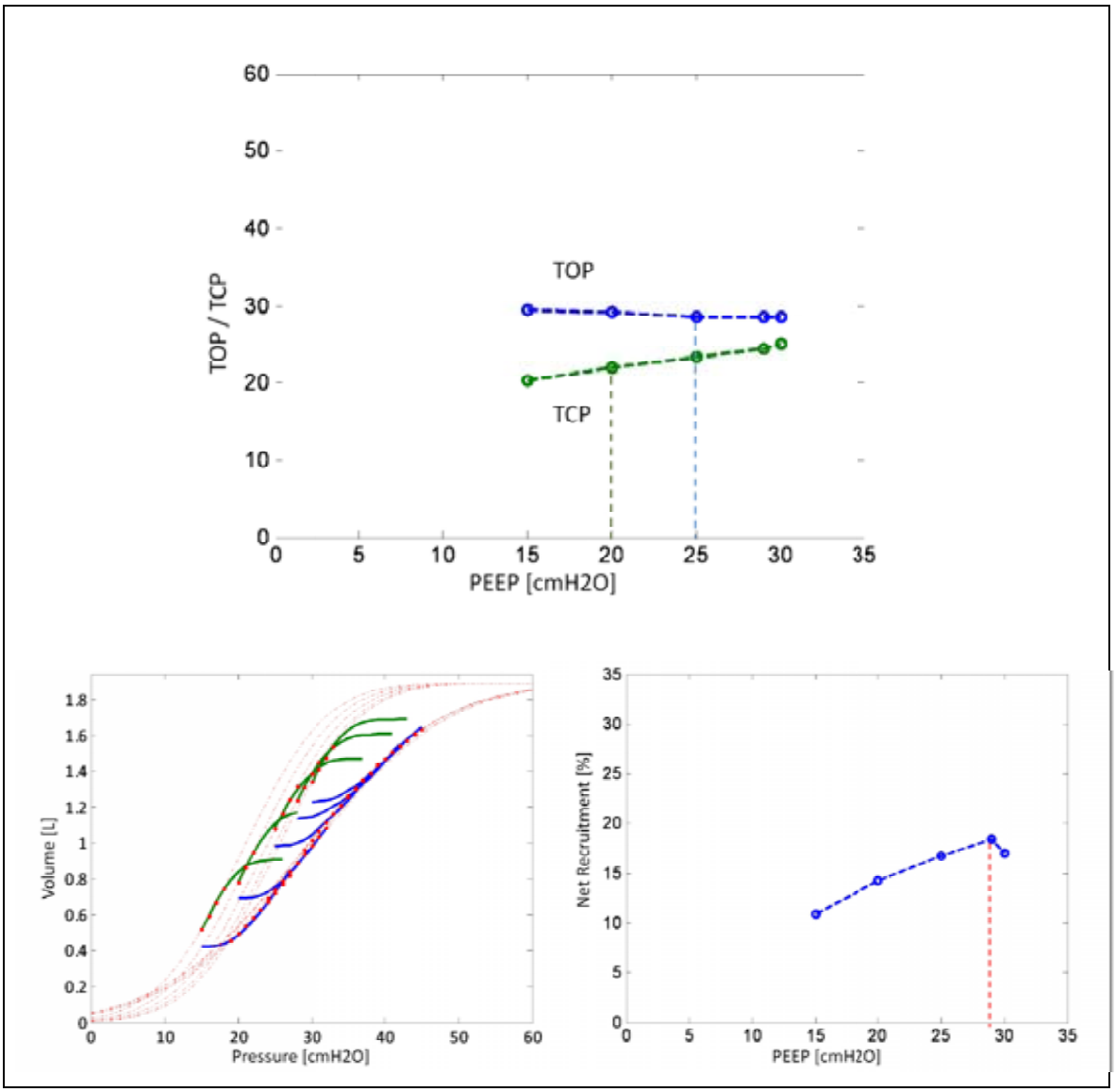

Figure C. 12 - Main plot shows TOP and TCP as a function of PEEP for Patient 9. Bottom left plot is the model fit. Bottom right indicates net recruitment

Table C. 12 - Clinically selected PEEP and Optimal PEEP indicated by TOP, TCP and net recruitment for Patient 9

Method	Optimum PEEP [cm H2O]	Reason
TOP	25	Recruitment maximised - Additional PEEP does not cause additional recruitment
TCP	20	Higher PEEP results in less de-recruitment but can risk VILI
Net Recruitment	29	Lower PEEP does not maximise recruitment, while higher PEEP is sub-optimal. But may risk VILI
Clinical Setting	10	Clinician selected

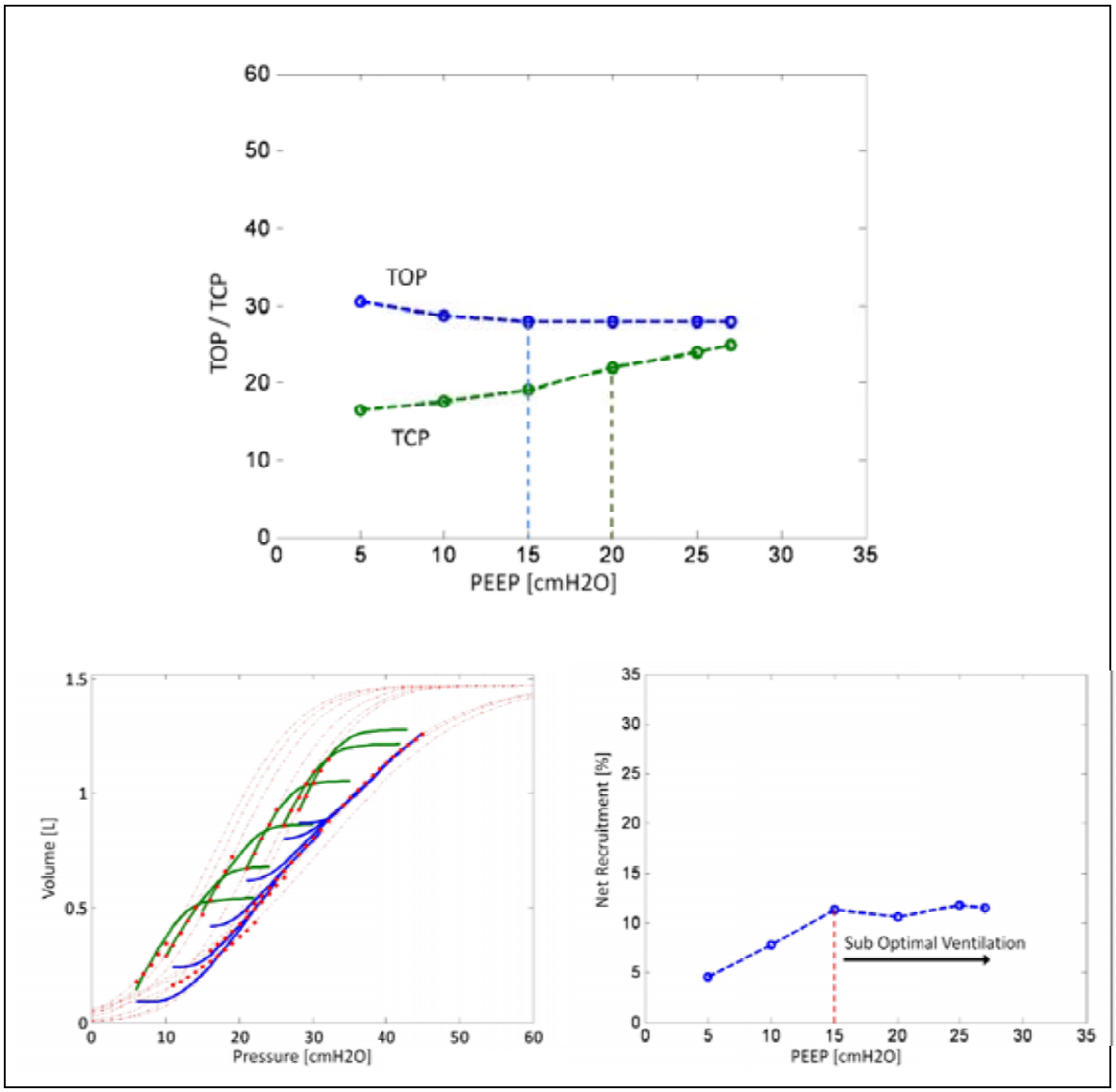

Figure C. 13 - Main plot shows TOP and TCP as a function of PEEP for Patient 10. Bottom left plot is the model fit. Bottom right indicates net recruitment

Table C. 13 - Clinically selected PEEP and Optimal PEEP indicated by TOP, TCP and net recruitment for Patient 10

Method	Optimum PEEP [cm H2O]	Reason
TOP	15	Recruitment maximised - Additional PEEP does not cause additional recruitment
TCP	20	Higher PEEP results in less de-recruitment but can risk VILI
Net Recruitment	15	Lower PEEP does not maximise recruitment, while higher PEEP is sub-optimal. But may risk VILI
Clinical Setting	10	Clinician selected

Appendix D – Measured dFRC Plots

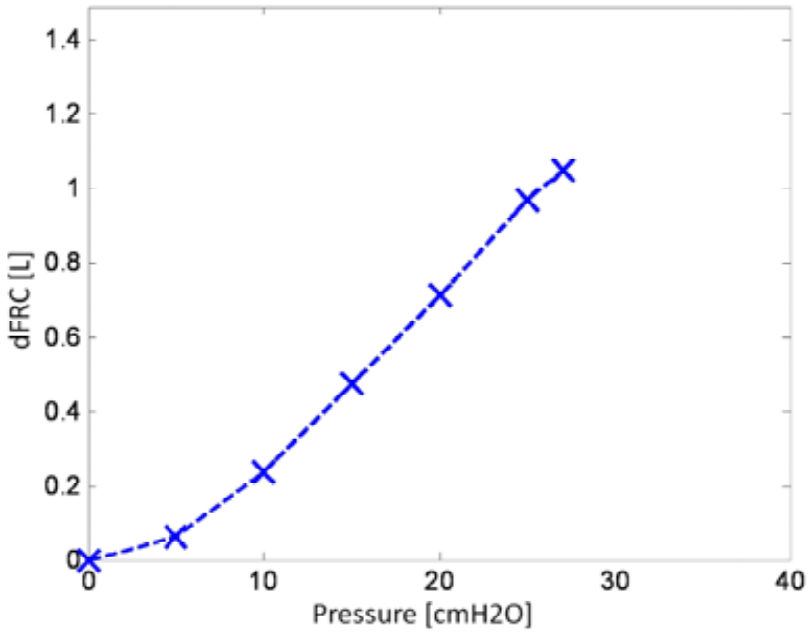

Figure D. 1 - PEEP vs Clinically measured dFRC for Group 2, Patient 1

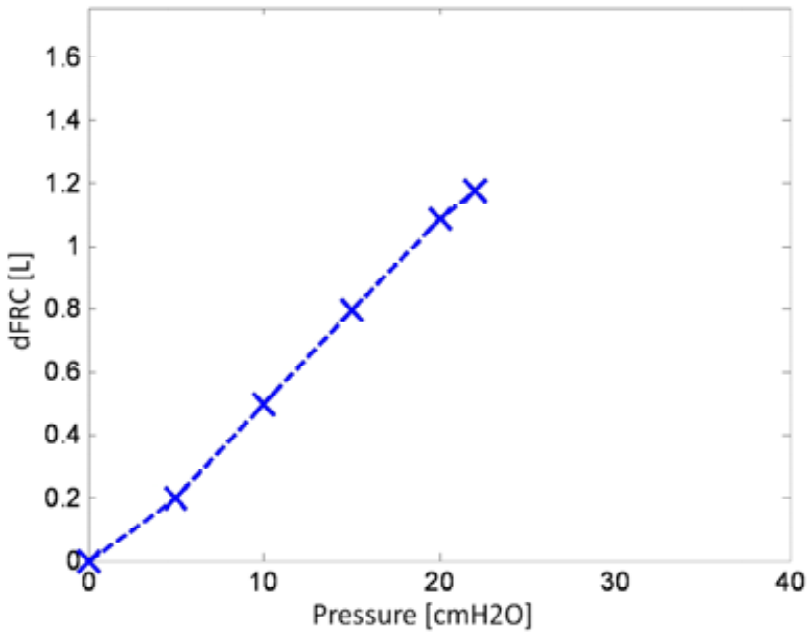

Figure D. 2 - PEEP vs Clinically measured dFRC for Group 2, Patient 2

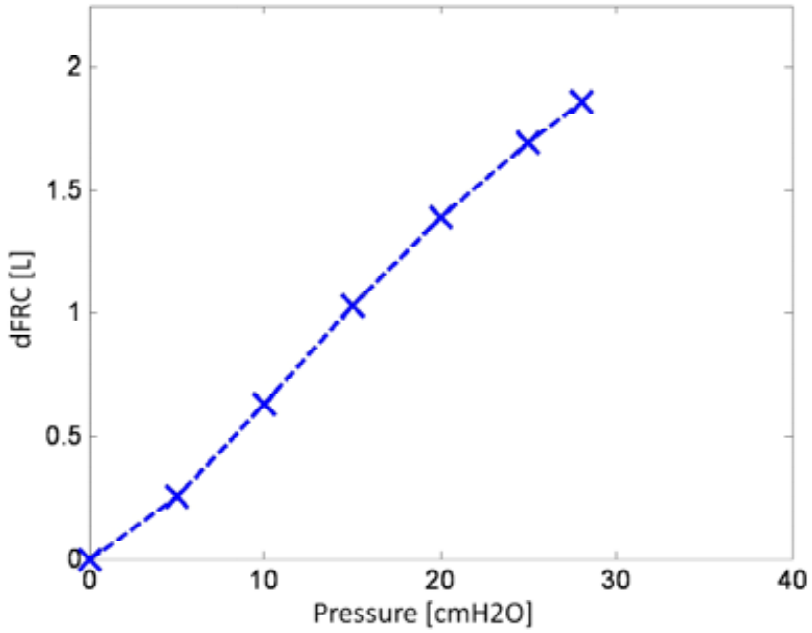

Figure D. 3 - PEEP vs Clinically measured dFRC for Group 2, Patient 3

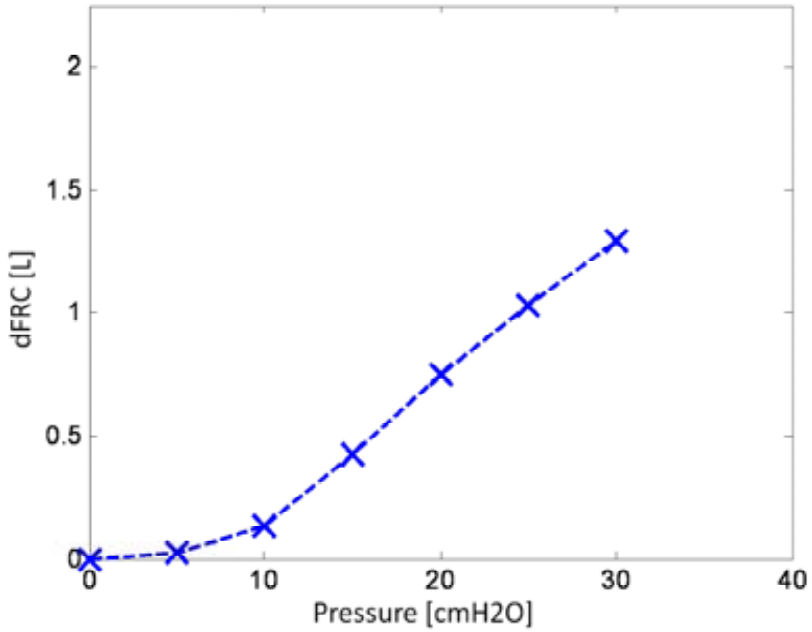

Figure D. 4 - PEEP vs Clinically measured dFRC for Group 2, Patient 4

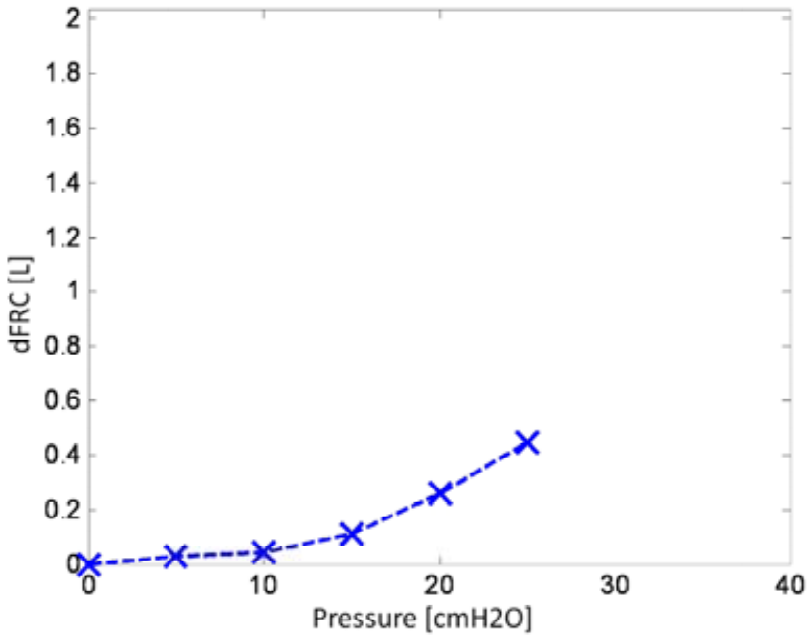

Figure D. 5 - PEEP vs Clinically measured dFRC for Group 2, Patient 5 – Trial 1

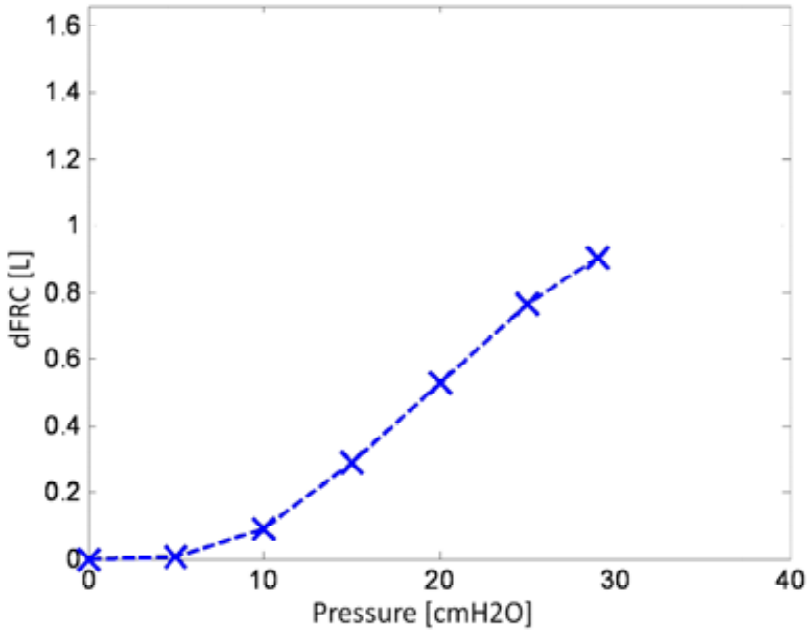

Figure D. 6 - PEEP vs Clinically measured dFRC for Group 2, Patient 5 – Trial 2

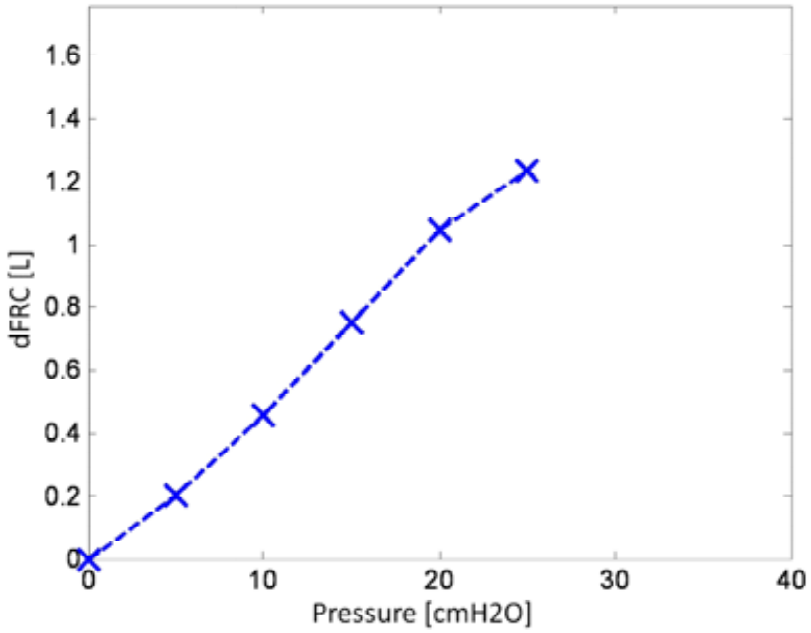

Figure D. 7 - PEEP vs Clinically measured dFRC for Group 2, Patient 6 – Trial 2

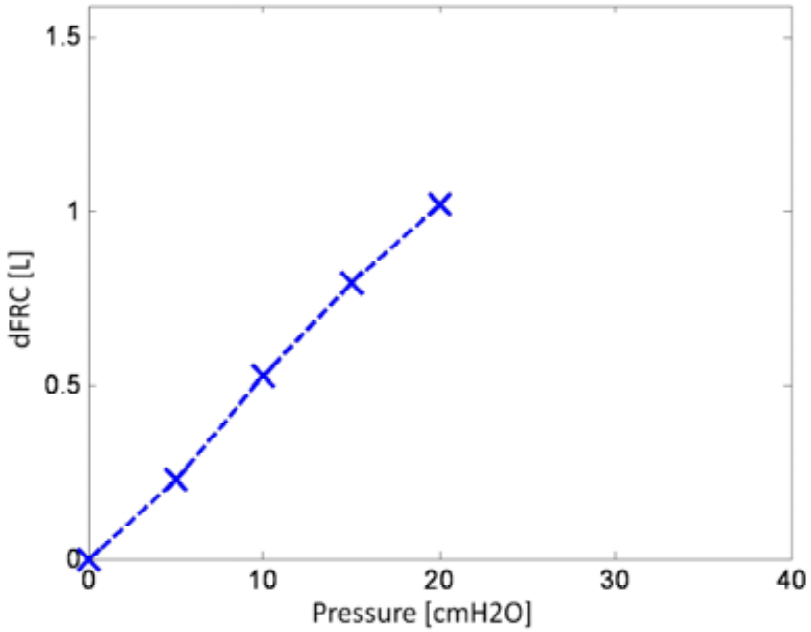

Figure D. 8 - PEEP vs Clinically measured dFRC for Group 2, Patient 6 – Trial 3

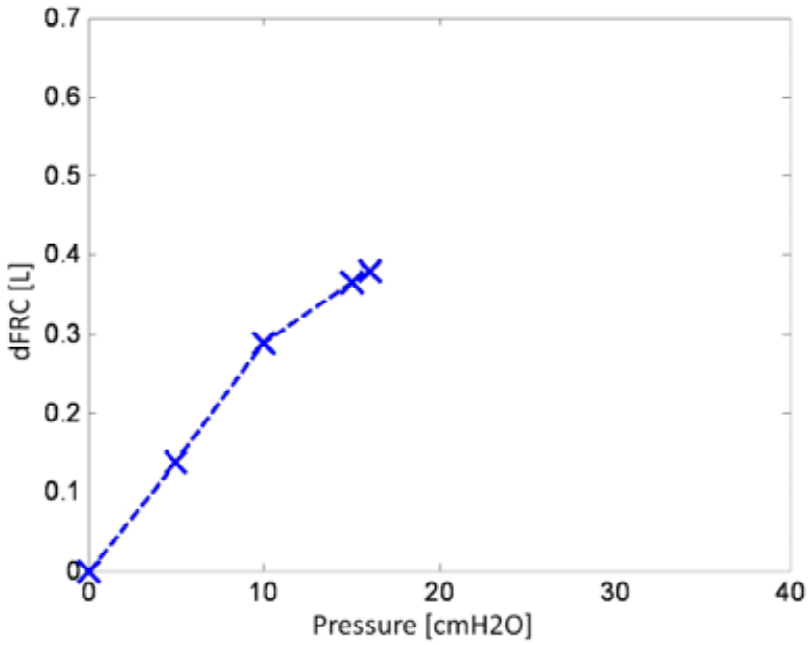

Figure D. 9 - PEEP vs Clinically measured dFRC for Group 2, Patient 7

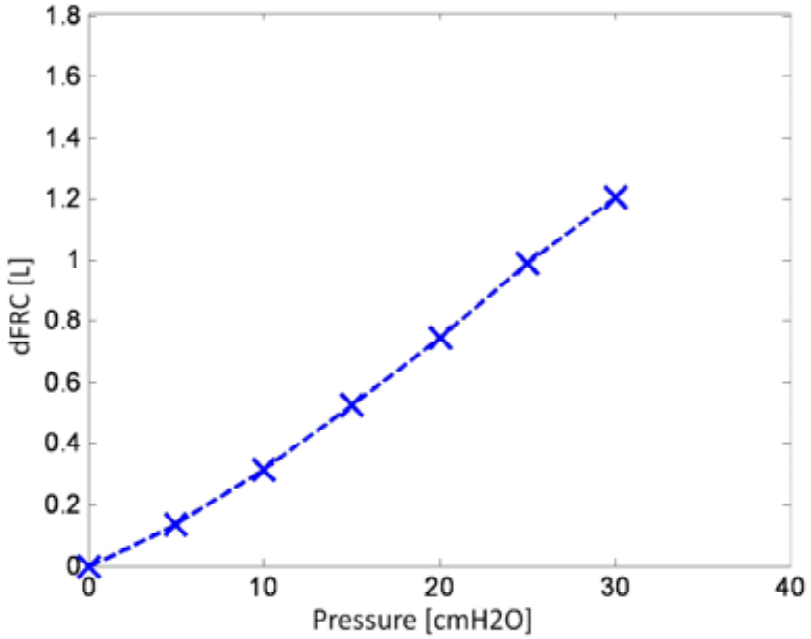

Figure D. 10 - PEEP vs Clinically measured dFRC for Group 2, Patient 8

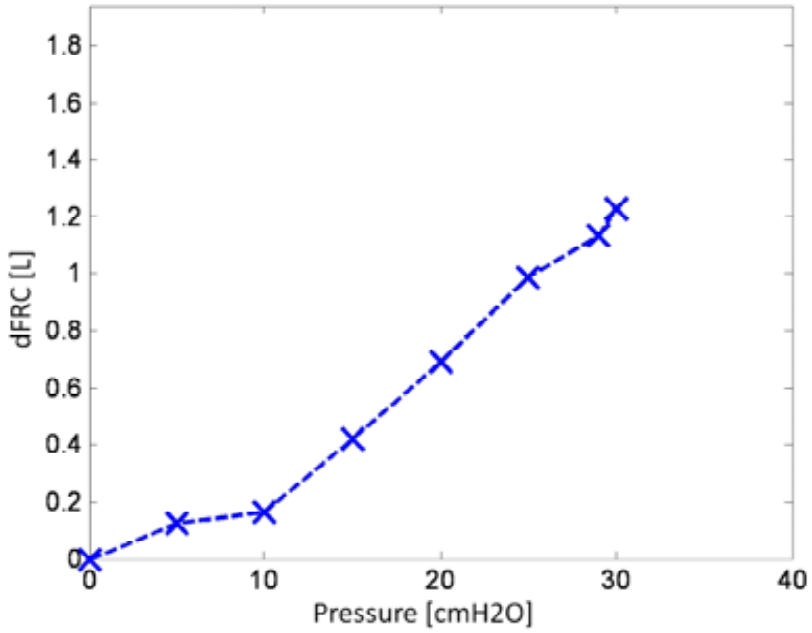

Figure D. 11 - PEEP vs Clinically measured dFRC for Group 2, Patient 9

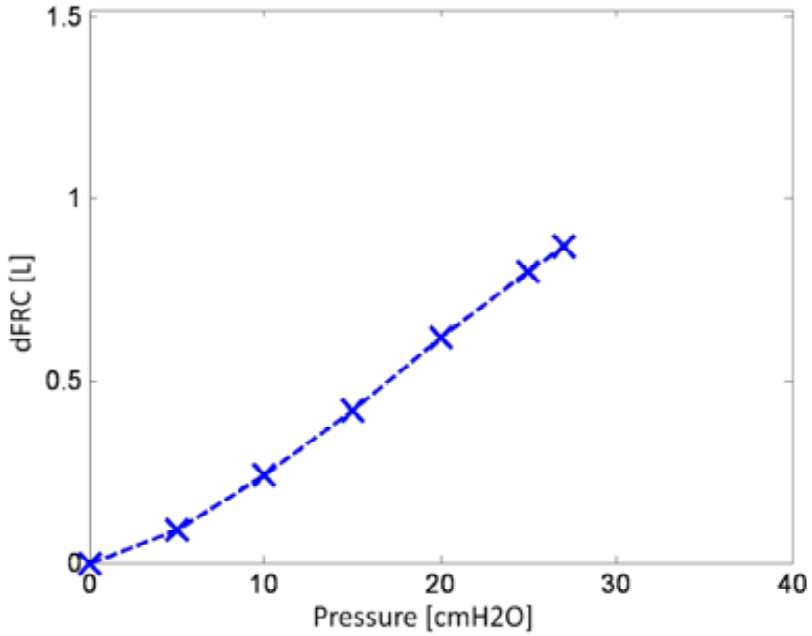

Figure D. 12 - PEEP vs Clinically measured dFRC for Group 2, Patient 10

References

Acosta, P., Santisbon, E. & Varon, J. (2007). The Use of Positive End-Expiratory Pressure in Mechanical Ventilation. *Critical Care Clinics,* 23 (2)**:** 251-261.

Adams, A. B., Simonson, D. A. & Dries, D. J. (2003). Ventilatory-induced lung injury. *Respir Care Clin N Am,* 9 (3)**:** 343 - 362.

Albaiceta, G. M., Piacentini, E., VillagrÃ¡, A., Lopez-Aguilar, J., Taboada, F. & Blanch, L. (2003). Application of continuous positive airway pressure to trace static pressure-volume curves of the respiratory system. *Crit Care Med,* 31 (10)**:** 2514-2519.

Albaiceta, G. M., Taboada, F., Parra, D., Luyando, L. H., Calvo, J., Menendez, R. & Otero, J. (2004). Tomographic Study of the Inflection Points of the Pressure-Volume Curve in Acute Lung Injury. *Am J Respir Crit Care Med,* 170 (10)**:** 1066-1072.

Amato, M. B. P., Barbas, C. S. V., Medeiros, D. M., Magaldi, R. B., Schettino, G. P., Lorenzi-Filho, G., Kairalla, R. A., Deheinzelin, D., Munoz, C., Oliveira, R., Takagaki, T. Y. & Carvalho, C. R. R. (1998). Effect of a Protective-Ventilation Strategy on Mortality in the Acute Respiratory Distress Syndrome. *N Engl J Med,* 338 (6)**:** 347-354.

Amir, K., Thomas, G. K., Robert, d. & Manuel, D. (1995). Comparison of dynamic and passive measurements of respiratory mechanics in ventilated newborn infants. *Pediatric Pulmonology,* 20 (4)**:** 258-264.

Andreassen, S., Egeberg, J., Schröter, M. P. & Andersen, P. T. (1996). Estimation of pulmonary diffusion resistance and shunt in an oxygen status model. *Computer Methods and Programs in Biomedicine,* 51 (1-2)**:** 95-105.

Andreassen, S., Rees, S. E., KjÃ¦rgaard, S. r., Thorgaard, P., Winter, S. M., Morgan, C. J., Alstrup, P. & Toft, E. (1999). Hypoxemia after coronary bypass surgery modeled by resistance to oxygen diffusion. *Crit Care Med,* 27 (11)**:** 2445-2453.

Artigas, A., Bernard, Gordon R., Carlet, J., Dreyfuss, D., Gattinoni, L., Hudson, L., Lamy, M., Marini, John J., Matthay, Michael A., Pinsky, Michael R., Spragg, R., Suter, Peter M. & the Consensus Committee (1998). The American-European Consensus Conference on ARDS, Part 2 . Ventilatory, Pharmacologic, Supportive Therapy, Study Design Strategies, and Issues Related to Recovery and Remodeling. *Am J Respir Crit Care Med,* 157 (4)**:** 1332-1347.

Ashbaugh, D. G., Bigelow, D. B., Petty, T. L. & Levine, B. E. (1967). Acute respiratory distress in adults. *Lancet,* 2 (7511)**:** 319-323.

Barbas, C. S. l. V., de Matos, G. F. J., Pincelli, M. P., da Rosa Borges, E., Antunes, T., de Barros, J. M., Okamoto, V., Borges, J. o. B., Amato, M. B. P. & Ribeiro de

Carvalho, C. R. (2005). Mechanical ventilation in acute respiratory failure: recruitment and high positive end-expiratory pressure are necessary. *Current Opinion in Critical Care,* 11 (1)**:** 18-28.

Baudouin, S. (1998). Improved survival in ARDS: chance, technology or experience? *Thorax,* 53 (4)**:** 237-238.

Ben-Tal, A. (2006). Simplified models for gas exchange in the human lungs. *Journal of Theoretical Biology,* 238**:** 474 - 495.

Bernard, G., Artigas, A., Brigham, K., Carlet, J., Falke, K., Hudson, L., Lamy, M., Legall, J., Morris, A. & Spragg, R. (1994). The American-European Consensus Conference on ARDS. Definitions, mechanisms, relevant outcomes, and clinical trial coordination. *Am J Respir Crit Care Med,* 149 (3)**:** 818-824.

Bernard, G. R. (2005). Acute Respiratory Distress Syndrome: A Historical Perspective. *Am J Respir Crit Care Med,* 172 (7)**:** 798-806.

Bersten, A. D. (1998). Measurement of overinflation by multiple linear regression analysis in patients with acute lung injury. *Eur Respir J,* 12 (3)**:** 526-532.

Bersten, A. D., Edibam, C., Hunt, T. & Moran, J. (2002). Incidence and Mortality of Acute Lung Injury and the Acute Respiratory Distress Syndrome in Three Australian States. *Am J Respir Crit Care Med,* 165 (4)**:** 443-448.

Bickenbach, J., Czaplik, M., Dembinski, R., Pelosi, P., Schroeder, W., Marx, G. & Rossaint, R. (2010). In vivo microscopy in a porcine model of acute lung injury. *Respiratory Physiology & Neurobiology,* 172 (3)**:** 192-200.

Brenner, D. J. & Hall, E. J. (2007). Computed Tomography -- An Increasing Source of Radiation Exposure. *N Engl J Med,* 357 (22)**:** 2277-2284.

Brochard, L., Roudot-Thoraval, F., Roupie, E., Delclaux, C., Chastre, J., Fernandex-Mondejar, E., Clementi, E., Mancebo, J., Factor, P., Matamis, D., Ranieri, M., Blanch, L., Rodi, G., Mentec, H., Dreyfuss, D., Ferrer, M., Brun-Buisson, C., Tobin, M. & Lemaire, F. (1998). Tidal Volume Reduction for Prevention of Ventilator-induced Lung Injury in Acute Respiratory Distress Syndrome. *Am J Respir Crit Care Med,* 158 (6)**:** 1831-1838.

Brower, R. G., Lanken, P. N., MacIntyre, N., Matthay, M. A., Morris, A., Ancukiewicz, M., Schoenfeld, D. & Thompson, B. T. (2004). Higher versus Lower Positive End-Expiratory Pressures in Patients with the Acute Respiratory Distress Syndrome. *N Engl J Med,* 351 (4)**:** 327-336.

Brower, R. G., Shanholtz, C. B., Fessler, H. E., Shade, D. M., White, P. J., Wiener, C. M., Teeter, J. G., Dodd-o, J. M., Almog, Y. & Piantadosi, S. (1999). Prospective, randomized, controlled clinical trial comparing traditional versus reduced tidal volume ventilation in acute respiratory distress syndrome patients. *Crit Care Med,* 27 (8)**:** 1492-1498.

Burrowes, K. S., Hunter, P. J. & Tawhai, M. H. (2005). Anatomically based finite element models of the human pulmonary arterial and venous trees including supernumerary vessels. *J Appl Physiol,* 99 (2)**:** 731-738.

Carney, D., DiRocco, J. & Nieman, G. (2005). Dynamic alveolar mechanics and ventilator-induced lung injury. *Crit Care Med,* 33 (3)**:** S122-S128.

Carney, D. E., Bredenberg, C. E., Schiller, H. J., Picone, A. l., McCann, U. G., Gatto, L. A., Bailey, G., Fillinger, M. & Nieman, G. F. (1999). The Mechanism of Lung Volume Change during Mechanical Ventilation. *Am J Respir Crit Care Med,* 160 (5)**:** 1697-1702.

Carvalho, A., Jandre, F., Pino, A., Bozza, F., Salluh, J., Rodrigues, R., Ascoli, F. & Giannella-Neto, A. (2007). Positive end-expiratory pressure at minimal respiratory elastance represents the best compromise between mechanical stress and lung aeration in oleic acid induced lung injury. *Critical Care,* 11 (4)**:** R86.

Chase, J. G., Shaw, G., Le Compte, A., Lonergan, T., Willacy, M., Wong, X.-W., Lin, J., Lotz, T., Lee, D. & Hann, C. (2008). Implementation and evaluation of the SPRINT protocol for tight glycaemic control in critically ill patients: a clinical practice change. *Critical Care,* 12 (2)**:** R49.

Cheng, W., DeLong, D. S., Franz, G. N., Petsonk, E. L. & Frazer, D. G. (1995). Contribution of opening and closing of lung units to lung hysteresis. *Respiration Physiology,* 102 (2-3)**:** 205-215.

Chiumello, D., Carlesso, E., Cadringher, P., Caironi, P., Valenza, F., Polli, F., Tallarini, F., Cozzi, P., Cressoni, M., Colombo, A., Marini, J. J. & Gattinoni, L. (2008). Lung Stress and Strain during Mechanical Ventilation for Acute Respiratory Distress Syndrome. *Am J Respir Crit Care Med,* 178 (4)**:** 346-355.

Cohen, B. L. (2008). The Linear No-Threshold Theory of Radiation Carcinogenesis Should Be Rejected. *J Am Physicians and Surgeons,* 13 (3)**:** 70 - 76.

Cournand, A., Motley, H. L., Werko, L. & Richards, D. W. J. R. (1947). Physiological studies of the effects of intermittent positive pressure breathing on cardiac output in man. *Am J Physiol,* 152 (1)**:** 162-174.

Crotti, S., Mascheroni, D., Caironi, P., Pelosi, P., Ronzoni, G., Mondino, M., Marini, J. J. & Gattinoni, L. (2001). Recruitment and Derecruitment during Acute Respiratory Failure . A Clinical Study. *Am J Respir Crit Care Med,* 164 (1)**:** 131-140.

Dasta, J. F., McLaughlin, T. P., Mody, S. H. & Piech, C. T. (2005). Daily cost of an intensive care unit day: The contribution of mechanical ventilation. *Crit Care Med,* 33 (6)**:** 1266-1271.

De Michele, M. & Grasso, S. (2006). Measurement of PEEP-induced alveolar recruitment: just a research tool? *Critical Care,* 10 (4)**:** 148.

Dreyfuss, D., Basset, G., Soler, P. & Saumon, G. (1985). Intermittent positive-pressure hyperventilation with high inflation pressures produces pulmonary microvascular injury in rats. *Am Rev Respir Dis,* 132 (4)**:** 880-884.

Dreyfuss, D. & Saumon, G. (1998). Ventilator-induced Lung Injury . Lessons from Experimental Studies. *Am J Respir Crit Care Med,* 157 (1)**:** 294-323.

Eberhard, L., Guttmann, J., Wolff, G., Bertschmann, W., Minzer, A., Kohl, H. J., Zeravik, J., Adolph, M. & Eckart, J. (1992). Intrinsic PEEP monitored in the ventilated ARDS patient with a mathematical method. *J Appl Physiol,* 73 (2)**:** 479-485.

Eichacker, P. Q., Gerstenberger, E. P., Banks, S. M., Cui, X. & Natanson, C. (2002). Meta-Analysis of Acute Lung Injury and Acute Respiratory Distress Syndrome Trials Testing Low Tidal Volumes. *Am J Respir Crit Care Med,* 166 (11)**:** 1510-1514.

Esteban, A., Anzueto, A., Frutos, F., Alia, I., Brochard, L., Stewart, T., Benito, S., Epstein, S., Apezteguia, S., Nightingale, P., Arroliga, A. & Tobin, M. (2002). Characteristics and outcomes in adult patients receiving mechanical ventilation: a 28-day international study. *Jama,* 287 (3)**:** 345-355.

Feinendegen, L. E. (2005). Evidence for beneficial low level radiation effects and radiation hormesis. *Br J Radiol,* 78 (925)**:** 3-7.

Feinendegen, L. F. & Pollycove, M. (2001). Biologic Responses to Low Doses of Ionizing Radiation: Detriment versus Hormesis - Part 1. Dose Responses of Cells and Tissues. *J Nuclear Med,* 43 (7)**:** N17.

Ferguson, N. D., Frutos-Vivar, F., Esteban, A., Anzueto, A., Alia, I., Brower, R. G., Stewart, T. E., Apezteguia, C., Gonzalez, M., Soto, L., Abroug, F. & Brochard, L. (2005). Airway pressures, tidal volumes, and mortality in patients with acute respiratory distress syndrome. *Crit Care Med,* 33 (1)**:** 21-30.

Fernández, R., Mancebo, J., Blanch, L., Benito, S., Calaf, N. & Net, A. (1990). Intrinsic PEEP on static pressure-volume curves. *Intensive Care Medicine,* 16 (4)**:** 233-236.

Forrester, J. S., Ganz, W., Diamond, G., McHugh, T., Chonette, D. W. & Swan, H. J. C. (1972). Thermodilution cardiac output determination with a single flow-directed catheter. *American Heart Journal,* 83 (3)**:** 306-311.

Foti, G., Cereda, M., Sparacino, M. E., De Marchi, L., Villa, F. & Pesenti, A. (2000). Effects of periodic lung recruitment maneuvers on gas exchange and respiratory mechanics in mechanically ventilated acute respiratory distress syndrome (ARDS) patients. *Intensive Care Medicine,* 26 (5)**:** 501-507.

Gajic, O., Dara, S. I., Mendez, J. L., Adesanya, A. O., Festic, E., Caples, S. M., Rana, R., St. Sauver, J. L., Lymp, J. F., Afessa, B. & Hubmayr, R. D. (2004). Ventilator-associated lung injury in patients without acute lung injury at the onset of mechanical ventilation *. *Crit Care Med,* 32 (9)**:** 1817-1824.

Gattinoni, L., Caironi, P., Cressoni, M., Chiumello, D., Ranieri, V. M., Quintel, M., Russo, S., Patroniti, N., Cornejo, R. & Bugedo, G. (2006). Lung Recruitment in Patients with the Acute Respiratory Distress Syndrome. *N Engl J Med,* 354 (17)**:** 1775-1786.

Gattinoni, L., Caironi, P., Pelosi, P. & Goodman, L. R. (2001). What Has Computed Tomography Taught Us about the Acute Respiratory Distress Syndrome? *Am J Respir Crit Care Med,* 164 (9)**:** 1701-1711.

Gattinoni, L., Chiumello, D., Carlesso, E. & Valenza, F. (2004). Bench-to-bedside review: Chest wall elastance in acute lung injury/acute respiratory distress syndrome patients. *Critical Care,* 8 (5)**:** 350 - 355.

Gattinoni, L., Eleonora, C. & Caironi, P. (2005). Monitoring of pulmonary mechanics in acute respiratory distress syndrome to titrate therapy. *Current Opinion in Critical Care,* 11 (3)**:** 252-258.

Gattinoni, L., Pelosi, P., Crotti, S. & Valenza, F. (1995). Effects of positive end-expiratory pressure on regional distribution of tidal volume and recruitment in adult respiratory distress syndrome. *Am J Respir Crit Care Med,* 151 (6)**:** 1807-1814.

Gattinoni, L., Pelosi, P., Suter, P. M., Pedoto, A., Vercesi, P. & Lissoni, A. (1998). Acute Respiratory Distress Syndrome Caused by Pulmonary and Extrapulmonary Disease . Different Syndromes? *Am J Respir Crit Care Med,* 158 (1)**:** 3-11.

Gattinoni, L. & Pesenti, A. (2005). The concept of "baby lung". *Intensive Care Medicine,* 31 (6)**:** 776 - 784.

GE Healthcare. 2006. *The INview Suite: SpiroDynamics and FRC INview*. http://www.gehealthcare.com/usen/respiratory_care/docs/CC4891A_INview_brochure.pdf

Girard, T. D. & Bernard, G. R. (2007). Mechanical Ventilation in ARDS. *Chest,* 131 (3)**:** 921-929.

Goode, K. M. (2003). Model-based development of a fuzzy logic advisor for artificially ventilated patients : a thesis presented for the degree of Doctor of Philosophy. *University of Sheffield, England*.

Grasso, S., Stripoli, T., De Michele, M., Bruno, F., Moschetta, M., Angelelli, G., Munno, I., Ruggiero, V., Anaclerio, R., Cafarelli, A., Driessen, B. & Fiore, T. (2007). ARDSnet Ventilatory Protocol and Alveolar Hyperinflation: Role of Positive End-Expiratory Pressure. *Am J Respir Crit Care Med,* 176 (8)**:** 761-767.

Grasso, S., Terragni, P., Mascia, L., Fanelli, V., Quintel, M., Herrmann, P. P., Hedenstierna, G., Slutsky, A. S. & Ranieri, V. M. (2004). Airway pressure-time curve profile (stress index) detects tidal recruitment/hyperinflation in experimental acute lung injury. *Crit Care Med,* 32 (4)**:** 1018-1027.

Halter, J. M., Steinberg, J. M., Schiller, H. J., DaSilva, M., Gatto, L. A., Landas, S. & Nieman, G. F. (2003). Positive End-Expiratory Pressure after a Recruitment Maneuver Prevents Both Alveolar Collapse and Recruitment/Derecruitment. *Am J Respir Crit Care Med,* 167 (12)**:** 1620-1626.

Hann, C. E., Chase, J. G., Desaive, T., Froissart, C. B., Revie, J., Stevenson, D., Lambermont, B., Ghuysen, A., Kolh, P. & Shaw, G. M. (2010). Unique parameter identification for cardiac diagnosis in critical care using minimal data sets. *Computer Methods and Programs in Biomedicine,* 99 (1)**:** 75-87.

Harris, R. S. (2005). Pressure-volume curves of the respiratory system. *Respir Care,* 50 (1)**:** 78-98.

Harris, R. S., Willey-Courand, D.-B., Head, C. A., Galletti, G. G., Call, D. M. & Venegas, J. G. (2002). Regional VA, Q, and VA/Q during PLV: effects of nitroprusside and inhaled nitric oxide. *J Appl Physiol,* 92 (1)**:** 297-312.

Hauber, H., Karp, D., Goldmann, T., Vollmer, E. & Zabel, P. (2010). Effect of low tidal volume ventilation on lung function and inflammation in mice. *BMC Pulmonary Medicine,* 10 (1)**:** 21.

Heinze, H., Schaaf, B., Grefer, J., Klotz, K. & Eichler, W. (2007). The Accuracy of the Oxygen Washout Technique for Functional Residual Capacity Assessment During Spontaneous Breathing. *Anesth Analg,* 104 (3)**:** 598-604.

Henzler, D., Pelosi, P., Dembinski, R., Ullmann, A., Mahnken, A., Rossaint, R. & Kuhlen, R. (2005). Respiratory compliance but not gas exchange correlates with changes in lung aeration after a recruitment maneuver: an experimental study in pigs with saline lavage lung injury. *Critical Care,* 9 (5)**:** R471 - R482.

Hickling, K. G. (1998). The Pressure-Volume Curve Is Greatly Modified by Recruitment . A Mathematical Model of ARDS Lungs. *Am J Respir Crit Care Med,* 158 (1)**:** 194-202.

Hickling, K. G. (2002). Reinterpreting the pressure-volume curve in patients with acute respiratory distress syndrome. *Current Opinion in Critical Care,* 8 (1)**:** 32-38.

Hoeper, M. M., Maier, R., Tongers, J., Niedermeyer, J., Hohlfeld, J. M., Hamm, M. & Fabel, H. (1999). Determination of Cardiac Output by the Fick Method, Thermodilution, and Acetylene Rebreathing in Pulmonary Hypertension. *Am J Respir Crit Care Med,* 160 (2)**:** 535-541.

Howman, S. F. (1999). Mechanical Ventilation: A Review and Update for Clinicians. *Hospital Physician,* 35 (12)**:** 26 - 36.

Hudson, L. D. & Steinberg, K. P. (1999). Epidemiology of Acute Lung Injury and ARDS. *Chest,* 116 (suppl 1)**:** 74S-82S.

ICRP (2008). *ICRP Publication 103: Recommendations of the ICRP - Annals of the ICRP*, 37 (2 - 4)

Jia, X., Malhotra, A., Saeed, M., Mark, R. G. & Talmor, D. (2008). Risk Factors for ARDS in Patients Receiving Mechanical Ventilation for > 48 h. *Chest,* 133 (4)**:** 853-861.

Johnston, C. J., Rubenfeld, G. D. & Hudson, L. D. (2003). Effect of Age on the Development of ARDS in Trauma Patients. *Chest,* 124 (2)**:** 653-659.

Jonson, B., Richard, J. C., Straus, C., Mancebo, J., Lemaire, F. & Brochard, L. (1999). Pressure-Volume Curves and Compliance in Acute Lung Injury . Evidence of Recruitment Above the Lower Inflection Point. *Am J Respir Crit Care Med,* 159 (4)**:** 1172-1178.

Jonson, B. & Svantesson, C. (1999). Elastic pressure-volume curves: what information do they convey? *Thorax,* 54 (1)**:** 82-87.

Jonson, B. & Uttman, L. (2007). Efficient gas exchange with low tidal volume ventilation in acute respiratory distress syndrome. *Journal of Organ Dysfunction,* 3 (2)**:** 82-89.

Kacmarek, R. M. (2005). Lung Protection: The Cost in Some Is Increased Work of Breathing. Is It Too High? *Respir Care,* 50 (12)**:** 1614-1616.

Kallet, R. H., Jasmer, R. M., Pittet, J.-F., Tang, J. F., Campbell, A. R., Dicker, R., Hemphill, C. & Luce, J. M. (2005). Clinical implementation of the ARDS network protocol is associated with reduced hospital mortality compared with historical controls. *Crit Care Med,* 33 (5)**:** 925-929.

Karason, S., Sondergaard, S., Lundin, S., Wiklund, J. & Stenqvist, O. (2000). Evaluation of pressure/volume loops based on intratracheal pressure measurements during dynamic conditions. *Acta Anaesthesiologica Scandinavica,* 44 (5)**:** 571-577.

Karbing, D., Kjaergaard, S., Smith, B., Espersen, K., Allerod, C., Andreassen, S. & Rees, S. (2007). Variation in the PaO2/FiO2 ratio with FiO2: mathematical and experimental description, and clinical relevance. *Critical Care,* 11 (6)**:** R118.

King, E., Jones, R. & Patakas, D. (1973). Evaluation of positive end-expiratory pressure therapy in the adult respiratory distress syndrome. *Can J Anesth,* 20 (4)**:** 546-558.

King, T. K. C., Weber, B., Okinaka, A., Friedman, S. A., Smith, J. P. & Briscoe, W. A. (1974). Oxygen Transfer in Catastrophic Respiratory Failure. *Chest,* 65 (4 Supplement)**:** 40S-44S.

Kwok, H. F. (2003). SIVA: An intelligent advisory system for intensive care ventilators : a thesis presented for the degree of Doctor of Philosophy. *University of Sheffield, England*.

Lapinsky, S. & Mehta, S. (2005). Bench-to-bedside review: Recruitment and recruiting maneuvers. *Crit Care,* 9 (1)**:** 60 - 65.

Leibowitz, A. B. & Oropello, J. M. (2007). The Pulmonary Artery Catheter in Anesthesia Practice in 2007: An Historical Overview With Emphasis on the Past 6 Years. *Seminars in Cardiothoracic and Vascular Anesthesia,* 11 (3)**:** 162-176.

Levy, M. M. (2002). Optimal PEEP in ARDS: Changing concepts and current controversies. *Critical Care Clinics,* 18 (1)**:** 15-33.

Lichtwarck-Aschoff, M., Kessler, V., Sjostrand, U. H., Hedlund, A., Mols, G., Rubertsson, S., Markstrom, A. M. & Guttmann, J. (2000). Static versus dynamic respiratory mechanics for setting the ventilator. *Br J Anaesth,* 85 (4)**:** 577-586.

Lorente, L., Villegas, J., Martín, M. M., Jiménez, A. & Mora, M. L. (2004). Catheter-related infection in critically ill patients. *Intensive Care Medicine,* 30 (8)**:** 1681-1684.

Lu, Q., Constantin, J. M., Nieszkowska, A., Elman, M., Vieira, S. & Rouby, J. J. (2006). Measurement of alveolar derecruitment in patients with acute lung injury: computerized tomography versus pressure–volume curve. *Crit Care,* 10 (3)**:** R95.

Lu, Q. & Rouby, J.-J. (2000). Measurement of pressure-volume curves in patients on mechanical ventilation: methods and significance. *Critical Care,* 4 (2)**:** 91 - 100.

Luecke, T. & Pelosi, P. (2005). Clinical review: Positive end-expiratory pressure and cardiac output. *Critical Care,* 9 (6)**:** 607 - 621.

Luecke, T., Roth, H., Herrmann, P., Joachim, A., Weisser, G., Pelosi, P. & Quintel, M. (2003). PEEP decreases atelectasis and extravascular lung water but not lung tissue volume in surfactant-washout lung injury. *Intensive Care Medicine,* 29 (11)**:** 2026-2033.

Luhr, O. R., Karlsson, M., Thorsteinsson, A., Rylander, C. & Frostell, C. G. (2000). The impact of respiratory variables on mortality in non-ARDS and ARDS patients requiring mechanical ventilation. *Intensive Care Medicine,* 26 (5)**:** 508-517.

Macnaughton, P. D. (2006). New ventilators for the ICU--usefulness of lung performance reporting. *Br J Anaesth***:** ael115.

Maggiore, S. M., Jonson, B., Richard, J.-C., Jaber, S., Lemaire, F. & Brochard, L. (2001). Alveolar Derecruitment at Decremental Positive End-Expiratory Pressure Levels in Acute Lung Injury . Comparison with the Lower Inflection Point, Oxygenation, and Compliance. *Am J Respir Crit Care Med,* 164 (5)**:** 795-801.

Maggiore, S. M., Richard, J. C. & Brochard, L. (2003). What has been learnt from P/V curves in patients with acute lung injury/acute respiratory distress syndrome. *Eur Respir J,* 22 (42_suppl)**:** 22s-26.

Malbouisson, L. M., Muller, J. C., Constantin, J. M., Lu, Q., Puybasset, L., Rouby, J. J. & The CT Scan ARDS Study Group (2001). Computed Tomography Assessment of Positive End-expiratory Pressure-induced Alveolar Recruitment in Patients with

Acute Respiratory Distress Syndrome. *Am J Respir Crit Care Med,* 163 (6)**:** 1444-1450.

Manzano, F., Yuste, E., Colmenero, M., Aranda, A., Garcia-Horcajadas, A., Rivera, R. & Fernandez-Mondejar, E. (2005). Incidence of acute respiratory distress syndrome and its relation to age. *Journal of Critical Care,* 20 (3)**:** 274-280.

Martini, F. H. (2006). *Fundamentals of Anatomy & Physiology - 7th Edition,* San Francisco, Pearson Benjamin Cummings.

McCann, U. G., Schiller, H. J., Carney, D. E., Gatto, L. A., Steinberg, J. M. & Nieman, G. F. (2001). Visual validation of the mechanical stabilizing effects of positive end-expiratory pressure at the alveolar level. *J Surg Res,* 99 (2)**:** 335-342.

McLean, S. E., Jensen, L. A., Schroeder, D. G., Gibney, N. R. & Skjodt, N. M. (2006). Improving Adherence to a Mechanical Ventilation Weaning Protocol for Critically Ill Adults: Outcomes After an Implementation Program. *Am J Crit Care,* 15 (3)**:** 299-309.

Mergoni, M., Volpi, A., Bricchi, C. & Rossi, A. (2001). Lower inflection point and recruitment with PEEP in ventilated patients with acute respiratory failure. *J Appl Physiol,* 91 (1)**:** 441-450.

Micceri, T. (1989). The unicorn, the normal curve, and other improbable creatures. *Psychological Bulletin,* 105 (1)**:** 156-166.

Michelet, P., Roch, A., Brousse, D., D'Journo, X. B., Bregeon, F., Lambert, D., Perrin, G., Papazian, L., Thomas, P., Carpentier, J. P. & Auffray, J. P. (2005). Effects of PEEP on oxygenation and respiratory mechanics during one-lung ventilation. *Br J Anaesth,* 95 (2)**:** 267-273.

Miranda, D. R., Gommers, D., Struijs, A., Dekker, R., Mekel, J., Feelders, R., Lachmann, B. & Bogers, A. J. (2005). Ventilator according to the open lung concept attenuates pulmonary inflammatory response in cardiac surgery. *Eur J Cardiothorac Surg,* 28 (6)**:** 889 - 895.

Moloney, E. D. & Griffiths, M. J. D. (2004). Protective ventilation of patients with acute respiratory distress syndrome. *Br J Anaesth,* 92 (2)**:** 261-270.

Moran, I., Zavala, E., Fernandez, R., Blanch, L. & Mancebo, J. (2003). Recruitment manoeuvres in acute lung injury/acute respiratory distress syndrome. *Eur Respir J,* 22 (42_suppl)**:** 37 - 42.

Mughal, M. M., Culver, D. A., Minai, O. A. & Arroliga, A. C. (2005). Auto-positive end-expiratory pressure: mechanisms and treatment. *Cleveland Clinic Journal of Medicine,* 72 (9)**:** 801-809.

NCRP (2002). Evaluation of the Linear-Nonthreshold Dose-Response Model for Ionizing Radiation (NCRP Report No 136). *J Radiological Protection,* 22 (3)**:** 331.

NRL (2009). Sources, Effects and Risks of Ionising Radiation. *New Zealand Ministry of Health*

Ochs, M., Nyengaard, J. R., Jung, A., Knudsen, L., Voigt, M., Wahlers, T., Richter, J. & Gundersen, H. J. G. (2004). The Number of Alveoli in the Human Lung. *Am J Respir Crit Care Med,* 169 (1)**:** 120-124.

Otis, A. B., Fenn, W. O. & Rahn, H. (1950). Mechanics of Breathing in Man. *J Appl Physiol,* 2 (11)**:** 592-607.

Parsons, P. E., Eisner, M. D., Thompson, B. T., Matthay, M. A., Ancukiewicz, M., Bernard, G. R., Wheeler, A. P. & Network, t. N. A. R. D. S. C. T. (2005). Lower tidal volume ventilation and plasma cytokine markers of inflammation in patients with acute lung injury. *Crit Care Med,* 33 (1)**:** 1-6.

Pavone, L., Albert, S., DiRocco, J., Gatto, L. & Nieman, G. (2007). Alveolar instability caused by mechanical ventilation initially damages the nondependent normal lung. *Critical Care,* 11 (5)**:** R104.

Pelosi, P., Bottino, N., Chiumello, D., Caironi, P., Panigada, M., Gamberoni, C., Colombo, G., Bigatello, L. M. & Gattinoni, L. (2003). Sigh in Supine and Prone Position during Acute Respiratory Distress Syndrome. *Am J Respir Crit Care Med,* 167 (4)**:** 521-527.

Pelosi, P., Goldner, M., Mckibben, A., Adams, A., Eccher, G., Caironi, P., Losappio, S., Gattinoni, L. & Marini, J. J. (2001). Recruitment and Derecruitment During Acute Respiratory Failure . An Experimental Study. *Am J Respir Crit Care Med,* 164 (1)**:** 122-130.

Peris, A., Zagli, G., Barbani, F., Tutino, L., Biondi, S., Di Valvasone, S., Batacchi, S., Bonizzoli, M., Spina, R., Miniati, M., Pappagallo, S., Giovannini, V. & Gensini, G. F. (2010). The value of lung ultrasound monitoring in H1N1 acute respiratory distress syndrome. *Anaesthesia,* 65 (3)**:** 294-297.

Phua, J., Badia, J. R., Adhikari, N. K. J., Friedrich, J. O., Fowler, R. A., Singh, J. M., Scales, D. C., Stather, D. R., Li, A., Jones, A., Gattas, D. J., Hallett, D., Tomlinson, G., Stewart, T. E. & Ferguson, N. D. (2009). Has Mortality from Acute Respiratory Distress Syndrome Decreased over Time?: A Systematic Review. *Am J Respir Crit Care Med,* 179 (3)**:** 220-227.

Piacentini, E., Wysocki, M. & Blanch, L. (2009). A new automated method versus continuous positive airway pressure method for measuring pressure–volume curves in patients with acute lung injury. *Intensive Care Medicine,* 35 (3)**:** 565-570.

Preston, R. J. (2003). The LNT model is the best we can do—today. *J Radiological Protection,* 23 (3)**:** 263.

Ramsey, C. D., Funk, D., Miller, R. R. I. & Kumar, A. (2010). Ventilator management for hypoxemic respiratory failure attributable to H1N1 novel swine origin influenza virus. *Critical Care Medicine,* 38**:** e58-e65.

Ranieri, V. M., Eissa, N. T., Corbeil, C., Chassé, M., Braidy, J., Matar, N. & Milic-Emili, J. (1991). Effects of positive end-expiratory pressure on alveolar recruitment and gas exchange in patients with the adult respiratory distress syndrome. *Am Rev Respir Dis,* 144 (3)**:** 544 - 551.

Ranieri, V. M., Suter, P. M., Tortorella, C., De Tullio, R., Dayer, J. M., Brienza, A., Bruno, F. & Slutsky, A. S. (1999). Effect of Mechanical Ventilation on Inflammatory Mediators in Patients With Acute Respiratory Distress Syndrome: A Randomized Controlled Trial. *Jama,* 282 (1)**:** 54-61.

Rees, S. E., Allerod, C., Kjaergaard, S., Toft, E., Thorgaard, P. & Andreassen, S. Year. Diagnosing Patient State in Intensive Care Patients Using the Intelligent Ventilator (INVENT) System. *In: Proceedings of the 8th Conference on AI in Medicine in Europe: Artificial Intelligence Medicine*, 2001.

Rees, S. E., Andreassen, S., Freundlich, M., Morgan, C., Carson, E. R. & Thorgaard, P. Year. Selecting ventilator settings using INVENT, a system including physiological models and penalty functions. *In: Proceedings of the Joint conference of European societies of Artificial Intelligence in Medicine and Medical Decision Making. Workshop, Computers in Anesthesia and Intensive Care*, 1999 Aalborg, Denmark.

Rees, S. E., Kjærgaard, S., Thorgaard, P., Malczynski, J., Toft, E. & Andreassen, S. (2002). The Automatic Lung Parameter Estimator (ALPE) System: Non-Invasive Estimation of Pulmonary Gas Exchange Parameters in 10-15 Minutes. *Journal of Clinical Monitoring and Computing,* 17 (1)**:** 43-52.

Register, S. D., Downs, J. B., Stock, M. C. & Kirby, R. R. (1987). Is 50% oxygen harmful? *Crit Care Med,* 15 (6)**:** 598-601.

Reynolds, H. N., McCunn, M., Borg, U., Habashi, N., Cottingham, C. & Bar-Lavi, Y. (1998). Acute respiratory distress syndrome: estimated incidence and mortality rate in a 5 million-person population base. *Critical Care,* 2 (29)**:** 29–34.

Ricard, J.-D., Dreyfuss, D. & Saumon, G. (2003). Ventilator-induced lung injury. *Eur Respir J,* 22 (42_suppl)**:** 2s-9.

Rouby, J.-J., Puybasset, L., Cluzel, P., Richecoeur, J., Lu, Q. & Grenier, P. (2000). Regional distribution of gas and tissue in acute respiratory distress syndrome. II. Physiological correlations and definition of an ARDS Severity Score. *Intensive Care Medicine,* 26 (8)**:** 1046-1056.

Rouby, J. J., Lu, Q. & Goldstein, I. (2002). Selecting the Right Level of Positive End-Expiratory Pressure in Patients with Acute Respiratory Distress Syndrome. *Am J Respir Crit Care Med,* 165 (8)**:** 1182-1186.

Rouby, J. J., Lu, Q. & Vieira, S. (2003). Pressure/volume curves and lung computed tomography in acute respiratory distress syndrome. *Eur Respir J,* 22 (42_suppl)**:** 27s-36.

Schiller, H. J., Steinberg, J., ., Halter, J., ., McCann, U., ., DaSilva, M., ., Gatto, L. A., Carney, D. & Nieman, G. (2003). Alveolar inflation during generation of a quasi-static pressure/volume curve in the acutely injured lung. *Crit Care Med,* 31 (4)**:** 1126-1133.

Sebel, P., Stoddart, D. M., Waldhorn, R. E., Wadmann, C. S. & Whitfield, P. (1985). *Respiration: The breath of life - 1st Edition,* New York, Torstar Books Inc.

Seeley, R. R., Stephens, T. D. & Tate, P. (2003). *Anatomy & Physiology - 6th Edition,* New York, McGraw-Hill.

Servillo, G., De Robertis, E., Coppola, M., Blasi, F., Rossano, F. & Tufano, R. (2000). Application of a computerised method to measure static pressure volume curve in acute respiratory distress syndrome. *Intensive Care Medicine,* 26 (1)**:** 11-14.

Stather, D. & Stewart, T. (2005). Clinical review: Mechanical ventilation in severe asthma. *Critical Care,* 9 (6)**:** 581 - 587.

Stewart, T. E., Meade, M. O., Cook, D. J., Granton, J. T., Hodder, R. V., Lapinsky, S. E., Mazer, C. D., McLean, R. F., Rogovein, T. S., Schouten, B. D., Todd, T. R. J., Slutsky, A. S. & The Pressure- and Volume-Limited Ventilation Strategy Group (1998). Evaluation of a Ventilation Strategy to Prevent Barotrauma in Patients at High Risk for Acute Respiratory Distress Syndrome. *N Engl J Med,* 338 (6)**:** 355-361.

Suchyta, M. R., Clemmer, T. P., Elliott, C. G., Orme, J. F., Morris, A. H., Jacobson, J. & Menlove, R. (1997). Increased Mortality of Older Patients With Acute Respiratory Distress Syndrome. *Chest,* 111**:** 1334-1339.

Sundaresan, A., Yuta, T., Hann, C. E., Geoffrey Chase, J. & Shaw, G. M. (2009). A minimal model of lung mechanics and model-based markers for optimizing ventilator treatment in ARDS patients. *Computer Methods and Programs in Biomedicine,* 95 (2)**:** 166-180.

Swan, A., Hunter, P. & Tawhai, M. (2008). Pulmonary Gas Exchange in Anatomically-Based Models of the Lung. *Integration in Respiratory Control,* 605 (5)**:** 184-189.

Takeuchi, M., Goddon, S., Dolhnikoff, M., Shimaoka, M., Hess, D., Amato, M. B. P. & Kacmarek, R. M. (2002). Set Positive End-expiratory Pressure during Protective Ventilation Affects Lung Injury. *Anesthesiology,* 97 (3)**:** 682-692.

Tawhai, M. H., Hunter, P., Tschirren, J., Reinhardt, J., McLennan, G. & Hoffman, E. A. (2004). CT-based geometry analysis and finite element models of the human and ovine bronchial tree. *J Appl Physiol,* 97 (6)**:** 2310-2321.

The ARDS Network (2000). Ventilation with Lower Tidal Volumes as Compared with Traditional Tidal Volumes for Acute Lung Injury and the Acute Respiratory Distress Syndrome. *N Engl J Med,* 342 (18)**:** 1301-1308.

Thompson, B. T., Hayden, D., Matthay, M. A., Brower, R. & Parsons, P. E. (2001). Clinicians' Approaches to Mechanical Ventilation in Acute Lung Injury and ARDS*. *Chest,* 120 (5)**:** 1622-1627.

Tubiana, M. (2005). Dose-effect relationship and estimation of the carcinogenic effects of low doses of ionizing radiation: The joint report of the Académie des Sciences (Paris) and of the Académie Nationale de Médecine. *Intl J Radiation Oncology,Biology,Physics,* 63 (2)**:** 317 - 319.

Tubiana, M., Nagataki, S., Feinendegen, L. E., Dimitroyannis, D. A., Frush, D. P., Goske, M. J., Hernanz-Schulman, M., Soyer, P., Varnholt, H., Brenner, D. J. & Hall, E. J. (2008). Computed Tomography and Radiation Exposure. *N Engl J Med,* 358 (8)**:** 850-853.

Vander, A., Sherman, J. & Luciano, D. (2001). *The Mechanism of Body Function - 7th Edition,* New York, McGraw-Hill.

Venegas, J. G., Harris, R. S. & Simon, B. A. (1998). A comprehensive equation for the pulmonary pressure-volume curve. *J Appl Physiol,* 84 (1)**:** 389-395.

Vidal Melo, M. F. (1998). Effect of cardiac output on pulmonary gas exchange: role of diffusion limitation with mismatch. *Respiration Physiology,* 113 (1)**:** 23-32.

Vieria, S. R. R., Puybasset, L., Lu, Q., Richecoeur, J., Cluzel, P., Coriat, P. & Rouby, J. J. (1999). A Scanographic Assessment of Pulmonary Morphology in Acute Lung Injury. Significance of the Lower Inflection Point Detected on the Lung Pressure-Volume Curve. *Am J Respir Crit Care Med,* 159 (5)**:** 1612 -1623.

Villar, J., Kacmarek, R. M., Pérez-Méndez, L. & Aguirre-Jaime, A. (2006). A high positive end-expiratory pressure, low tidal volume ventilatory strategy improves outcome in persistent acute respiratory distress syndrome: A randomized, controlled trial. *Crit Care Med,* 34 (5)**:** 1311-1318.

Wandrup, J. H. (1992). Oxygen uptake in the lungs: Shortcuts in clinical assessment of pulmonary oxygenation. *Blood Gas News,* 1**:** 3-5.

Wandrup, J. H. (1995). Quantifying pulmonary oxygen transfer deficits in critically ill patients. *Acta Anaesthesiologica Scandinavica,* 39 (s107)**:** 37-44.

Wang, A., Mahfouf, M., Mills, G. H., Panoutsos, G., Linkens, D. A., Goode, K., Kwok, H. F. & Dena, M. (2010). Intelligent model-based advisory system for the management of ventilated intensive care patients: Hybrid blood gas patient model. *Computer Methods and Programs in Biomedicine,* 99 (2).

Ware, L. B. & Matthay, M. A. (2000). The Acute Respiratory Distress Syndrome. *N Engl J Med,* 342 (18)**:** 1334-1349.

Yuta, T. (2007). Minimal model of lung mechanics for optimising ventilator therapy in critical care : a thesis presented for the degree of Doctor of Philosophy. *University of Canterbury, New Zealand*.

Yuta, T., Chase, J. G., Shaw, G. M. & Hann, C. Year. Dynamic models of ARDS lung mechanics for optimal patient ventilation. *In: Proceedings of the 26th International Conf of IEEE Engineering in Med and Biology Society (EMBC 2004)*, 2004 San Francisco, CA.

Zilberberg, Marya D. & Epstein, Scott K. (1998). Acute Lung Injury in the Medical ICU . Comorbid Conditions, Age, Etiology, and Hospital Outcome. *Am J Respir Crit Care Med,* 157 (4)**:** 1159-1164.